Dissertation zur Erlangung des Doktorgrades
der Fakultät für Chemie und Pharmazie
der Ludwig-Maximilians-Universität München

# Lanthanum (Oxo)nitridosilicates: Syntheses, Properties and the Use of Synchrotron Radiation for Structure Elucidation

Dajana Durach

aus

Bonn, Deutschland

2016

Erklärung

Diese Dissertation wurde im Sinne von § 7 der Promotionsordnung vom 28. November 2011 von Herrn Prof. Dr. W. Schnick betreut.

Eidesstattliche Versicherung

Diese Dissertation wurde eigenständig und ohne unerlaubte Hilfe erarbeitet.

München, den 11.04.2016

…….

(Dajana Durach)

Dissertation eingereicht am 11.4.2016

1. Gutachter Prof. Dr. W. Schnick

2. Gutachter Prof. Dr. O. Oeckler

Mündliche Prüfung am 24.05.2016

*Für meine Familie*

# Acknowledgement

Mein ganz besonderer Dank gebührt Herrn Prof. Dr. Wolfgang Schnick für die Gelegenheit meine Doktorarbeit in seinem Arbeitskreis anzufertigen. Die vielfältigen Mittel und die große Freiheit den Fragestellungen eigenständig auf den Grund zu gehen, sowie die hervorragenden Arbeitsbedingungen waren die beste Voraussetzung für diese Arbeit. Auch für die Möglichkeit Ergebnisse in wissenschaftlichen Fachzeitschriften bzw. auf (inter)nationalen Tagungen darzustellen sowie der Gelegenheit zur aktiven Beteiligung an der Kooperation mit Lumileds gebührt großer Dank.

Herrn Prof. Dr. Oliver Oeckler danke ich für die Übernahme des Korreferats und vor allem für die vielen gemeinsamen Projekte, die maßgeblich dazu beigetragen haben meiner Doktorarbeit den nötigen Feinschliff zu gegeben.

Frau Prof. Dr. Christina Scheu, sowie den Herrn Prof. Dr. Konstantin Karaghiosoff, Prof. Dr. Hans-Christian Böttcher und Prof. Dr. Dirk Johrendt danke ich für die Bereitschaft, als weitere Prüfer zur Verfügung zu stehen.

Auch möchte ich mich bei allen Beteiligten des Kooperationsprojekts mit Lumileds bedanken. Dabei möchte ich vor allem Dr. Peter J. Schmidt und Petra Huppertz hervorheben, die durch zahlreiche Lumineszenzmessungen und spannende Diskussionen meine Doktorarbeit bereichert haben. Ich freue mich sehr, dass ich durch diese enge Zusammenarbeit ein fundiertes Wissen über moderne Beleuchtungstechnologie aufbauen konnte, und dass durch unsere gemeinsame Forschung nachhaltige Ergebnisse geschaffen werden konnten.

Desweiteren bedanke ich mich ganz herzlich bei meinen Kooperationspartnern Dr. Felix Fahrnbauer, Peter Schultz und Lukas Neudert für die tolle Zusammenarbeit. Die Projekte mit Euch haben mir sehr viel Spaß gemacht.

Ferner danke ich auch Herrn Dr. Constantin Hoch und Herrn Dr. Peter Mayer für die zahlreichen Einkristalluntersuchungen und auch für den intensiven Beistand bei diversen Problemdatensätzen. Herrn Christian Minke danke ich für die zahlreichen Stunden am REM, die stets mit netten Gesprächen verbunden waren.

Frau Olga Lorenz, Herrn Thomas Miller und Herrn Wolfgang Wünschheim danke ich für die stete Hilfe bei allerlei organisatorischen, computertechnischen und sicherheitsrelevanten Fragen.

Besonderer Dank gilt Herrn Dr. Philipp Pust, der stets ein offenes Ohr für meine Fragen hatte und mir vieles von dem was diese Arbeit erfolgreich gemacht hat beibrachte.

Auch meinen Praktikanten Philipp Angloher, Mareike Czuppa, Niklas Keller, Niklas Cordes und Pamina Hirler gilt großer Dank, da sie mich mit viel Einsatz unterstützt haben.

Ich danke natürlich auch allen bisher nicht erwähnten Mitgliedern der Arbeitskreise Schnick, Johrendt, Lotsch, Schmedt auf der Günne, Oeckler und Hoch für die großartige Stimmung im zweiten Stock. Ich freue mich während meiner Promotion in einigen von Euch wahre Freunde gefunden zu haben.

Meiner Familie danke ich für Ihre stetige Unterstützung und dafür, dass Sie mir auch in den stressigsten Zeiten immer wieder dabei geholfen hat zur Ruhe zu kommen. Ohne euch wäre ich nicht wo ich jetzt bin.

Zum Schluss möchte ich noch meinem Freund Felix danken, dass er während des gesamten Studiums durch sämtliche Höhen und Tiefen mit mir gegangen ist. Sein Vertrauen in mich und seine Unterstützung haben mich stets bestärkt und mir die nötige Kraft gegeben.

*Es ist nicht genug, zu wissen, man muß auch anwenden;*

*es ist nicht genug, zu wollen, man muß auch tun!*

(Johann Wolfgang von Goethe)

# Table of Contents

# 1 Introduction

At the latest with the discovery of $La_3Si_6N_{11}:Ce^{3+}$ [1] the importance of lanthanum (oxo)nitridosilicates was recognized, since this material supplemented the great structural variability of lanthanum (oxo)nitridosilicates (chapter 2) by outstanding luminescence properties (chapter 3). Owing to this feature, some lanthanum (oxo)nitridosilicates already found broad application as luminescent materials (phosphors) for phosphor-converted pc-LEDs.[2] As such, lanthanum (oxo)nitridosilicates will further gain importance as especially in times of energy saving, there is a continuously growing demand for highly efficient and stable phosphors for application in pc-LEDs.

Usually, (oxo)nitridosilicates do not occur naturally, as oxygen and water have an ubiquitous presence in our world. The only known exception is sinoite, $Si_2N_2O$, which however was found in meteorites.[3,4] Chemical bonds to nitrogen are typically less stable than bonds to oxygen and thus most solid nitrides are thermodynamically less stable than the corresponding oxides. As a general consequence, usually only highly condensed nitridosilicates are stable in air and towards hydrolysis, as the high degree of condensation kinetically prevents the dissociation.[5] Therefore, the bonding situation in oxo- and nitridosilicates is significantly different, although both compounds are characterized by building blocks formed by $SiN_4$ or $SiO_4$ tetrahedra, respectively. Oxosilicates additionally exhibit a smaller structural diversity than nitridosilicates, since they are restricted to terminal ($O^{[1]}$) and simply bridging ($O^{[2]}$) oxygen. The Si-N distances, by contrast, are larger and less ionic than Si-O distances, which both might be the reason for the possible threefold ($N^{[3]}$) and even fourfold ($N^{[4]}$) linkage of neighboring tetrahedral centers. Furthermore, $SiN_4$ tetrahedra can share both common corners as well as common edges, while $SiO_4$ tetrahedra nearly exclusively share common corners.[6,7] The only exception might be fibrous $SiO_2$, whose existence has not yet been unambiguously substantiated.[8] On the basis of the structural variety of nitridosilicates an extended range for the degree of condensation $\kappa = n(Si):n(N)$ is found. For oxosilicates, κ can reach values between ¼, corresponding to non-condensed tetrahedral anions, and ½ in $SiO_2$, whereas in nitridosilicates, κ has a maximum value of ¾, e.g. in $Si_3N_4$.[6,9] As a direct consequence of the structural features of nitridosilicates these compounds build non-condensed,[10] one-dimensional,[11,12] and layer-

like silicate substructures[13] next to three-dimensional silicate frameworks, like in $EA_2Si_5N_8$ (*EA* = Sr, Ba)[14] (Figure 2).

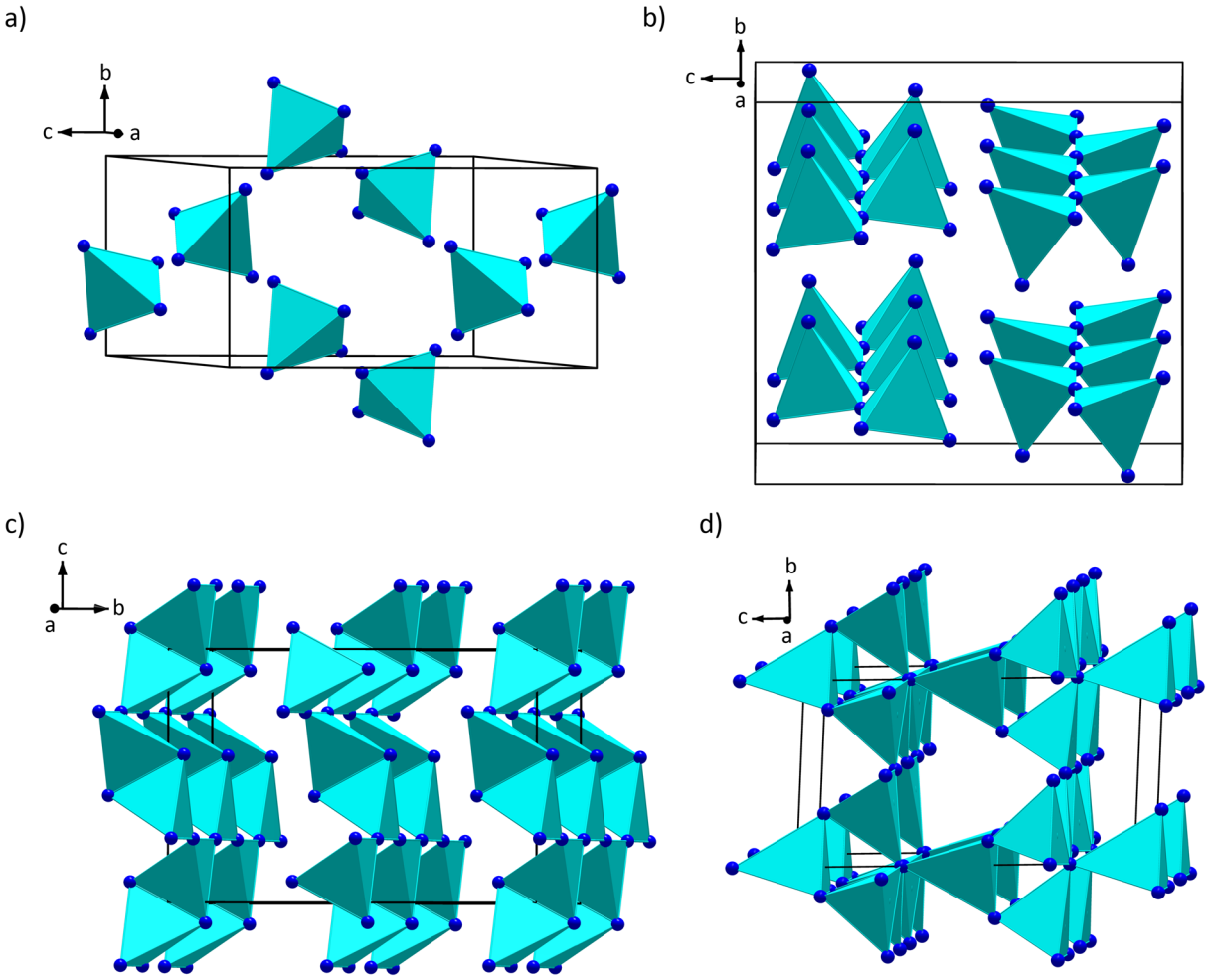


Figure 2. Silicate substructure of a) $Ca_4SiN_4$ (isolated $SiN_4$ tetrahedra)[10] b) $Eu_2SiN_3$ (non-branched single-chains of corner sharing $SiN_4$ tetrahedra)[12] c) $BaSiN_2$ (sheets of corner and edge sharing $SiN_4$ tetrahedra)[13] and d) $MYbSi_4N_7$ (M = Eu, Sr, Ba; highly condensed network of corner sharing $SiN_4$ tetrahedra and $[N(SiN_3)_4]$building blocks with N[4].[27-29] $SiN_4$ tetrahedra are depicted in turquoise.

Associated with these structural opportunities nitridosilicates show several promising materials properties. The currently most important application of nitridosilicates is their already mentioned utilization as phosphors for pc-LEDs.[15,16] This topic will be discussed in chapter 3 in detail. Nitridosilicates also offer potential as nonlinear optic materials, which can be used in computer and optical signal processing devices, optical frequency conversion, and telecommunications.[17-19] Moreover, nitridosilicates can be applied as heat sink materials, due to their high thermal conductivity.[20,21] Lithium nitridosilicates, on the other

hand, show lithium ion conductivity,[22] e.g. in $Li_2SiN_2$[23-25] and $Li_8SiN_4$,[26] which raises potential as solid-state electrolytes in batteries.

The focus of this thesis is based on the development of an innovative synthesis route to expand the compound class of lanthanum (oxo)nitridosilicates and the investigation of the optical properties of the respective lanthanide-doped compounds. The first part deals with the synthesis and characterization of novel lanthanum (oxo)nitridosilicates with different dimensionalities of the silicate substructure. In the second part calcium lanthanum (oxo)nitridosilicates with intriguing luminescence properties are discussed. These compounds enable efficient codoping und thus the fabrication of high-performance warm-white 1pc-LEDs. In the third part, investigations with synchrotron microfocus radiation are presented, which enables the analysis of particles with a volume even smaller than 1 $\mu m^3$ and thus allows for the characterization of further novel lanthanum (oxo)nitridosilicates. Additionally, a promising characterization method is presented, which combines transmission electron microscopy and synchrotron microfocus radiation and provides the possibility of analyzing the same particle by TEM and X-ray diffraction.

## References


[1] N. Kijima, T. Seto, N. Hirosaki, *ECS Trans.* **2009**, *25*, 247.

[2] http://www.semicontaiwan.org/en/sites/semicontaiwan.org/files/docs/mitsubishifinal_ke_fen_xiang_.pdf, visited on 7th December **2015**.

[3] W. H. Baur, *Nature* **1972**, *240*, 461.

[4] A. Bischoff, T. Grund, T. Jording, B. Heying, R.-D. Hoffmann, U. Ch. Rodewald, R. Pöttgen, *Z. Naturforsch. B* **2005**, *60b*, 1231.

[5] W. Schnick, *Angew. Chem. Int. Ed. Engl.* **1993**, *32*, 806.

[6] M. Zeuner, S. Pagano, W. Schnick, *Angew. Chem. Int. Ed.* **2011**, *50*, 7754.

[7] W. Schnick, H. Huppertz, *Chem. Eur. J.* **1997**, *3*, 679.

[8] A. Weiss, A. Weiss, *Z. Anorg. Allg. Chem.* **1954**, *276*, 95.

[9] F. Liebau, *Naturwissenschaften* **1962**, *49*, 481.

[10] H. Yamane, H. Morito, *Inorg. Chem.* **2013**, *52*, 5559.

[11] S. Lupart, M. Zeuner, S. Pagano, W. Schnick, *Eur. J. Inorg. Chem.* **2010**, 2636.

[12] M. Zeuner, S. Pagano, P. Matthes, D. Bichler, D. Johrendt, T. Harmening, R. Pöttgen, W. Schnick, *J. Am. Chem. Soc.* **2009**, *131*, 11242.

[13] Z. A. Gàl, P. M. Mallinson, H. J. Orchard, S. J. Clarke, *Inorg. Chem.* **2004**, *43*, 3998.

[14] T. Schlieper, W. Milius, W. Schnick, *Z. Anorg. Allg. Chem.* **1995**, *621*, 1380.

[15] S. Schmiechen, P. Pust, P. J. Schmidt, W. Schnick, *Nachr. Chem.* **2014**, *62*, 847.

[16] R. Müller-Mach, G. Müller, M. R. Krames, H. A. Höppe, F. Stadler, W. Schnick, T. Jüstel, P. Schmidt, *Phys. Status Solidi A* **2005**, *202*, 1727.

[17] M. S. Bhamra, D. J. Fray, *J. Mater. Sci.* **1995**, *30*, 5381.

[18] S. R. Marder, G. D. Stucky, J. E. Sohn, *Materials for Nonlinear Optics: Chemical* Perspectives, ACS Symp. Ser., **1991**, *455*.

[19] H. Lutz, S. Joosten, J. Hoffmann, P. Lehmeier, A. Seilmeier, H. A. Höppe, W. Schnick, J. *Phys. Chem. Solids* **2004**, *65*, 1285.

[20] G. A. Slack, *J. Phys. Chem. Solids* **1973**, *34*, 321.

[21] M. Kitayama, K. Hirao, K. Watari, M. Toriyama, S. Kanzaki, *J. Am. Ceram. Soc.* **2001**, *84*, 353.

[22] E. Narimatsu, Y. Yamamoto, T. Takeda, T. Nishimura, N. Hirosaki, *J. Mater. Res.* **2011**, *26*, 1133.

[23] S. Pagano, M. Zeuner, S. Hug, *Eur. J. Inorg. Chem.* **2009**, 1579.

[24] B. Song, J. K. Jian, G. M. Cai, M. Lei, H. Q. Bao, H. Li, Y. P. Xu, W. Y. Wang, J. C. Han, X. L. Chen, *Solid State Ionics* **2009**, *180*, 29.

[25] A. J. Anderson, R. G. Blair, S. M. Hick, R. B. Kaner, *J. Mater. Chem.* **2006**, *16*, 1318.

[26] J. Lang, J.-P. Charlot, *Rev. Chim. Miner.* **1970**, *7*, 121.

[27] H. Huppertz, W. Schnick, *Acta Crystallogr. Sect C* **1997**, *53*, 1751.

[28] H. Huppertz, W. Schnick, *Angew. Chem. Int. Ed. Engl.* **1996**, *108*, 2115.

[29] H. Huppertz, W. Schnick, *Z. Anorg. Allg. Chem.* **1997**, *623*, 212.

# 2 Lanthanum (Oxo)nitridosilicates and their Structural Variety

## 2.1 Introduction

Owing to the great structural variability and promising properties of (oxo)nitridosilicates (chapter 1), scientists are constantly looking for new (oxo)nitridosilicates. Thus, meanwhile several lanthanum (oxo)nitridosilicates with diverse structures are known (Table 1).

**Table 1.** Crystal structures of already known lanthanum (oxo)nitridosilicates.

| compound | linking pattern of the $SiN_{4-x}O_x$ tetrahedral |
|---|---|
| $La_5[Si_3NO_{11}]O$[1] | non-condensed tetrahedra |
| $La_3[SiN_3O]O$[2] | non-condensed tetrahedra |
| $La_4Si_2N_2O_7$[3] | corner-sharing double tetrahedra |
| $LaSiNO_2$[4] | corner-sharing *dreier* rings[14,15] |
| $La_{16}[Si_8N_{22}][SiON_3]_2$[5] | infinite chains of branched corner- and edge-sharing tetrahedra; non-condensed tetrahedra |
| $La_5Si_3N_9$[6] | infinite branched chains of corner-sharing tetrahedra |
| $LiLa_5Si_4N_{10}O$[7] | loop-branched *dreier* single chains of corner-sharing tetrahedra |
| $Li_5La_5Si_4N_{12}$[8] | non-branched *zweier* chains of corner-sharing tetrahedra |
| $La_3Si_8N_{11}O_4$[9] | three-dimensional network of corner- and edge-sharing tetrahedra; corner-sharing *fünfer* rings |
| $La_7Si_6N_{15}$[10] | complex interrupted network of corner-sharing tetrahedra |
| $LaSi_3N_5$[11] | three-dimensional network of corner-sharing *fünfer* rings |
| $La_3Si_6N_{11}$[12] | three-dimensional network of corner-sharing *vierer* and *achter* rings |
| $La_{4-x}Ca_xSi_{12}O_{3+x}N_{18-x}:Eu^{2+}$[13] | three-dimensional network of corner-sharing tetrahedra |

A synthetic approach to lanthanum (oxo)nitridosilicates is facilitated by high-temperature reactions with temperatures of at least 1200 °C (Table 2). Only $Li_5La_5Si_4N_{12}$ was synthesized at lower temperatures (900 °C), as a flux technique utilizing metallic Li was used (Table 2.). This approach enables the solvation of a variety of metals,[16] inorganic salts and even complex anions.[17] Additionally, the solubility of nitrogen is enhanced when alkali metals are

added to the reaction mixture.[18] This seems to be a crucial factor for the syntheses of nitrides in liquid alkali metals. Consequently, this approach enables the synthesis of several (oxo)nitridosilicates by temperatures lower than 1000 °C.[18,19] However, the used alkali metal often incorporates into the (oxo)nitridosilicates.[18] Besides, LaSi ,LaN, $La_2O_3$, $LaHal_3$ (Hal = F, Cl), La, $Si_3N_4$, "$Si(NH)_2$", $SiO_2$, Si and $N_2$ turned out to be promising starting materials on the route to lanthanum (oxo)nitridosilicates (Table 2).

**Table 2.** Conditions for the synthesis of already known lanthanum (oxo)nitridosilicates.

| compound | synthesis temperature | starting materials |
|---|---|---|
| $La_5[Si_3NO_{11}]O$[1] | 1300 °C | $La_2O_3$, $Si_3N_4$, $SiO_2$ |
| $La_3[SiN_3O]O$[2] | 1600 °C | La,$La_2O_3$, "$Si(NH)_2$" |
| $La_4Si_2N_2O_7$[4] | 1500 °C | $La_2O_3$, $Si_3N_4$, $SiO_2$ |
| $LaSiNO_2$[4] | 1550 °C | $La_2O_3$, $Si_3N_4$, $SiO_2$ |
| $La_{16}[Si_8N_{22}][SiON_3]_2$[5] | 1600 °C | LaN, "$Si(NH)_2$", $SiO_2$ |
| $La_5Si_3N_9$[6] | 1625 °C | La, "$Si(NH)_2$" |
| $LiLa_5Si_4N_{10}O$[7] | 1200 °C | $LaF_3$, "$Si(NH)_2$", $LiN_3$ |
| $Li_5La_5Si_4N_{12}$[8] | 900 °C | $LaCl_3$, "$Si(NH)_2$", $NaN_3$, Li |
| $La_3Si_8N_{11}O_4$[4] | 1600 °C | $La_2O_3$, $Si_3N_4$, $SiO_2$ |
| $La_7Si_6N_{15}$[10] | 1625 °C | LaN, "$Si(NH)_2$" |
| $LaSi_3N_5$[11] | 2000 °C | $La_2O_3$, $Si_3N_4$ |
| $La_3Si_6N_{11}$[12] | 1500 °C | La, Si, $N_2$ atmosphere |
| $La_{4-x}Ca_xSi_{12}O_{3+x}N_{18-x}:Eu^{2+}$[13] | 1525 °C | $La_2O_3$, $Si_3N_4$, CaO, $Eu_2O_3$ |

Next to the mentioned flux methods, precursor approaches, combining crystalline metal amide precursors and "$Si(NH)_2$" are used for the synthesis of (oxo)nitridosilicates,[20] as amides show a high reactivity and decompose under thermal treatment solely to metal nitrides and imides.[21] In the course of this work, an enhancement of the latter method was established (chapter 2.2 and 2.3) in order to avoid thermodynamic sinks and the synthesis of known compounds. Thereby, the novel lanthanum (oxo)nitridosilicates $La_{16.32}Ba_{1.82}Sr_{7.86}[Si_{60}N_{92.32}O_{3.68}]O_{12}$, $La_{13.68}Sr_{12.32}[Si_{60}N_{96}]F_{6.32}O_{5.68}$ (chapter 2.2) $La_3[SiN_4]F$ and $La_3[SiN_3O]O$ (chapter 2.3) have been obtained.

## References


[1] S. Titeux, M. Gervais, P. Verdier, Y. Laurent, *Mater. Sci. Forum* **2000**, *325*, 17.

[2] J. A. Kechele, C. Schmolke, S. Lupart, W. Schnick, *Z. Anorg. Allg. Chem.* **2010**, *636*, 176.

[3] J. Takahashi, H. Yamane, N. Hirosaki, Y. Yamamoto, T. Suehiro, T. Kamiyama, M. Shimada, *Chem. Mater.* **2003**, *15*, 1099.

[4] M. Mitomo, F. Izumi, S. Horiuchi, Y. Matsui, *J. Mater. Sci.* **1982**, *17*, 2359.

[5] C. Schmolke, S. Lupart, W. Schnick, *Solid State Sci.* **2009**, *11*, 305.

[6] C. Schmolke, D. Bichler, D. Johrendt, W. Schnick, *Solid State Sci.* **2009**, *11*, 389.

[7] S. Lupart, W. Schnick, *Z. Anorg. Allg. Chem.* **2012**, *638*, 94.

[8] S. Lupart, M. Zeuner, S. Pagano, W. Schnick, *Eur. J. Inorg. Chem.* **2010**, 2636.

[9] R. K. Harris, M. J. Leach, *Chem. Mater.* **1992**, *4*, 260.

[10] C. Schmolke, O. Oeckler, D. Bichler, D. Johrendt, W. Schnick, *Chem. Eur. J.* **2009**, *15*, 9215.

[11] Z. Inoue, M. Mitomo, N. Li, *J. Mater. Sci.* **1980**, *15*, 2915.

[12] M. Woike, W. Jeitschko, *Inorg. Chem.* **1995**, *34*, 5105.

[13] W. B. Park, N. Shin, K.-P. Hong, M. Pyo, K.-S. Sohn, *Adv. Funct. Mater.* **2012**, *22*, 2258.

[14] F. Liebau, *Structural Chemistry of Silicates*, Springer, Berlin, **1985**.

[15] The term *dreier* ring was coined by Liebau and is derived from the German word “drei”; a *dreier* ring comprises three tetrahedral centers.

[16] P. Hubberstey, P. G. Roberts, *J. Chem. Soc. Dalton Trans.* **1994**, 667.

[17] R. J. Pulham, P. Hubberstey, *J. Nucl. Mater.* **1983**, *115*, 239.

[18] S. Pagano, S. Lupart, M. Zeuner, W. Schnick, *Angew. Chem. Int. Ed.* **2009**, *48*, 6335.

[19] Z. A. Gál, P. M. Mallinson, H. J. Orchard, S. J. Clarke, *Inorg. Chem.* **2004**, *43*, 3998.

[20] M. Zeuner, F. Hintze, W. Schnick, *Chem. Mater.* **2009**, *21*, 336.

[21] M. Zeuner, S. Pagano, W. Schnick, *Angew. Chem. Int. Ed.* **2011**, *50*, 7754.

# 2.2 Lanthanum (Oxo)nitridosilicates: From Ordered to Disordered Crystal Structures

published in: *Z. Anorg. Allg. Chem.* **2016**, *642*, 101-106.

authors: Dajana Durach and Wolfgang Schnick

DOI: DOI: 10.1002/zaac.201500730



http://onlinelibrary.wiley.com/doi/10.1002/zaac.201500730/abstract

**Abstract.** The homeotypic compounds $La_{16.32}Ba_{1.82}Sr_{7.86}[Si_{60}N_{92.32}O_{3.68}]O_{12}$ and $La_{13.68}Sr_{12.32}[Si_{60}N_{96}]F_{6.32}O_{5.68}$ were synthesized at high temperature (1600/1500 °C) in a radio-frequency furnace. The crystal structures [$I\bar{4}3m$ (no. 217), $Z$ = 1, $a$ = 13.3360(10)/13.3258(10) Å and $V$ = 2371.8(5)/2366.4(5) Å$^3$] were solved and refined on basis of single-crystal X-ray diffraction data and were corroborated by lattice-energy calculations (Madelung part of lattice energy, MAPLE) powder X-ray diffraction data and FTIR spectroscopy. They consist of a three-dimensional network of all side corner sharing $SiN_{4-x}O_x$ tetrahedra. The framework is characterized by double dreier rings. $La_{16.32}Ba_{1.82}Sr_{7.86}[Si_{60}N_{92.32}O_{3.68}]O_{12}$ represents an oxonitridosilicate oxide and $La_{13.68}Sr_{12.32}[Si_{60}N_{96}]F_{6.32}O_{5.68}$ a nitridosilicate fluoride oxide, as the crystal structures contain non-condensed ($O^{[0]}$/O,$F^{[0]}$) anions. The first compound is isotypic to $Sr_3Ln_{10}Si_{18}Al_{12}O_{18}N_{36}$ (*Ln* = Ce, Pr, Nd; $Z$ = 2), whereas the latter describes a disordered model of the crystal structure, which is homeotypic to the mentioned SiAlONs.

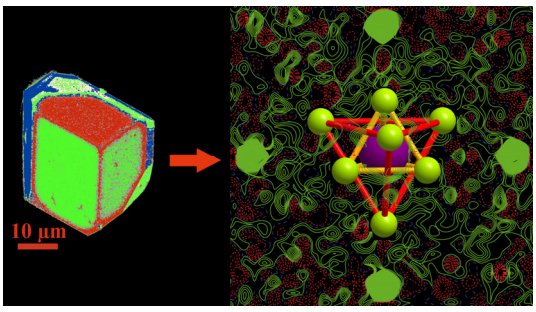

## 2.2.1 Introduction

(Oxo)nitridosilicates represent a promising compound class as they show interesting materials properties, e.g. luminescence of $Eu^{2+}$ or $Ce^{3+}$ doped samples, which are correlated with their crystal structure.[1-5] Consequently, there is a keen interest in new (oxo)nitridosilicates with auspicious crystal structures. Typically, such compounds consist of $Si(N,O)_4$ tetrahedra. The nitrogen facilitates the linkage of the tetrahedra with one to four other $Si(N,O)_4$ tetrahedra. Furthermore, $SiN_4$ tetrahedra can share common corners as well as common edges. Thus, (oxo)nitridosilicates show a pronounced structural variability. Consequently, (oxo)nitridosilicates with non-condensed,[6,7] one-dimensional,[8,9] and layer-like crystal structures[10] are known next to compounds consisting of a three-dimensional framework, like $EA_2Si_5N_8$ (*EA* = Sr, Ba).[11] As this compound class has a great tendency to build highly condensed crystal structures, the quantity of less condensed crystal structures is still minor compared to classical oxosilicates. From a thermodynamic point of view, chemical bonds to nitrogen are less stable than the bonds to oxygen, thus most of the less condensed (oxo)nitridosilicates are sensitive towards hydrolysis, whereas the high degree of condensation of (oxo)nitridosilicates with three-dimensional frameworks usually prevents dissociation kinetically.[1,12] A synthetic approach to this compound class is facilitated by high-temperature reactions,[13,14] flux methods[6,8,9] and precursor routes.[1,15] For high-temperature syntheses often radio-frequency furnaces have been used, which allow fast heating and high quenching rates. Flux methods are based on the significant solubility of nitrogen in liquid alkali metals (Na or Li). For precursor routes metal amides have been used frequently, as they have a high reactivity and thermal decomposition feasibility, which lead to metal nitrides and imides.[1]

In this contribution, we report on synthesis and crystal structure elucidation of $La_{16.32}Ba_{1.82}Sr_{7.86}[Si_{60}N_{92.32}O_{3.68}]O_{12}$ and $La_{13.68}Sr_{12.32}[Si_{60}N_{96}]F_{6.32}O_{5.68}$, two (oxo)nitridosilicates with a high degree of condensation, which were synthesized with a combination of a high-temperature and precursor approach.

## 2.2.2 Results and Discussion

### 2.2.2.1 Single-Crystal Structure Analyses

$La_{16.32}Ba_{1.82}Sr_{7.86}[Si_{60}N_{92.32}O_{3.68}]O_{12}$ and $La_{13.68}Sr_{12.32}[Si_{60}N_{96}]F_{6.32}O_{5.68}$ can be obtained as air and hydrolysis stable byproducts of high-temperature reactions, which are probably based on the decomposition of the used hydrides (decomposition of $BaH_2/SrH_2$: 675 °C)[16] and their reaction with $LaF_3$ to $BaF_2/SrF_2$. These products resublimate at the reactor wall of the radio-frequency furnace. The remaining Ba/Sr/F reacts with $La_2O_3$ and the precursors $La(NH_2)_3$ and $Si(NH)_2$ to colorless crystals of $La_{13.68}Sr_{12.32}[Si_{60}N_{96}]F_{6.32}O_{5.68}$ and brown crystals of $La_{16.32}Ba_{1.82}Sr_{7.86}[Si_{60}N_{92.32}O_{3.68}]O_{12}$, respectively (Figure 1). Consequently, the latter represents in addition to e.g. $Sr_3Ln_{10}Si_{18}Al_{12}O_{18}N_{36}$ (*Ln* = Ce, Pr, Nd),[17] t-$La_3SiN_3O$,[13] and $LiLa_5Si_4N_{10}O$[8] another oxonitridosilicate (SiON) with colored crystals. Possibly, the color originates from color centers.

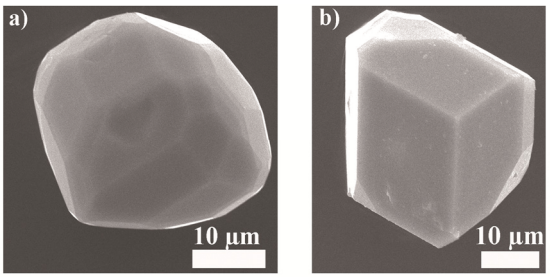


**Figure 1.** SEM images of the investigated single-crystals of $La_{16.32}Ba_{1.82}Sr_{7.86}[Si_{60}N_{92.32}O_{3.68}]O_{12}$ (a) and $La_{13.68}Sr_{12.32}[Si_{60}N_{96}]F_{6.32}O_{5.68}$ (b).

Both compounds crystallize in the cubic space group $I\bar{4}3m$ (no. 217). All atoms except the Sr split position of $La_{13.68}Sr_{12.32}[Si_{60}N_{96}]F_{6.32}O_{5.68}$ (Table 2) were refined anisotropically. The crystallographic data are summarized in Table 1. For the atomic coordinates and isotropic displacement parameters see Table 2. The anisotropic displacement parameters are given in the Supporting Information (Table S1).

**Table 1.** Crystallographic data of the single-crystal structure determination of $La_{16.32}Ba_{1.82}Sr_{7.86}[Si_{60}N_{92.32}O_{3.68}]O_{12}$ and $La_{13.68}Sr_{12.32}[Si_{60}N_{96}]F_{6.32}O_{5.68}$.

| | $La_{16.32}Ba_{1.82}Sr_{7.86}[Si_{60}N_{92.32}O_{3.68}]O_{12}$ | $La_{13.68}Sr_{12.32}[Si_{60}N_{96}]F_{6.32}O_{5.68}$ |
|---|---|---|
| Molar mass/g·mol$^{-1}$ | 6435.35 | 6221.09 |
| Crystal system | Cubic | |
| Space group | $I\bar{4}3m$ (no. 217) | |
| $a$/Å | 13.3360(10) | 13.3258(10) |
| Cell Volume/Å$^3$ | 2371.8(5) | 2366.4(5) |
| Formula units per unit cell | 1 | |
| Density/g·cm$^{-3}$ | 4.506 | 4.366 |
| μ/mm$^{-1}$ | 13.153 | 13.772 |
| Temperature/K | 293(2) | |
| Diffractometer | Bruker D8 Quest (microfocus and graphite monochromator) | |
| Radiation/Å | Mo-K$\alpha$ (0.71073) | |
| $F$(000) | 2943 | 2862 |
| 2θ range/° | 3.055 ≤ 2θ ≤ 52.146 | 3.057 ≤ 2θ ≤ 52.119 |
| Total no. of reflections | 58260 | 60337 |
| Independent reflections | 2526 | 2516 |
| Refined parameters | 53 | 56 |
| Goodness of fit | 1.056 | 1.134 |
| $R_1$ (all data)/$R_1$ [$F^2>2\sigma(F^2)$] | 0.0610/0.0400 | 0.0688/0.0405 |
| $wR_2$ (all data)/w$R_2$ [$F^2>2\sigma(F^2)$] | 0.0786/0.0710 | 0.0542/0.0491 |

**Table 2.** Atomic coordinates and isotropic displacement parameters/Å$^2$ of $La_{16.32}Ba_{1.82}Sr_{7.86}[Si_{60}N_{92.32}O_{3.68}]O_{12}$ and $La_{13.68}Sr_{12.32}[Si_{60}N_{96}]F_{6.32}O_{5.68}$ with standard deviations in parentheses.

| Atom | *x* | *y* | *z* | $U_{eq}$ | *s.o.f.* |
|---|---|---|---|---|---|
| $La_{16.32}Ba_{1.82}Sr_{7.86}[Si_{60}N_{92.32}O_{3.68}]O_{12}$ | | | | | |
| La,Sr1 | 0.12963(2) | *x* | 0.44760(3) | 0.01107(7) | 0.68/0.32 |
| Ba,Sr2 | 0 | 0 | 0 | 0.0421(6) | 0.09/0.910 |
| Si1 | 0.29787(17) | 0 | 0 | 0.0069(3) | 1 |
| Si2 | 0.20619(8) | *x* | 0.04817(12) | 0.0070(2) | 1 |
| Si3 | 0.35037(8) | *x* | 0.19123(12) | 0.0070(2) | 1 |
| O1 | ¼ | ½ | 0 | 0.0161(11) | 1 |
| N,O2 | 0.4283(2) | *x* | 0.1274(4) | 0.0108(7) | 127/150; 23/150 |
| N3 | 0.2843(3) | *x* | 0.1076(4) | 0.0119(7) | 1 |
| N4 | 0.0783(2) | *x* | 0.2254(4) | 0.0091(6) | 1 |
| N5 | 0.2725(3) | *x* | 0.4202(3) | 0.0085(6) | 1 |
| $La_{13.68}Sr_{12.32}[Si_{60}N_{96}]F_{6.32}O_{5.68}$ | | | | | |
| La,Sr1 | 0.12961(2) | *x* | 0.44711(2) | 0.00912(5) | 0.57/0.43 |
| Sr2A | 0.4690(6) | *x* | *x* | 0.035(3) | 0.171(12) |
| Sr2B | 0.0208(8) | *x* | *x* | 0.047(9) | 0.079(12) |
| Si1 | 0.29832(13) | 0 | 0 | 0.0049(2) | 1 |
| Si2 | 0.20616(6) | *x* | 0.04805(9) | 0.00494(16) | 1 |
| Si3 | 0.35036(6) | *x* | 0.19103(9) | 0.00516(17) | 1 |
| F1,O1 | ¼ | ½ | 0 | 0.0123(7) | 0.5267/0.4733 |
| N2 | 0.42831(16) | *x* | 0.1265(3) | 0.0074(5) | 1 |
| N3 | 0.28424(19) | *x* | 0.1072(3) | 0.0104(6) | 1 |
| N4 | 0.07831(18) | *x* | 0.2258(3) | 0.0072(5) | 1 |
| N5 | 0.27222(18) | *x* | 0.4203(2) | 0.0063(5) | 1 |

Both compounds derive from $Sr_3Ln_{10}Si_{18}Al_{12}O_{18}N_{36}$ (*Ln* = Ce, Pr, Nd; *Z* = 2),[17] as $La_{16.32}Ba_{1.82}Sr_{7.86}[Si_{60}N_{92.32}O_{3.68}]O_{12}$ is isotypic and $La_{13.68}Sr_{12.32}[Si_{60}N_{96}]F_{6.32}O_{5.68}$ is homeotypic to these SiAlONs. La and Ba as well as N, F, and O were distributed on basis of EDX measurements, MAPLE calculations (Table 3) and the results of the neutron powder diffraction of $Sr_3Pr_{10}Si_{18}Al_{12}O_{18}N_{36}$.[17] This is explained in detail in the chapter on MAPLE calculations below. Free refinement of the respective site occupation factors of the heavy atom sites yielded their occupation with Sr. To obtain charge neutrality the refined site

occupation factors were fixed (Table 2). The absence of N-H groups was confirmed by FTIR spectroscopy (Figure S2, Supporting Information). $La_{16.32}Ba_{1.82}Sr_{7.86}[Si_{60}N_{92.32}O_{3.68}]O_{12}$ and $La_{13.68}Sr_{12.32}[Si_{60}N_{96}]F_{6.32}O_{5.68}$ are characterized by a three-dimensional network of all site corner sharing ($Q^4$-type) $SiN_{4-x}O_x$ tetrahedra (Figure 2a). The tetrahedra consist of $N,O^{[2]}/O^{[2]}$ and $N^{[3]}$ atoms ($X^{[2]}/X^{[3]}$: interconnection of two/three tetrahedra). This leads to a degree of condensation $\kappa = n(Si):n(N/O) = 0.625$. The tetrahedra build double *dreier* rings,[18] which result in *vierer* rings. Thereby, the $Si_3N_{3-x}O_x$ units of the *dreier* rings exhibit chair conformation and the $Si_4N_{4-x}O_x$ units of the *vierer* rings saddle conformation (Figure 2b, 2c). Moreover, the double *dreier* rings are connected via $SiN_{4-x}O_x$ tetrahedra. Additionally, both compounds contain isolated $O^{[0]}$ and $O,F^{[0]}$ positions, respectively. They are coordinated in a tetrahedral manner by four La,Sr1 atoms. The resulting tetrahedra are condensed in a way that they build *vierer* and *sechser* rings resulting in a β-cage of the isolated anions (Figure 2d, 2e). Next to La,Sr1, which is coordinated by ten anions, there is a second heavy atom site surrounded by twelve anions, thus Friauf polyhedra are formed (Figure 2d). They are arranged in a body centered cubic packing.

In $La_{16.32}Ba_{1.82}Sr_{7.86}[Si_{60}N_{92.32}O_{3.68}]O_{12}$ and $Sr_3Ln_{10}Si_{18}Al_{12}O_{18}N_{36}$ (*Ln* = Ce, Pr, Nd) Ba/Sr2 and Sr2, respectively, occupy a special site with Wyckoff no. 2*a* (0,0,0) and show enlarged displacement parameters. This points towards disorder around this position, however crystal structure refinement does not lead to a convincing disorder model.[17] In contrast, the crystal structure refinement of $La_{13.68}Sr_{12.32}[Si_{60}N_{96}]F_{6.32}O_{5.68}$ yielded no electron density on (0,0,0) and a disorder model, in which the second heavy atom site partly occupies two Wyckoff sites (8*c*). This results in the structural motif of two differently sized tetrahedra around (0,0,0), one formed of Sr2A and the other of Sr2B (Figure 3). Free refinement of the respective occupation factors [*s.o.f*(Sr2A): 0.68(4); *s.o.f*(Sr2B): 0.32(4)] results in a mutually exclusive but overall full occupation.

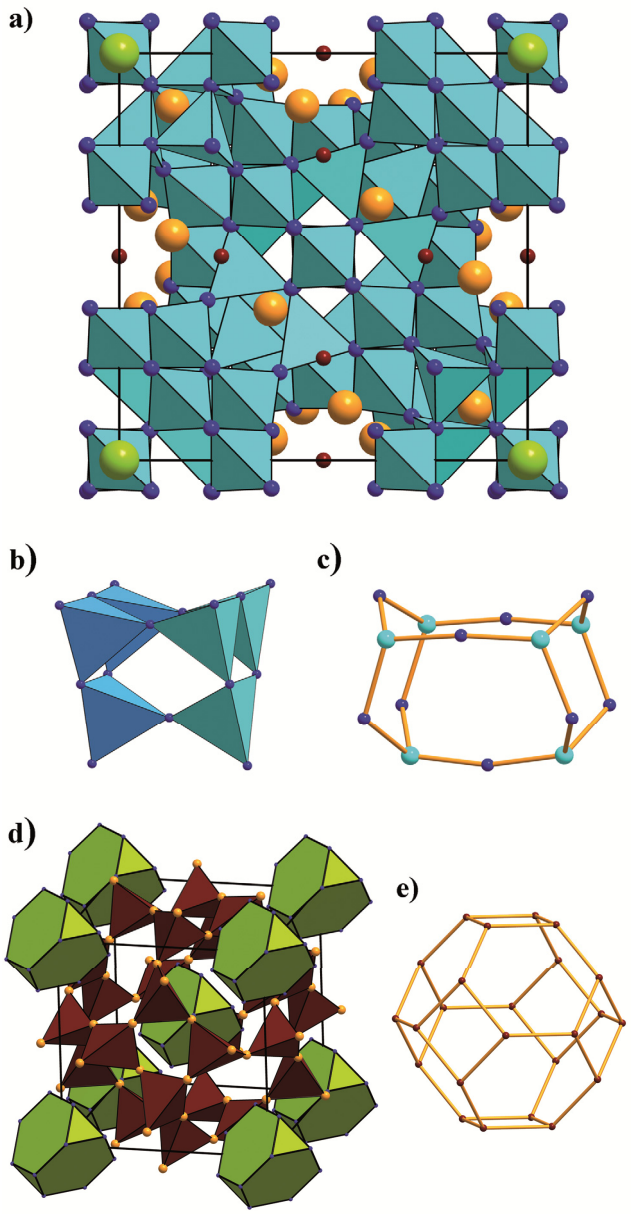


**Figure 2.** (a) Crystal structure of $La_{16.32}Ba_{1.82}Sr_{7.86}[Si_{60}N_{92.32}O_{3.68}]O_{12}$ and idealized model of $La_{13.68}Sr_{12.32}[Si_{60}N_{96}]F_{6.32}O_{5.68}$; with $SiN_{4-x}O_x$ tetrahedra (turquoise), N/N,O (blue), O/O,F (red), La,Sr (orange), Sr,Ba/Sr (green), unit cell is displayed; (b) and (c) double *dreier* ring with one *vierer* ring as characteristic building block of the silicate network; (d) polyhedral visualization of the crystal structures with Sr,Ba/$SrN_{12-x}O_x$ (green) units forming Friauf polyhedra and $O(La,Sr)_4$ tetrahedra (red); (e) β-cage of condensed O/O,F atoms (red).

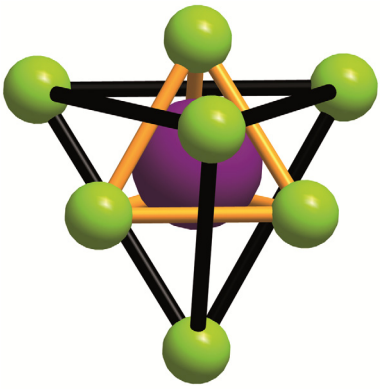

**Figure 3.** Sr sites (green) in $La_{13.68}Sr_{12.32}[Si_{60}N_{96}]F_{6.32}O_{5.68}$. Sr2A leads to the larger and Sr2B to the smaller tetrahedra. Position (0,0,0) is highlighted blue.

To exclude that the disorder model can be described with a model in lower symmetry the electron density of $La_{13.68}Sr_{12.32}[Si_{60}N_{96}]F_{6.32}O_{5.68}$ was plotted in *P*1 (Figure 4d, e, and f). As Sr2 shows only electron density around (0,0,0) an ordered model could be precluded in this case. In contrast, the electron density of $La_{16.32}Ba_{1.82}Sr_{7.86}[Si_{60}N_{92.32}O_{3.68}]O_{12}$ in *P*1 shows concentrated electron density on (0,0,0) (Figure 4a, b, and c).

The distances Si-N [1.669(4)-1.771(3) Å] and Si-N,O [1.680(5) Å] are in good agreement with other (oxo)nitridosilicates, e.g. $Sr_2Si_5N_8$ [Si-N: 1.653(9)-1.7865(5) Å][11] and $Ce_{10}[Si_{10}O_9N_{17}]Br$ [Si-N/O: 1.664(4)-1.709(7) Å].[19] The La,Sr-N [2.628(4)-3.117(5) Å] La,Sr-N,O [2.635(5)-2.967(3) Å], La,Sr-O [2.4605(2) Å] and La,Sr-O,F [2.4604(2) Å] bond lengths also correspond with other (oxo)nitridosilicates as well as the Sr-N [2.939(16)-3.043(6) Å] and Sr,Ba-N [3.350(5) Å] distances.[11,17,20-23] Moreover, all distances agree well with the sum of the ionic radii.[24]

A comparison of the powder diffraction patterns of the both samples with the theoretical powder diffraction patterns, simulated on the basis of single-crystal structure elucidation, show that $La_{16.32}Ba_{1.82}Sr_{7.86}[Si_{60}N_{92.32}O_{3.68}]O_{12}$ occurs as side phase and $La_{13.68}Sr_{12.32}[Si_{60}N_{96}]F_{6.32}O_{5.68}$ as main phase of the sample (Figure S1, Supporting Information).

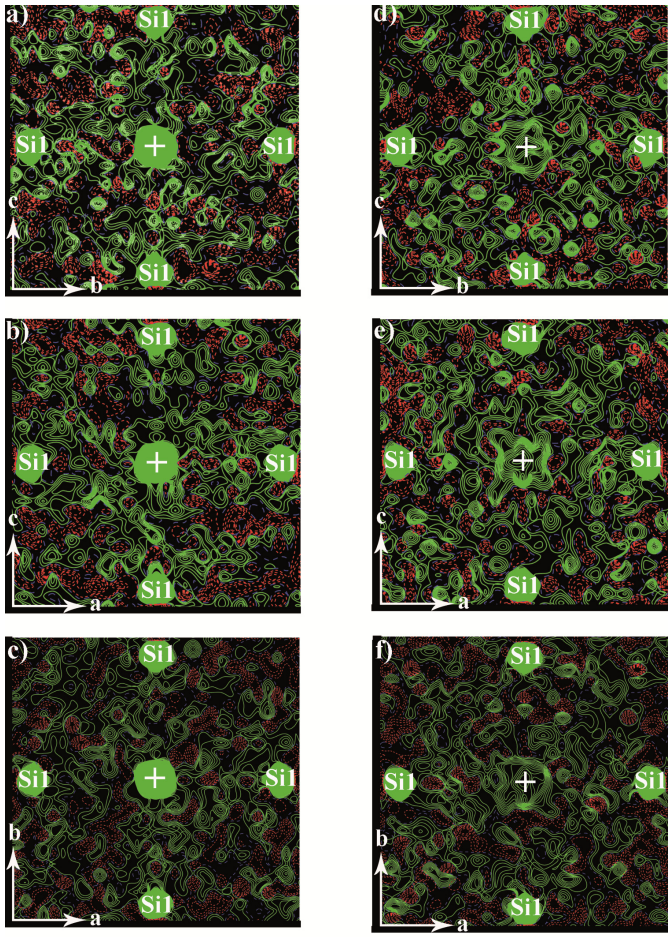


**Figure 4.** Electron density of $La_{16.32}Ba_{1.82}Sr_{7.86}[Si_{60}N_{92.32}O_{3.68}]O_{12}$ (a, b, c) and $La_{13.68}Sr_{12.32}[Si_{60}N_{96}]F_{6.32}O_{5.68}$ (d, e, f) without symmetry restrains on the planes (100) at $x = 0$ (a, d), (010) at $y = 0$ (b, e), (001) at $z = 0$ (c, f); site (0,0,0) is highlighted with a white cross; contour level 0.8 e·Å$^{-3}$ (green = positive electron density, red = negative electron density).

### 2.2.2.2 Lattice-Energy Calculations (MAPLE)

MAPLE calculations were performed to prove the electrostatic consistency of the crystal structures.[24-27] Thereby, solely electrostatic interactions, which depend on the charge, distances, and the coordination spheres of the constituting ions, were taken into account. As mentioned before these calculations are especially useful to determine the site occupancies of F, N, O, and La, Ba, respectively, as theses ions can hardly be distinguished by conventional X-ray diffraction owing to their similar X-ray scattering factors (Table 3). In addition to the MAPLE calculations the results of the EDX analysis and of the neutron powder diffraction pattern of $Sr_3Pr_{10}Si_{18}Al_{12}O_{18}N_{36}$, which yielded occupation of the terminal and one bridging anion position with O[17] served as a basis for the assignment of the atoms

types. For $La_{13.68}Sr_{12.32}[Si_{60}N_{96}]F_{6.32}O_{5.68}$ an idealized structure model was used, as the consideration of partly occupied sites with the MAPLE software is not possible. Consequently, Sr2A and Sr2B were shifted from Wyckoff position 8*c* [point symmetry: .3*m*; $x = y = z = 0.4690(6)$; $x = y = z = 0.0208(8)$] to a fully occupied "average" Wyckoff position 2*a* [point symmetry: $\bar{4}3m$, $x = y = z = 0$]. For both compounds the calculated partial MAPLE values of Si and N are consistent with reference values,[28-31] whereas the value of La,Sr1 and N,O2 range between those of the constituting ions, as expected. The terminal anion sites, Sr,Ba2 and Sr2 are insignificantly smaller than the characteristic range. The minor deviation between the overall MAPLE value of both compounds and the sum of those of the binary compounds that formally constitute them corroborate the electrostatic balance of the refined crystal structure.

**Table 3.** Partial MAPLE values and MAPLE sums /kJ·mol$^{-1}$ for $La_{16.32}Ba_{1.82}Sr_{7.86}[Si_{60}N_{92.32}O_{3.68}]O_{12}$ and $La_{13.68}Sr_{12.32}[Si_{60}N_{96}]F_{6.32}O_{5.68}$.[a)]

| $La_{16.32}Ba_{1.82}Sr_{7.86}[Si_{60}N_{92.32}O_{3.68}]O_{12}$ model | | | $La_{13.68}Sr_{12.32}[Si_{60}N_{96}]F_{6.32}O_{5.68}$ model | | |
|---|---|---|---|---|---|
| La/Sr1 | 3450 | +91/50 $BaSiN_2$[32] | La/Sr1 | 3117 | +308/25 $SrSiN_2$[32] |
| Sr/Ba2 | 1379 | +393/50 $SrSiN_2$[32] | Sr2 | 1409 | +1192/75 ß-$Si_3N_4$[33] |
| Si1 | 9680 | + 1258/75 α-$Si_3N_4$[33] | Si1 | 9732 | +584/75 LaN[34] |
| Si2 | 9579 | +392/75 $La_2O_3$[35] | Si2 | 9800 | +158/75 $LaF_3$[22] |
| Si3 | 9910 | +88/15 LaN[34] | Si3 | 9964 | +142/75 $La_2O_3$[35] |
| O1[0] | 1643 | | O/F1[0] | 948 | |
| N/O2[2] | 4912 | | N2[2] | 5453 | |
| N3[2] | 5437 | | N3[2] | 5315 | |
| N4[3] | 6073 | | N4[3] | 6016 | |
| N5[3] | 6000 | | N5[3] | 5975 | |
| Σ = 1228268 | | Σ = 1228860<br>Δ = 0.04% | Σ = 1225300 | | Σ = 1222573<br>Δ = 0.22% |

a) Typical partial MAPLE values /kJ·mol$^{-1}$: $La^{3+}$: 3500-5100; $EA^{2+}$: 1500-2100 (*EA* = Sr, Ba) $Si^{4+}$: 9000-10200; $(N^{[3]})^{3-}$: 5000-6200; $(N^{[2]})^{3-}$: 4600-6000; $F^-$: 465-599; $(O^{[0]})^{2-}$: 1871-1913.[28-31]

Partial exchange of Ba with La in $La_{16.32}Ba_{1.82}Sr_{7.86}[Si_{60}N_{92.32}O_{3.68}]O_{12}$, under consideration of charge neutrality, yielded MAPLE values, which are not consistent with reference values, thus an occupation of the second heavy atom site with La is unlikely. As the refined Ba content correspond to the EDX analysis occupation of the first heavy atom site with Ba

seems to be unlikely as well. But as the partial MAPLE values of Sr and Ba show the same characteristic range this cannot be fully precluded. According to the EDX analysis $La_{13.68}Sr_{12.32}[Si_{60}N_{96}]F_{6.32}O_{5.68}$ contains F, which usually do not occupy bridging sites. Therefore, F could only be located on the isolated anion position. Due to charge neutrality this site must be mixed occupied with both O and F. The occupation of this site with N and F is highly improbable, as this model leads to MAPLE values which do not agree with reference values.

## 2.2.3 Conclusions

High-temperature syntheses yielded to the lanthanum (oxo)nitridosilicates $La_{16.32}Ba_{1.82}Sr_{7.86}[Si_{60}N_{92.32}O_{3.68}]O_{12}$ and $La_{13.68}Sr_{12.32}[Si_{60}N_{96}]F_{6.32}O_{5.68}$. Single-crystal structure refinement shows that the Ba containing compound is isotypic to $Sr_3Ln_{10}Si_{18}Al_{12}O_{18}N_{36}$ (*Ln* = Ce, Pr, Nd; *Z* = 2),[17] whereas $La_{13.68}Sr_{12.32}[Si_{60}N_{96}]F_{6.32}O_{5.68}$ describes a homeotypic disordered variant. This was corroborated by investigations of the electron density. Both crystal structures were confirmed by means of powder X-ray diffraction data, MAPLE calculations and FTIR spectroscopy. The syntheses were, analogous to $La_3SiN_4F$[7] and $La_3BaSi_5N_9O_2:Ce^{3+}$,[36] based on $LaF_3$, hydrides and amides. Consequently, they are further examples that show that the mentioned route is particularly suitable for the synthesis of new lanthanum (oxo)nitridosilicates with diverse crystal structures.

## 2.2.4 Experimental Section

### 2.2.4.1 General

The starting materials were handled under exclusion of oxygen and moisture using either an argon-filled glove box (Unilab, MBraun, Garching; $O_2$ <1 ppm; $H_2O$ <1 ppm) or flame-dried glassware attached to a vacuum line.

### 2.2.4.2 Synthesis of $La_{13.68}Sr_{12.32}[Si_{60}N_{96}]F_{6.32}O_{5.68}$

$LaF_3$ (20.3 mg, 0.10 mmol), "$Si(NH)_2$" (35.6 mg, 0.61 mmol synthesized according to *Winter* et al.),[37] $La(NH_2)_3$ (20.1 mg, 0.11 mmol synthesized according to *Jacobs* et al.),[38] $SrH_2$

(42.7 mg, 0.48 mmol), and $La_2O_3$ (1.8 mg, 0.01 mmol) were thoroughly mixed in an agate mortar and filled into a tungsten crucible, which was placed in a water-cooled silica glass reactor of a radio-frequency furnace (Typ AXIO 10/450, max. electrical output 10 kW, Hüttinger Elektronik, Freiburg).[14] Subsequently, the crucible was heated in a purified nitrogen atmosphere to 1500 °C within 1 h, maintained at that temperature for 10 h, and cooled to 900 °C in 43.75 h, and finally quenched to room temperature by switching off the furnace. The reaction yielded an inhomogeneous product with colorless crystals of air and hydrolysis stable $La_{13.68}Sr_{12.32}Si_{60}F_{6.32}O_{5.68}N_{96}$.

### 2.2.4.3 Synthesis of $La_{16.32}Ba_{1.82}Sr_{7.86}[Si_{60}N_{92.32}O_{3.68}]O_{12}$

$LaF_3$ (20.3 mg, 0.10 mmol), "$Si(NH)_2$" (35.6 mg, 0.61 mmol synthesized according to *Winter* et al.),[37] $La(NH_2)_3$ (20.1 mg, 0.11 mmol synthesized according to *Jacobs* et al.),[38] $SrH_2$ (14.2 mg, 0.16 mmol), $BaH_2$ (44.2 mg, 0.32 mmol), and $La_2O_3$ (3.0 mg, 0.01 mmol) were thoroughly ground and filled into a tungsten crucible. The crucible was heated in a radio-frequency furnace in a nitrogen atmosphere within 1 h to 1600 °C, maintained at that temperature for 10 h, cooled to 900 °C in 43.75 h, and finally quenched to room temperature by switching off the furnace. The reaction affords an inhomogeneous sample with brown crystals of $La_{16.32}Ba_{1.82}Sr_{7.86}[Si_{60}N_{92.32}O_{3.68}]O_{12}$ which are stable in air and resistant against hydrolysis.

### 2.2.4.4 Single-Crystal X-ray Diffraction

Single crystals of the samples were isolated from the product under a microscope and were mounted on Kapton foil sample holders (micromount, MiTeGen, Ithaca). X-ray diffraction data were recorded with a Bruker D8 Quest diffractometer (Mo-$K_{\alpha1}$ radiation, microfocus and Goebel mirror optic). Absorption corrections of the respective data were done using the multi-scan method (SADABS).[39] The crystal structures were solved with Direct Methods (SHELXS) and refined by full-matrix least-squares methods (SHELXL).[40]

Further details of the crystal structures investigations may be obtained from the Fachinformationszentrum Karlsruhe, 76344 Eggenstein-Leopoldshafen, Germany (Fax: +49-7247-808-666; E-Mail: crysdata@fiz-karlsruhe.de, http://www.fiz-karlsruhe.de/request for deposited data.html) on quoting the depository numbers CSD-429945 and CSD-429946.

### 2.2.4.5 Powder X-ray Diffraction

The samples were pulverized in agate mortars and enclosed in glass capillaries. Powder diffraction data were recorded with a STOE STADI P diffractometer (Mo-$K_{\alpha1}$ radiation, Ge(111) monochromator, MYTHEN 1 K detector) in Debye-Scherrer setup. Simulated powder diffraction patterns were calculated on the basis of the single-crystal structure data with the use of the WinXPOW program package.[41]

### 2.2.4.6 SEM and EDX Spectroscopy

The chemical composition and morphology of the crystals were investigated with a JEOL JSM, equipped with a Si/Li EDX detector 7418 (Oxford Instruments) and operated at 30 kV. To provide electrical conductivity on the sample surfaces, the crystals were prepared on conductive adhesive films and coated with carbon (BAL-TEC MED 020, Bal Tec AG). The EDX measurements of the both compounds yielded in average compositions of La/Ba/Sr/Si 16:3:5:60 or La/Sr/Si/F 12:10:60:10 (normalized according to the Si content; four measurements on the crystals used for single-crystal X-ray diffraction; the atomic content of N and O was excluded as they are over-determined, due to the limitations of the method). These measurements corroborate the sum formulas of the both compounds obtained from single-crystal structure refinement and MAPLE calculations. Moreover they preclude the presence of other elements than La, Sr, Si, N, O and F/ Ba.

### 2.2.4.7 FTIR Spectroscopy

The IR spectrum of the both compounds was recorded with a Perkin-Elmer BXII spectrometer mounting ATR (attenuated total reflection) technology.

## 2.2.5 References


[1] M. Zeuner, S. Pagano, W. Schnick, *Angew. Chem. Int. Ed.* **2011**, *50*, 7754.

[2] N. Hirosaki, R.-J. Xie, *Appl. Mater. Interfaces* **2011**, *3*, 811.

[3] V. Bachmann, T. Jüstel, A. Meijerink, C. Ronda, P. J. Schmidt, *J. Lumin.* **2006**, *121*, 441.

[4] S. Schmiechen, P. Strobel, C. Hecht, T. Reith, M. Siegert, P.J. Schmidt, P. Huppertz, D. Wiechert, W. Schnick, *Chem. Mater* **2015**, *27*, 1780.

[5] Y. Q. Li, A. C. A. Delsing, G. DeWith, H. T. Hintzen, *Chem. Mater.* **2005**, *17*, 3242.

[6] H. Yamane, H. Morito, *Inorg. Chem.* **2013**, *52*, 5559.

[7] D. Durach, W. Schnick, *Eur. J. Inorg. Chem.* **2015**, 4095.

[8] S. Lupart, M. Zeuner, S. Pagano, W. Schnick, *Eur. J. Inorg. Chem.* **2010**, 2636.

[9] M. Zeuner, S. Pagano, P. Matthes, D. Bichler, D. Johrendt, T. Harmening, R. Pöttgen, W. Schnick, *J. Am. Chem. Soc.* **2009**, *131*, 11242.

[10] Z. A. Gàl, P. M. Mallinson, H. J. Orchard, S. J. Clarke, *Inorg. Chem.* **2004**, *43*, 3998.

[11] T. Schlieper, W. Milius, W. Schnick, *Z. Anorg. Allg. Chem.* **1995**, *621*, 1380.

[12] W. Schnick, *Angew. Chem. Int. Ed. Engl.* **1993**, *32*, 806.

[13] J. A. Kechele, C. Schmolke, S. Lupart, W. Schnick, *Z. Anorg. Allg. Chem.* **2010**, *636*, 176.

[14] W. Schnick, H. Huppertz, R. Lauterbach, *J. Mater Chem.* **1999**, *9*, 289.

[15] M. Zeuner, F. Hintze, W. Schnick, *Chem. Mater.* **2009**, *21*, 336.

[16] W. Grochala, P. Edwards, *Chem. Rev.* **2004**, *104*, 1283.

[17] R. Lauterbach, E. Irran, P. F. Henry, M. T. Weller, W. Schnick, *J. Mater. Chem.* **2000**, *10*, 1357.

[18] F. Liebau, *Structural Chemistry of Silicates*, Springer, Berlin, **1985**.

[19] A. Lieb, W. Schnick, *J. Solid State Chem.* **2005**, *178*, 3323.

[20] C. Schmolke, S. Lupart, W. Schnick, *Solid State Sci.* **2009**, *11*, 305.

[21] R. Lauterbach, W. Schnick, *Z. Anorg. Allg. Chem.* **1998**, *624*, 1154.

[22] T. Schleid, H. M. Bunz, *Z. Anorg. Allg. Chem.* **1999**, *625*, 1377.

[23] A. Akella, D. A. Keszler, *Chem. Mater.* **1995**, *7*, 1299.

[24] R. D. Shannon, *Acta Crystallogr. Sect. A.* **1976**, *32*, 751.

[25] R. Hübenthal, *MAPLE, Programm zur Berechnung des Madelunganteils der Gitterenergie*, **1993**, v. 4.

[26] R. Hoppe, *Angew. Chem. Int. Ed. Engl.* **1970**, *9*, 25.

[27] R. Hoppe, R. Homann, *Z. Anorg. Allg. Chem.* **1970**, *379*, 193.

[28] H. A. Höppe, Doctoral Thesis, University of Munich (LMU), Germany, **2003**.

[29] K. Köllisch, Doctoral Thesis, University of Munich (LMU), Germany, **2001**.

[30] R. Lauterbach, Doctoral Thesis, University of Bayreuth, Germany, **1999**.

[31] P. Cortona, *Phys. Rev.* B **1992**, *46*, 2008.

[32] Z. A. Gal, P. M. Mallinson, H. J. Orchard, S. J. Clarke, *Inorg. Chem.* **2004**, *43*, 3998.

[33] M. Billy, J. C. Labbè, A. Selvaraj, G. Roult, *Mater. Res. Bull.* **1983**, *18*, 921.

[34] W. Klemm, G. Winkelmann, *Z. Anorg. Allg. Chem.* **1956**, *288*, 87.

[35] O. Greis, *J. Solid State Chem.* ***1980***, *34*, 39.

[36] D. Durach, L. Neudert, O. Oeckler, W. Schnick, *Chem. Mater.* **2015**, 27, 4832.

[37] H. Lange, G. Wotting, G. Winter, *Angew. Chem. Int. Ed.* **1991**, *30*, 1579.

[38] B. Gieger, H. Jacobs, C. Hadenfeldt, *Z. Anorg. Allg. Chem.* **1974**, *410*, 104.

[39] G. M. Sheldrick, *SADABS, Multi-Scan Absorption Correction*, Bruker-AXS: WA, **2012**, v. 2.

[40] G. M. Sheldrick, *Acta Crystallogr. Sect. A* **2008**, *64*, 112.

[41] *WINXPOW, Program for powder data handling*, Stoe & Cie GmbH, Darmstadt, Germany, **2007**, v. 2.21.

# 2.3 Non-Condensed (Oxo)nitridosilicates: $La_3[SiN_4]F$ and the Polymorph o-$La_3[SiN_3O]O$

published in: *Eur. J. Inorg. Chem.* **2015**, 4095-4100

authors: Dajana Durach and Wolfgang Schnick

DOI: 10.1002/ejic.201500644



http://onlinelibrary.wiley.com/doi/10.1002/ejic.201500644/abstract

**Abstract.** The isotypic compounds $La_3[SiN_4]F$ and $La_3[SiN_3O]O$ were synthesized in a radio-frequency furnace at 1600 °C. The crystal structures [*Pnma* (no. 62), $Z = 4$; $La_3(SiN_4)F$: $a = 9.970(3)$, $b = 7.697(2)$, $c = 6.897(2)$ Å, $V = 529.3(3)$ Å$^3$; La3(SiON3)O: $a = 9.950(2)$, $b = 7.6160(15)$, $c = 6.9080(14)$ Å, $V = 523.48(18)$ Å$^3$] were elucidated from single-crystal X-ray diffraction data and corroborated by Rietveld refinement, lattice-energy calculations (Madelung part of lattice energy, MAPLE) and Raman/FTIR spectroscopy. Both compounds are homeotypic with $Na_2Pr[GeO_4]OH$ forming a network of vertex-sharing $FLa_6$/$OLa_6$ octahedra, whose voids are filled with non-condensed $SiN_4$/$SiN_3O$ tetrahedra. o-$La_3[SiON_3]O$ is the orthorhombic polymorph of this compound, which probably represents the high-temperature modification, whereas the tetragonal polymorph t-$La_3[SiON_3]O$ represents the low-temperature modification. While the space group of the t-polymorph [*I*4/*mcm* (no. 140)] differs from the new $La_3[SiN_4]F$ and o-$La_3[SiN_3O]O$, the crystal structure contains the same linking pattern.

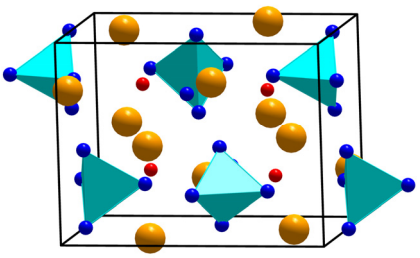

## 2.3.1 Introduction

(Oxo)nitridosilicates are promising compounds, as they show manifold and outstanding materials properties, e.g. luminescence of $Eu^{2+}$- or $Ce^{3+}$-doped samples.[1-5] Consequently, chemists and materials scientists are constantly looking for new (oxo)nitridosilicates. Formally, (oxo)nitridosilicates derive from oxosilicates by substituting all or a part of O by N. The characteristic building blocks of these compounds are $SiN_4$ or $SiN_{4-x}O_x$ tetrahedra, respectively. Apart from this analogy the structural variability of (oxo)nitridosilicates is distinctively greater. In oxosilicate structures containing tetrahedra, O is only known as terminal ($O^{[1]}$) or simply bridging ($O^{[2]}$) atom. N by contrast also facilitates threefold ($N^{[3]}$) and even fourfold ($N^{[4]}$) linkage of neighboring tetrahedral centers in (oxo)nitridosilicates. Moreover, $SiN_4$ tetrahedra can share both common corners as well as common edges,[6] whereas $SiO_4$ tetrahedra, except for fibrous $SiO_2$,[7] whose existence has not yet been proven unequivocally, share exclusively common corners. As a consequence, (oxo)nitridosilicates show a wide range of possible structures. Next to three-dimensional frameworks[8-10] also layer-like structures, like in *EA*$SiN_2$ (*EA* = Sr, Ba),[11] or one-dimensional structures like in $Li_5RE_5Si_4N_{12}$ (*RE* = La, Ce)[12] and $Eu_2SiN_3$[13] have been found. Even non-condensed structures like in $La_3[SiN_3O]O$[14] and the recently published $Ca_4SiN_4$[15] are known from literature. However, (oxo)nitridosilicates have a more pronounced tendency to form highly condensed networks as oxosilicates. Hence the structural variety of less condensed (oxo)nitridosilicates is still minor compared to oxosilicates. Due to the missing kinetic prevention of hydrolysis in less condensed (oxo)nitridosilicates, these compounds are usually air- and moisture-sensitive. A synthetic approach is enabled by the use of low-temperature approaches as well as high-temperature syntheses.[1,12-15]

Here we report on the syntheses and structural characterization of the ortho-(oxo)nitridosilicates $La_3[SiN_4]F$ and $La_3[SiN_3O]O$, which were synthesized by high-temperature approaches using reactive starting materials. The latter compound is the orthorhombic polymorph of $La_3[SiN_3O]O$[14] and is described in the following as o-$La_3[SiN_3O]O$, whereas the former tetragonal polymorph is designated as t-$La_3[SiN_3O]O$.

## 2.3.2 Results and Discussion

### 2.3.2.1 Syntheses

$La_3[SiN_4]F$ and o-$La_3[SiN_3O]O$ were obtained by high-temperature reactions. The driving force of these syntheses is probably the decomposition of $BaH_2$ (decomposition at 675 °C)[16] and its reaction with $LaZ_3$ ($Z$ = F, Br) to reactive lanthanum and $BaZ_2$, whereas the latter one resublimates at the reactor wall of the radio-frequency furnace. The lanthanum reacts with the precursors $Si(NH)_2$,[17] $La(NH_2)_3$[18] and the remaining $LaF_3$ and $La_2O_3$ to a heterogeneous product with red crystals of $La_3[SiN_4]F$ and o-$La_3[SiN_3O]O$, respectively (Figure 1).

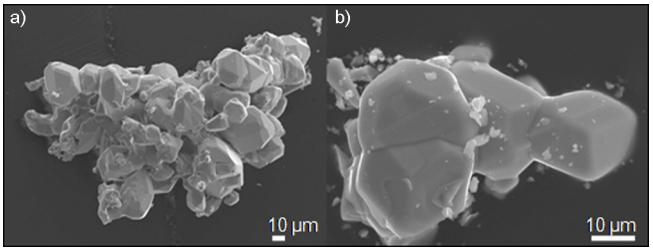


**Figure 1.** SEM images of crystals of $La_3[SiN_4]F$ (a) and o-$La_3[SiN_3O]O$ (b).

Even though Ba is a component of the reaction mixture, and although charge neutrality could be maintained by arbitrary exchange of LaN and BaO units, incorporation of Ba into the products is not very likely as the ionic radius of $Ba^{2+}$ (1.42 Å) is considerably larger than the ionic radius of $La^{3+}$ (1.16 Å), whereas the ionic radii of $N^{3-}$ (1.46 Å) and $O^{2-}$ (1.40 Å) are rather similar.[19] Moreover, the EDX analyses of the products preclude incorporation of Ba. Although $LaBr_3$ was used in the same molar ratio as $LaF_3$, o-$La_3[SiN_3O]O$ was obtained instead of "$La_3[SiN_4]Br$". Consequently, the unit cell probably offers not enough space for an integration of Br, as the ionic radius of $Br^-$ (1.96 Å) is significantly larger than the ionic radius of $F^-$ (1.33 Å), whereas the ionic radius of the latter one and $O^{2-}$ (1.40 Å) are very similar.[19] Another possible reason for the formation of o-$La_3[SiN_3O]O$ rather than "$La_3[SiN_4]Br$" is that the incorporation of O (conceivably originating from $La_2O_3$) is probably favored over the incorporation of Br.

Besides, e.g., $La_5Si_3N_9$,[20] $LiLa_5Si_4N_{10}O$[21] and t-$La_3SiN_3O$,[14] the products $La_3[SiN_4]F$ and o-$La_3[SiN_3O]O$ are further examples for lanthanum (oxo)nitridosilicates with colored crystals. It is unclear whether the color of the crystals originates from defects or color centers.

### 2.3.2.2 Single-Crystal Structure Analyses

The crystal structures of $La_3[SiN_4]F$ and o-$La_3[SiN_3O]O$ were solved and refined in the orthorhombic space group *Pnma* (no. 62). All atoms were refined anisotropically. The crystallographic data are summarized in Table 1, the atomic coordinates and isotropic displacement parameters are given in Table 2. For the anisotropic displacement parameters see Table S1 in the Supporting Information.

**Table 1.** Crystallographic data of the single-crystal structure determination of $La_3[SiN_4]F$ and o-$La_3[SiN_3O]O$.

| Formula | $La_3[SiN_4]F$ | o-$La_3[SiN_3O]O$ |
|---|---|---|
| Crystal system | orthorhombic | |
| Space group | *Pnma* (no. 62) | |
| *a* [Å] | 9.970(3) | 9.950(2) |
| *b* [Å] | 7.697(2) | 7.6160(15) |
| *c* [Å] | 6.897(2) | 6.9080(14) |
| Cell volume [$Å^3$] | 529.3(3) | 523.48(18) |
| Formula units per unit cell | 4 | |
| Density [$gcm^{-3}$] | 6.524 | 6.583 |
| μ [$mm^{-1}$] | 23.912 | 24.172 |
| Temperature [K] | 293(2) | |
| Diffractometer | Bruker D8 Quest (microfocus and graphite monochromator) | |
| Radiation ($\lambda$ [Å]) | Mo-K$\alpha_1$ (0.71073) | |
| *F*(000) | 888 | |
| θ range [°] | $3.592 \leq \theta \leq 27.496$ | $3.591 \leq \theta \leq 26.988$ |
| Total no. of reflections | 10723 [$R_{int} = 0.0275$] | 9577 [$R_{int} = 0.0985$] |
| Independent reflections | 649 | 618 |
| Refined parameters | 49 | |
| Goodness of fit | 1.175 | 1.137 |
| $R_1$ (all data)<br>$R_1$ [$F^2>2\sigma(F^2)$] | 0.0128,<br>0.0119 | 0.0475,<br>0.0278 |
| $wR_2$ (all data)<br>w$R_2$ [$F^2>2\sigma(F^2)$] | 0.0280,<br>0.0277 | 0.0495,<br>0.0466 |
| $\Delta\rho_{max}$, $\Delta\rho_{min}$ [$e \cdot Å^{-3}$] | 0.611/-0.673 | 1.391/-1.516 |

**Table 2.** Atomic coordinates and isotropic displacement parameters [Å$^2$] of $La_3[SiN_4]F$ and o-$La_3[SiN_3O]O$ with standard deviations in parentheses.

| Atom | | *x* | *y* | *z* | $U_{eq}$ | *s.o.f.* |
|---|---|---|---|---|---|---|
| $La_3[SiN_4]F$ | | | | | | |
| La1 | 8*d* | 0.33437(2) | 0.02444(2) | 0.09691(3) | 0.00897(7) | 1 |
| La2 | 4*c* | 0.46756(2) | ¼ | 0.58960(3) | 0.00607(7) | 1 |
| Si1 | 4*c* | 0.10437(12) | ¼ | 0.30930(17) | 0.0050(2) | 1 |
| F1 | 4*c* | 0.2254(3) | ¼ | 0.8389(4) | 0.0182(6) | 1 |
| N1 | 8*d* | 0.0746(3) | 0.0579(3) | 0.1906(4) | 0.0089(5) | 1 |
| N2 | 4*c* | 0.0074(4) | ¼ | 0.5217(6) | 0.0081(7) | 1 |
| N3 | 4*c* | 0.2746(4) | ¼ | 0.3726(5) | 0.0077(7) | 1 |
| o-$La_3[SiN_3O]O$ | | | | | | |
| La1 | 8*d* | 0.32591(5) | 0.02393(6) | 0.09310(8) | 0.00995(14) | 1 |
| La2 | 4*c* | 0.47174(7) | ¼ | 0.59922(12) | 0.00794(17) | 1 |
| Si1 | 4*c* | 0.1000(3) | ¼ | 0.3086(5) | 0.0068(7) | 1 |
| O1 | 4*c* | 0.2223(9) | ¼ | 0.8368(13) | 0.017(2) | 1 |
| N/O2 | 8*d* | 0.0669(7) | ¼ | 0.1916(10) | 0.0103(15) | ¾/¼ |
| N/O3 | 4*c* | 0.0067(10) | ¼ | 0.5169(15) | 0.011(2) | ¾/¼ |
| N/O4 | 4*c* | 0.2707(10) | ¼ | 0.3651(15) | 0.014(2) | ¾/¼ |

Both compounds represent ortho-(oxo)nitridosilicates, which are homeotypic to $Na_2Pr[GeO_4]OH$.[22] They are characterized by non-condensed ($Q^0$-type) $SiN_4$ and $SiN_3O$ tetrahedra, respectively. This is a reason for the air and hydrolysis sensitivity of the compounds. The three crystallographically independent anion positions of the $SiN_3O$ tetrahedra of o-$La_3[SiN_3O]O$ are mixed-occupied with N and O in an atomic ratio of ¾:¼ (Table 2) Next to the $N^{[1]}$/$N,O^{[1]}$ atoms of $La_3[SiN_4]F$/o-$La_3[SiN_3O]O$, which form the tetrahedra, there are isolated $F^{[0]}$/$O^{[0]}$ positions, which are coordinated in a distorted octahedral manner by six La atoms. These $FLa_6$/$OLa_6$ octahedra are interconnected with each other by common vertices, thus a three-dimensional network is formed, whereas the $SiN_4$/$SiN_3O$ tetrahedra are positioned in the voids between the octahedra (Figure 2a, c). The absence of N-H groups was confirmed by Fourier transform infrared (FTIR) and Raman spectroscopy, respectively (Figures S2 and S3 in the Supporting Information). There are two crystallographically independent La sites, which are surrounded by eight and nine (N/F)/(N,O/O) atoms, respectively (Figure 3a).

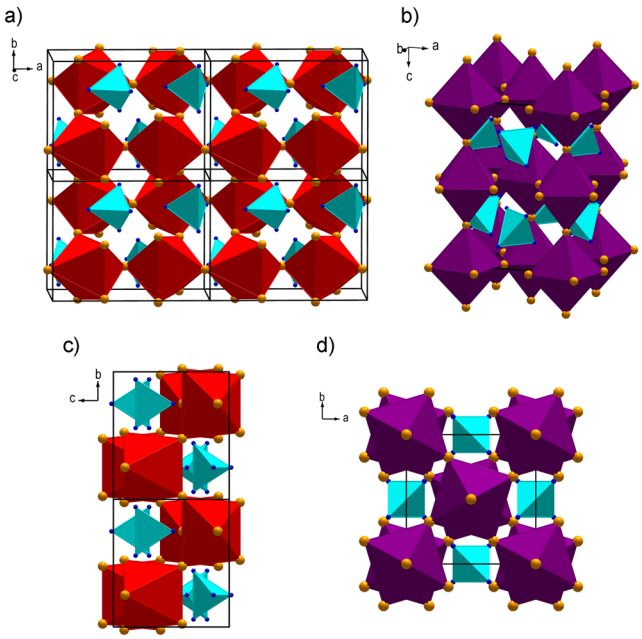


**Figure 2.** (a, c) Structure of $La_3[SiN_4]F$ and o-$La_3[SiN_3O]O$. (b, d) Structure of t-$La_3[SiN_3O]O$. The $SiN_4$/$SiN_3O$ tetrahedra are depicted in turquoise, the $FLa_6$/$OLa_6$ octahedra in red/violet. The blue spheres symbolize the N/N,O and the orange ones the La atoms.

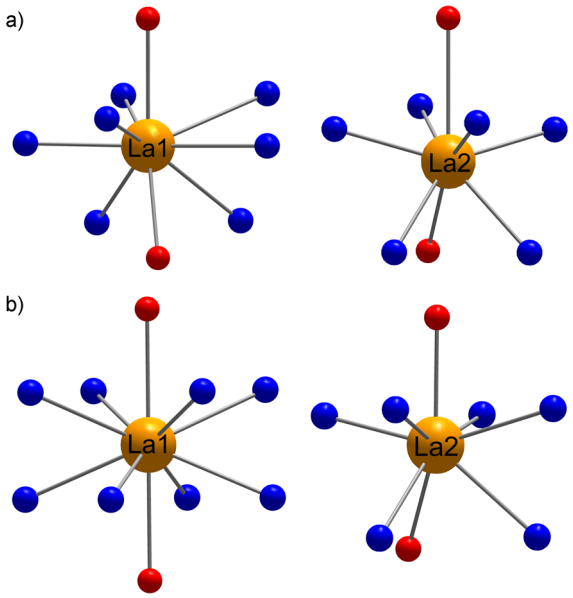


**Figure 3.** (a) Coordination spheres of the lanthanum sites in $La_3[SiN_4]F$ and o-$La_3[SiN_3O]O$ (a) and in t-$La_3[SiN_3O]O$ (b) (red: O/F atoms; blue N/N,O atoms).

Although the t-polymorph of $La_3[SiN_3O]O$ was synthesized with an analogous temperature program as both of the new compounds, it crystallizes in the tetragonal space group *I*4/*mcm* (no. 140) with $a = 6.8224(10)$ and $c = 11.074(2)$ Å. Its structure also consists of a three-dimensional network of $OLa_6$ octahedra, whereas the non-condensed $SiN_3O$ tetrahedra fill the voids of the network. There is only one crystallographically independent anion position of the $SiN_3O$ tetrahedra. This site is mixed occupied with N and O in an atomic ratio of ¾:¼.[14] Compared to the structure of $La_3[SiN_4]F$/o-$La_3[SiN_3O]O$ the octahedra are less distorted (Figure 2a, b). Furthermore, the octahedra are more twisted against each other along [001] than the $FLa_6/OLa_6$ polyhedra in both compounds along [100], and the $SiN_3O$ tetrahedra in t-$La_3[SiN_3O]O$ are congruent to each other, whereas the $SiN_4/SiN_3O$ tetrahedra of $La_3[SiN_4]F$/o-$La_3[SiN_3O]O$ are tilted against each other by 180° along [100] (Figure 2c, d). The t-polymorph also contains two crystallographically independent La sites, which, however, are coordinated by eight and ten (N,O/O) atoms, respectively (Figure 3b).[14]

Due to the structural differences the density of the two polymorphs differs, and as t-$La_3[SiN_3O]O$ has a larger density (6.686 g $cm^{-3}$)[14] than o-$La_3[SiN_3O]O$ (6.583 g $cm^{-3}$) it probably represents the thermodynamically stable product at room temperature. Consequently, the t-polymorph presumably represents the low-temperature and the o-polymorph the high-temperature modification. As there is no simple group/subgroup relation between the two modifications, the phase transition is probably of first order.

The distances Si-N [1.716(3)-1.755(4) Å] and Si-N,O [1.692(7)-1.743(11) Å] of $La_3[SiN_4]F$ and o-$La_3[SiN_3O]O$ are in the typical range for terminal Si-N/N,O bonds; similar values were observed in other (oxo)nitridosilicates, e.g. $La_{16}[Si_8N_{22}][SiON_3]_2$ [Si-N,O 1.689(5)-1.743(8) Å][23] and $CeSi_3N_5$ [Si-N 1.699(7)-1.761(6) Å].[20] The La-N and La-N,O bond lengths are also in good agreement with the interatomic distances in $La_{16}[Si_8N_{22}][SiON_3]_2$ [La-N 2.424(7)-3.191(8) Å; La-N,O 2.399(7)-3.141(8) Å].[23] The La-F and La-O distances agree with those in other lanthanum compounds.[24-26] Moreover, all distances correspond well with the sum of the ionic radii.[19] Rietveld refinement of powder X-ray diffraction data confirmed the structures of $La_3[SiN_4]F$ and o-$La_3[SiN_3O]O$ determined from single-crystal data (Figure 4, Table S2 and Figure S1 in the Supporting Information).

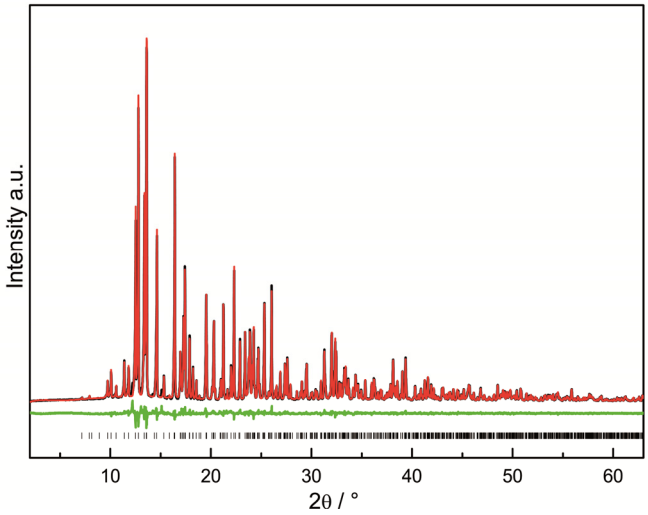


**Figure 4.** Rietveld refinement of the powder diffraction pattern of collected crystals of $La_3[SiN_4]F$. Observed (black line) and calculated (red line) X-ray powder diffraction pattern as well as difference profile (green line). The vertical bars indicate positions of Bragg reflections.

### 2.3.2.3 Lattice-Energy Calculations (MAPLE)

By means of MAPLE (Madelung part of lattice energy) calculations the electrostatic consistency of the crystal structures was proven (Table 3).[19,27-29] Thereby, exclusively electrostatic interactions, which depend on the charge, distance, and the coordination spheres of the constituting ions, were taken into account.

**Table 3.** Partial MAPLE values and MAPLE sums [kJ $mol^{-1}$] for $La_3[SiN_4]F$ and o-$La_3[SiN_3O]O$.[a]

| $La_3[SiN_4]F$ | | Model | o-$La_3[SiN_3O]O$ | | Model |
|---|---|---|---|---|---|
| La1 | 3904 | +1/3 $LaF_3$[24] | La1 | 3937 | +3 LaN[35] |
| La2 | 4474 | +1/3 β-$Si_3N_4$[34] | La2 | 4474 | +$SiO_2$[36] |
| Si1 | 10144 | + 8/3 LaN[35] | Si1 | 9847 | |
| F1 | 548 | | O1 | 1821 | |
| N1 | 4617 | | N/O2 | 4052 | |
| N2 | 4734 | | N/O3 | 4119 | |
| N3 | 4765 | | N/O4 | 4189 | |
| | Σ = 41700 | Σ = 41532<br>Δ = 0.4% | | Σ = 40418 | Σ = 40037<br>Δ = 0.9% |

[a] Typical partial MAPLE values [kJ·$mol^{-1}$]: $La^{3+}$: 3500-5100; $Si^{4+}$: 9000-10200; $(N^{[1]})^{3-}$: 4300-5000 $(N,O^{[1]})^{2.75-}$: 3725-4450; $F^-$: 465-599; $(O^{[0]})^{2-}$: 1871-1913.[24,30-33]

These calculations are especially useful to determine the anion site occupancies as F, N and O could not be distinguished by X-ray diffraction due to their similar X-ray scattering factors. Therefore F, N and O were distributed to the light atom positions on the basis of the crystal structure of t-$La_3[SiN_3O]O$. This distribution was corroborated by lattice energy calculations as the calculated partial MAPLE values of La, Si, N, O and F are in good agreement with reference values,[24,30-33] whereas the values of the mixed $N/O^{[1]}$ sites range between those of $N^{[1]}$ and $O^{[1]}$, as anticipated. As La1 has a higher coordination number and consequently a higher average bond length the partial MAPLE value is smaller than the value of La2.[27,28] This is consistent with the MAPLE values of the homeotypic $Na_2Pr[GeO_4]OH$ as La1 occupies the Na and La2 the Pr position. The minor deviations of 0.4 and 0.9 % between the overall MAPLE values of $La_3[SiN_4]F$ and o-$La_3[SiN_3O]O$ and the formally constituting compounds (1/3 $LaF_3$[24] + 1/3 β-$Si_3N_4$[34] + 8/3 LaN[35] or 3 LaN + $SiO_2$[36]) corroborate the refined crystal structures.

Additionally, the MAPLE calculations exclude the even occupation of all anion positions with N and O or N and F as well as the occupation of the isolated anion position $X^{[0]}$ with N as these options (all in consideration of charge neutrality) lead to MAPLE values, which do not agree with reference values.

## 2.3.3 Conclusion

The crystal structures of $La_3[SiN_4]F$ and o-$La_3[SiN_3O]O$ were successfully determined on the basis of single-crystal X-ray diffraction data. Moreover, the structures were confirmed by Rietveld refinement of powder X-ray diffraction data, MAPLE calculations, FTIR and Raman spectroscopy. The compounds represent ortho-(oxo)nitridosilicates, whereas $La_3[SiN_4]F$ is the second example for an ortho-nitridosilicate,[15] and o-$La_3[SiN_3O]O$ forms a new orthorhombic polymorph next to the tetragonal t-$La_3[SiN_3O]O$.[14] As both polymorphs are synthesized with analogous temperature programs, the mentioned synthesis approach, which is based on reactive starting materials, guides the way to so far unknown lanthanum nitridosilicates. Furthermore, the syntheses of both compounds show that this route leads to less condensed structures as well, next to nitridosilicates with a three-dimensional network as $La_3BaSi_5N_9O_2$.[37] Consequently, this synthesis approach could probably help to discover more high- and even less-condensed nitridosilicates, although this group of compounds has

a stronger tendency to form condensed networks than classical oxosilicates.[1] Moreover, the mentioned synthesis approach enables access to an ortho-nitridosilicate even with a high-temperature route, although $Ca_4SiN_4$[15] was obtained at low temperatures up to 900 °C.

## 2.3.4 Experimental Section

### 2.3.4.1 General

All manipulations were performed under exclusion of moisture and oxygen in either an argon-filled glove box (Unilab, MBraun, Garching; $O_2 < 1$ ppm; $H_2O < 1$ ppm) or in flame-dried glassware of a Schlenk line attached to a vacuum line.

### 2.3.4.2 Synthesis of $La_3[SiN_4]F$

$LaF_3$ (69.8 mg, 0.36 mmol, Sigma-Aldrich, 99.99%), $La(NH_2)_3$ (50.0 mg, 0.27 mmol, synthesized according to Jacobs et al.),[18] $BaH_2$ (63.0 mg, 0.45 mmol, Materion, 99.7%) and $Si(NH)_2$ (18.9 mg, 0.33 mmol, synthesized according to Winter et al.)[17] were thoroughly ground in an agate mortar and filled into a tungsten crucible. Subsequently, the crucible was placed in a water-cooled silica glass reactor of a radio-frequency furnace (Typ AXIO 10/450, max. electrical output 10 kW, Hüttinger Elektronik, Freiburg).[38] Under purified nitrogen, the crucible was heated to 1600 °C within 1 h, maintained at that temperature for 10 h, then cooled to 900 °C within 43.75 h, and finally quenched to room temperature by switching off the furnace. The reaction yielded an inhomogeneous product with air- and hydrolysis-sensitive red crystals of $La_3[SiN_4]F$.

### 2.3.4.3 Synthesis of o-$La_3[SiN_3O]O$

$LaBr_3$ (134.9 mg, 0.36 mmol, Sigma-Aldrich, 99.9%), $La(NH_2)_3$ (50.0 mg, 0.27 mmol, synthesized according to Jacobs et al.),[18] $La_2O_3$ (7.0 mg, 0.021 mmol, Alfa Aesar, 99.99%), $BaH_2$ (62.3 mg, 0.45 mmol, Materion, 99.7%) and $Si(NH)_2$ (12.9 mg, 0.22 mmol, synthesized according to Winter et al.)[17] were thoroughly ground and filled into a tungsten crucible. The crucible was heated in a radio-frequency furnace analogously to the synthesis of $La_3[SiN_4]F$. o-$La_3[SiN_3O]O$ was obtained in form of air- and hydrolysis-sensitive red crystals in a heterogeneous sample.

#### 2.3.4.4 Single-Crystal X-ray Diffraction

Single crystals of $La_3[SiN_4]F$ and o-$La_3[SiN_3O]O$ were isolated from the product under a microscope (glove box), enclosed in glass capillaries and sealed under argon. Single-crystal X-ray diffraction data were collected with a Bruker D8 Quest diffractometer (Mo-$K_\alpha$ radiation, microfocus and graphite monochromator). Absorption corrections of the respective data were done with SADABS.[39] The crystal structures were solved with Direct Methods (SHELXS) and refined by full-matrix least-squares methods (SHELXL).[40] Further details of the crystal structure investigations may be obtained from the Fachinformationszentrum Karlsruhe, 76344 Eggenstein-Leopoldshafen, Germany (fax: +49-7247-808-666; e-mail: crysdata@fiz-karlsruhe.de), on quoting the depository numbers CSD-429558 and -429559.

#### 2.3.4.5 Powder X-ray Diffraction

Powder samples were prepared by pulverizing the products in agate mortars and enclosing them in glass capillaries. For the phase-pure powder sample of $La_3[SiN_4]F$ single crystals were collected under a microscope and processed as described before. Powder-diffraction data were collected with a STOE STADI P diffractometer [Mo-$K_{\alpha1}$ radiation ($\lambda$ = 0.70930 Å), Ge(111) monochromator, MYTHEN 1K detector] in Debye-Scherrer geometry. Simulations of powder diffraction patterns were conducted by using the WinXPOW program package[41] on the basis of the single-crystal structure data. Rietveld refinements were performed by using the TOPAS Academic package.[42]

#### 2.3.4.6 SEM and EDX Spectroscopy

To analyze the chemical composition and the morphology of the obtained crystals, a JEOL JSM 6500F field emission scanning electron microscope (SEM), operated at 12/26 kV, equipped with an Si/Li EDX detector 7418 (Oxford Instruments), was used. In order to ensure electrical conductivity on the sample surfaces, they were prepared on conductive adhesive films and coated with carbon (BAL-TEC MED 020, Bal Tec AG). The EDX analyses of both compounds resulted in average compositions of La/Si/F, 3.0:1.0:0.8 or La/Si, 3.0:1.0 (normalized according to the La content; four measurements on different crystals; the atomic content of N and O were excluded, due to the air and hydrolysis sensitivity of the products). These measurements corroborate the obtained empirical formulas of $La_3[SiN_4]F$

and o-$La_3[SiN_3O]O$ and preclude the presence of other elements than La, Si, N, F and O within the sensitivity range of the method.

#### 2.3.4.7 FTIR and Raman Spectroscopy

The IR spectrum of $La_3[SiN_4]F$ was recorded using a KBr pellet with a Spectrum BX II spectrometer (Perkin-Elmer, Waltham MA, USA) (Figure S2 in the Supporting Information). To obtain the Raman spectrum of a crystal of o-$La_3[SiN_3O]O$ enclosed in a glass capillary, a confocal LabRAM HR UV/Vis (HORIBA Jobin Yvon) Raman microscope (Olympus BX 41) with a SYMPHONY CCD detection system and an He-Ne laser ($\lambda$ = 633 nm) was used (Figure S3 in the Supporting Information).

## 2.3.3 References


[1] M. Zeuner, S. Pagano, W. Schnick, *Angew. Chem. Int. Ed.* **2011**, *50*, 7754.

[2] N. Hirosaki, R.-J. Xie, *Appl. Mater. Interfaces* **2011**, *3*, 811.

[3] V. Bachmann, T. Jüstel, A. Meijerink, C. Ronda, P. J. Schmidt, *J. Lumin.* **2006**, *121*, 441.

[4] Y. Q. Li, A. C. A. Delsing, G. DeWith, H. T. Hintzen, *Chem. Mater.* **2005**, *17*, 3242.

[5] S. Schmiechen, P. Strobel, C. Hecht, T. Reith, M. Siegert, P.J. Schmidt, P. Huppertz, D. Wiechert, W. Schnick, *Chem. Mater* **2015**, *27*, 1780.

[6] W. Schnick, H. Huppertz, *Chem. Eur. J.* **1997**, *3*, 679.

[7] A. Weiss, A. Weiss, *Z. Anorg. Allg. Chem.* **1954**, *276*, 95.

[8] Z. Inoue, M. Mitomo, N. Li, *J. Mater. Sci.* **1980**, *15*, 2915.

[9] T. Schlieper, W. Milius, W. Schnick, *Z. Anorg. Allg. Chem.* **1995**, *621*, 1380.

[10] H. Huppertz, W. Schnick, *Acta Crystallogr. Sect. C* **1997**, *53*, 1751.

[11] Z. A. Gàl, P. M. Mallinson, H. J. Orchard, S. J. Clarke, *Inorg. Chem.* **2004**, *43*, 3998.

[12] S. Lupart, M. Zeuner, S. Pagano, W. Schnick, *Eur. J. Inorg. Chem.* **2010**, 2636.

[13] M. Zeuner, S. Pagano, P. Matthes, D. Bichler, D. Johrendt, T. Harmening, R. Pöttgen, W. Schnick, *J. Am. Chem. Soc.* **2009**, *131*, 11242.

[14] J. A. Kechele, C. Schmolke, S. Lupart, W. Schnick, *Z. Anorg. Allg. Chem.* **2010**, *636*, 176.

[15] H. Yamane, H. Morito, *Inorg. Chem.* **2013**, *52*, 5559.

[16] W. Grochala, P. Edwards, *Chem. Rev.* **2004**, *104*, 1283.

[17] H. Lange, G. Wotting, G. Winter, *Angew. Chem. Int. Ed. Engl.* **1991**, *30*, 1579.

[18] B. Gieger, H. Jacobs, C. Hadenfeldt, *Z. Anorg. Allg. Chem.* **1974**, *410*, 104.

[19] R. D. Shannon, *Acta Crystallogr. Sect. A* **1976**, *32*, 751.

[20] C. Schmolke, D. Bichler, D. Johrendt, W. Schnick, *Solid State Sci.* **2009**, *11*, 389.

[21] S. Lupart, M. Zeuner, S. Pagano, W. Schnick, *Eur. J. Inorg. Chem.* **2010**, 2636.

[22] A. N. Kornev, G. P. Klientova, B. A. Maximov, V. V. Ilyukhin, N. V. Belov, *Dokl. Akad. Nauk SSSR* **1972**, *206*, 1109.

[23] C. Schmolke, S. Lupart, W. Schnick, *Solid State Sci.* **2009**, *11*, 305.

[24] T. Schleid, H. M. Bunz, *Z. Anorg. Allg. Chem.* **1999**, *625*, 1377.

[25] K. Fukuda, T. Iwata, E. Champion, *Powder Diffr.* **2006**, *21*, 300.

[26] H. Lehnert, H. Boysen, P. Dreier, Y. Yu, *Z. Kristallogr.* **2000**, *215*, 145.

[27] R. Hoppe, *Angew. Chem. Int. Ed. Engl.* **1970**, *9*, 25.

[28] R. Hoppe, R. Homann, *Z. Anorg. Allg. Chem.* **1970**, *379*, 193.

[29] R. Hübenthal, *MAPLE, Programm zur Berechnung des Madelunganteils der Gitterenergie*, **1993**, v. 4.

[30] H. A. Höppe, Doctoral Thesis, University of Munich (LMU), Germany, **2003**.

[31] K. Köllisch, Doctoral Thesis, University of Munich (LMU), Germany, **2001**.

[32] R. Lauterbach, Doctoral Thesis, University of Bayreuth, Germany, **1999**.

[33] P. Cortona, *Phys. Rev. B* **1992**, *46*, 2008.

[34] M. Billy, J. C. Labbè, A. Selvaraj, G. Roult, *Mater. Res. Bull.* **1983**, *18*, 921.

[35] W. Klemm, G. Winkelmann, *Z. Anorg. Allg. Chem.* **1956**, *288*, 87.

[36] J. Kim Zajonz, S. Werner, H. Schulz, *Z. Kristallogr.* **1999**, *214*, 324.

[37] D. Durach, L. Neudert, O. Oeckler, W. Schnick, *Chem. Mater.* **2015**, *27*, 4832.

[38] W. Schnick, H. Huppertz, R. Lauterbach, *J. Mater Chem.* **1999**, *9*, 289.

[39] G. M. Sheldrick, *SADABS, Multi-Scan Absorption Correction*, Bruker-AXS: WA, **2012**, v. 2.

[40] G. M. Sheldrick, *Acta Crystallogr., Sect. A* **2008**, *64*, 112.

[41] *WINXPOW, Program for powder data handling*, Stoe & Cie GmbH, Darmstadt, Germany, **2007**, v. 2.21.

[42] A. Coelho, *TOPAS Academic* 2007, Coelho Software, Brisbane, Australia, **2007**.

# 3 Lanthanum (Oxo)nitridosilicates as Phosphor Materials

## 3.1 Introduction

Since the development of efficient light-emitting diodes (LEDs) light stands for far more than just brightness. It helps to define areas, shape rooms, provide energy, influence our moods, improve security and transfer information.[1] Consequently, LEDs already found broad application in several areas. For example, numerous stores have already changed their illumination to LEDs as they help to save energy and to eliminate inventory erosion due to IR and UV damage. The long lifetime of LEDs also decreases the maintenance costs. In the automotive sector, LEDs gain importance since calculations for automotive forward lighting based on different light technologies reveal that a traditional system uses almost five times the power of an LED system. Therefore, an LED system is associated with a smaller $CO_2$ emission than a traditional one.[2] Multichip LEDs for front headlamps can also generate more light from a small package than any other comparable product, thus the design flexibility for headlamps is considerably expanded.[3] Besides, LEDs enable mobile iris scanning. This becomes more and more popular as a means of biometric identification, which makes sensitive applications such as online banking and online shopping significantly safer.[4]

Next to the mentioned examples, there are nowadays numerous further applications for LEDs, but it was a long journey to the development of efficient LEDs, which meet the requirements of the customers. In 1962, *Holonyak* et al. developed the first commercially available LED emitting in the visible spectral region. This diode consisted of a GaAsP semiconductor and showed red emission. In the following years several different semiconductors, like InGaP and GaAlAs, were investigated and allowed for the access to all colors of the visible spectrum.[5] The functional principle of these LEDs is based on electron-hole transitions between different layers of semiconducting materials (p- and n-doped). The color of the emitted light is directly correlated to the band gap energy of the used semiconducting material. As these LEDs show several disadvantages, like low efficiencies, limited current densities and therefore also low brightness, they found no application in general illumination. Moreover, the development of an efficient blue LED proved to be very

difficult, since no suitable semiconductor in the required quality was available. In the 1970s the new crystal growth technique MOVPE (Metalorganic Vapor Phase Epitaxy) arose and enabled *Akasaki* and *Amano* in 1986 to synthesize high quality device-grade GaN, a direct band gap semiconducting material for blue LEDs.[6,7] Challenges associated with the p-doping of GaN could be solved by treating the samples with an electron beam or by thermal annealing. These treatments were investigated and described by *Nakamura*.[8,9] A further crucial step towards the development of efficient LEDs was the growth and p-doping of alloys (AlGaN, InGaN), which are required for the production of heterojunctions. Here, the recombination processes occur more efficiently, as shown by *Akasaki`s* and *Nakamura`s* research groups.[10,11] Since these results pave the way toward *efficient blue light-emitting diodes which has enabled bright and energy-saving white light sources*, the Nobel Prize was awarded to *Isamu Akasaki*, *Hirosho Amano* and *Shuji Nakamura* in 2014.[12]

As soon as efficient blue- to UV-emitting primary LEDs were available, the demand of phosphor-converted (pc-) LEDs arose, since the latter show a highly tunable emission and even enable the emission of white light with high quality, thus they are promising candidates for several applications. The functional principle of pc-LEDs is based on the stimulation of the emission of a down-conversion phosphor material by a primary light source. Thereby, the conversion of light is based on excitation and emission processes of rare earth ions incorporated as dopant in the crystal structure of the host compound.[5] Usually 5*d*→4*f* emission is favored, as shown e.g. by $Eu^{2+}$ or $Ce^{3+}$.[13] The emission process is strongly affected by the host lattice of the dopant, as the 5*d* orbitals of the lanthanides are significantly influenced by its surrounding, in contrast to the 4*f* orbitals which are shielded by the 6*s* and 5*d* orbitals.[14,15] These influences on the emission process of $Eu^{2+}$ and $Ce^{3+}$ are shown in Figure 3.1.1. The energetic position of the 5*d* level depends on the chemical bond between the dopant and the ligands, thus the more covalent the bonding, the more the 5*d* level is lowered in comparison to the free ion (so-called nephelauxetic effect). Additionally, the crystal field around the dopant leads to degeneration of the 5*d* orbitals (crystal field splitting). After excitation of an electron from the 4f ground state to the lowest 5d state, non-radiative relaxation to the lowest energy of the excited state occurs. Consequently, the emission wavelength is higher (red shifted) than the excitation wavelength (Stokes shift).

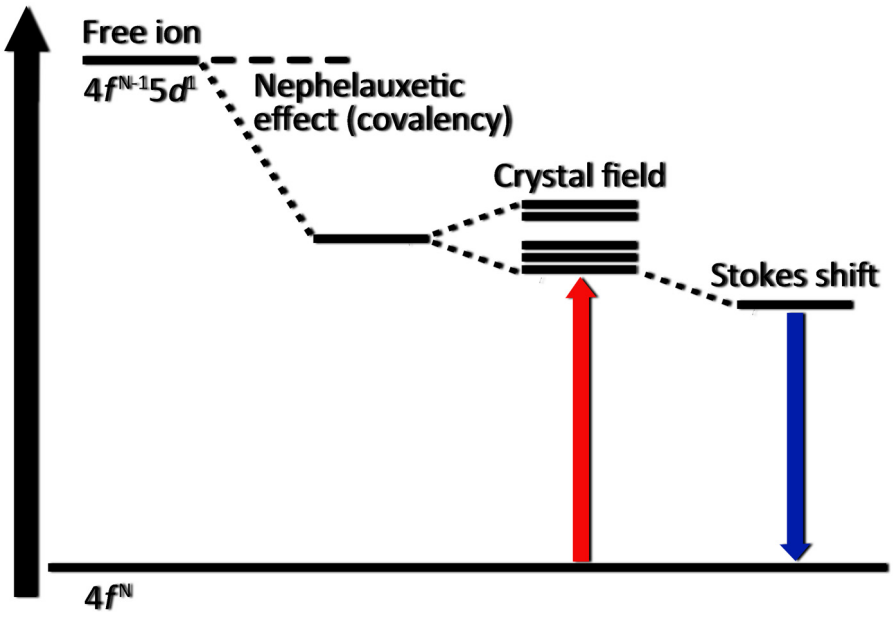


**Figure 3.1.1.** Scheme of excitation and emission processes in $Eu^{2+}$ or $Ce^{3+}$ considering influencing effects like the crystal field around the activator site and the nephelauxetic effect as well as the Stokes shift.

On the basis of several energy level overlaps, the large number of allowed transitions and the significant influence of the coordination sphere of the dopant on the emission $Eu^{2+}$ and $Ce^{3+}$ exhibit a broad band emission. $Eu^{3+}$, by contrast, shows a well-defined line emission of 4*f*→4*f* transitions. As mentioned before, 4*f* orbitals are shielded by 6*s* and 5*d* orbitals, thus the emission of $Eu^{3+}$ is not affected by the host lattice. Since 4*f*→4*f* transitions are partly forbidden, the emission intensity is limited, whereby application in high-power LEDs is not possible, since the high pump rates would cause a saturation of the $Eu^{3+}$ excited state due to the long decay of the *f-f* transition (in the order of ms).[16] However, $Eu^{2+}$ exhibits an intense partly allowed (spin-forbidden, parity-allowed) *f-d* transition and $Ce^{3+}$ a spin- and parity-allowed *f-d* transition. Consequently, their emissions show short decay times ($Eu^{2+}$: in the order of µs; $Ce^{3+}$: ns) thus they are the dopants of choice for phosphor materials applied in high-luminance pc-LEDs. Besides a short decay time, potential phosphor materials have to meet several further requirements.[17] A high chemical and thermal stability are indispensable for the product lifetime and during the manufacturing. Additionally, high quantum efficiencies (QE) close to 100% are essential for a nearly non-dissipative light conversion. As modern blue-emitting high-power LEDs are usually operated at currents of

about 350 mA, which results in temperatures up to 150 °C at the chips surfaces due to ohmic resistance, a weak thermal quenching of the applied phosphor materials is crucial.
Nowadays, garnet-type compounds, e.g. $Y_3Al_5O_{12}:Ce^{3+}$ (YAG:$Ce^{3+}$),[18,19] as well as nitridosilicates, e.g. $(Ba,Sr)_2Si_5N_8:Eu^{2+}$[20-23] and $(La,Ca)_3Si_6N_{11}:Ce^{3+}$[24] have been established as phosphor materials for pc-LEDs. Therefore, luminescence properties of (oxo)nitridosilicates in general and the potential of lanthanum (oxo)nitridosilicates as phosphor material in particular are discussed more detailed in the following chapter. Additionally, two novel lanthanum oxonitridosilicates with outstanding luminescence properties are presented and compared to the luminescence properties of YAG:$Ce^{3+}$.

## References


[1] http://www.osram-os.com/osram_os/en/company/vision--mission/index.jsp, visited on 23th December **2015**.

[2] http://www.osram-os.com/osram_os/en/company/forward-thinking/environment-protection/index.jsp, visited on 23th December **2015**.

[3] http://www.osram-os.com/osram_os/en/press/press-releases/led-for-automotive,-consumer,-industry/2015/pace-award-2015-goes-to-osram-opto-semiconductors/index.jsp, visited on 23th December **2015**.

[4] http://www.osram-os.com/osram_os/en/news--events/spotlights/success-stories/2015 /research-award-for-osram-ired/index.jsp, visited on 23th December **2015**.

[5] C. Ronda, *Luminescence*, Wiley-VCH Verlag, Weinheim, Germany, **2008**.

[6] H. M. Manasevit, F. M. Erdman, W. I. Simpson, *J. Electrochem. Soc.* **1971**, *118*, 1864.

[7] H. Amano, N. Sawaki, I. Akasaki, Y. Toyoda, *Appl. Phys. Lett.* **1986**, *48*, 353.

[8] S. Nakamura, N. Iwasa, M. Senoh, T. Mukai, *Jpn. J. Appl. Phys.* **1992**, *31*, 1258.

[9] S. Nakamura, T. Mukai, M. Senoh, N. Iwasa, *Jpn. J. Appl. Phys.* **1992**, *31*, L139.

[10] H. Murakami, T. Asahi, H. Amano, K. Hiramatsu, N. Sawaki, I. Akasaki, *J. Crystal Growth* **1991**, *115*, 648.

[11] S. Nakamura, T. Mukai, *Jpn. J. Appl. Phys.* **1992**, *31*, L1457.

[12] J. Heber, *Nat. Phys.* **2014**, *10*, 791.

[13] H. A. Höppe, *Angew. Chem. Int. Ed.* **2009**, *48*, 3572.

[14] G. Blasse, B. Grabmaier, *Luminescent Materials*, Springer, Berlin, Germany, **1994**.

[15] S. Shionoya, W. M. Yen, H. Yamamoto, *Phosphor Handbook*; CRC Press: Boca Raton, **2006**.

[16] M. R. Krames, G. O. Müller, R. B. Müller-Mach, H.-H. Bechtel, P. J. Schmidt, *PCT Int. Appl.* WO 2010131133, A1, **2010**.

[17] G. Blasse, A. Bril, *Appl. Phys. Lett.* **1967**, *11*, 53.

[18] A. A. Setlur, *Electrochem. Soc. Interface* **2009**, *18*, 32.

[19] D. J. Robbins, *J. Electrochem. Soc.* **1979**, *126*, 1550.

[20] R. Müller-Mach, G. Müller, M. R. Krames, H. A. Höppe, F. Stadler, W. Schnick, T. Jüstel, P. Schmidt, *Phys. Status Solidi A* **2005**, *202*, 1727.

[21] Y. Q. Li, J. E. J. van Steen, J. W. H. van Krevel, G. Botty, A. C. A. Delsing, F. J. DiSalvo, G. de With, H. T. Hintzen, *J. Alloys Compd*. **2006**, *417*, 273.

[22] M. Zeuner, S. Pagano, W. Schnick, *Angew. Chem. Int. Ed.* **2011**, *50*, 7754.

[23] H. A. Höppe, H. Lutz, P. Morys, W. Schnick, A. Seilmeier, *J. Phys. Chem. Solids*, **2000**, *61*, 2001.

[24] T. Suehiro, N. Hirosaki, R.-J. Xie, *Appl. Mater. Interfaces* **2011**, *3*, 811.

# 3.2 $La_5CaSi_{12}N_{17}O_7\square_2$ and $La_{3.7}Ca_{2.3}Si_{12}N_{11.7}O_{14.3}$: Two Promising Host Lattices for $Eu^{2+}$- and $Ce^{3+}$-doping Towards Phosphor Materials with Highly Tunable Luminescence

patent in progress: Dajana Durach, Peter J. Schmidt and Wolfgang Schnick

**Abstract.** $La_5CaSi_{12}N_{17}O_7\square_2$ and $La_{3.7}Ca_{2.3}Si_{12}N_{11.7}O_{14.3}$ were synthesized by high-temperature reactions (1600 / 1400 °C) in a radio-frequency furnace. The crystal structures [*P*4*bm* (no. 100), $Z = 1$, $a = 10.1505(3)$ / $10.0881(4)$ Å $c = 4.8806(2)$/ $4.9234(2)$ Å, $V = 502.86(4)$ / $501.05(4)$ Å$^3$] were solved and refined on basis of single-crystal X-ray diffraction data. Accuracy of the structure determinations were confirmed by Rietveld refinements. FTIR spectroscopy proves the absence of N-H bonds. $La_5CaSi_{12}N_{17}O_7\square_2$ and $La_{3.7}Ca_{2.3}Si_{12}N_{11.7}O_{14.3}$ are built up by a three-dimensional network with *vierer* and *achter* rings of all side vertex sharing $Si(N,O)_4$ tetrahedra. They are homeotypic to $La_3Si_6N_{11}$ ($Z = 2$) as they are characterized by the same network but contain an additional isolated O site. Moreover, both compounds show intriguing luminescent properties upon doping with $Ce^{3+}$ or $Eu^{2+}$ or being codoped with $Ce^{3+}$ and $Eu^{2+}$. Consequently, the luminescence of doped $La_5CaSi_{12}N_{17}O_7\square_2$ and $La_{3.7}Ca_{2.3}Si_{12}N_{11.7}O_{14.3}$ can be easily tuned, thus both are promising candidates for application in phosphor-converted pc-LEDs.

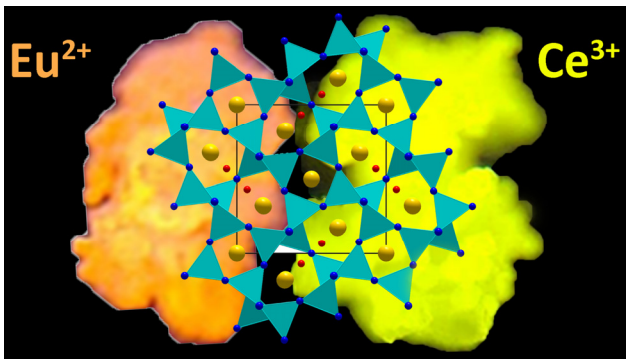

## 3.2.1 Introduction

The invention of efficient blue light-emitting diodes (LEDs) has paved the way for the development of energy-saving white phosphor-converted pc-LEDs with high performance.[1] Since pc-LEDs show significant advantages e. g. long lifetime, small size, low heat build-up, environmental compatibility and high efficiency, they already found broad application, for example in industry and general lighting and were additionally used as design elements e.g. in living rooms, offices or cars. Consequently, they convince as pioneering light source.[2-5] Currently, $Y_3Al_5O_{12}:Ce^{3+}$ ($YAG:Ce^{3+}$) has been established as yellow-emitting phosphor for white-light pc-LEDs. It shows excellent thermal and chemical stability and highly efficient luminescence. Moreover, its emission can be easily shifted to different emission maxima by substitution of the cation sites with e.g. $Gd^{3+}$. However, 1pc-LEDs (LEDs based on a single phosphor approach) with $YAG:Ce^{3+}$ as phosphor yielded only cool-white light.[6,7] To achieve warm-white light, which is, due to its relaxing effect, commonly used for general lighting, a multi-phosphor approach is necessary, which e.g. combines $YAG:Ce^{3+}$ with the red emitting phosphor $(Ca,Sr)AlSiN_3:Eu^{2+}$.[8,9] The latter combines the compound classes of nitridosilicates and nitridoaluminates, which turned out to be excellent host lattices for doping with $Eu^{2+}$ or $Ce^{3+}$, as they are frequently chemically and thermally inert, due to their highly cross-linked nitridic network structures. Additionally, phosphor materials of these compound classes usually show a red-shifted photoluminescence, since they have partially covalent bonds between the activator (dopant) and the N (nephelauxetic effect). Owing to these properties $Eu^{2+}$-doped nitridosilicates and nitridoaluminates like $(Ba,Sr)_2Si_5N_8:Eu^{2+}$ and $Sr[LiAl_3N_4]:Eu^{2+}$ are applied as red emitting component in commercially available warm-white pc-LEDs.[10-15] Furthermore, $Ce^{3+}$-doped nitridosilicates are auspicious candidates for phosphors in warm-white 1pc-LEDs, as their emission is red shifted, due to the nephelauxetic effect. In this context the promising phosphor $(La,Ca)_3Si_6N_{11}:Ce^{3+}$ can be mentioned. This material enables the fabrication of 1pc-LEDs with good thermal stability, emitting in the 2600-3800 K color temperature range.[16] But as the requirements regarding new solid-state lighting technologies and devices still increase, the investigation of new nitridosilicates with promising luminescent properties is continuously spurred.

In this contribution we report on the investigation and properties of the two novel (oxo)nitridosilicate oxides $La_5CaSi_{12}N_{17}O_7\square_2$ and $La_{3.7}Ca_{2.3}Si_{12}N_{11.7}O_{14.3}$, which derive from

$La_3Si_6N_{11}$ ($Z = 2$)[17] and exhibit promising luminescence by being doped with $Ce^{3+}$or $Eu^{2+}$, or being codoped with $Ce^{3+}$ and $Eu^{2+}$.

## 3.2.2 Experimental Section

### 3.2.2.1 Syntheses

All synthesis steps were performed under exclusion of moisture and oxygen in either an argon-filled glove box (Unilab, MBraun, Garching; $O_2 < 1$ ppm; $H_2O < 1$ ppm) or in flame-dried glassware on a Schlenk line attached to a vacuum line. For the synthesis of $La_5CaSi_{12}N_{17}O_7\square_2$, 0.10 mmol (23.2 mg) $LaF_3$ (Sigma-Aldrich, 99.99%) 0.11 mmol (20.1 mg) $La(NH_2)_3$,[18] 0.48 mmol (20.0 mg) $CaH_2$ (Materion, 99.7%) and 0.62 mmol (35.6 mg) of "$Si(NH)_2$"[19] were thoroughly ground in an agate mortar and filled into a tungsten crucible. Then the crucible was placed in a water-cooled silica glass reactor of a radio-frequency furnace (type AXIO 10/450, maximal electrical output 10 kW, Hüttinger Elektronik, Freiburg)[20] heated under purified $N_2$-atmosphere to 1600 °C within 1 h, maintained at that temperature for 10 h, then cooled to 900 °C in 44 h, and finally quenched to room temperature by switching off the furnace. The resulting product consists of colorless crystals of $La_5CaSi_{12}N_{17}O_7\square_2$. Addition of $CeF_3$ as dopant (1.2 mol% Ce (0.003 mmol, 0.5 mg); Alfa Aesar, 99.99%) to the starting materials yielded yellow crystals of $La_5CaSi_{12}N_{17}O_7\square_2$:$Ce^{3+}$, which show intensive yellow luminescence under irradiation with blue light. Orange crystals of $La_5CaSi_{12}N_{17}O_7\square_2$:$Eu^{2+}$ could be obtained by using $EuF_3$ as dopant (4.3 mol% Eu (1.9 mg, 0.009 mmol) Sigma Aldrich, 99,99%). These crystals exhibit orange luminescence under excitation with blue light. The doped and nondoped compounds show high oxygen and hydrolysis stability as contact with air and water over several hours does not lead to a decomposition of the crystals.

To obtain crystals of $La_{3.7}Ca_{2.3}Si_{12}N_{11.7}O_{14.3}$, 0.10 mmol (23.2 mg) $LaCl_3$ (Alfa Aesar, 99.99%), 0.48 mmol (20.1 mg) $CaH_2$ (Materion, 99.7%) and 0.24 mmol (100.0 mg) of "$Si_2(NH)_3 \cdot 6NH_4Cl$"[21] were mixed in an agate mortar and filled into a tungsten crucible. Subsequently, the crucible was heated in a radio-frequency furnace under $N_2$-atmosphere to 900 °C within 5 min, then heated to 1400 °C within 4 h and finally quenched to room temperature by switching off the furnace. The reaction yielded an inhomogeneous powder of colorless, air and hydrolysis sensitive crystals next to colorless crystals of

$La_{3.7}Ca_{2.3}Si_{12}N_{11.7}O_{14.3}$, which in contrast exhibit high air and water stability. To decompose the hydrolysis sensitive byproducts the sample was washed with $H_2O$. Addition of $CeF_3$ (2.1 mol% Ce (002 mmol, 0.4 mg) Alfa Aesar, 99.99%) or $EuF_3$ (2.0 mol% (0.002 mmol, 0.4 mg) Sigma Aldrich, 99,99%) as dopant to the reaction mixture leads to yellow crystals of $La_{3.7}Ca_{2.3}Si_{12}N_{11.7}O_{14.3}:Ce^{3+}$ or orange crystals of $La_{3.7}Ca_{2.3}Si_{12}N_{11.7}O_{14.3}:Eu^{2+}$, respectively, whereas the air and hydrolysis sensitive product stays colorless. The orange crystals exhibit orange luminescence under irradiation with blue light while the yellow crystals show luminescence in the yellow spectral range. The colorless phase, in contrast, reveals no luminescence properties.

### 3.2.2.2 Single-Crystal X-ray Diffraction

Single crystals of $La_5CaSi_{12}N_{17}O_7\square_2:Ce^{3+}$ and $La_{3.7}Ca_{2.3}Si_{12}N_{11.7}O_{14.3}:Ce^{3+}$ were mounted on Kapton foil sample holders (micromount, MiTeGen, Ithaca). Subsequently, X-ray diffraction data were collected with a Bruker D8 Quest diffractometer (Mo-$K_\alpha$ radiation, microfocus and Goebel mirror optic) and a D8 Venture diffractometer (Mo-$K_\alpha$ radiation, microfocus rotating anode and Goebel mirror optic), respectively. The data were corrected for absorption effects using the multiscan method (SADABS).[22] The crystal structures were solved using direct methods (SHELXS) and refined by full matrix least-squares methods (SHELXL).[23]

### 3.2.2.3 Electron Microscopy

For scanning electron microscopy (SEM) as well as for energy-dispersive X-ray (EDS) spectroscopy a JEOL JSM, equipped with a Si/Li EDS detector 7418 (Oxford Instruments) was used. EDS spectra were collected with an accelerating voltage of 15 kV and 12 kV, respectively. Preparation on conductive adhesive films and coating with carbon (BAL-TEC MED 020, Bal Tec AG) ensure the electrical conductivity of the sample surfaces.

### 3.2.2.4 Powder X-ray Diffraction

Powder diffraction data were collected with a STOE STADI P diffractometer (Stoe & Cie, Darmstadt) in Debye-Scherrer geometry (Mo-K$\alpha_1$ radiation, $\lambda = 0.70930$ Å, Ge(111) monochromator, MYTHEN 1K detector). Rietveld refinement was carried out using TOPAS-Academic.[24]

#### 3.2.2.5 UV-Vis Spectroscopy

Reflectance spectra were recorded with a JASCO V-650 UV/Vis spectrophotometer with a deuterium and a halogen lamp (Czerny-Turner monochromator with 1200 lines/mm concave grating, photomultiplier tube detector). The measurements were carried out between 200 nm and 800 nm with 1 nm step size. The band gap of $La_5CaSi_{12}N_{17}O_7\square_2$ was derived from acquired data by drawing two line tangents to the slope of the reflectance curve. The point of intersection of the tangents was estimated as the value of the band gap.

#### 3.2.2.6 Luminescence

Luminescence properties of microcrystalline bulk samples in PTFE holders were investigated using an in-house built system based on a 5.3'' integrating sphere and a spectrofluorimeter equipped with a 150 W Xe lamp, two 500 mm Czerny-Turner monochromators, 1800 1/mm lattices, and 250/500 nm lamps with a spectral range from 230 to 820 nm. Excitation wavelength was chosen to 440 nm. The emission spectra were measured between 460 nm and 800 nm with 1 nm step size. For color point calculations the same spectral range was used. Excitation spectra were measured between 350 nm and 530 nm with 2 nm step size. Comparison of the integrated emission intensities and absorption at excitation wavelength with standard materials ($BaSO_4$, Merck p.a.; commercial SCASN:Eu, Mitsubishi Chemical) yielded the internal quantum efficiencies of samples. Thermal quenching of the samples was investigated in a temperature range from room temperature to 323 °C (step size 25 °C) with an AvaSpec-2048 Spectrometer. Excitation wavelength was chosen to 450 nm.

#### 3.2.2.6 FTIR Spectroscopy

The infrared spectra of the samples were recorded with a Perkin Elmer BXII spectrometer mounting ATR (attenuated total reflection) technology.

### 3.2.3 Results and Discussion

#### 3.2.3.1 Syntheses and Chemical Analyses

Both syntheses are based on reactive precursors. To obtain $La_5CaSi_{12}N_{17}O_7\square_2$, $La(NH_2)_3$ and "$Si(NH)_2$" were used as starting materials, which recently have established as promising precursors for the syntheses of novel Lanthanum (oxo)nitridosilicates.[25-27] Moreover, the

use of "$Si_2(NH)_3 \cdot 6\,NH_4Cl$", which was used as reactant for the synthesis of $La_{3.7}Ca_{2.3}Si_{12}N_{11.7}O_{14.3}$, also seems to offer an auspicious route to novel (oxo)nitridosilicates, since it provides another stoichiometric proportion of Si and N and another oxidation state of Si as the common precursors $Si_3N_4$ and "$Si(NH)_2$".[28] Contaminated commercially acquired starting materials are probably the source of the incorporated O of both compounds. SEM-EDS measurements yielded an average composition of La/Ca/Si/Ce = 5.0:1.9:12.2:0 ($La_5CaSi_{12}N_{17}O_7\square_2$:$Ce^{3+}$) and of La/Ca/Si/Ce = 3.7:2.9:11.1:0.2 ($La_{3.7}Ca_{2.3}Si_{12}N_{11.7}O_{14.3}$:$Ce^{3+}$) (normalized according to the La content; six point measurements at different positions; the atomic content of N and O was excluded as they are under-determined, due to the limitations of the method). Consequently, they confirm the sum formulas obtained from single-crystal structure refinements. Although the EDS measurements did only detect the Ce-content of the latter compound the presence of Ce in both samples is proven unequivocally by luminescence measurements. The morphology of the samples is depicted in Figure 1. FTIR spectroscopy corroborated the absence of N-H and O-H groups (Figure S1 in the Supporting Information). Thus, the combination of EDS measurements and FTIR spectroscopy prove the absence of any other elements than La, Ca, Si, N and O.

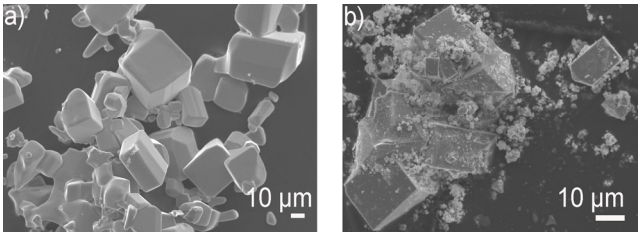


**Figure 1.** SEM images of (a) crystals of $La_5CaSi_{12}N_{17}O_7\square_2$:$Ce^{3+}$ and (b) crystals of $La_{3.7}Ca_{2.3}Si_{12}N_{11.7}O_{14.3}$:$Ce^{3+}$ covered with the amorphous byproduct.

### 3.2.3.2 Single-Crystal Structure Analyses

The crystal structures of $La_5CaSi_{12}N_{17}O_7\square_2$:$Ce^{3+}$ and $La_{3.7}Ca_{2.3}Si_{12}N_{11.7}O_{14.3}$:$Ce^{3+}$ were solved and refined in the tetragonal space group *P4bm* (no. 100). The small amount of $Ce^{3+}$ was neglected in the refinement of the crystal structures because of its insignificant contribution to the scattering density. Inversion twinning had to be taken into account. All atoms were refined anisotropically. The crystallographic details are given in Table 1.

**Table 1.** Crystallographic data of the single-crystal structure determination of $La_5CaSi_{12}N_{17}O_7\square_2$ and $La_{3.7}Ca_{2.3}Si_{12}N_{11.7}O_{14.3}$.

| parameter | comment | comment |
|---|---|---|
| formula | $La_5CaSi_{12}N_{17}O_7\square_2$ | $La_{3.7}Ca_{2.3}Si_{12}N_{11.7}O_{14.3}$ |
| crystal system | tetragonal | |
| space group | *P*4*bm* (no. 100) | |
| lattice parameters/Å | *a* = 10.1505(3) *c* = 4.8806(2) | *a* = 10.0881(4) *c* = 4.9234(2) |
| cell volume/$Å^3$ | 502.86(4) | 501.05(4) |
| formula units per unit cell | 1 | |
| density/$g\cdot cm^{-3}$ | 4.695 | 4.427 |
| $\mu/mm^{-1}$ | 11.449 | 9.153 |
| T/K | 293(2) | |
| diffractometer | Bruker D8 Quest | Bruker D8 Venture |
| radiation/Å | Mo-*Kα* (*λ* = 0.71073) | |
| F(000) | 648 | 621 |
| θ range/deg | $2.838 \le \vartheta \le 27.479$ | $4.139 \le \vartheta \le 27.444$ |
| independent reflections | 631 [$R_{int}$ = 0.0459] | 625 [$R_{int}$ = 0.0235] |
| refined parameters | 62 | |
| twin ratio | 0.03(4)/0.97 | 0.01(4)/0.99 |
| goodness of fit | 1.137 | 1.169 |
| *R*1 (all data / for $F^2 > 2\sigma(F^2)$) | 0.0180/0.0161 | 0.0178/0.0174 |
| *wR*2 (all data / for $F^2 > 2\sigma(F^2)$) | 0.0365/0.0362 | 0.0460/0.0457 |
| $\Delta\rho_{max}$ , $\Delta\rho_{min}$ / $e\cdot Å^{-3}$ | 0.780, -0.687 | 0.933, -0.664 |

Table S1 shows the atomic coordinates and isotropic displacement parameters and table S2 the anisotropic displacement parameters (both in the Supporting Information).

The respective site occupation factors of the heavy atom sites were refined freely to determine their occupation with La and Ca, respectively. Afterwards the refined site occupation factors were fixed to preserve charge neutrality (Table S1 in the Supporting Information). The assignment of N and O was based on Paulings'[29] rule and charge neutrality.

$La_5CaSi_{12}N_{17}O_7\square_2$ and $La_{3.7}Ca_{2.3}Si_{12}N_{11.7}O_{14.3}$ are characterized by a three-dimensional network of all side vertex sharing ($Q^4$-type) $Si(N,O)_4$ tetrahedra, consisting of $(N,O)^{[2]}$ and $N^{[3]}$ atoms ($X^{[2]}/X^{[3]}$: interconnection of two/three tetrahedra) (Figure 2a). This leads to a degree of condensation κ = n(Si):n(N,O) = 6/11. The $Si(N,O)_4$ tetrahedra are condensed to *vierer* and

*achter* rings.[30,31] Theses rings are interconnected via common edges, thus planes in [110] were formed. The planes are interlinked along [001] by units of two vertex sharing $Si(N,O)_4$ tetrahedra (Figure 2b, c). Next to the $(N,O)^{[2]}$ and $N^{[3]}$ atoms, there is one isolated $O^{[0]}$ site, which is coordinated by two heavy atom sites.[32] $La_5CaSi_{12}N_{17}O_7\square_2$ contains a half-occupied $O^{[0]}$ position and $La_{3.7}Ca_{2.3}Si_{12}N_{11.7}O_{14.3}$ a fully-occupied $O^{[0]}$ position.

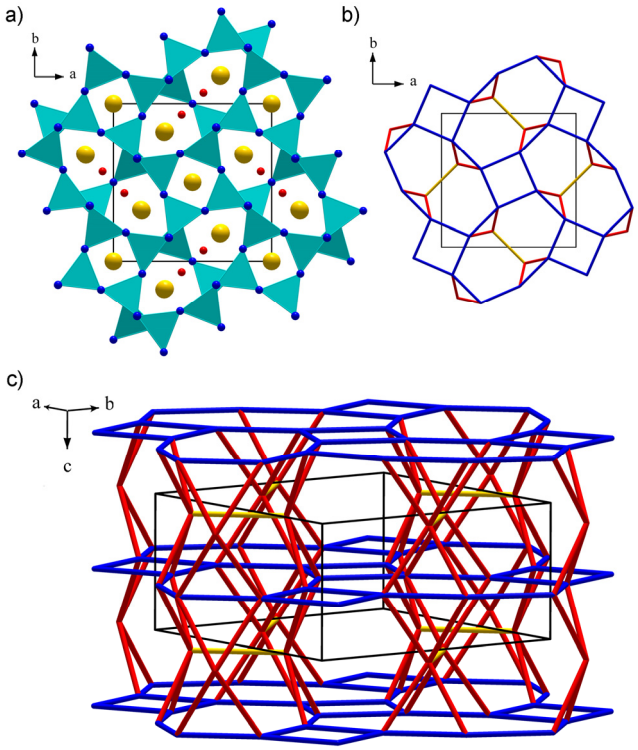


**Figure 2.** (a) Crystal structure of $La_5CaSi_{12}N_{17}O_7\square_2$ and $La_{3.7}Ca_{2.3}Si_{12}N_{11.7}O_{14.3}$ in projection along [001] with $Si(N,O)_4$ tetrahedra (turquoise), N/(N,O) atoms (blue), O atoms (red) and La/(La,Ca) atoms (yellow); (b,c) topological representation of the structure, *achter* and *vierer* rings are represented by blue and units of two vertex sharing $Si(N,O)_4$ tetrahedra by yellow lines. Due to the presence of $N^{[3]}$ atoms only each blue and yellow lines represents a Si-N-Si bond; unit cell shown in black.

$La_3Si_6N_{11}$ ($Z$ = 2) is characterized by the same three-dimensional network, but with respect to the missing $O^{[0]}$ position both compounds are homeotypic to $La_3Si_6N_{11}$.[17]

$La_5CaSi_{12}N_{17}O_7\square_2$ and $La_{3.7}Ca_{2.3}Si_{12}N_{11.7}O_{14.3}$ exhibit two crystallographically independent heavy-atom sites. La1/(La,Ca1) is coordinated by eight (N,O) atoms in a slightly distorted quadratic antiprism arrangement (Table S1 in the Supporting Information, Figure 3a). The second heavy atom site (La,Ca2A/La2B)/(La,Ca2A/La,Ca2B) can be described with a split

position, which is surrounded by eight and nine N/(N,O) atoms, respectively (Table S1 in the Supporting Information, Figure 3b).

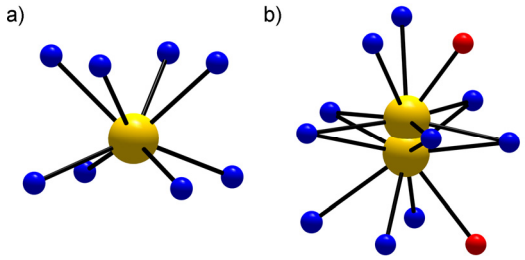


**Figure 3.** (a) Coordination spheres of the heavy atom sites in $La_5CaSi_{12}N_{17}O_7\square_2$ and $La_{3.7}Ca_{2.3}Si_{12}N_{11.7}O_{14.3}$ (a) X1; (b) (La,Ca)2A/X2B ($La_5CaSi_{12}N_{17}O_7\square_2$: X = La; $La_{3.7}Ca_{2.3}Si_{12}N_{11.7}O_{14.3}$: X = (La,Ca); yellow: La and (La,Ca) atoms; red: O atoms; blue N/(N,O) atoms).

The bond lengths of Si-N [1.766(7)-1.788(4) Å] and Si-N,O [1.698(2)-1.739(5) Å] are in good agreement with comparable compounds, such as $Sr_2Si_5N_8$ [Si-N: 1.653(9)-1.786(5) Å][33] $Ca_2Si_5N_8$ [Si-N: Å][34] and $La_{16}[Si_8N_{22}][SiON_3]_2$ [Si-N,O: 1.689(5)-1.743(8) Å].[35] The La-O [2.353(18) Å], La-N,O [2.593(11)-2.791(12) Å], La,Ca-O [2.363(10)-2.751(6) Å], La,Ca-N [2.892(7)-2.926(7) Å] and La,Ca-N,O [2.557(5)-2.847(5) Å] distances correspond to those in other La and Ca compounds.[19,20,36-38] Additionally, all distances are in good agreement with the sum of the ionic radii.[39] In order to determine the bulk phase composition of the samples as well as the accuracy of the structure elucidation from single-crystal X-ray diffraction Rietveld refinements of X-ray powder diffraction data have been carried out (Figure S2, S3 and Table S3 in the Supporting Information). They show that $La_5CaSi_{12}N_{17}O_7\square_2$ was synthesized without any significant byproducts and that the powder diffractogram of the sample containing $La_{3.7}Ca_{2.3}Si_{12}N_{11.7}O_{14.3}$ exhibits only a few weak reflections which, however, cannot be ascribed to the target phase.

### 3.2.3.3 UV-Vis Spectroscopy

The optical band gap of both compounds was, owing to the amorphous byproduct of the sample containing $La_{3.7}Ca_{2.3}Si_{12}N_{11.7}O_{14.3}$ (see Syntheses), exemplarily determined by means of solid-state UV-Vis spectroscopy on the nondoped sample of $La_5CaSi_{12}N_{17}O_7\square_2$ (Figure 4). Due to the absorption of the host lattice the reflectance spectra show a broad absorption band around 275 nm, corresponding to the white body color. Accordingly, the band gap was estimated to be ~4.3 eV.

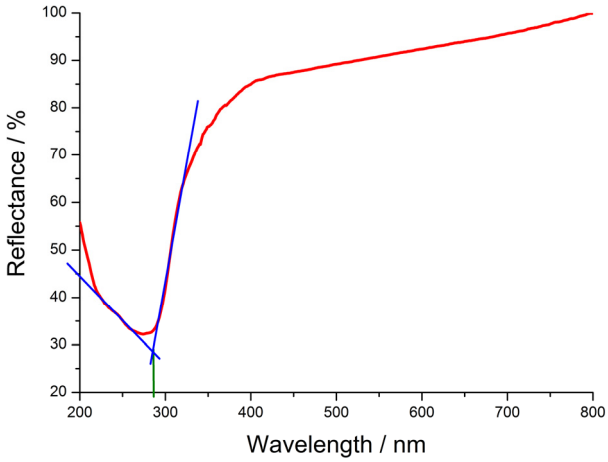


**Figure 4.** UV-Vis reflectance spectra of nondoped $La_5CaSi_{12}N_{17}O_7\square_2$ with plotted tangents to the slope of the reflectance curve (blue). The point of intersection of the tangents is marked by a green line.

### 3.2.3.4 Luminescence

Luminescence measurements of $Eu^{2+}$, $Ce^{3+}$ as well as of $Eu^{2+}$ and $Ce^{3+}$ codoped samples of $La_5CaSi_{12}N_{17}O_7\square_2$ and $La_{3.7}Ca_{2.3}Si_{12}N_{11.7}O_{14.3}$, respectively, were performed on thick bed powder material.

Excitation of $Ce^{3+}$-doped $La_5CaSi_{12}N_{17}O_7\square_2$ and $La_{3.7}Ca_{2.3}Si_{12}N_{11.7}O_{14.3}$ [nominal doping level of: 1.2 mol% ($La_5CaSi_{12}N_{17}O_7\square_2$)/ 2.1 mol% ($La_{3.7}Ca_{2.3}Si_{12}N_{11.7}O_{14.3}$)] with 440 nm yielded emission spectra with the characteristic broadband emission of the 5d-4f transition of $Ce^{3+}$ (Figure 5). The emission band of $La_5CaSi_{12}N_{17}O_7\square_2$:$Ce^{3+}$ peaks at 565 nm with a fwhm of ~ 127.2 nm (~ 3744 $cm^{-1}$) and CIE (Commission Internationale de l'Éclairage) color coordinates of $x = 0.471$ and $y = 0.510$, which results in a greenish yellow luminescence. $La_{3.7}Ca_{2.3}Si_{12}N_{11.7}O_{14.3}$:$Ce^{3+}$ shows yellow luminescence, as its emission band shows a maximum at 578 nm with a fwhm of ~ 141.4 nm (~ 4010 $cm^{-1}$) and CIE color coordinates of $x = 0.489$ and $y = 0.495$. The internal quantum efficiency of the samples reaches values of 62% ($La_5CaSi_{12}N_{17}O_7\square_2$:$Ce^{3+}$) and 46% ($La_{3.7}Ca_{2.3}Si_{12}N_{11.7}O_{14.3}$:$Ce^{3+}$), although their syntheses are not yet optimized with regard to doping concentration, morphology and particle size. The lower internal quantum efficiency of the latter compound is attributable to the amorphous, non-luminescent side phase of the sample (see Syntheses), which could not be separated for luminescent measurements. Besides, both samples show relative low thermal quenching at 150 °C with a relative emission intensity of ~ 70% (Figure S4 in the Supporting

Information). Additionally, they can be excited very well by blue light as originating from a (Ga,In)N-LED, since their excitation spectra peak at ~ 450 nm ($La_5CaSi_{12}N_{17}O_7\square_2:Ce^{3+}$) or rather ~ 466 nm ($La_{3.7}Ca_{2.3}Si_{12}N_{11.7}O_{14.3}:Ce^{3+}$) (Figure 5). The emission of $La_5CaSi_{12}N_{17}O_7\square_2:Ce^{3+}$ and $La_{3.7}Ca_{2.3}Si_{12}N_{11.7}O_{14.3}:Ce^{3+}$ is comparable to other, industrially applied $Ce^{3+}$-doped LED phosphor materials, such as $(La,Ca)_3Si_6N_{11}:Ce^{3+}$ ($\lambda_{em}$ = 577 - 581 nm; fwhm ~ 3800 $cm^{-1}$),[16] $CaAlSiN_3:Ce^{3+}$ ($\lambda_{em}$ = 580 nm; fwhm ~ 3900 $cm^{-1}$),[40] and $YAG:Ce^{3+}$ ($\lambda_{em}$ = 550 - 570 nm; fwhm ~ 3700 $cm^{-1}$).[41] The relatively broad emission with double band shape of these and the title compounds is based on the two levels of the $4f^1$ ground state configuration of $Ce^{3+}$, separated by approximately 2000 $cm^{-1}$.[42]

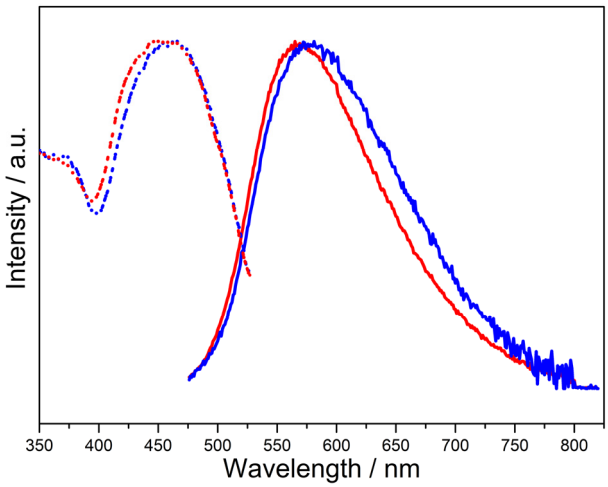


**Figure 5.** Excitation (dotted line) and emission (solid line) spectra of $La_5CaSi_{12}N_{17}O_7\square_2:Ce^{3+}$ (1.2 mol% Ce) (red) and $La_{3.7}Ca_{2.3}Si_{12}N_{11.7}O_{14.3}:Ce^{3+}$ (2.1 mol% Ce) (blue).

Due to the similar luminescence properties of the both $Ce^{3+}$-doped samples, $La_5CaSi_{12}N_{17}O_7\square_2$ was used for further luminescence investigations, as it shows no significant side phase. Upon excitation of $Eu^{2+}$-doped $La_5CaSi_{12}N_{17}O_7\square_2$ [nominal doping level of 4.3 mol%] with 440 nm yellow-orange luminescence was detected. The emission band peaks at 586 nm with a fwhm of ~ 57.7 nm (~ 1664 $cm^{-1}$) and CIE color coordinates of $x$ = 0.544 and $y$ = 0.453 (Figure 6). Moreover, $La_5CaSi_{12}N_{17}O_7\square_2:Eu^{2+}$ can be efficiently excited by blue light, as the excitation spectrum shows a maximum at ~ 430 nm (Figure 6). Compared to $(Sr,Ba)_2Si_5N_8:Eu^{2+}$ ($\lambda_{em}$ = 590 - 625 nm; fwhm ~ 2050-2600 $cm^{-1}$), which already found broad application in industry, the fwhm of $La_5CaSi_{12}N_{17}O_7\square_2:Eu^{2+}$ is rather narrow.[11,13,15,43]

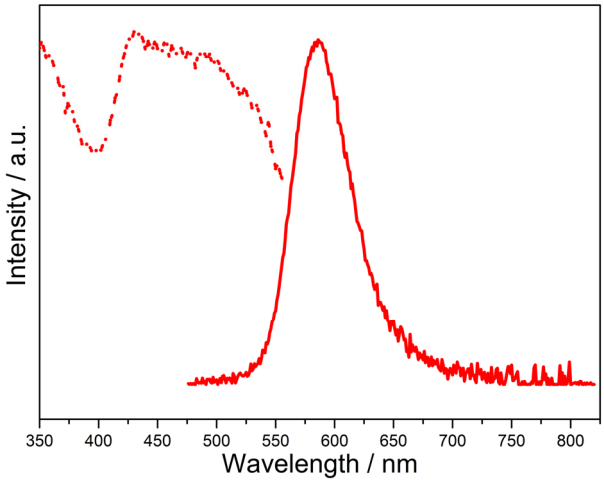


**Figure 6.** Excitation (dotted line) and emission (solid line) spectra of $La_5CaSi_{12}N_{17}O_7\square_2:Eu^{2+}$ (4.3 mol% Eu).

To investigate the luminescence of the samples doped with $Eu^{2+}$ and $Ce^{3+}$, exemplarily codoped $La_5CaSi_{12}N_{17}O_7\square_2$ [nominal doping level of: 1.9 mol% Ce and 0.1 mol% Eu] was excited with 440 nm. The emission spectra peaks at 581 nm with a fwhm of ~ 125.8 nm (~ 3609 $cm^{-1}$) and CIE color coordinates of $x = 0.491$ and $y = 0.495$ (Figure 7). The internal quantum efficiency of the nonoptimized sample is 64%. Analogous to the $Ce^{3+}$-doped samples $La_5CaSi_{12}N_{17}O_7\square_2:Ce^{3+},Eu^{2+}$ exhibits relative low thermal quenching at 150 °C with a relative emission intensity of ~ 70% (Figure S4 in the Supporting Information). Since the excitation spectrum shows a maximum at 462 nm, the sample can also be excited efficiently by blue light (Figure 7).

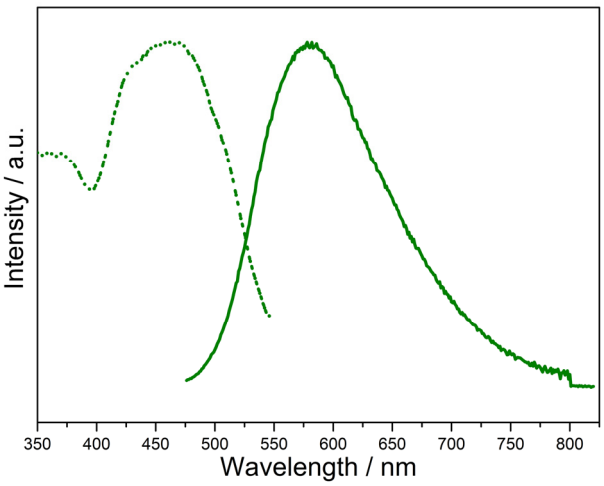


**Figure 7.** Excitation (dotted line) and emission (solid line) spectra of $La_5CaSi_{12}N_{17}O_7\square_2:Ce^{3+},Eu^{2+}$ (1.9 mol% Ce and 0.1 mol% Eu).

The luminescence measurements prove that regardless of the concentration of the dopants, the band gap of $La_5CaSi_{12}N_{17}O_7\square_2$ and $La_{3.7}Ca_{2.3}Si_{12}N_{11.7}O_{14.3}$ is much larger than the optical transition of the phosphors. According to the UV-Vis measurement the bang gap is ~ 4.3 eV, corresponding to 288 nm. Consequently, excitations bridging the band gap of both compounds should not influence the optical properties in the visible region. The emission spectra of the $Ce^{3+}$-doped samples (Figure 5) show that increasing $Ce^{3+}$ content leads to a red shift of the emission. Additionally, codoping with $Eu^{2+}$ and $Ce^{3+}$ also leads to a red shifted emission (Figure 7). In comparison to the emission of an investigated YAG:$Ce^{3+}$ sample ($\lambda_{em}$ = 550 nm; fwhm ~ 2994 $cm^{-1}$, $x$ = 0.432 and $y$ = 0.549) $Ce^{3+}$ and codoped $La_5CaSi_{12}N_{17}O_7\square_2$ as well as $Ce^{3+}$-doped $La_{3.7}Ca_{2.3}Si_{12}N_{11.7}O_{14.3}$ show a significant red shifted emission, which enables the production of 1pc-LEDs with warmer color temperature. This is also corroborated by the CIE diagram (Figure 8).

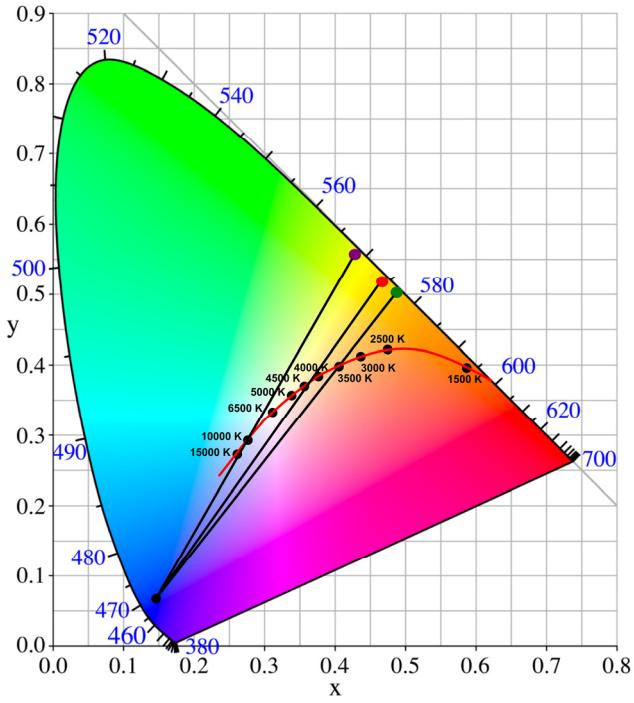


**Figure 8.** CIE 1931 chromaticity diagram showing the color coordinates of the YAG:$Ce^{3+}$ (violet) sample, $La_5CaSi_{12}N_{17}O_7\square_2$:$Ce^{3+}$ (red) $La_{3.7}Ca_{2.3}Si_{12}N_{11.7}O_{14.3}$:$Ce^{3+}$ (green) and $La_5CaSi_{12}N_{17}O_7\square_2$:$Ce^{3+}$,$Eu^{2+}$ (green).

The color coordinates of $La_5CaSi_{12}N_{17}O_7\square_2$:$Ce^{3+}$, $La_{3.7}Ca_{2.3}Si_{12}N_{11.7}O_{14.3}$:$Ce^{3+}$, $La_5CaSi_{12}N_{17}O_7\square_2$:$Ce^{3+}$,$Eu^{2+}$ and the YAG:$Ce^{3+}$ sample are positioned in the yellow spectral range. The combination with a 450 nm InGaN LED yields white 1pc-LEDs. The combination of

the blue LED with $La_5CaSi_{12}N_{17}O_7\square_2$:$Ce^{3+}$leads to a crossing of the black body curve at ~ 4300 K and the combination with $La_{3.7}Ca_{2.3}Si_{12}N_{11.7}O_{14.3}$:$Ce^{3+}$ and $La_5CaSi_{12}N_{17}O_7\square_2$:$Ce^{3+}$,$Eu^{2+}$, respectively, to a crossing of the black body curve at ~ 3500 K. Consequently, under irradiation with 450 nm all three compounds show a warmer correlated color temperature than the YAG:$Ce^{3+}$ sample (~ 10000 K). With $La_{3.7}Ca_{2.3}Si_{12}N_{11.7}O_{14.3}$:$Ce^{3+}$ or $La_5CaSi_{12}N_{17}O_7\square_2$:$Ce^{3+}$,$Eu^{2+}$ it is even possible to create a warm-white 1pc-LED,without any further optimization steps.

## 3.2.4 Conclusion

High temperature reactions with reactive starting materials yielded the oxonitridosilicate oxides $La_5CaSi_{12}N_{17}O_7\square_2$ and $La_{3.7}Ca_{2.3}Si_{12}N_{11.7}O_{14.3}$. Both compounds are homeotypic to $La_3Si_6N_{11}$ ($Z$ = 2),[17] as they are characterized by the same three-dimensional network but contain an additional isolated oxygen site. The unit cells of $La_5CaSi_{12}N_{17}O_7\square_2$ and $La_{3.7}Ca_{2.3}Si_{12}N_{11.7}O_{14.3}$ offer enough space for this position, since the ionic radius of $Ca^{2+}$ (1.80 Å)[44] is significantly smaller than the ionic radius of $La^{3+}$ (1.95 Å),[44] thus the occupation of the oxygen site increases with increasing Ca content. Additionally, $La_5CaSi_{12}N_{17}O_7\square_2$ and $La_{3.7}Ca_{2.3}Si_{12}N_{11.7}O_{14.3}$ show promising luminescence properties. Under irradiation with blue light doping with $Ce^{3+}$ yielded, white luminescence, which depending on the doping level covers the neutral white to warm-white spectral region. Under these conditions $Eu^{2+}$-doped samples show yellow-orange luminescence. Consequently, $La_5CaSi_{12}N_{17}O_7\square_2$ and $La_{3.7}Ca_{2.3}Si_{12}N_{11.7}O_{14.3}$ can be doped significantly with $Ce^{3+}$ and $Eu^{2+}$, which is probably based on the content of a trivalent (La) and divalent (Ca) cation. These features enable codoping of the samples which leads to a red shift of the $Ce^{3+}$ luminescence. Owing to these different doping possibilities the luminescence of $La_5CaSi_{12}N_{17}O_7\square_2$ and $La_{3.7}Ca_{2.3}Si_{12}N_{11.7}O_{14.3}$ can be tuned by the used dopant, codoping and the dopant content. Due to this marked tunability the presented compounds are promising materials for application in neutral to warm-white 1pc-LEDs.

## 3.2.5 References


[1] J. Heber, *Nat. Phys.* **2014**, *10*, 791.

[2] E. F. Schubert, J.-K. Kim, *Science* **2005**, *308*, 1274.

[3] M. S. Shur, A. Zukauskas, *Proc. IEEE* **2005**, *93*, 1691.

[4] Y. Narukawa, J. Narita, T. Sakamoto, T. Yamada, H. Narimatsu, M. Sano, T. Mukai, *Phys. Status Solidi A* **2007**, *204*, 2087.

[5] J. Y. Tsao, M. E. Coltrin, M. H. Crawford, J. A. Simmons, *Proc. IEEE* **2010**, *98*, 1162.

[6] A. A. Setlur, *Electrochem. Soc. Interface* **2009**, *18*, 32.

[7] D. J. Robbins, *J. Electrochem. Soc.* **1979**, *126*, 1550.

[8] K. Uheda, N. Hirosaki, H. Yamamoto, *Phys. Status Solidi A* **2006**, *203*, 2712.

[9] K. Uheda, N. Hirosaki, Y. Yamamoto, A. Naito, T. Nakajima, H. Yamamoto, *Electrochem*. *Solid-State Lett.* **2006**, *9***,** H22.

[10] P Pust, V. Weiler, C. Hecht, A. Tücks, A. S. Wochnik, A. -K. Henß, D. Wiechert, C. Scheu, P. J. Schmidt, W. Schnick, *Nat. Mater.* **2014**, *13*, 891.

[11] R. Müller-Mach, G. Müller, M. R. Krames, H. A. Höppe, F. Stadler, W. Schnick, T. Jüstel, P. Schmidt, *Phys. Status Solidi A* **2005**, *202*, 1727.

[12] Y. Q. Li, J. E. J. van Steen, J. W. H. van Krevel, G. Botty, A. C. A. Delsing, F. J. DiSalvo, G. de With, H. T. Hintzen, *J. Alloys Compd*. **2006**, *417*, 273.

[13] M. R. Krames, G. O. Müller, R. B. Müller-Mach, H.-H. Bechtel, P. J. Schmidt, *PCT Int. Appl.* WO 2010131133, A1, **2010**.

[14] M. Zeuner, S. Pagano, W. Schnick, *Angew. Chem. Int. Ed.* **2011**, *50*, 7754.

[15] H. A. Höppe, H. Lutz, P. Morys, W. Schnick, A. Seilmeier, *J. Phys. Chem. Solids*, **2000**, *61*, 2001.

[16] T. Suehiro, N. Hirosaki, R.-J. Xie, *Appl. Mater. Interfaces* **2011**, *3*, 811.

[17] M. Woike, W. Jeitschko, *Inorg. Chem.*, **1995**, *34*, 5105.

[18] B. Gieger, H. Jacobs, C. Hadenfeldt, *Z. Anorg. Allg. Chem.* **1974**, *410*, 104.

[19] H. Lange, G. Wotting, G. Winter, *Angew. Chem. Int. Ed.* **1991**, *30*, 1579.

[20] W. Schnick, H. Huppertz, R. Lauterbach, *J. Mater Chem.* **1999**, *9*, 289.

[21] M. Besson, *C. R. Acad. Sci.* **1890**, *110*, 518.

[22] G. M. Sheldrick, *SADABS, Multi-Scan Absorption Correction*, Bruker-AXS, WA, USA, **2012**, v. 2.

[23] G. M. Sheldrick, *Acta Crystallogr. Sect. A* **2008**, *64*, 112.

[24] A. Coelho, *TOPAS Academic* 2007, Coelho Software, Brisbane, Australia, **2007**.

[25] D. Durach, W. Schnick, *Eur. J. Inorg. Chem.* **2015**, 4095.

[26] D. Durach, L. Neudert, O. Oeckler, W. Schnick, *Chem. Mater.* **2015**, *27*, 4832.

[27] D. Durach, W. Schnick, *Z. Anorg. Allg. Chem.* **2016**, *642*, 101.

[28] D. Durach, F. Fahrnbauer, O. Oeckler, W. Schnick, *Inorg. Chem.* **2015**, *54*, 8727.

[29] P. E. D. Morgan, *J. Mater. Sci.* **1986**, *21*, 4305.

[30] F. Liebau, *Structural Chemistry of Silicates*, Springer, Berlin, **1985**.

[31] The term *vierer* (*achter*) ring was coined by Liebau and is derived from the German word “vier” (“acht”); a *vierer* (*achter*) ring comprises four (eight) tetrahedral centers.

[32] J. Shropshire, P. P. Keat, P. A. Vaughan, *Z. Kristallogr.* **1959**, *112*, 409.

[33] T. Schlieper, W. Milius, W. Schnick, *Z. Anorg. Allg. Chem.* **1995**, *621*, 1380.

[34] T. Schlieper, W. Milius, W. Schnick, *Z. Anorg. Allg. Chem.* **1995**, *621*, 1037.

[35] C. Schmolke, S. Lupart, W. Schnick, *Solid State Sci.* **2009**, *11*, 305.

[36] J. A. Kechele, C. Schmolke, S. Lupart, W. Schnick, *Z. Anorg. Allg. Chem.* **2010**, *636*, 176.

[37] K. Fukuda, T. Iwata, E. Champion, *Powder Diffr.* **2006**, *21*, 300.

[38] K. Mori, R. Kiyanagi, M. Yonemura, K. Iwase, T. Salto, K. Itoh, M. Sugiyama, T. Kamiyama, T. Fukunaga, *J. Solid State Chem.* **2006**, *179, 3286.*

[39] R. D. Shannon, *Acta Crystallogr. Sect. A.* **1976**, *32*, 751.

[40] Y. Q. Li, N. Hirosaki, R.-J. Xie, T. Takeda, M. Mitomo, *Chem. Mater.* **2008**, *20*, 6704.

[41] T. Moriguchi, Y. Noguchi, K. Sakanao, Y. Shimizu, US 5998925 A, **1997**.

[42] G. Blasse, B. C. Grabmaier, Luminescent Materials, Springer, Berlin, Heidelberg, NY, **1994**.

[43] M. Zeuner, P. J. Schmidt, W. Schnick, *Chem. Mater.* **2009**, *21*, 2467.

[44] J.C. Slater, *J. Chem. Phys.* **1964**, *41*, 3199.

# 4 Combination of Electron Microscopy and Synchrotron X-ray Diffraction for Structure Elucidation of Lanthanum (Oxo)nitridosilicates

## 4.1 Introduction

Many solid-state syntheses lead to heterogeneous samples containing microcrystalline compounds. The characterization of such materials represents a challenge, as conventional single-crystal X-ray diffraction of crystals smaller than 1000 $\mu m^3$ becomes increasingly difficult. Powder X-ray diffraction is in many cases inadequate for a detailed structure elucidation, particularly if the sample contains complex unknown structure types. Characterization by means of electron crystallography is an attractive alternative. However, due to dynamic diffraction effects and experimental limitations, the precision of the results lags behind that of X-ray single-crystal diffraction data.[1-4] Nevertheless, electron microscopy is an important tool for the discovery and pre-characterization of novel phases regarding their compositions and structural aspects, especially their metrics. For a detailed structure characterization of such samples, investigations with microfocused synchrotron radiation are well suited. This approach yields datasets with high quality, comparable to laboratory X-ray diffraction data. Recently developed lens systems based on Be, Si or Al allow unprecedented brilliance and intensity by microfocusing.[5] Until now mounting and centering of the tiny crystals of the phase sought-after in the microfocused beam was very laborious and time-consuming. In 2015, *Oeckler* et al. described an experimental solution for many such problems by a combination of electron microscopy and synchrotron microdiffraction. In a first step the inhomogeneous sample is prepared on a transmission electron microscopy grid. Then the desired crystal is selected by means of energy-dispersive X-ray spectroscopy and selected area electron diffraction. Subsequently, the very crystal is focused in the microfocused beam by a telescope with large magnification as well as by X-ray fluorescence, using the copper crossbars of the grid as "landmarks".[6,7] Consequently, this elaborate approach is a powerful tool for the characterization of so far unknown compounds, which could only be obtained as microcrystals in a heterogeneous sample. This is proven by chapter 4.2, which describes the characterization of a novel lanthanum oxonitridosilicates

with the combination of electron microscopy and synchrotron microdiffraction. Sections 4.3 and 4.4 represent the investigation of hitherto unidentified lanthanum (oxo)nitridosilicates with microfocused synchrotron radiation.

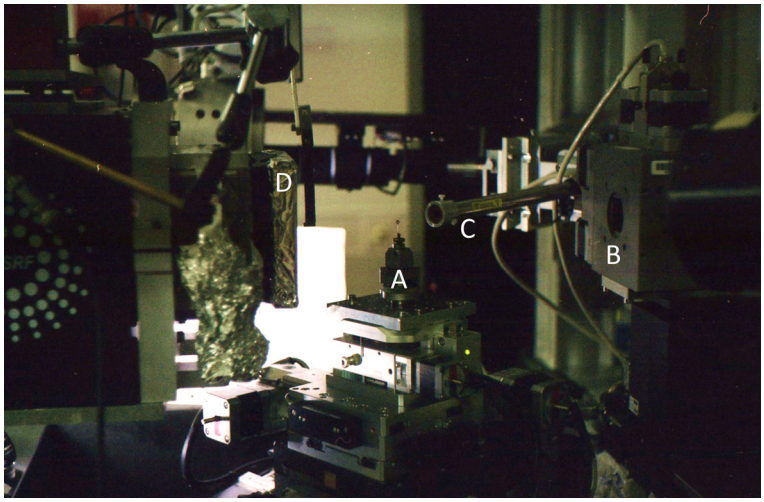


**Figure 1.** (a) Experimental setup for microfocus diffraction experiments at ID11 with mounted copper grid (A), primary beam outlet (B), fluorescence (C) and Frelon 2K CCD detector (D).

## References

[1] U. Kolb, E. Mugnaioli, T. E. Gorelik, *Cryst. Res. Technol.* **2011**, *46*, 542.

[2] G. van Tendeloo, S. Bals, S. van Aert, J. Verbeeck, D. van Dyck, *Adv. Mater.* **2012**, *24*, 5655.

[3] L. Palatinus, V. Petricek, C. A. Corrêa, *Acta Crystallogr. Sect. A* **2015**, *71*, 235.

[4] T. Willhammar, X. Zou, *Z. Kristallogr.* **2013**, *228*, 11.

[5] C. G. Schroer, B. Benner, T. F. Günzler, M. Kuhlmann, J. Patommel, B. Lengeler, A. Somogyi, T. Weitkamp, C. Rau, A. Snigirev, I. Snigireva, *Proc. of the SPIE Meeting* **2004**, *5535*, 701.

[6] F. Fahrnbauer, T. Rosenthal, T. Schmutzler, G. Wagner, G. B. M. Vaughan, J. P. Wright, O. Oeckler, *Angew. Chem. Int. Ed.* **2015**, *54*, 10020.

[7] F. Fahrnbauer, *Doktoral Thesis*, Leipzig University, **2015**.

# 4.2 $La_3BaSi_5N_9O_2:Ce^{3+}$ - A Yellow Phosphor with an Unprecedented Tetrahedra Network Structure Investigated by Combination of Electron Microscopy and Synchrotron X-ray Diffraction

published in: *Chem. Mater.* **2015**, *27*, 4832-4838

authors: Dajana Durach, Lukas Neudert, Peter J. Schmidt, Oliver Oeckler and Wolfgang Schnick

DOI: 10.1021/acs.chemmater.5b01702



http://pubs.acs.org/doi/abs/10.1021/acs.chemmater.5b01702

**Abstract.** Due to the relationship between structure and luminescence properties, detailed crystal structure determination for microcrystalline phosphors is necessary for a profound understanding of materials properties. The yellow phosphor $La_3BaSi_5N_9O_2:Ce^{3+}$ ($\lambda_{max}$ = 578 nm; fwhm ~4700 $cm^{-1}$) was characterized by a combination of transmission electron microscopy (TEM) and synchrotron microfocus diffraction as only agglomerates of crystals with a maximum size of a few µm could be obtained yet. $La_3BaSi_5N_9O_2:Ce^{3+}$ was synthesized from $LaF_3$, $La(NH_2)_3$, $BaH_2$, $Si(NH)_2$, and $CeF_3$ in a radio frequency furnace. It crystallizes in space group $Pmn2_1$ (no. 31) with $a$ = 9.5505(8), $b$ = 19.0778(16), $c$ = 12.1134(9) Å, and $Z$ = 8. Its interrupted three-dimensional tetrahedra network contains *zehner* and *dreier* rings of vertex-sharing $SiN_4$ and $SiN_2O_2$ tetrahedra. The crystal structure was confirmed by high-resolution TEM and Z-contrast scanning TEM. The element distribution was derived by bond-valence sum calculations. The infrared spectrum proves the absence of N-H bonds.

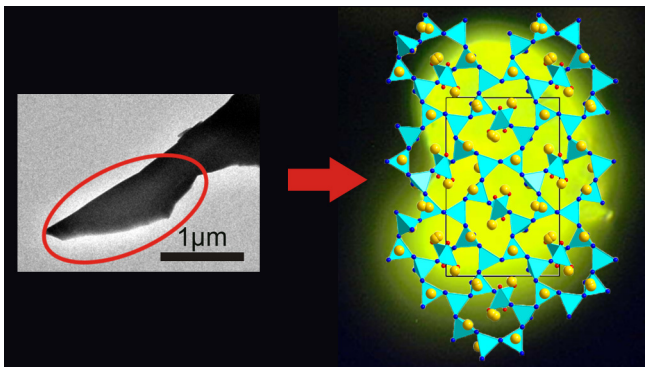

## 4.2.1 Introduction

In 2014, the Nobel Prize in Physics was awarded to Akasaki, Amano, and Nakamura *"for the invention of efficient blue light-emitting diodes which has enabled bright and energy-saving white light sources"*.[1] This emphasizes the importance of light-emitting diodes (LEDs) which are typically combined with luminescent materials to phosphor-converted pc-LEDs that produce white light. Owing to their excellent properties such as long lifetime, energy efficiency, small volume, and environmental compatibility, they convince as light source now and in the future.[2-5] Presently, most white-light pc-LEDs are produced by combining a blue primary (In,Ga)N LED chip with yellow-emitting $(Y,Gd)_3(Al,Ga)_5O_{12}:Ce^{3+}$ ($YAG:Ce^{3+}$). This phosphor shows a broad yellow emission and excellent chemical and thermal stability. However, this combination yields only cool-white light.[6,7] In order to achieve warm-white light for general lighting, a multiphosphor approach is necessary, which combines at least two phosphors, e.g. a broadband green-yellow with an orange-red emitting one.[8] As nitridoaluminates and nitridosilicates can be thermally and chemically inert due to their highly condensed structures, they turned out to be excellent phosphors. Moreover, they have partially covalent bonds between the activator (dopant) and N, which leads to red-shifted photoluminescence (nephelauxetic effect). Thus, $Eu^{2+}$-doped nitridoaluminates and nitridosilicates such as $(Ba,Sr)_2Si_5N_8:Eu^{2+}$[9-12] or $(Ca,Sr)SiAlN_3:Eu^{2+}$[13-16] are applied as red emitting component in commercially available warm-white pc-LEDs.[8,17] Owing to the nephelauxetic effect, the luminescence of nitridosilicates is shifted to warmer color temperatures. Thus, $Ce^{3+}$-doped nitridosilicates have great potential for application in warm-white pc-LEDs based on a single-phosphor approach (1pc-LEDs). An outstanding example for this is $(La,Ca)_3Si_6N_{11}:Ce^{3+}$.[18] White 1pc-LEDs using this phosphor emit in the 2600-3800 K color temperature range and show good thermal stability.

The continuous development of new solid-state lighting technologies and devices and a growing demand motivate the search for new nitridosilicate phosphors. However, structure elucidation of such new phosphors often proved difficult and time-consuming, and either large single crystals or phase-pure samples were usually necessary. Commonly, a single-particle-diagnosis approach is used, which enables the determination of luminescence and crystal structures of rather small single crystals up to 10 µm.[19] Yet, many explorative syntheses lead to inhomogeneous and microcrystalline products with crystal size below a few µm. Consequently, structure characterization with conventional single-crystal X-ray

diffraction is no longer possible. Here, we apply an approach that combines transmission electron microscopy (TEM) and synchrotron microfocus diffraction. This method allows for the analysis of particles with a volume even smaller than 1 $\mu m^3$ and furthermore provides the possibility of analyzing the same particle by TEM and X-ray diffraction.[20] In contrast to structure determination by electron crystallography, e.g. with automated electron diffraction tomography (ADT) or rotation electron diffraction (RED),[21-25] this method allows a much more accurate determination of bond lengths, mixed occupancies and displacement parameters. Data acquired with microfocused synchrotron radiation yielded the crystal structure of the novel yellow phosphor $La_3BaSi_5N_9O_2:Ce^{3+}$ discussed in this contribution.

## 4.2.2 Experimental Section

### 4.2.2.1 Synthesis

For the synthesis of $La_3BaSi_5N_9O_2:Ce^{3+}$ (with 2 mol% Ce), 0.15 mmol (29.8 mg) of $LaF_3$ (Sigma-Aldrich, 99.99%), 0.17 mmol (31 mg) of $La(NH_2)_3$,[26] 0.48 mmol (66.8 mg) of $BaH_2$ (Materion, 99.7%), 0.55 mmol (32.2 mg) of $Si(NH)_2$,[27] and 0.006 mmol (1.2 mg) of $CeF_3$ as dopant (Alfa Aesar, 99.99%) were mixed in an agate mortar and filled into a tungsten crucible. These steps were performed under argon atmosphere in a glovebox (Unilab, MBraun, Garching; $O_2 < 1$ ppm; $H_2O < 1$ ppm). Subsequently, the crucible was placed in a water-cooled silica glass reactor of a radio frequency furnace (type AXIO 10/450, maximal electrical output 10 kW, Hüttinger Elektronik, Freiburg),[28] heated under $N_2$-atmosphere to 1600 °C within 1 h, maintained at that temperature for 10 h, then cooled to 900 °C in 44 h, and finally quenched to room temperature by switching off the furnace. The reaction yielded an inhomogeneous sample with small aggregates of yellow crystals with a maximum size of a few µm (Figure S1), which show yellow luminescence after excitation with blue light. Moreover the crystals have high air and water stability. Contact with air and water over several hours does not lead to a decomposition of the crystals.

### 4.2.2.2 Electron Microscopy

For scanning electron microscopy (SEM), a JSM 6500F instrument (JEOL) with a Si/Li energy-dispersive X-ray (EDX) detector (Oxford Instruments, model 7418) was used. EDX spectra were collected with an accelerating voltage of 12 kV. In order to ensure electrical

conductivity on the sample surface, it was coated with carbon by means of an electron beam evaporator (BAL-TEC MED 020, Bal Tec AG).

For TEM investigations, the crushed polycrystalline aggregates of $La_3BaSi_5N_9O_2:Ce^{3+}$ were dispersed in absolute ethanol and drop-cast on copper finder grids coated with a holey carbon film (S166-2, Plano GmbH, Germany). The grids were fixed on double-tilt holders. Selected area electron diffraction (SAED), high resolution TEM (HRTEM), scanning TEM using a high-angle annular dark-field detector (STEM-HAADF), and EDX measurements were acquired on a Titan 80-300 (FEI, USA) with a field emission gun operated at 300 kV, equipped with a TEM TOPS 30 EDX spectrometer (EDAX, Germany). Images were recorded using an UltraScan 1000 camera (Gatan, USA, resolution: 2k × 2k). Further SAED and EDX measurements were done on a Jeol 2010 (Jeol, Germany) with a thermal emitter operated at 200 keV, equipped with an EDAX Apollo XLT EDX detector (EDAX Germany) and a TemCam F216 camera (TVIPS, Germany, resolution: 2k × 2k). HRTEM and SAED data were evaluated using the programs Digital Micrograph[29] (including Fourier filtering of the HRTEM images) and JEMS.[30] EDX data were processed with ES Vision[31] and EDAX TEAM.[32]

#### 4.2.2.3 Single-Crystal X-ray Diffraction

The X-ray diffraction data of $La_3BaSi_5N_9O_2:Ce^{3+}$ were collected at beamline ID11 of the ESRF in Grenoble (Ge(111) double-crystal monochromator, Frelon CCD detector)[33] with a wavelength of $\lambda = 0.33510$ Å. The beam was focused to 4.5 µm in horizontal direction and 0.5 µm in vertical direction with a beryllium lens system.[34] A single-crystalline tip (ca. 1 µm · 0.5 µm) of a crystallite was centered in the beam with the help of the fluorescence signal. Diffraction data were indexed with SMART[35] and integrated with SAINT.[36] Scaling and absorption correction were done with SADABS.[37] In addition, a correction for the incomplete absorption in the CCD phosphor was applied.[38] The structure was solved by direct methods (SHELXS) and refined by full matrix least-squares methods (SHELXL).[39]

#### 4.2.2.4 Powder X-ray Diffraction

Powder diffraction data were collected with a STOE STADI P diffractometer (Mo-$K\alpha_1$ radiation, $\lambda = 0.70930$ Å, Ge(111) monochromator, MYTHEN 1K detector) in Debye-Scherrer geometry. Simulated powder diffraction patterns were calculated using the WinXPOW

program package[40] on the basis of the single-crystal structure data. Rietveld refinement was performed by using TOPAS-Academic.[41]

#### 4.2.2.5 Luminescence

The luminescence was analyzed with a luminescence microscope, consisting of a HORIBA Fluoromax4 spectrofluorimeter system attached to an Olympus BX51 microscope via fiber optics. Using an excitation wavelength of 440 nm with a spectral width of 10 nm, the emission spectra were measured between 460 and 780 nm with 2 nm step size. This spectral range was also used for color point calculations. Excitation spectra were measured between 385 and 520 nm with 2 nm step size.

#### 4.2.2.6 FTIR Spectroscopy

The Fourier transform infrared spectrum (FTIR) spectrum of $La_3BaSi_5N_9O_2:Ce^{3+}$ was recorded using a KBr pellet with a Spectrum BX II spectrometer (PerkinElmer, Waltham MA, USA).

### 4.2.3 Results and Discussion

#### 4.2.3.1 Synthesis and Chemical Analysis

The synthesis is probably based on the decomposition of $BaH_2$ (decomposition at 675 °C),[42] and its reaction with $LaF_3$ to $BaF_2$, which resublimates at the reactor wall of the radio frequency furnace. Subsequently, the remaining Ba reacts with the dopant and the precursors $La(NH_2)_3$ and $Si(NH)_2$ to $La_3BaSi_5N_9O_2:Ce^{3+}$. The incorporated O supposedly originates from contamination of commercially acquired starting materials. $La_3BaSi_5N_9O_2:Ce^{3+}$ forms small yellow crystals, whose size could not be increased so far by variation of synthesis conditions. The sum formula obtained from single-crystal structure refinement and bond-valence sum calculations is corroborated by SEM-EDX analyses as the measurements result in an average composition of $La_{3.00(17)}Ba_{0.49(4)}Si_{4.4(2)}N_{12.0(4)}O_{2.34(11)}$ (sum formula normalized according to the La content; four measurements on different crystals; unusually large errors are due to La/Ba line overlap and the simultaneous presence of light and very heavy elements). Although Ce was not detected by EDX, its presence is proven unequivocally by luminescence measurements.

### 4.2.3.2 Single-Crystal Structure Analysis

As only agglomerates with low scattering intensity of the crystals could be separated, their characterization was not possible with conventional single-crystal X-ray diffraction. As no phase-pure sample could be obtained and the powder pattern suggested a novel compound with a very complex structure, crystal-structure determination by means of powder X-ray diffraction was also not feasible. As the product shows interesting luminescence properties, it was investigated by a combination of TEM and synchrotron microfocus diffraction. Therefore, the agglomerates were crushed in order to obtain small single crystals which were then dispersed on a TEM grid. An appropriate tip of a crystallite of $La_3BaSi_5N_9O_2:Ce^{3+}$ was selected by means of EDX and SAED (Figure 1).

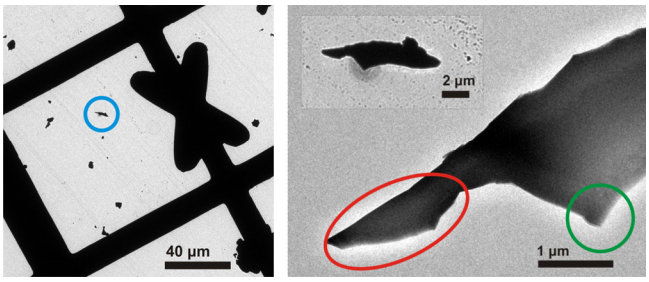


**Figure 1.** Bright-field image of the selected crystal (blue circle) and investigated areas of the microcrystal; green: for TEM, red: for microfocused synchrotron beam.

Indexing of the SAED patterns (Figure 2) leads to orthorhombic metrics with so far unknown lattice parameters ($a$ = 10.37, $b$ = 19.1, $c$ = 12.21 Å). Further electron diffraction patterns along [100], [010], and [001] confirm the orthorhombic metrics of $La_3BaSi_5N_9O_2$ and the reflection condition $h0l$: $h + l = 2n$ for a (010) $n$-glide plane is fulfilled.

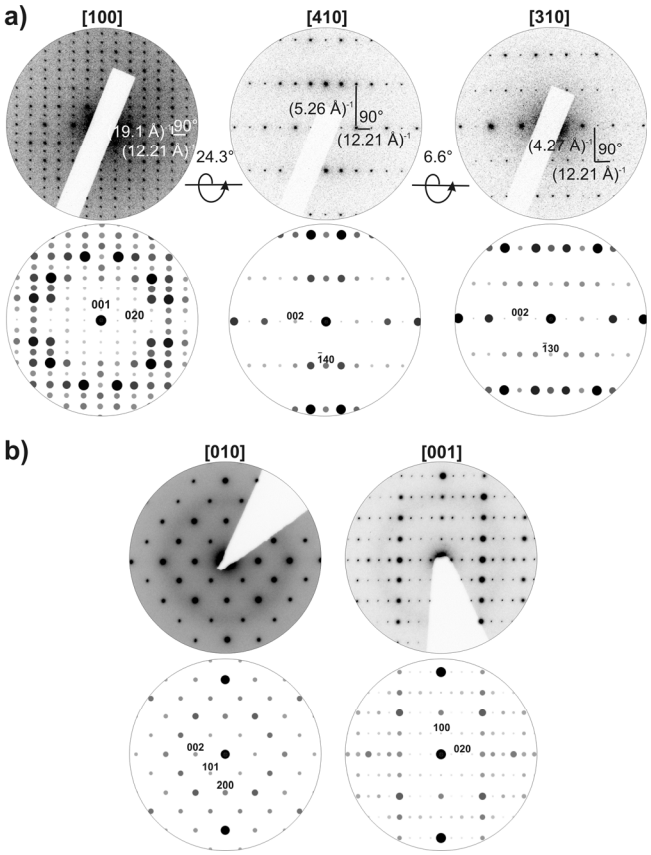


**Figure 2.** (a) SAED tilt series (maximum deviation between experimental and simulated tilt angles 1.5°) of the $La_3BaSi_5N_9O_2:Ce^{3+}$ microcrystal investigated by synchrotron radiation; experimental SAED pattern with some highlighted 1/d-values (top), simulated SAED patterns with selected reflections labeled with indices (bottom, selected reflections labeled with indices, kinematical intensities according to the final structure model), (b) experimental SAED patterns along [010] and [001] obtained from thin regions of different crystallites of $La_3BaSi_5N_9O_2:Ce^{3+}$ (top) and corresponding, simulated SAED patterns (bottom, selected reflections are labeled with indices).

Consequently, the selected crystal was investigated by microfocused radiation. The crystal structure was solved and refined in space group $Pmn2_1$. Inversion twinning had to be taken into account. The crystallographic data are summarized in Table 1, and the atomic parameters are given in the Supporting Information (Tables S1, S2).[43] Due to its insignificant contribution to the scattering density, $Ce^{3+}$ was neglected in the refinement of the crystal structure as well as for bond-valence sum calculations (BVS) (Tables S3, S4). The distribution of La and Ba as well as of N and O is based on BVS calculations and EDX measurements and is explained in detail in the chapter on BVS calculations below.

**Table 1.** Crystallographic Data of the Single-Crystal Structure Determination of $La_3BaSi_5N_9O_2$.

| parameter | comment |
|---|---|
| formula | $La_3BaSi_5N_9O_2$ |
| crystal system | orthorhombic |
| space group | $Pmn2_1$ (no. 31) |
| lattice parameters/Å | $a$ = 9.5505(8), $b$ = 19.0778(16), $c$ = 12.1134(9) |
| cell volume/Å$^3$ | 2207.1(3) |
| formula units per unit cell | 8 |
| density/g·cm$^{-3}$ | 5.132 |
| μ/mm$^{-1}$ | 2.045 |
| T/K | 298(2) |
| radiation/Å | synchrotron ( λ = 0.3351) |
| F(000) | 3008 |
| θ range/deg | 1.4 ≤ θ ≤ 12.9 |
| independent reflections | 5514 [$R_{int}$ = 0.0518] |
| refined parameters | 296 |
| twin ratio | 0.51(8)/0.49 |
| goodness of fit | 1.036 |
| $R1$ (all data/for $F^2 > 2\sigma(F^2)$) | 0.0357/0.0343 |
| $wR2$ (all data/for $F^2 > 2\sigma(F^2)$) | 0.0859/0.0848 |
| $\Delta\rho_{max}$ , $\Delta\rho_{min}$/e·Å$^{-3}$ | 1.841, -1.777 |

$La_3BaSi_5N_9O_2$ is characterized by a three-dimensional network of vertex-sharing $Q^4$- and $Q^2$-type $SiN_4/SiN_2O_2$ tetrahedra in the ratio of $Q^4/Q^2$ = 4/1 (Figure 3a). This leads to a degree of condensation κ = n(Si):n(N,O) = 0.45. In the network, there are singly bridging $N^{[2]}$ atoms and terminal $O^{[1]}$ atoms. The absence of N-H groups was confirmed by FTIR spectroscopy (Figure S3). The $SiN_4$ tetrahedra form *sechser* rings, which are condensed to *zehner* rings. These *zehner* rings are interconnected by *dreier* rings, which are composed of two $SiN_4$ and one $SiN_2O_2$ tetrahedra (Figure 3a, 3c, 3d).[44,45] Thus, although nitridosilicates with κ < 0.5 usually tend to form layered or less-condensed structures,[45] an interrupted three-dimensional network with *zehner* ring channels along [100] is formed (Figure 3b). An interrupted tetrahedra framework based on a degree of condensation smaller than 0.5 was also observed for $M_7Si_6N_{15}$ (M = La, Ce, Pr).[46] The unique topology of the network[47] of $La_3BaSi_5N_9O_2$ , keeping the 2-coordinated nodes forming the *dreier* rings, is represented by

the point symbol $\{3.6^3.7^2\}_2\{3\}\{6^6\}_2$. The Si-N [1.670(10)-1.773(8) Å] and Si-O [1.647(14)-1.709(14) Å] distances are in good agreement with comparable compounds, such as $Sr_2Si_5N_8$ [1.653(9)-1.786(5) Å][48] and $Pr_2Si_2O_7$.[1.519-1.712 Å][49] as well as with the sum of the ionic radii.[50]

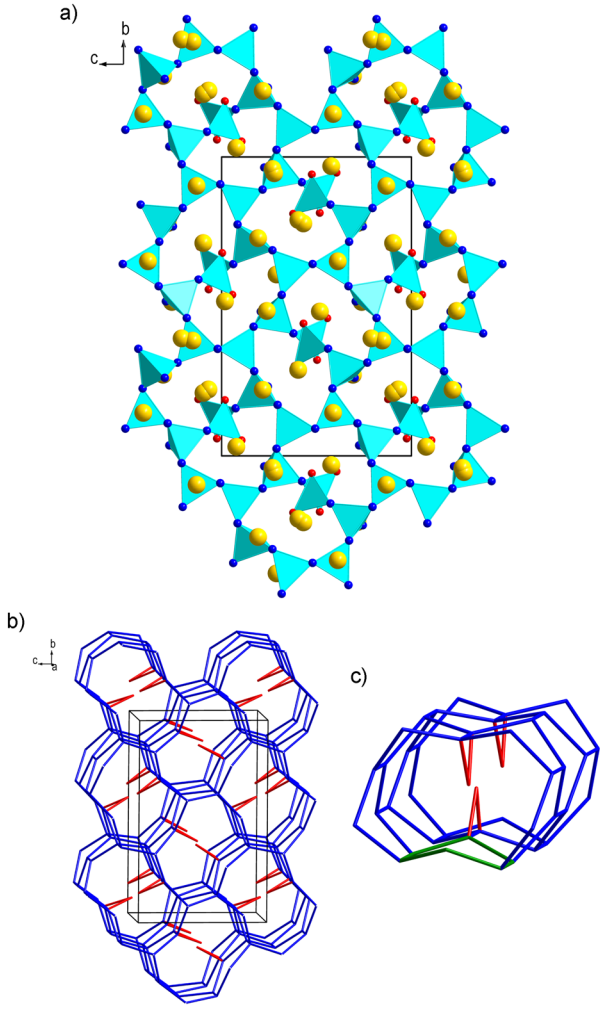


**Figure 3.** (a) Structure of $La_3BaSi_5N_9O_2$ in projection along [100] with $SiN_4/SiN_2O_2$ tetrahedra (turquoise), N atoms (blue), O atoms (red), and La/Ba atoms (yellow), unit cell outlined in black; (b) topological representation of $La_3BaSi_5N_9O_2$, *zehner* rings are represented by blue and *dreier* rings by red lines. Each connecting line represents a Si-N-Si bond; (c,d) detailed representation of *zehner* rings (blue), which are condensed with *sechser* (d: green) and *dreier* (red) rings.

The crystal structure contains 12 crystallographically independent heavy-atom sites. Bond-valence sum calculations (see below and Tables S3, S4) suggest that all positions are mixed occupied with La and Ba. The sites La3/Ba3, La5/Ba5, and La9/Ba9 were described with split positions (each containing La and Ba) with site occupation factors of 0.755(17):0.244(17),

0.213(17):0.286(17), and 0.039(2):0.460(2), respectively. In order to maintain a charge neutral formula, the site occupation factors were fixed to ratios of 0.750:0.250, 0.215:0.285, and 0.040:0.460, respectively (see chapter on BVS calculations below). La1/Ba1-La4/Ba4, La5B/Ba5B, La7/Ba7, La10/Ba10, and La11/Ba11 are 8-fold coordinated by $N^{3-}$ and $O^{2-}$. The sites La8/Ba8 and La9A/Ba9A are 8-fold coordinated by $N^{3-}$. For the sites La5A/Ba5A, La6/Ba6, La9B/Ba9B, and La12/Ba12 a coordination with nine anions is observed, whereas La6/Ba6, La9B/Ba9B, and La12/Ba12 are exclusively surrounded by $N^{3-}$ and La5A/Ba5A is surrounded by $N^{3-}$ and $O^{2-}$. All cations coordination spheres correspond to nonregular polyhedra (Figure 4). The bond lengths of La/Ba-N [2.419(12)-3.22(2) Å] and La/Ba-O [2.40(2)-2.908(19) Å] correspond to those in other lanthanum and barium compounds as well as to the sum of the ionic radii.[50-53]

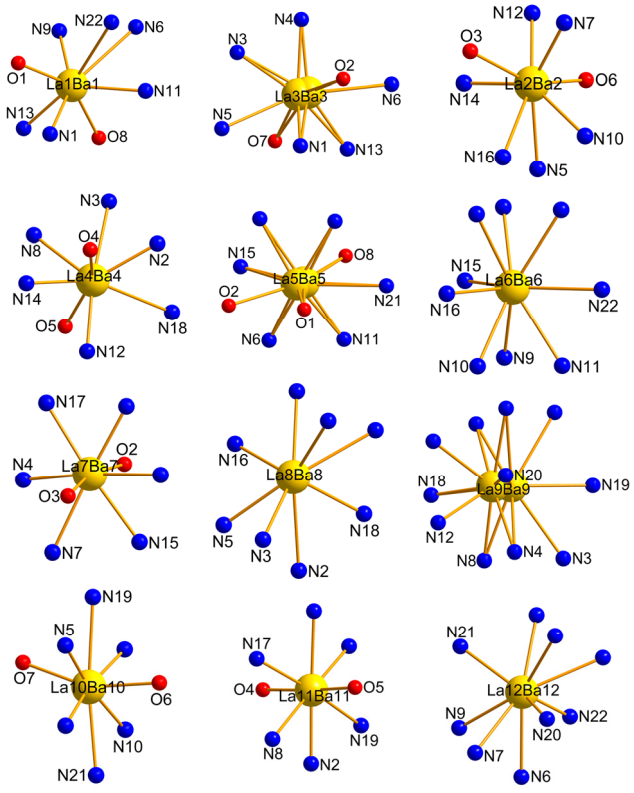


**Figure 4.** Coordination spheres of the heavy-atom sites in $La_3BaSi_5N_9O_2$.

A Rietveld refinement based on powder X-ray diffraction data (Figure S2) shows that the sample is composed of 93% $La_3BaSi_5N_9O_2$ and 7% $LaSi_3N_5$. In addition, there are a few weak reflections which cannot be ascribed to any known compound. The refinement also confirms the structure determined by single-crystal structure analysis.

#### 4.2.3.3 Bond-Valence Sum Calculations

Due to the very similar scattering factors of La and Ba, it is impossible to distinguish these atoms by X-ray diffraction. The same is true concerning the differentiation between N and O. Moreover, charge neutrality could be maintained by arbitrary exchange of LaN and BaO units. Thus, BVS calculations were performed to determine the cation site occupancies.[54] The calculations were based on the fact that terminal anion positions would preferentially be occupied by O rather than by N (Pauling's rules),[55] whereas all other light-atom sites were assumed to be occupied by N. The validity of this assumption is corroborated by EDX measurements, which leads to a comparable ratio of N and O. On the basis of this assumption, the BVS of the cations were determined (Table S3, S4). Thereby, the BVS of each heavy atom site was determined for La as well as for Ba. Optimizing the weighted average BVS for each site so that it corresponds to the site valence[54] yielded to the relative occupation of the heavy-atom sites. This calculation led to a sum formula with 0.14 negative excess charges. These were evenly distributed over all heavy atoms sites by adjusting the site occupancies in order to achieve a neutral formula. The negligible deviation between the refined and fixed site occupation factors as well as between the oxidation states and the BVS of the heavy atom sites that was achieved by this strategy confirms that the structure model is consistent (Table S4). Additionally, the La/Ba ratio is also corroborated by EDX measurements.

#### 4.2.3.4 Electron Microscopy

Simulations of HRTEM images along [001] based on the structure model of $La_3BaSi_5N_9O_2$ obtained by X-ray structure refinement are consistent with the experimental images (Figure 5). This is supported by STEM-HAADF images along [001]. Real structure effects were also observed, e.g. an antiphase boundary along ⟨010⟩ specified by an antiphase vector $p = 1/4b$ (Figure 6). Due to the large difference of the atomic numbers in $La_3BaSi_5N_9O_2$, only the heavy atoms La and Ba are visible in STEM-HAADF images.

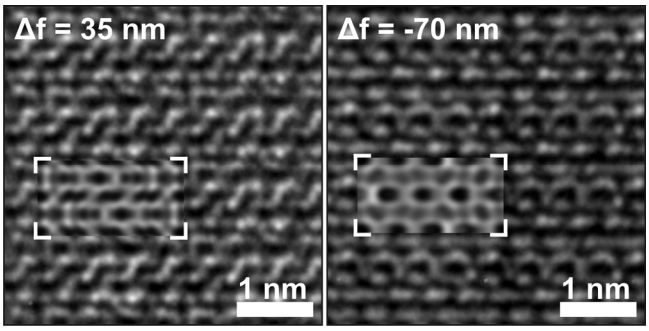


**Figure 5.** Fourier filtered HRTEM images along [001] with different defocus values Δf, insets: simulated images in the size of one unit cell (multislice method,[30] $C_s$ = 0.6 nm, spread of focus = 3.6 nm, beam semiconvergence = 25 mrad, layer thickness ~ 25 nm).

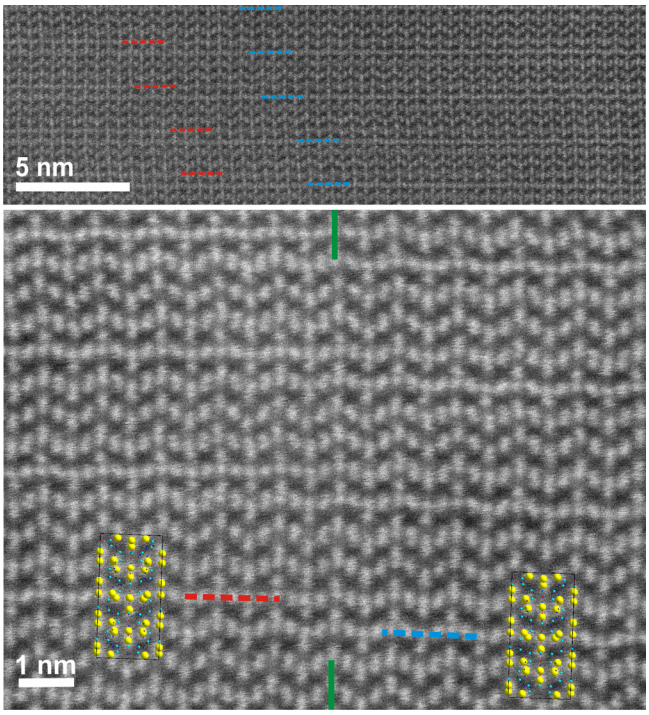


**Figure 6.** STEM-HAADF images along [001] at different magnifications with structure projections (unit cell contents) of $La_3BaSi_5N_9O_2$, antiphase boundary highlighted with green lines and domain positions visualized by red and blue lined.

### 4.2.3.5 Luminescence

Luminescence measurements were performed on isolated aggregates of $La_3BaSi_5N_9O_2:Ce^{3+}$ (2 mol% $Ce^{3+}$, nominal composition). All particles show comparable yellow emission under irradiation with blue light. Exemplary emission and excitation spectra are depicted in Figure 7. Excitation at 440 nm yields an emission spectrum with the characteristic broadband

emission of the 5d-4f transition of $Ce^{3+}$. The emission band peaks at 578 nm with a fwhm of ~167.4 nm (~4700 $cm^{-1}$) and CIE (Commission Internationale de l'Éclairage) color coordinates of $x = 0.464$ and $y = 0.493$. The excitation spectrum shows a broad band with maximum intensity at approximately 385-455 nm, thus the material can be excited very well by blue light as originating from a (Ga,In)N-LED.

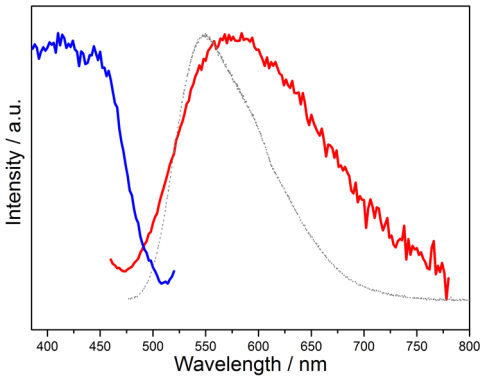


**Figure 7.** Excitation (blue) and emission (red) spectra of $La_3BaSi_5N_9O_2:Ce^{3+}$ in comparison to the emission of a $YAG:Ce^{3+}$ sample (gray).

Emissions comparable to $La_3BaSi_5N_9O_2:Ce^{3+}$ are also observed by other industrially applied LED phosphor materials such as $(La,Ca)_3Si_6N_{11}:Ce^{3+}$ ($\lambda_{em}$ = 577-581 nm; fwhm ~3800 $cm^{-1}$),[18] $CaAlSiN_3:Ce^{3+}$ ($\lambda_{em}$ = 580 nm; fwhm ~3900 $cm^{-1}$),[56] and $YAG:Ce^{3+}$ ($\lambda_{em}$ = 550-570 nm; fwhm ~3700 $cm^{-1}$).[57] These compounds as well as $La_3BaSi_5N_9O_2:Ce^{3+}$ show a relatively broad emission with double band shape as the $4f^1$ ground state configuration of $Ce^{3+}$ yields two levels separated by approximately 2000 $cm^{-1}$.[58] Compared to the emission of $YAG:Ce^{3+}$ (Figure 7, $\lambda_{em}$ = 550 nm; fwhm ~2994 $cm^{-1}$, $x = 0.432$ and $y = 0.549$) $La_3BaSi_5N_9O_2:Ce^{3+}$ shows a red-shifted and a markedly broader emission, so that a broader color range can be covered. Both aspects lead to a warmer color temperature under excitation with blue light. The warmer color temperature is also proven by the CIE diagram (Figure 8). The color coordinates of $La_3BaSi_5N_9O_2:Ce^{3+}$ and $YAG:Ce^{3+}$ are positioned in the yellow spectral range. The combination with a 450 nm InGaN LED yields white 1pc-LEDs, whereas the combination with $La_3BaSi_5N_9O_2:Ce^{3+}$ leads to a crossing of the blackbody curve at a warmer correlated color temperature (~4000 K) than that with $YAG:Ce^{3+}$ (~10000 K). The broad emission spectrum of $La_3BaSi_5N_9O_2:Ce^{3+}$ most likely originates from the superposition of light emitted from multiple chemically different sites.[59] Moreover the asymmetric coordination of the sites might increase the width of the emission, as asymmetric dopant site environment leads

to stronger structural relaxation around the activator in its excited state and consequently to a broad, red-shifted emission.[59] Since $La_3BaSi_5N_9O_2:Ce^{3+}$ shows a large number of different substitutable sites, which are additionally asymmetrically coordinated (Figure 4), its host lattice is especially suitable for broad band emission

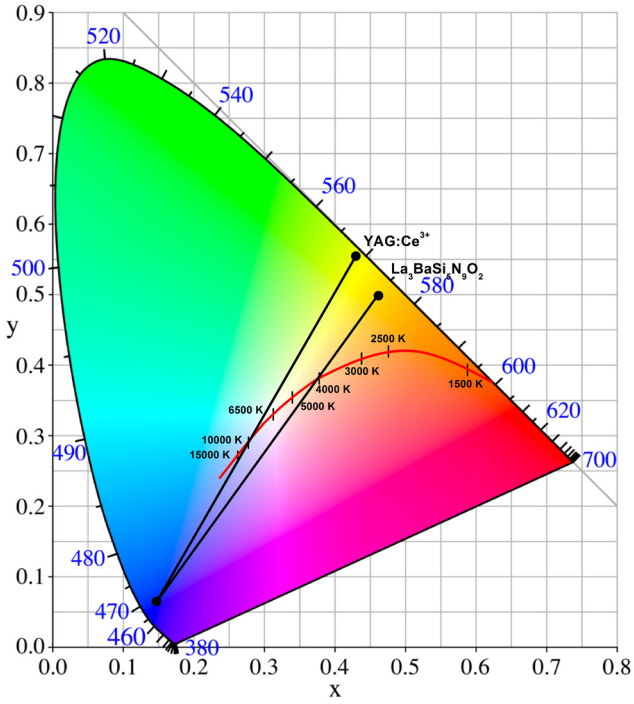


**Figure 8.** CIE 1931 chromaticity diagram showing the color coordinates of $La_3BaSi_5N_9O_2:Ce^{3+}$ and the $YAG:Ce^{3+}$ sample.

## 4.2.4 Conclusion

The lanthanum barium nitridosilicate $La_3BaSi_5N_9O_2:Ce^{3+}$ could be obtained from reactive starting materials. It exhibits a new type of interrupted tetrahedra network and shows intense yellow emission under irradiation of blue light. Compared to $YAG:Ce^{3+}$, the emission yields a warmer color temperature. This synthesis approach might offer an intriguing way to new lanthanum nitridosilicates, which might have potential as phosphors for pc-LEDs.

By combination of TEM and synchrotron microfocus diffraction, it was possible to analyze the small crystals of $La_3BaSi_5N_9O_2:Ce^{3+}$, which occur as aggregates of crystals with a maximum size of only a few µm. Compared with other methods for micro- or nanocrystal analysis like ADT and RED, this approach allows for a precise structure refinement, which e.g.

clearly reveals split positions and renders data suitable for BVS calculations. Consequently, this method is a powerful tool for the analysis of single particles of new promising phosphors, even with complicated structures not accessible by powder X-ray diffraction or conventional single-crystal measurements. With a detailed knowledge of their structures, it might be possible to draw conclusions about the relation between structures and properties which is necessary for a systematic tuning of the luminescence properties. Moreover, the information on the crystal structures could probably accelerate the development of syntheses to phase-pure samples. Both aspects could help to push forward the research of phosphor materials for LEDs.

## 4.2.5 References

[1] J. Heber, *Nat. Phys.* **2014**, *10*, 791.

[2] E. F. Schubert, J.-K. Kim, *Science* **2005**, *308*, 1274.

[3] M. S. Shur, A. Zukauskas, *Proc. IEEE* **2005**, *93*, 1691.

[4] Y. Narukawa, J. Narita, T. Sakamoto, T. Yamada, H. Narimatsu, M. Sano, T. Mukai, *Phys. Status Solidi A* **2007**, *204*, 2087.

[5] J. Y. Tsao, M. E. Coltrin, M. H. Crawford, J. A. Simmons, *Proc. IEEE* **2010**, *98*, 1162.

[6] A. A. Setlur, *Electrochem. Soc. Interface* **2009**, *18*, 32.

[7] D. J. Robbins, *J. Electrochem. Soc.* **1979**, *126*, 1550.

[8] M. Zeuner, S. Pagano, W. Schnick, *Angew. Chem. Int. Ed.* **2011**, *50*, 7754.

[9] R. Müller-Mach, G. Müller, M. R. Krames, H. A. Höppe, F. Stadler, W. Schnick, T. Jüstel, P. Schmidt, *Phys. Status Solidi A* **2005**, *202*, 1727.

[10] Y. Q. Li, J. E. J. van Steen, J. W. H. van Krevel, G. Botty, A. C. A. Delsing, F. J. DiSalvo, G. de With, H. T. Hintzen, *J. Alloys Compd*. **2006**, *417*, 273.

[11] M. R. Krames, G. O. Müller, R. B. Müller-Mach, H.-H. Bechtel, P. J. Schmidt, *PCT Int. Appl.* WO 2010131133, A1, **2010**.

[12] H. A. Höppe, H. Lutz, P. Morys, W. Schnick, A. Seilmeier, *J. Phys. Chem. Solids*, **2000**, *61*, 2001.

[13] R.-J. Xie, N. Hirosaki, K. Sakuma, Y. Yamamoto, M. Mitomo, *Appl. Phys. Lett.* **2004**, *84*, 5404.

[14] R.-J. Xie, N. Hirosaki, M. Mitomo, Y. Yamamoto, T. Suehiro, K. Sakuma, *J. Phys. Chem. B* **2004**, *108*, 12027.

[15] K. Uheda, N. Hirosaki, H. Yamamoto, *Phys. Status Solidi A* **2006**, *203*, 2712.

[16] K. Uheda, N. Hirosaki, Y. Yamamoto, A. Naito, T. Nakajima, H. Yamamoto, *Electrochem*. *Solid-State Lett.* **2006**, *9*, H22.

[17] S. Schmiechen P. Pust, P. J. Schmidt, W. Schnick, *Nachr. Chem.* **2014**, *62*, 847.

[18] T. Suehiro, N. Hirosaki, R.-J. Xie, *Appl. Mater. Interfaces* **2011**, *3*, 811.

[19] N. Hirosaki, T. Takeda, S. Funahashi, R.-J. Xie, *Chem. Mater.* **2014**, *26*, 4280.

[20] F. Fahrnbauer, T. Rosenthal, T. Schmutzler, G. Wagner, G. B. M. Vaughan, J. P. Wright, O. Oeckler, *Angew. Chem. Int. Ed.* **2015**, *54*, 10020.

[21] U. Kolb, T. Gorelik, C. Kübel, M. T. Otten, D. Hubert, *Ultramicroscopy* **2007**, *107*, 507.

[22] U. Kolb, T. Gorelik, M. T. Otten, *Ultramicroscopy* **2008**, *108*, 763.

[23] E. Mugnaioli, T. Gorelik, U. Kolb, *Ultramicroscopy* **2009**, *109*, 758.

[24] U. Kolb, E. Mugnaioli, T. E. Gorelik, *Cryst. Res. Technol.* **2011**, *46*, 542.

[25] D. Zhang, P. Oleynikov, S. Hovmöller, X. Zou, *Z. Kristallogr.* **2010**, *225*, 94.

[26] B. Gieger, H. Jacobs, C. Hadenfeldt, *Z. Anorg. Allg. Chem.* **1974**, *410*, 104.

[27] H. Lange, G. Wotting, G. Winter, *Angew. Chem. Int. Ed.* **1991**, *30*, 1579.

[28] W. Schnick, H. Huppertz, R. Lauterbach, *J. Mater Chem.* **1999**, *9*, 289.

[29] *Digital Micrograph*, Gatan Software Team, Pleasanton, USA, **1999**, v3.6.1.

[30] P. A. Stadelmann, *JEMS*, CIME-EPFL, Ecublens, Switzerland, **1999-2008**, v3.3425U2008.

[31] *ES Vision*, Emispec Systems Inc., Tempe, USA, **1994 - 2002**, v4.0.164.

[32] *TEAM*, EDAX AMETEK, Wiesbaden, Germany, **2013**, v3.4.1.

[33] J. C. Labiche, O. Mathon, S. Pascarelli, M. A. Newton, G. G. Ferre, C. Curfs, G. Vaughan, A. Homs, D. F. Carreiras, *Rev. Sci. Instrum.* **2007**, *78*, 091301.

[34] G. B. M. Vaughan, J. P. Wright, A. Bytchkov, C. Curfs, C. Grundlach, M. Orlova, L. Erra, H. Gleyzolle, T. Buslaps, A. Götz, G. Suchet, S. Petitdemange, M. Rossat, L. Margulies, W. Ludwig, A. Snigirey, I. Snigireva, H. O. Sorensen, E. M. Lauridsen, U. L. Olsen, J. Oddershede, H. F. Poulsen, *Science* **2010**, 457.

[35] J. L. Chambers, K. L. Smith, M. R. Pressprich, Z. Jin, *SMART*, Bruker-AXS, Madison, USA, **1997-1998**, v. 5.059.

[36] *SAINT*, Bruker-AXS, Madison, USA, **1997-2002**, v. 6.36A.

[37] G. M. Sheldrick, *SADABS, Multi-Scan Absorption Correction*, Bruker-AXS, WA, USA, **2012**, v. 2.

[38] G. Wu, B. L. Rodrigues, P. Coppens, *J. Appl. Crystallogr.* **2002**, *35*, 356.

[39] G. M. Sheldrick, *Acta Crystallogr., Sect. A* **2008**, *64*, 112.

[40] *WINXPOW, Program for powder data handling*, Stoe & Cie GmbH, Darmstadt, Germany, **2007**, v. 2.21.

[41] A. Coelho, *TOPAS Academic* 2007, Coelho Software, Brisbane, Australia, **2007**.

[42] W. Grochala, P. Edwards, *Chem. Rev.* **2004**, *104*, 1283.

[43] Further details of the crystal structure investigation can be obtained from the Fachinformationszentrum Karlsruhe, 76344 Eggenstein-Leopoldshafen, Germany (fax: (+49)7247-808-666; e-mail: crysdata@fiz-karlsruhe.de) on quoting the depository number CSD- 429510.

[44] F. Liebau, *Structural Chemistry of Silicates*, Springer, Berlin, **1985**.

[45] The term *dreier* (*sechser*, *zehner*) ring was coined by Liebau and is derived from the German word “drei” (“sechs”, “zehn”); a *dreier* (*sechser, zehner*) ring comprises three (six, ten) tetrahedra centers.

[46] C. Schmolke, O. Oeckler, D. Bichler, J. Johrendt, W. Schnick, *Chem. Eur. J.* **2009**, *15*, 9215.

[47] a) V. A. Blatov, M. O’Keeffe, D. M. Proserpio, *CrystEngComm* **2010**, *12*, 44; b) V. A. Blatov, A. P. Shevchenko, D. M. Proserpio, *Cryst. Growth Des.* **2014**, *14*, 3576.

[48] T. Schlieper, W. Milius, W. Schnick, *Z. Anorg. Allg. Chem.* **1995**, *621*, 1380.

[49] J. Feschle, *Z. Kristallogr.* **1971**, *133*, 364.

[50] R. D. Shannon, *Acta Crystallogr. Sect. A.* **1976**, *32*, 751.

[51] C. Schmolke, S. Lupart, W. Schnick, *Solid State Sci.* **2009**, *11*, 305.

[52] H. Katscher, G. Bissert, F. Liebau, *Z. Kristallogr.* **1973**, *137*, 146.

[53] A. C. Tas, M. Akinc, *J. Am. Ceram. Soc.* **1994**, *77*, 2968.

[54] A. S. Wills, *VaList,* University College London, UK, **2010**, v. 4.0.7.

[55] P. E. D. Morgan, *J. Mater. Sci.* **1986**, *21*, 4305.

[56] Y. Q. Li, N. Hirosaki, R.-J. Xie, T. Takeda, M. Mitomo, *Chem. Mater.* **2008**, *20*, 6704.

[57] T. Moriguchi, Y. Noguchi, K. Sakanao, Y. Shimizu, US 5998925 A, **1997**.

[58] G. Blasse, B. C. Grabmaier, Luminescent Materials, Springer, Berlin, Heidelberg, NY, **1994**.

[59] A. Meijerink, G. Blasse, *J. Lumin.* **1989**, *43*, 283.

# 4.3 $La_6Ba_3[Si_{17}N_{29}O_2]Cl$ – An Oxonitridosilicate Chloride with Exceptional Structural Motifs

published in: *Inorg. Chem.* **2015**, *54*, 8727-8732

authors: Dajana Durach, Felix Fahrnbauer, Oliver Oeckler and Wolfgang Schnick

DOI: 10.1021/acs.inorgchem.5b01368



http://pubs.acs.org/doi/abs/10.1021/acs.inorgchem.5b01368

**Abstract.** The oxonitridosilicate chloride $La_6Ba_3[Si_{17}N_{29}O_2]Cl$ was synthesized by a high-temperature reaction in a radiofrequency furnace starting from $LaCl_3$, $BaH_2$, and the ammonolysis product of $Si_2Cl_6$. Diffraction data of a micrometer-sized single crystal were obtained using microfocused synchrotron radiation at beamline ID11 of the ESRF. EDX measurements on the same crystal confirm the chemical composition. The crystal structure [space group $P6_3/m$ (no. 176), $a = 9.8117(14)$, $c = 19.286(6)$ Å, $Z = 2$] contains an unprecedented interrupted three-dimensional network of vertex-sharing $SiN_4$ and $SiN_3O$ tetrahedra. The $SiN_4$ tetrahedra form *dreier* rings. Twenty of the latter condense in a way that the Si atoms form icosahedra. Each icosahedron is connected to others via six $SiN_4$ tetrahedra that are part of *dreier* rings and via six $Q^3$-type $SiN_3O$ tetrahedra. Rietveld refinements confirm that the final product contains only a small amount of impurities. Lattice energy (MAPLE) and bond-valence sum (BVS) calculations show that the structure is electrostatically well balanced. Infrared spectroscopy confirms the absence of N-H bonds.

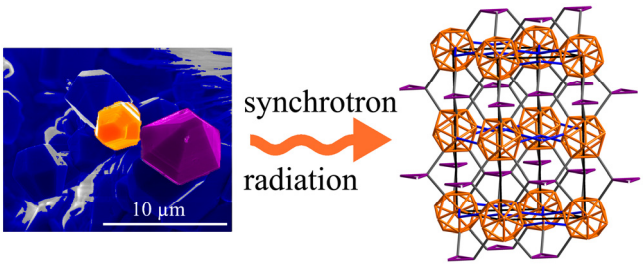

## 4.3.1 Introduction

Silicon and oxygen are the most abundant elements in the earth's crust, and more than 1000 representatives of silicate structures are known. Among others, silicates find applications in ceramics and glass industries. Nonoxidic ceramics exhibit pronounced covalent bonding character which results generally in high mechanical, thermal, and chemical stability.[1] In this context, (oxo)nitridosilicates turned out to be a promising extension of the classical silicate materials class.[2] In addition, compounds like $Li_2SiN_2$, $Li_8SiN_4$, and $Li_{14}Ln_5[Si_{11}N_{19}O_5]O_2F_2$, with Ln = Ce and Nd, emerged as lithium ion conductors, which makes them interesting for potential applications in lithium batteries.[3-7] Moreover, nitridosilicates such as $M_2Si_5N_8$ with M = Ca and Sr seem suitable as nonlinear optical (NLO) materials.[8] Nowadays, $Eu^{2+}$-doped (oxo)nitridosilicates are indispensable luminescence materials for phosphor-converted light-emitting diodes (pc-LEDs).[9,10] The reason for the diverse and tunable properties of these compounds lies in their broad structural variety. The structural entities of oxosilicates are largely limited to $SiO_4$ tetrahedra with either terminal $O^{[1]}$ or singly bridging $O^{[2]}$ atoms. In contrast, (oxo)nitridosilicates are typically built up from $Si(O,N)_4$ tetrahedra with $N^{[1]}$, $N^{[2]}$, $N^{[3]}$, and $N^{[4]}$ atoms bridging up to four neighboring tetrahedral centers. This variability allows for a wide range of additional structural possibilities. Moreover, except for fibrous $SiO_2$,[11] whose existence has not yet been proven unequivocally, $SiO_4$ tetrahedra share only common vertices, whereas nitridosilicates can contain both vertex- and edge-sharing tetrahedra.[12] Due to these structural possibilities and the resulting outstanding properties, the search for novel (oxo)nitridosilicates has been pursued frequently. Synthetic approaches like high-temperature syntheses, flux methods, and precursor routes enabled suitable access to this compound class.[13-15] However, syntheses often lead to inhomogeneous samples containing microcrystalline compounds. This situation impedes structure determination by means of conventional single-crystal or powder X-ray diffraction. However, diffraction data of micrometer-sized single crystals can be acquired using synchrotron radiation as recently developed Be and Al lenses allow unprecedented brilliance by microfocusing.[16-19] This approach leads to the structure elucidation of the novel compound $La_6Ba_3[Si_{17}N_{29}O_2]Cl$, one of the few oxonitridosilicate chlorides among $Nd_{10}Si_{10}O_9N_{17}Cl$,[20] $Ln_4Si_4O_{3+x}N_{7-x}Cl_{1-x}O_x$ (Ln = Ce, Pr, Nd; $x \approx 0.2$),[21] and $Ba_3Si_3N_5OCl$.[22]

## 4.3.2 Experimental Section

### 4.3.2.1 Synthesis

For the synthesis of $La_6Ba_3[Si_{17}N_{29}O_2]Cl$, $LaCl_3$ (23.2 mg, 0.095 mmol, 99.99%, Alfa Aesar), "$Si_2(NH)_3{\cdot}6NH_4Cl$"[23] (100.0 mg, 0.237 mmol), and $BaH_2$ (66.7 mg, 0.479 mmol, 99.7%, Materion) were thoroughly ground in an agate mortar and filled into a tungsten crucible. These steps were performed under argon atmosphere in a glovebox (Unilab, MBraun, Garching; $O_2 < 1$ ppm; $H_2O < 1$ ppm). Then the crucible was placed into a radiofrequency furnace (type AXIO 10/450, max electrical output 10 kW, Hüttinger Elektronik, Freiburg),[13] heated under $N_2$ atmosphere to 900 °C within 5 min, subsequently heated to 1600 °C within 4 h, and finally quenched to room temperature by switching off the furnace. The reaction affords an inhomogeneous sample with small, turquoise crystals of $La_6Ba_3[Si_{17}N_{29}O_2]Cl$ which are resistant to hydrolysis. To remove soluble byproducts the sample was washed with water. Addition of $CeF_3$ or $EuF_3$ (0.4 mg, 0.002 mmol, 99.99%, Alfa Aesar/0.4 mg, 0.002 mmol, 99.99% Aldrich) as doping agent to the reaction mixture results in no marked change of color and does not lead to luminescence of the crystals of $La_6Ba_3[Si_{17}N_{29}O_2]Cl$.

### 4.3.2.2 Elemental Analysis and Spectroscopy

The chemical composition and morphology of the crystals were analyzed with a LEO 1530 field-emission scanning electron microscope (SEM) operated at 20 kV and equipped with an energy-dispersive Si/Li detector 7418 (Oxford Instruments). To provide electrical conductivity on the sample surface it was coated with carbon (electron beam evaporator CED 030, Balzers). Fourier transform infrared (FTIR) spectroscopy was carried out with a PerkinElmer BXII spectrometer mounting ATR (attenuated total reflection) technology.

### 4.3.2.3 Crystal Structure Analysis

For single-crystal structure investigations, crystals of $La_6Ba_3[Si_{17}N_{29}O_2]Cl:Ce^{3+}$ were mounted on Kapton foil sample holders (micromount, MiTeGen, Ithaca). X-ray diffraction data were collected at beamline ID11 of the ESRF in Grenoble (Ge(111) double-crystal monochromator, Frelon 2K CCD detector).[24] The beam ($\lambda = 0.33510$ Å) was focused to ~4.5 µm in the horizontal direction and ~2 µm in the vertical direction with a beryllium lens system.[16] The reflections of the dominant crystal in an aggregate were indexed with SMART,[25] integrated with SAINT,[26] and semi-empirically absorption corrected using SADABS.[27] In addition, a

correction was applied in order to account for the systematic error owing to the diffraction-angle dependence of the beam path length through the CCD phosphor.[28] The structure was solved by direct methods and refined by full matrix least-squares methods with SHELX.[29] Powder X-ray diffraction data were collected with a STOE STADI P diffractometer (Mo $K\alpha_1$ radiation, $\lambda$ = 0.70930 Å, Ge(111) monochromator, MYTHEN 1K detector) in modified Debye-Scherrer geometry. Rietveld refinement was carried out using the TOPAS-Academic package.[30]

## 4.3.3 Results and Discussion

### 4.3.3.1 Synthesis and Sample Characterization

$La_6Ba_3[Si_{17}N_{29}O_2]Cl$ was synthesized at high temperature, the driving force presumably being the decomposition of $BaH_2$ around 675 °C[31] and its reaction to $BaCl_2$ with chlorine originating from $LaCl_3$. Among other intermediates, probably La metal is formed, which reacts with the remaining Ba, $LaCl_3$, and the precursor "$Si_2(NH)_3{\cdot}6NH_4Cl$" to form turquoise crystals of $La_6Ba_3[Si_{17}N_{29}O_2]Cl$ (Figure 1). The incorporated O supposably originates from contamination of commercially acquired starting materials.

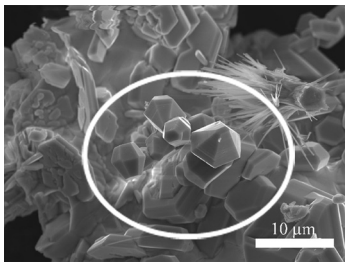


**Figure 1.** SEM image of crystals of $La_6Ba_3[Si_{17}N_{29}O_2]Cl:Ce^{3+}$ (white circle).

Crystal structure investigations were performed on a crystal of a sample doped with $Ce^{3+}$ (see above). Consequently, the same crystal was used for EDX analysis, which yields an average composition of La/Ba/Si/Cl/Ce = 6.0:3.5:13.3:1.0:0.14 (normalized according to the La content; four-point measurements at different positions; the atomic content of N and O was excluded as they are underdetermined, due to the limitations of the method). The heavy element ratios are in good agreement with the sum formula obtained from single-crystal structure refinement, which is consistent with bond-valence sum (BVS) and MAPLE

(Madelung part of lattice energy) calculations (see below). The absence of N-H and O-H groups was confirmed by infrared spectroscopy (Figure S2, Supporting Information). Consequently, the combination of the results of EDX measurements and infrared spectroscopy excludes the presence of elements other than La, Ba, Si, N, O, Cl, and Ce. In order to determine the bulk phase composition of the washed sample, a Rietveld refinement of powder X-ray diffraction data was performed (Figure S1, Table S1). It shows that the sample contains $La_6Ba_3[Si_{17}N_{29}O_2]Cl$ as the main phase and $BaCl_2$ as byproduct. A few weak reflections cannot be ascribed to any known compound.

#### 4.3.3.2 Crystal Structure of $La_6Ba_3[Si_{17}N_{29}O_2]Cl$

Due to the limited scattering power of the micrometer-sized crystals, microfocused synchrotron radiation was used for single-crystal investigations. As it was impossible to isolate and handle such tiny single crystals, the investigated sample consisted of several fragments; however, the reflections of one individual could be selected in a straightforward fashion and yielded a data set with high quality. The crystal structure of $La_6Ba_3[Si_{17}N_{29}O_2]Cl$ was solved and refined in space group $P6_3/m$ (no. 176) with $a = 9.8117(14)$ Å and $c = 19.286(6)$ Å. In the refinement as well as for BVS and MAPLE calculations, $Ce^{3+}$ was neglected because of its insignificant contribution to the scattering density. The distribution of La and Ba as well as of N and O was fixed as indicated by MAPLE and BVS calculations; for detailed explanations see the sections on Bond-Valence Sum Calculations and MAPLE Calculations below. The crystallographic data of $La_6Ba_3[Si_{17}N_{29}O_2]Cl$ are summarized in Table 1, and the atomic parameters are listed in Table 2. All atoms were refined anisotropically (Table S2 in the Supporting Information).[32]

**Table 1.** Crystallographic Data and Details of the Structure Refinement of $La_6Ba_3[Si_{17}N_{29}O_2]Cl$ at Room Temperature.

| | |
|---|---|
| formula | $La_6Ba_3[Si_{17}N_{29}O_2]Cl$ |
| cryst. syst. | hexagonal |
| space group | $P6_3/m$ (no. 176) |
| $a$ (Å) | 9.8117(14) |
| $c$ (Å) | 19.286(6) |
| cell volume (Å$^3$) | 1607.9(7) |
| $Z$ | 2 |
| density (g·cm$^{-3}$) | 4.54 |
| μ (mm$^{-1}$) | 1.611 |
| radiation | synchrotron (λ = 0.33510 Å, ID11 at ESRF) |
| $F$(000) | 1968 |
| θ range (deg) | 1.96 ≤ θ ≤ 14.70 |
| total no. of reflns | 21886 |
| no. of independent reflns | 1985 [$R$(int) = 0.0304] |
| no. of refined params | 95 |
| extinction param | 0.0031 |
| GOF | 1.30 |
| $R$1 (all data/for $F^2 > 2\sigma(F^2)$) | 0.0171/0.0169 |
| $wR$2 (all data/for $F^2 > 2\sigma(F^2)$) | 0.0397/0.0396 |
| $\Delta\rho_{max}$, $\Delta\rho_{min}$ (e/Å$^3$) | 1.755; −1.051 |

**Table 2.** Atomic Coordinates, Isotropic Displacement Parameters, and Site Occupancies of $La_6Ba_3[Si_{17}N_{29}O_2]Cl$ at Room Temperature.[a]

| atom | | *x* | *y* | *Z* | $U_{eq}$ [Å$^2$] | s.o.f. |
|---|---|---|---|---|---|---|
| La1 | 12*i* | 0.53306(2) | 0.47894(2) | 0.39098(2) | 0.00793(5) | 1 |
| Ba2 | 6*h* | 0.16199(3) | 0.29913(3) | ¼ | 0.01178(6) | 1 |
| Si1 | 6*h* | 0.75300(9) | 0.54355(9) | ¼ | 0.00492(13) | 1 |
| Si2 | 4*f* | 2/3 | 1/3 | 0.50460(5) | 0.00530(16) | 1 |
| Si3 | 12*i* | 0.20747(6) | 0.12253(6) | 0.38315(3) | 0.00472(10) | 1 |
| Si4 | 12*i* | 0.67463(7) | 0.81638(6) | 0.46847(3) | 0.00492(10) | 1 |
| N1 | 4*e* | 0 | 0 | 0.36301(16) | 0.0058(5) | 1 |
| N2 | 12*i* | 0.7991(2) | 0.7374(2) | 0.45792(9) | 0.0062(3) | 1 |
| N3 | 12*i* | 0.2345(2) | 0.3081(2) | 0.39609(9) | 0.0067(3) | 1 |
| N4 | 12*i* | 0.5059(2) | 0.3480(2) | 0.52299(10) | 0.0080(3) | 1 |
| N5 | 12*i* | 0.7942(2) | 0.6655(2) | 0.32130(9) | 0.0087(3) | 1 |
| N6 | 6*h* | 0.5486(3) | 0.4142(3) | ¼ | 0.0080(4) | 1 |
| O7 | 4*f* | 2/3 | 1/3 | 0.41468(14) | 0.0086(4) | 1 |
| Cl1 | 4*f* | 1/3 | 2/3 | 0.2718(3) | 0.0542(16) | ½ |

[a]For anisotropic displacement parameters, cf. Table S2 in the Supporting Information.

In contrast to the oxonitridosilicate chlorides $Nd_{10}Si_{10}O_9N_{17}Cl$ and $Ln_4Si_4O_{3+x}N_{7-x}Cl_{1-x}O_x$ (Ln = Ce, Pr, Nd; $x \approx 0.2$), which represent layer silicates,[20,21] and $Ba_3Si_3N_5OCl$, which consists of a zeolite-like framework,[22] the crystal structure of $La_6Ba_3[Si_{17}N_{29}O_2]Cl$ is characterized by an unprecedented interrupted three-dimensional network. It consists of vertex-sharing $Q^4$- and $Q^3$-type $SiN_4/SiN_3O$ tetrahedra with a ratio of $Q^4/Q^3 = 15/2$ (Figure 2), which results in a degree of condensation κ= n(Si):n(N,O) = 0.55. The $Q^3$-type tetrahedra exhibit one terminal $O^{[1]}$ and three singly bridging $N^{[2]}$ atoms, whereas the $Q^4$-type tetrahedra consist of four $N^{[2]}$ or two $N^{[2]}$ and two $N^{[3]}$ (interconnection of three tetrahedra) atoms.

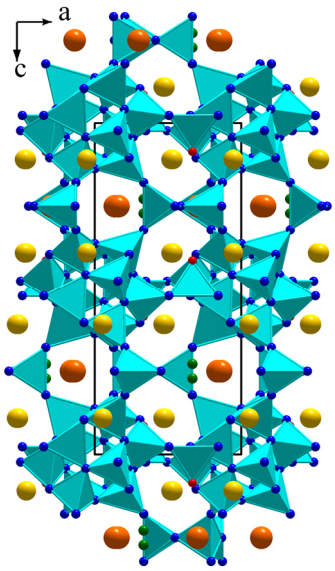


**Figure 2.** Crystal structure of $La_6Ba_3[Si_{17}N_{29}O_2]Cl$ in projection along [010] with $Si(N,O)_4$ tetrahedra (turquoise), N (blue), O (red), La (yellow), Ba (orange), and semi-occupied Cl positions (green); the unit cell is displayed.

The $Q^4$-type $SiN_4$ tetrahedra form *dreier* rings,[33,34] 20 of which condense in a way that the Si atoms form icosahedra (note that in skeletal representations not all edges of this polyhedron correspond to Si-N-Si bonds due to the presence of $N^{[3]}$ atoms, Figure 3e). Each icosahedron is connected to others via six $SiN_4$ tetrahedra that are part of *dreier* rings and via six $Q^3$-type $SiN_3O$ tetrahedra (Figure 3a, 3b, 3d, and 3e). In addition, the structure is characterized by *sechser* and *siebener* rings, which are built up by the tetrahedra of the Si atoms of the icosahedra and the $Q^3$-type tetrahedra. Six edges of the icosahedron are part of the *sechser* rings, and 18 edges are part of the *siebener* rings (Figure 3f and 3g). The novel topology of the framework is characterized by the point symbol $\{3.6.7^4\}_3\{3^5.4^5.6^2.7^3\}_{12}\{6^3\}_2$ as calculated with the program TOPOS.[35] Despite the complexity of the network it is a hierarchical derivative[36, 37] of the simple NiAs structure type,[38] with the centers of the icosahedra on the Ni and the centers of the *dreier* rings on the As positions (Figure 3c).

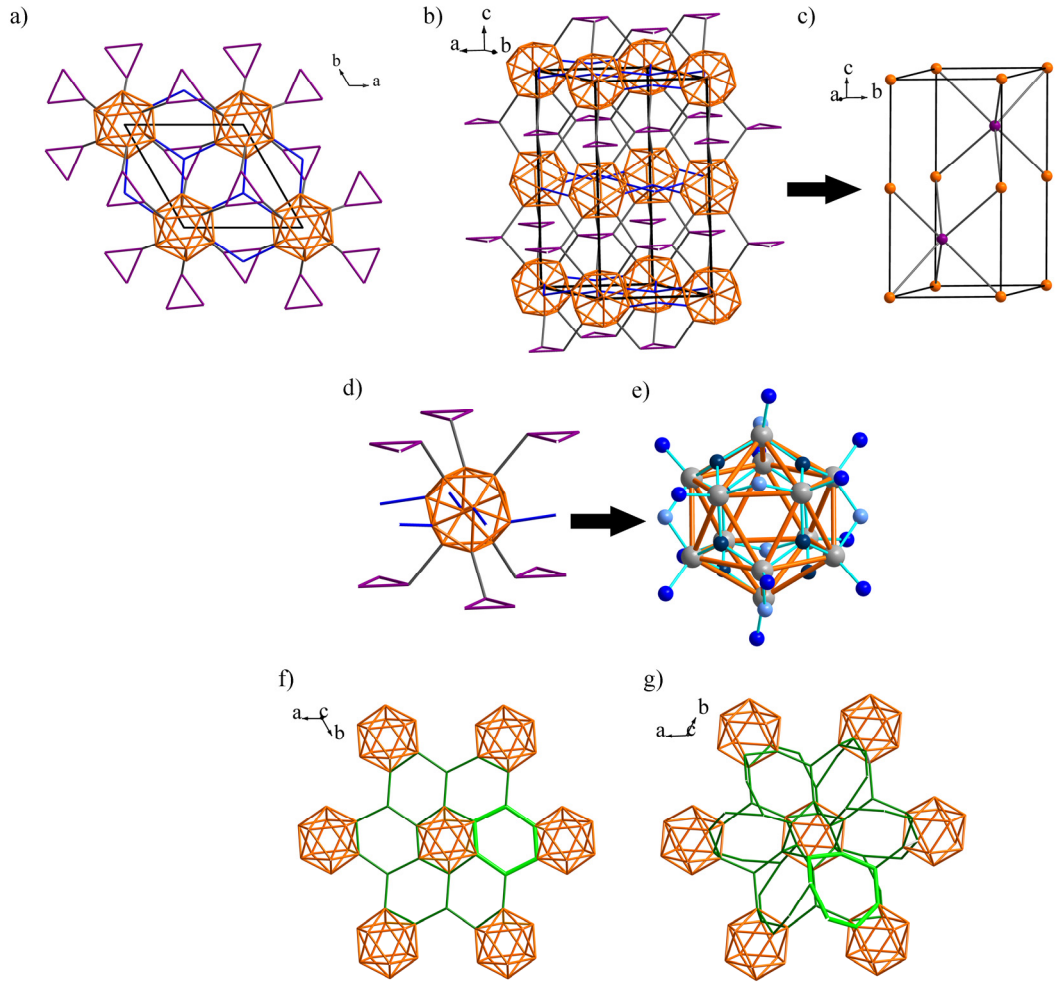


**Figure 3.** (a and b) Topological representations of $La_6Ba_3[Si_{17}N_{29}O_2]Cl$; (c) simplification of the topology of $La_6Ba_3[Si_{17}N_{29}O_2]Cl$ as a variant of the NiAs structure type (centers of icosahedra orange; centers of *dreier* rings violet); (d) icosahedra (orange) connected via six *dreier* rings (violet) and six $Q^3$-type tetrahedra (blue) as characteristic buildings blocks of the silicate network; (e) interconnection of the Si atoms of one icosahedron (Si gray; $N^{[3]}$ dark blue; $N^{[2]}$ blue/light blue); due to the presence of $N^{[3]}$ atoms only each Si-$N^{[2]}$-Si bond corresponds to an edge of the icosahedron; (f and g) topological representation of the *sechser* and *siebener* rings (green); each connecting line of the *dreier*, *sechser*, and *siebener* rings represents a Si-N-Si bond.

$La_6Ba_3[Si_{17}N_{29}O_2]Cl$ contains a half-occupied Cl split position (Table 2). This site is coordinated by three Ba atoms forming a decentered trigonal coordination sphere (Figure 4a). A similar coordination of Cl atoms was observed in other oxo- and oxonitridosilicates, e.g., $Nd_{10}[Si_{10}O_9N_{17}]Cl$[20] and $Tb_3Cl_5[SiO_4]$.[39] Additionally, the refined crystal structure exhibits two crystallographically independent heavy-atom sites. BVS as well as MAPLE calculations (Table 3 and 4) indicate one La and one Ba site (Table 2). La is 7-fold coordinated by six N and one O atom, which results in a distorted single-capped octahedron

(Figure 4b). The Ba site is irregularly coordinated by nine N atoms and the Cl split position (50%/50%) (Figure 4c).

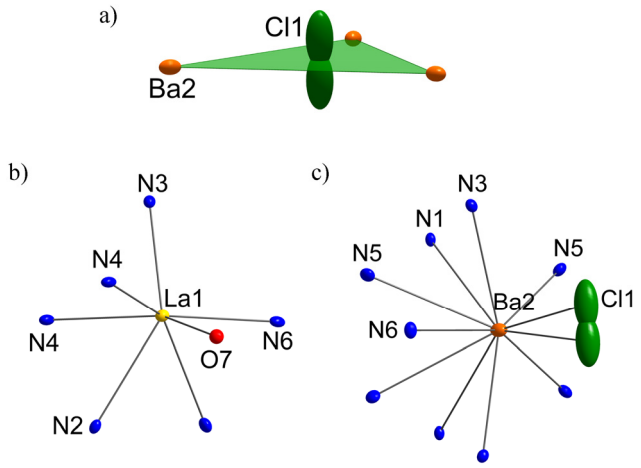


**Figure 4.** Coordination sphere of the Cl split position (a) and the heavy-atom sites (b and c) of $La_6Ba_3[Si_{17}N_{29}O_2]Cl$ (anisotropic displacement ellipsoids with 60% probability).

The distances Si-N [1.6914(18)-1.8145(9) Å] and Si-O [1.734(3) Å] are in good agreement with other (nitrido)silicates as well as the La-N [2.5361(19)-2.8796(18) Å] and Ba-N [2.8725(19)-3.374(3) Å] distances.[40-43] The La-O [2.4168(6) Å] and Ba-Cl [3.1535(8) Å] distances correspond to those in other lanthanum or barium compounds.[44,45] Additionally, all mentioned distances are in good agreement with the sum of the ionic radii.[46]

#### 4.3.3.3 Bond-Valence Sum Calculations

As mentioned before, BVS calculations[47] were performed in order to reasonably assign sites to N or O and La or Ba, respectively, despite their very similar X-ray scattering factors. Charge neutrality alone can be preserved by arbitrary exchange of LaN and BaO units and thus is not a sufficient constraint in structure refinements. Pauling's rules[48] and the fact that $X^{[3]}$ (X = N,O) is usually not occupied by O served as a basis. Consequently, the bridging anion positions were assumed to be occupied by N and the terminal anion positions by O. This assumption is corroborated by neutron powder diffraction of other oxonitridosilicates, where a similar contribution of N and O was observed.[21] On the basis of this O/N distribution, the BVS of the cations and anions were determined (Table 3) and indicate one La and one Ba site. This leads to a charge-neutral formula, which is additionally corroborated by EDX measurements.

**Table 3.** Bond-Valence Sums for $La_6Ba_3[Si_{17}N_{29}O_2]Cl$ and Expected Oxidation States.

| | BVS | oxidation state |
|---|---|---|
| La1 | 3.05 | +3 |
| Ba2 | 2.14 | +2 |
| Si1 | 3.82 | +4 |
| Si2 | 4.02 | +4 |
| Si3 | 3.78 | +4 |
| Si4 | 3.89 | +4 |
| Cl | 0.46 | -1[i] |
| N1[3] | 2.66 | -3 |
| N2[3] | 3.08 | -3 |
| N3[2] | 2.97 | -3 |
| N4[2] | 3.07 | -3 |
| N5[2] | 3.02 | -3 |
| N6[2] | 2.54 | -3 |
| O7[1] | 2.20 | -2 |
| | | [i] sof = ½ |

#### 4.3.3.3 MAPLE Calculations

In order to further confirm the electrostatic consistency of the crystal structure, lattice energies were calculated using the MAPLE concept (Table 4).[46,49-51] This solely takes into account electrostatic interactions, which depend on the coordination spheres, the charge, and the distances of the constituting ions. As the MAPLE software cannot consider partially occupied positions, an idealized structure model of $La_6Ba_3[Si_{17}N_{29}O_2]Cl$ was set up by shifting Cl from Wyckoff position 4*f* (point symmetry: 3..; $x = 1/3$, $y = 2/3$, $z = 0.2718$) to a fully occupied "average" Wyckoff position 2*c* (point symmetry: $\bar{6}$..; $x = 1/3$, $y = 2/3$, $z = 1/4$). The calculated partial MAPLE values of La, Ba, Si, N, and O are consistent with the characteristic ranges.[2,52-55] The partial MAPLE value of Cl is slightly smaller than reference values.[56,57] Therefore, as the exchange of the La and Ba position with consideration of charge neutrality leads to MAPLE values outside of the characteristic ranges, the occupation of the atoms sites is corroborated. The minor deviation of 0.27% of the overall MAPLE value of $La_6Ba_3[Si_{17}N_{29}O_2]Cl$ and the sum of those of the binary compounds that formally constitute $La_6Ba_3[Si_{17}N_{29}O_2]Cl$ confirms the electrostatic balance of the refined crystal structure.

**Table 4.** Partial MAPLE Values and MAPLE Sums [kJ/mol] for $La_6Ba_3[Si_{17}N_{29}O_2]Cl$ as Well As Typical Partial MAPLE Values.

| $La_6Ba_3[Si_{17}N_{29}O_2]Cl$ | BVS | typical partial MAPLE values[2,52-56] |
|---|---|---|
| La1 | 4032 | $Ln^{3+}$: 3500-5100 |
| Ba2 | 1708 | $Ba^{2+}$: 1500-2000 |
| Si1 | 10264 | $Si^{4+}$: 9000-10200 |
| Si2 | 9978 | |
| Si3 | 9677 | |
| Si4 | 9776 | |
| Cl | 289 | $Cl^-$: 307-357 |
| $N1^{[3]}$ | 5835 | $N^{[3]3-}$: 5000-6200 |
| $N2^{[3]}$ | 6084 | |
| $N3^{[2]}$ | 5427 | |
| $N4^{[2]}$ | 5396 | $N^{[2]3-}$: 4600-6000 |
| $N5^{[2]}$ | 5281 | |
| $N6^{[2]}$ | 5100 | |
| $O7^{[1]}$ | 2494 | $O^{[1]2-}$: 2000-2800 |
| | ∑ = 362 093 | |
| $2/3\ La_2O_3 + 14/3\ LaN + 1/2\ BaCl_2 + 5/6\ Ba_3N_2 + 17/3\ \beta\text{-}Si_3N_4 \rightarrow La_6Ba_3[Si_{17}N_{29}O_2]Cl$ | | |
| 9461 + 38 470 + 1103 + 10 129 + 301 963 → | | 361 127<br>Δ = 0.27% |

## 4.3.4 Conclusion

A high-temperature reaction yielded a novel oxonitridosilicate chloride $La_6Ba_3[Si_{17}N_{29}O_2]Cl$, characterized by an unprecedented tetrahedra network. The structure elucidation shows how microfocused synchrotron radiation is well suited to precisely determine the structure of microcrystals even with complex structures which could not be characterized by conventional single-crystal or powder X-ray diffraction. This approach is a powerful tool as knowledge of the structure could foster the development of syntheses to phase-pure samples and by comprehension of the relation between structures and properties which is necessary for a systematic improvement of properties. The usefulness of BVS and MAPLE calculations was demonstrated by applying these methods for a reasonable assignment of N and O as well as of Ba and La. Using $BaH_2$ as a starting material appears essential as it

decomposes and presumably reacts with $LaCl_3$ to $BaCl_2$ and finely dispersed and reactive La. Furthermore, the use of the precursor "$Si_2(NH)_3 \cdot 6NH_4Cl$" seems to play an important role to obtain novel (oxo)nitridosilicates as this starting material provides another stoichiometric proportion of Si and N and another oxidation state of Si as the common precursors $Si_3N_4$ and $Si(NH)_2$.[58] Consequently, this combination of starting materials appears to be a promising route which might lead to the discovery of further new (oxo)nitridosilicates with intriguing structural features and properties.

## 4.3.5 References


[1] A. K. Cheetham, G. Férey, T. Loiseau, *Angew. Chem. Int. Ed.* **1999**, *38*, 3268.

[2] M. Zeuner, S. Pagano, W. Schnick, *Angew. Chem. Int. Ed.* **2011**, *50*, 7754.

[3] J. Lang, J.-P. Charlot, *Rev. Chim. Miner.* **1970**, *7*, 121.

[4] H. Hillebrecht, J. Churda, L. Schröder, H. G. v. Schnering, *Z. Kristallogr. Suppl.* **1993**, *6*, 80.

[5] D. R. MacFarlane, J. Huang, M. Forsyth, *Nature* **1999**, *402*, 792.

[6] M. S. Bhamra, D. J. Fray, *J. Mater. Sci.* **1995**, *30*, 5381.

[7] S. Lupart, G. Gregori, J. Maier, W. Schnick, *J. Am. Chem. Soc.* **2012**, *134*, 10132.

[8] H. Lutz, S. Joosten, J. Hoffmann, P. Lehmeier, A. Seilmeier, H. A. Höppe, W. Schnick, *J. Phys. Chem. Solids* **2004**, *65*, 1285.

[9] R. Müller-Mach, G. Müller, M. R. Krames, H. A. Höppe, F. Stadler, W. Schnick, T. Jüstel, P. Schmidt, *Phys. Status Solidi A* **2005**, *202*, 1727.

[10] H. A. Höppe, H. Lutz, P. Morys, W. Schnick, A. Seilmeier, *J. Phys. Chem. Solids* **2000**, *61*, 2001.

[11] A. Weiss, A. Weiss, *Z. Anorg. Allg. Chem.* **1954**, *276*, 95.

[12] W. Schnick, H. Huppertz, *Chem. Eur. J.* **1997**, *3*, 679.

[13] W. Schnick, H. Huppertz, R. Lauterbach, *J. Mater. Chem.* **1999**, *9*, 289.

[14] Z. A. Gal, P. M. Mallinson, H. J. Orchard, S. J. Clarke, *Inorg. Chem.* **2004**, *43*, 3998.

[15] M. Zeuner, F. Hintze, W. Schnick, *Chem. Mater.* **2009**, *21*, 336.

[16] G. B. M. Vaughan, J. P. Wright, A. Bytchkov, C. Curfs, C. Grundlach, M. Orlova, L. Erra, H. Gleyzolle, T. Buslaps, A. Götz, G. Suchet, S. Petitdemange, M. Rossat, L. Margulies,

W. Ludwig, A. Snigirey, I. Snigireva, H. O. Sorensen, E. M. Lauridsen, U. L. Olsen, J. Oddershede, H. F. Poulsen, *Science* **2010**, 457.

[17] F. Fahrnbauer, T. Rosenthal, T. Schmutzler, G. Wagner, G. B. M. Vaughan, J. P. Wright, O. Oeckler, *Angew. Chem. Int. Ed.* **2015**, *54*, 10020.

[18] N. Hirosaki, T. Takeda, S. Funahashi, R.-J Xie, *Chem. Mater.* **2014**, *26*, 4280.

[19] B. Lengeler, C. G. Schroer, B. Benner, A. Gerhardus, T. F. Günzler, M. Kuhlmann, J. Meyer, C. Zimprich, *J. Synchrotron Radiat.* **2002**, *9*, 119.

[20] A. Lieb, W. Schnick, *J. Solid State Chem.* **2005**, *178*, 3323.

[21] A. Lieb, M. T. Weller, P. F. Henry, R. Niewa, R. Pöttgen, R.-D. Hoffmann, H. E. Höfer, W. Schnick, *J. Solid State Chem.* **2005**, *178*, 976.

[22] A. J. D. Barnes, T. J. Prior, M. G. Francesconi, *Chem. Commun.* **2007**, 4638.

[23] J. Besson, *Comptes rendus* **1890**, *110*, 518.

[24] J. C. Labiche, O. Mathon, S. Pascarelli, M. A. Newton, G. G. Ferre, C. Curfs, G. Vaughan, A. Homs, D. F. Carreiras, *Rev. Sci. Instrum.* **2007**, *78*, 091301.

[25] J. L. Chambers, K. L. Smith, M. R. Pressprich, Z. Jin, *SMART*, Bruker-AXS, Madison, USA, **1997-1998**, v. 5.059.

[26] *SAINT*, Bruker-AXS, Madison, USA, **1997-2002**, v. 6.36A.

[27] G. M. Sheldrick, *SADABS, Multi-Scan Absorption Correction*, Bruker-AXS, WA, USA, **2012**, v. 2.

[28] G. Wu, B. L. Rodrigues, P. Coppens, *J. Appl. Crystallogr.* **2002**, *35*, 356.

[29] G. M. Sheldrick, *Acta Crystallogr., Sect. A* **2008**, *64*, 112.

[30] A. Coelho, *TOPAS Academic* 2007, Coelho Software, Brisbane, Australia, **2007**.

[31] W. Grochala, P. Edwards, *Chem. Rev.* **2004**, *104*, 1283.

[32] Further details of the crystal structure investigation can be obtained from the Fachinformationszentrum Karlsruhe, 76344 Eggenstein-Leopoldshafen, Germany (fax: (+49)7247-808-666; e-mail: crysdata@fiz-karlsruhe.de) on quoting the depository number CSD- 429711.

[33] F. Liebau, *Structural Chemistry of Silicates*, Springer, Berlin, **1985**.

[34] The term *dreier* (*sechser, siebener*) ring was coined by Liebau and is derived from the German word “drei” (”sechs”, “sieben”). A *dreier* (*sechser, siebener*) ring comprises three (six, seven) tetrahedra centers.

[35] a) V. A. Blatov, M. O'Keeffe, D. M. Proserpio, *CrystEngComm* **2010**, *12*, 44; b) V. A. Blatov, A. P. Shevchenko, D. M. Proserpio, *Cryst. Growth Des.* **2014**, *14*, 3576.

[36] W. Carrillo-Cabrera, N. Caroca-Canales, H. G. v. Schnering, *Z. Anorg. Allg. Chem.* **1994**, *620*, 247.

[37] M. O'Keeffe, M. Eddaoudi, H. Li, T. Reineke, O. M. Yaghi, *J. Solid State Chem.* **2000**, *152*, 3.

[38] A. F. Holleman, E. Wiberg, N. Wiberg, Lehrbuch der Anorganischen Chemie, de Gruyter, Berlin, **1995**.

[39] M. Petter, I. Hartenbach, T. Nikelski, T. Schleid, *Z. Kristallogr.* **2004**, *21*, 177.

[40] C. Schmolke, S. Lupart, W. Schnick, *Solid State Sci.* **2009**, *11*, 305.

[41] K. I. Machida, G. Y. Adachi, J. Shiokawa, M. Shimada, M. Koizumi, *Acta Crystallogr. Sect. B* **1982**, *38*, 386.

[42] H. Yamane, F. J. DiSalvo, *J. Alloys Compd.* **1996**, *240*, 33.

[43] H. Huppertz, W. Schnick, *Chem. Eur. J*. **1997**, *3*, 249.

[44] M. Abed, H. K. Müller-Buschbaum, *J. Alloys Compd*. **1992**, *190*, 61.

[45] H. Müller-Bunz, T. Schleid, *Z. Anorg. Allg. Chem.* **2000,** *626*, 2549.

[46] R. D. Shannon, *Acta Crystallogr. Sect. A.* **1976**, *32*, 751.

[47] A. S. Wills, *VaList,* University College London, UK, **2010**, v. 4.0.7.

[48] P. E. D. J. Morgan, *J. Mater. Sci.* **1986**, *21*, 4305.

[49] R. Hoppe, *Angew. Chem. Int. Ed. Engl.* **1970**, *9*, 25.

[50] R. Hoppe, R. Homann, *Z. Anorg. Allg. Chem.* **1970**, *379*, 193.

[51] R. Hübenthal, *MAPLE, Programm zur Berechnung des Madelunganteils der Gitterenergie*, **1993**, v. 4.

[52] H. A. Höppe, Doctoral Thesis, University of Munich (LMU), Germany, **2003**.

[53] K. Köllisch, Doctoral Thesis, University of Munich (LMU), Germany, **2001**.

[54] R. Lauterbach, Doctoral Thesis, University of Bayreuth, Germany, **1999**.

[55] P. Cortona, *Phys. Rev.* B **1992**, *46*, 2008.

[56] J. T. Chen, G. C. Guo, J. S. Huang, Q. E. Zhang, *Acta Crystallogr. Sect. C* **1996**, *52*, 2123.

[57] W. H. J. Zachariasen, *J. Chem. Phys.* **1948**, *16*, 254.

[58] H. Lange, G. Wötting, G. Winter, *Angew. Chem. Int. Ed. Engl.* **1991**, *30*, 1579.

# 4.4 From Minor Side Phases to Bulk Samples of Lanthanum Oxonitridosilicates – An Investigation with Microfocused Synchrotron Radiation

published in: *Inorg. Chem.* **2016**, *55*, 3624-3629

authors: Dajana Durach, Peter Schultz, Oliver Oeckler and Wolfgang Schnick

DOI: 10.1021/acs.inorgchem.6b00143



http://pubs.acs.org/doi/abs/10.1021/acs.inorgchem.6b00143

**Abatract.** Microcrystals of the oxonitridosilicate oxide $La_{11}Si_{13}N_{27.636}O_{1.046}:Ce^{3+}$ were obtained by exploratory high-temperature synthesis starting from La, $La(NH_2)_3$, $Si(NH)_2$, $BaH_2$, and $CeF_3$. Owing to the small size of the crystals, microfocused synchrotron radiation was used for structure investigations (space group $Cmc2_1$ (No. 36), $a$ = 9.5074(4) Å, $b$ = 32.0626(9) Å, $c$ = 18.5076(8) Å, $Z$ = 8, $R1$(all) = 0.0267). The crystal structure consists of an unprecedented interrupted three-dimensional network of vertex-sharing $SiN_{4-x}O_x$ tetrahedra that form channels of *siebener* rings along [100]. Moreover, the structure is characterized by layers of condensed *sechser* rings in a boat conformation and *vierer* rings, which are alternatingly stacked with layers of *vierer* and *dreier* rings. Several split positions indicate two different local structure variants. Infrared spectroscopy confirms the absence of N-H bonds. Powder X-ray diffraction data show that bulk samples contain only a small amount of $La_{11}Si_{13}N_{27.636}O_{1.046}:Ce^{3+}$. However, once the exact composition was determined from structure analysis, it was possible to optimize the synthesis using fluorides as starting materials. Thereby, bulk samples of the homeotypic compound $La_{11}Si_{13}N_{27.376}O_{0.936}F$ were obtained and investigated.

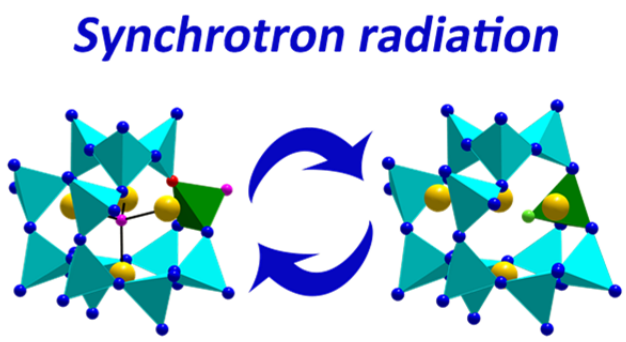

## 4.4.1 Introduction

(Oxo)nitridosilicates are a promising class of compounds, as they show fascinating material properties: e.g., ionic conductivity or luminescence of $Ce^{3+}$- or $Eu^{2+}$-doped samples.[1] For example, materials such as $Li_2SiN_2$, $Li_8SiN_4$, and $Li_{14}Ln_5[Si_{11}N_{19}O_5]O_2F_2$ (Ln = Ce, Nd) have been reported as $Li^+$ conductors, suggesting their possible application in lithium batteries.[2-6] Moreover, the discovery of $Eu^{2+}$-doped $M_2Si_5N_8$ (M = Ca, Sr, Ba) and $MSi_2O_2N_2$ (M = Ca, Sr, Ba) pushed forward the development of phosphor-converted light-emitting diodes (pc-LEDs), as the latter compounds exhibit efficient luminescence.[7,8] Accordingly, there is a general interest in (oxo)nitridosilicates with novel structures, even when the new compounds do not show exceptional properties at first glance.

(Oxo)nitridosilicates are characterized by more or less condensed $SiN_{4-x}O_x$ tetrahedra. In such network structures, nitrogen atoms can afford interconnection of one to four neighboring tetrahedral centers as well as the possibility of both corner sharing and edge sharing of these moieties.[9] In addition to noncondensed structures (e.g., $La_3SiN_4F$), chainlike, layerlike, and three dimensionally extended structures are known as well.[10-16] However, as bonds to N are less stable than bonds to O, most less condensed (oxo)nitridosilicates are sensitive to moisture, whereas highly condensed (oxo)nitridosilicates are typically inert toward hydrolysis.[17] These facts, in addition to the omnipresence of oxygen, could be the reason why sinoite $Si_2N_2O$, which usually originates from meteorites, is the only naturally occurring Si/O/N compound.[18,19] A synthetic approach to (oxo)nitridosilicates was established by high-temperature reactions, flux methods utilizing e.g. metallic sodium, and precursor routes on the basis of metal amides.[14,20,21] Since syntheses often yield inhomogeneous and microcrystalline samples, structure elucidation with conventional single-crystal or powder X-ray diffraction is often not feasible. As shown in previous investigations, microfocused synchrotron radiation gives access to data sets with high quality and consequently facilitates precise structure refinements.[22,23] Moreover, this method enables analysis of particles with a volume even smaller than 1 $\mu m^3$.[24]

In this contribution we report on the characterization of micrometer-sized crystals of $La_{11}Si_{13}N_{27.636}O_{1.046}$ by microfocused synchrotron radiation, identifying a novel oxonitridosilicate oxide with an exceptional framework topology. Subsequently, detailed knowledge of the crystal structure and thus the analytical composition has enabled synthesis optimization in order to obtain phase-pure bulk samples.

## 4.4.2 Results and Discussion

### 4.4.2.1 Synthesis and Sample Characterization

Micrometer-sized crystals of $La_{11}Si_{13}N_{27.636}O_{1.046}:Ce^{3+}$ (Figure 1a, b) were obtained as a side phase in products of a high-temperature reaction starting from a mixture of La, $La(NH_2)_3$,[25] $Si(NH)_2$,[26] $BaH_2$, and $CeF_3$ as dopant. The knowledge of the structure (see Crystal Structure of $La_{11}Si_{13}N_{27.636}O_{1.046}:Ce^{3+}$) and thus the information on the exact composition enabled synthesis optimization. In contrast, previous attempts based on the approximate composition determined by EDX were not successful. $LaF_3$, $La(NH_2)_3$,[25] $Si(NH)_2$,[26] and $BaH_2$ were used as starting materials, as this synthesis approach had already yielded several new lanthanum (oxo)nitridosilicates.[10,22] Although $BaH_2$ forms $BaF_2$ with F from $LaF_3$, a small amount of F is integrated in the target phase; thus, $La_{11}Si_{13}N_{27.376}O_{0.936}F$ was obtained (Figure 1 c). It exhibits a disordered structure similar to those of solid solutions of $La_{11}Si_{13}N_{28-x}O_{0.5+1.5x}:Ce^{3+}$ (which might thus also contain traces of F below the detection limit of EDX, see below). The oxygen incorporated in both compounds can probably be traced back to contamination of the starting materials

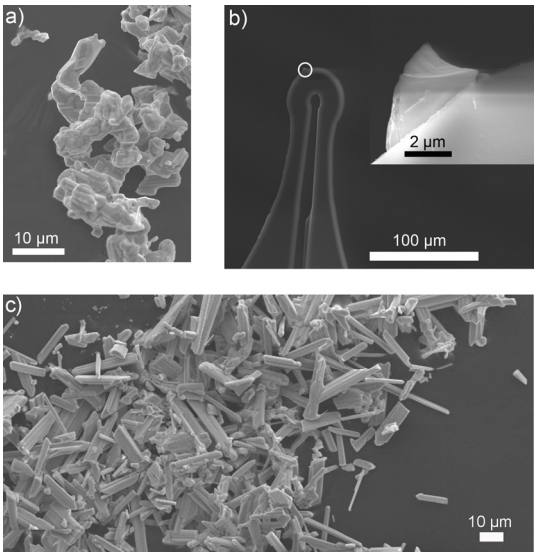


**Figure 1.** SEM images of (a) crystals of $La_{11}Si_{13}N_{27.636}O_{1.046}:Ce^{3+}$, (b) the investigated crystal (white circle and enlarged inset) of the sample mounted on a Kapton foil sample holder and (c) the optimized sample consisting of the homeotypic compound $La_{11}Si_{13}N_{27.376}O_{0.936}F$.

EDX analyses of crystals of $La_{11}Si_{13}N_{27.636}O_{1.046}:Ce^{3+}$ and $La_{11}Si_{13}N_{27.376}O_{0.936}F$ yielded the average compositions La/Si/Ce = 11.0/12.4/0.4 and La/Si/F = 11.0/12.1/1.4, respectively (normalized according to the La content; the atomic content of N and O could not be determined precisely due to the limitations of the analytical method). The determined element ratios are consistent with the sum formulas obtained from single-crystal structure refinements. The infrared spectra of both compounds (Figure S2 in the Supporting Information) confirm the absence of N-H and O-H bonds. Owing to the results of the EDX measurements and IR spectroscopy the investigated phases contain no other elements than La, Si, N, O, and Ce or F, respectively.

#### 4.4.2.2 Crystal Structure of $La_{11}Si_{13}N_{27.636}O_{1.046}:Ce^{3+}$

The low scattering power of the micrometer-sized crystals of $La_{11}Si_{13}N_{27.636}O_{1.046}:Ce^{3+}$ impeded characterization by conventional single-crystal X-ray diffraction. Crystal structure determination by means of powder X-ray diffraction was also not applicable, as initially no phase-pure sample could be obtained. Consequently, microfocused synchrotron radiation was used for single-crystal diffraction. The crystal structure was solved and refined in space group $Cmc2_1$ (No. 36). In the structure refinement, inversion twinning had to be taken into account. Owing to its small amount and lack of scattering contrast in comparison to that of $La^{3+}$, $Ce^{3+}$ was neglected in the refinement. Crystallographic data are given in Table 1, and the atomic parameters are given in Table S1 in the Supporting Information. The structure contains several split and not fully occupied positions. Thus, $La_{11}Si_{13}N_{27.636}O_{1.046}$ can be interpreted as a disordered structure with some alternative local atom arrangements. The predominant atom arrangement formally corresponds to the sum formula $La_{11}Si_{13}N_{28}O_{0.5}$, whereas a hypothetical structure that contains only the atom positions with lower occupancies would yield the composition $La_{11}Si_{13}N_{27}O_2$. Below, these hypothetical end members of a solid solution series of $La_{11}Si_{13}N_{28-x}O_{0.5+1.5x}$ are labeled as variants A ($La_{11}Si_{13}N_{28}O_{0.5}$; $x = 0$) and B ($La_{11}Si_{13}N_{27}O_2$; $x = 1$). One split position (La8C/8D) is present in both variants. The occupancies of the split positions were refined while retaining full total occupancy for all split atom sites (i.e., A and B or C and D, Table S1). Occupancy factors of atoms belonging to variants A and B, respectively, were constrained to the same values. On the basis of this approach, the investigated crystal with $x = 0.364$ formally corresponds to a solid solution with 63.6(3)% of variant A and 36.4(3)% of variant B. All cations except

Si15A/Si15B and Si16A/Si16B were refined anisotropically (Table S2 in the Supporting Information). The distribution of O and N is based on Pauling's rules[27] and charge neutrality.[28]

**Table 1.** Crystallographic data and details of the structure refinement of $La_{11}Si_{13}N_{27.636}O_{1.046}:Ce^{3+}$.

| | |
|---|---|
| formula | $La_{11}Si_{13}N_{27.636}O_{1.046}$ |
| cryst. syst. | orthorhombic |
| space group | $Cmc2_1$ (No. 36) |
| *a* (Å) | 9.566(12) |
| *b* (Å) | 32.269(19) |
| *c* (Å) | 18.667(11) |
| cell volume (Å$^3$) | 5762(9) |
| *Z* | 8 |
| density (g·cm$^{-3}$) | 5.296 |
| μ (mm$^{-1}$) | 9.273 |
| temperature (K) | 293(2) |
| radiation | synchrotron ($\lambda$ = 0.3099 Å) |
| F(000) | 8086 |
| θ range (deg) | $0.97 \leq \theta \leq 15.05$ |
| $d_{min}$ (Å) | 0.60 |
| total no. of rflns | 67652 |
| no. of indep. Rflns | 14300 ($R_{int}$ = 0.0342) |
| no. of refined params | 407 |
| twin ratio | 0.132(7)/0.868 |
| GOF | 1.348 |
| *R*1 (all data/for $F^2 > 2\sigma(F^2)$) | 0.0267/0.0246 |
| *wR*2 (all data/for $F^2 > 2\sigma(F^2)$) | 0.0502/0.0498 |
| $\Delta\rho_{max}$ , $\Delta\rho_{min}$ (e/Å$^3$) | 2.896 ; -1.846 |

A single crystal of $La_{11}Si_{13}N_{27.376}O_{0.936}F$ was investigated using a laboratory X-ray diffractometer. The refinement shows that $La_{11}Si_{13}N_{27.376}O_{0.936}F$ and $La_{11}Si_{13}N_{27.636}O_{1.046}$ form homeotypic solid solutions. The structures show the same framework and space group. However, $La_{11}Si_{13}N_{27.376}O_{0.936}F$ contains an additional discrete F atom site, and for the sake of charge neutrality, one discrete O site was assumed to be occupied by F instead of O. As the resolution of the obtained data set ($d_{min}$ = 0.77 Å) is inferior to that of the synchrotron data

set ($d_{min}$ = 0.60 Å), the two variants could only be identified on the basis of the knowledge of their presence originating from the refinement of the synchrotron data set (Tables S3 and S4 in the Supporting Information).

According to Pauling's rules[27] and charge neutrality in the predominant variant A, all anion positions of the $SiN_4$ network are occupied with N, whereas the isolated anion position is occupied with O. The degree of condensation amounts to $\kappa = n(Si):n(N) = 0.46$. Although nitridosilicates with $\kappa < 0.5$ tend to form layered or less-condensed structures,[29] the structure determination shows an interrupted three-dimensional framework of vertex-sharing $Q^4$-, $Q^3$-, and $Q^2$-type $SiN_4$ tetrahedra (Figure 2a, b) with the ratio $Q^4/Q^3/Q^2 = 10/2/1$. Interrupted tetrahedral networks with $\kappa < 0.5$ were also observed for $M_7Si_6N_{15}$ (M = La, Ce, Pr)[30] and $La_3BaSi_5N_9O_2$.[22] The $Q^4$-type tetrahedra exhibit four singly bridging $N^{[2]}$ atoms, whereas the $Q^3$-type tetrahedra consist of three singly bridging $N^{[2]}$ atoms and one terminal $N^{[1]}$ atom. The $Q^2$-type tetrahedra contain two singly bridging $N^{[2]}$ and two terminal $N^{[1]}$ atoms. In addition, there are discrete oxide anions $O^{[0]}$, which are 4-fold coordinated by La as, for example, in $La_2O_3$.[31] The $SiN_4$ tetrahedra are condensed to form *siebener* ring channels along [100] (Figure 2c). The asymmetric interconnection of the *siebener* rings (Figure 2b) is not compatible with centrosymmetry. Selected $SiN_4$ tetrahedra form layers extending along [110] which consist of condensed *sechser* rings in boat conformation and *vierer* rings. These layers are alternatingly stacked with other layers consisting of *dreier* and *vierer* rings (Figure 2c).[30,32] This topology has not been found in any other compound so far. It is characterized by the point symbol $\{3.4.5.6.7.8\}_2\{3.6^3.7^2\}_4\{3.7^2\}_2\{3\}\{4.6^2.8^3\}\{4.6^3.8^2\}\{6^5.8\}\{6^6\}$, as calculated with the program TOPOS.[33]

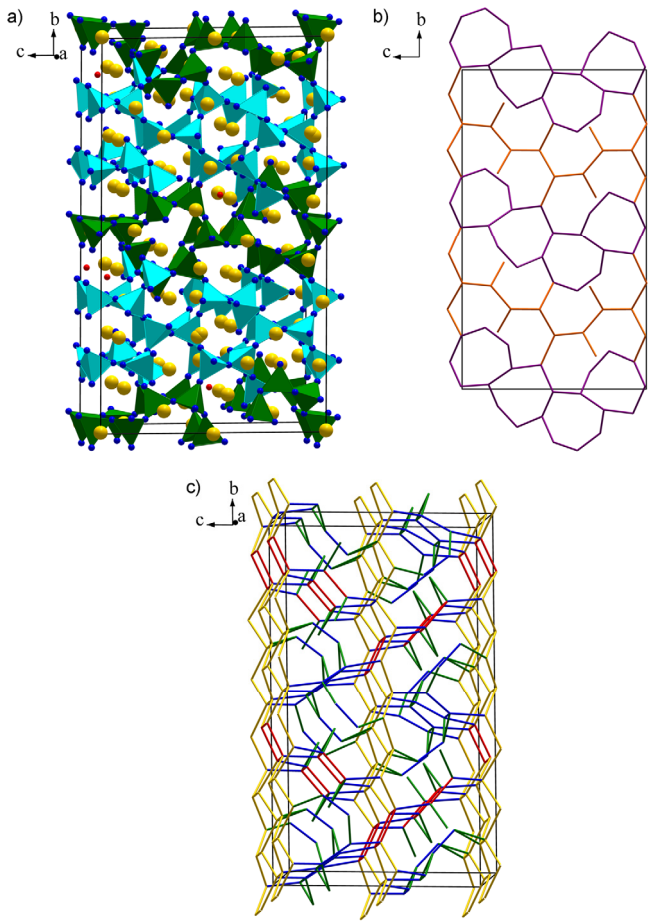


**Figure 2. (**a) Crystal structure of $La_{11}Si_{13}N_{28}O_{0.5}$ (predominant variant A of the atom positions in $La_{11}Si_{13}N_{27.636}O_{1.046}$) projected along [100] with $SiN_4$ tetrahedra (turquoise and green; the green area represents the location of the main differences between the two local structure variants), La (yellow), O (red), and the unit cell shown in black. (b) Topological representation of $La_{11}Si_{13}N_{28}O_{0.5}$ projected along [100], *siebener* rings represented by violet lines. (c) Slightly tilted view highlighting *dreier* rings by green lines, *vierer* rings by red lines, and *sechser* rings by yellow lines (each connecting line represents a Si-N-Si bond).

The crystal structure contains 16 crystallographically independent La sites, one of which is described with the split positions La8C and La8D. The site occupation factors were refined to 0.79(4) for La8C and 0.21(4) for La8D, while retaining full total occupation. All heavy atoms are located in non-regular polyhedra coordinated by 7-10 anions (Figure 3).

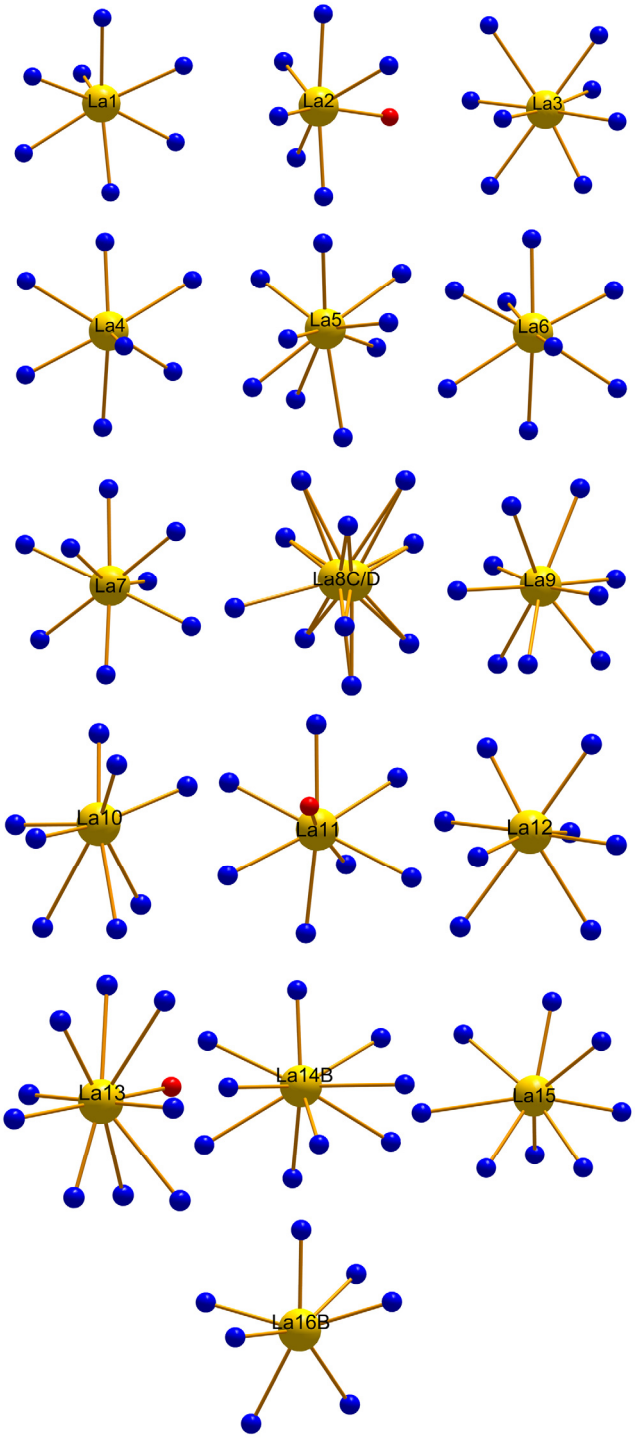


**Figure 3.** Coordination spheres of the La atoms (yellow) in $La_{11}Si_{13}N_{28}O_{0.5}$ (predominant variant A of the atom positions in $La_{11}Si_{13}N_{27.636}O_{1.046}$). N atoms are shown in blue and O atoms in red.

The Si–N distances (1.655(8)-1.792(9) Å) correspond to those in other nitridosilicates, such as $La_{16}[Si_8N_{22}][SiON_3]_2$ (Si-N 1.689(8)-1.815(8) Å)[34] and $BaSi_7N_{10}$ (Si-N 1.644(3)-1.774(3) Å).[35] The La-N and La-O bond lengths are in good agreement with those in other

lanthanum compounds,[35-37] and all interatomic distances are in accordance with the sum of the ionic radii.[38]

The differences between the local variants A and B are located in the area highlighted in green in Figure 2a. The building units present in this area are depicted in Figure 4. In variant B, N39A is replaced by O37B. This leads to an alternative orientation of the associated $SiN_{4-x}O_x$ tetrahedra, which creates space for an additional position O41B. In order to obtain charge neutrality for arrangement B, the partially occupied anion O37B position belonging exclusively to this variant was assigned as O.

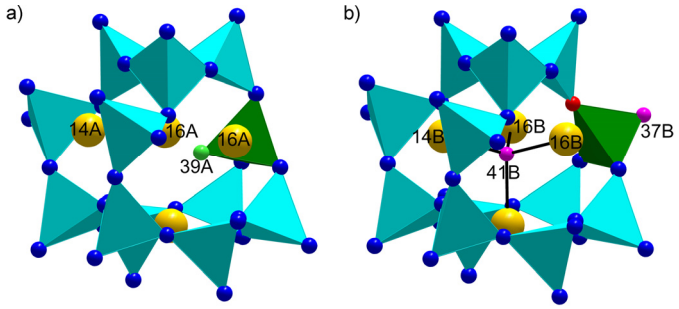


**Figure 4.** Detailed representation of the rings within the green area of Figure 3a, showing the differences between the two possible structure variants (a) A and (b) B. La atoms are shown in yellow, O positions in pink or red, and N atoms in blue and green.

Despite the several split positions of $La_{11}Si_{13}N_{27.636}O_{1.046}$, it might be possible that small regions of the investigated crystal show a higher structural order. These regions can probably be increased with a synthesis offering an increased cooling rate.

In order to determine the phases of the sample containing $La_{11}Si_{13}N_{27.636}O_{1.046}:Ce^{3+}$, its powder diffraction pattern was compared with calculated patterns of known lanthanum nitridosilicates and of $La_{11}Si_{13}N_{27.636}O_{1.046}$ as calculated on the basis of single-crystal data. It was found that the sample contains $La_{11}Si_{13}N_{27.636}O_{1.046}$ only as a side phase next to $La_{16}[Si_8N_{22}][Si_3ON_3]_2$,[34] $La_5Si_3N_9$,[39] and other unknown phases (Figure S1 in the Supporting Information). In contrast, Rietveld refinement of the powder X-ray diffraction data of the product of the optimized synthesis (washed with $H_2O$), on the basis of the exact knowledge of the composition, shows $La_{11}Si_{13}N_{27.376}O_{0.936}F$ as a single phase (Figure 5, Table S5 in the Supporting Information). The profile fit was based on the results of the single-crystal investigation of $La_{11}Si_{13}N_{27.376}O_{0.936}F$ (Tables S3 and S4 in the Supporting Information); only lattice parameters were refined.

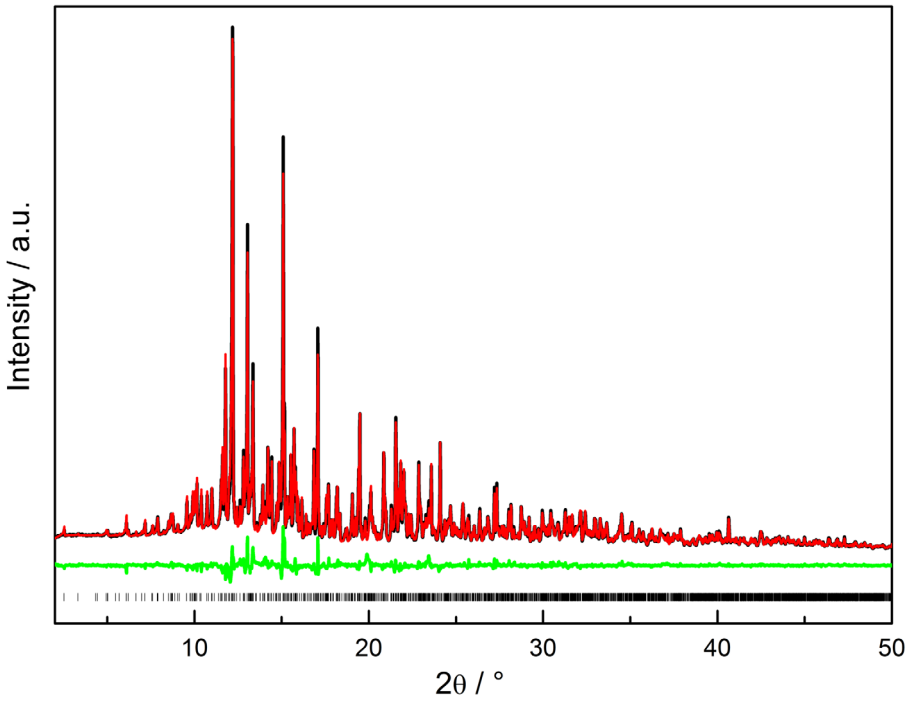


**Figure 5.** Rietveld refinement for the powder diffraction pattern of the washed ($H_2O$) sample of $La_{11}Si_{13}N_{27.376}O_{0.936}F$: observed (black line) and calculated (red line) X-ray powder diffraction patterns as well as difference profile (green line). The black vertical bars indicate positions of Bragg reflections.

## 4.4.3 Conclusion

Investigations of microcrystals of $La_{11}Si_{13}N_{27.636}O_{1.046}:Ce^{3+}$ revealed a novel lanthanum oxonitridosilicate oxide with an unprecedented interrupted network. The investigation shows how microfocused synchrotron radiation is well suited to precisely elucidate the structure of microcrystals with rather limited scattering power obtained as minority phases. In addition, the structure refinement of $La_{11}Si_{13}N_{27.636}O_{1.046}:Ce^{3+}$ demonstrates how such data can be exploited to describe complex structures with split positions and local disorder, as the high intensity of the synchrotron radiation yielded data sets with resolution higher than that of conventional X-ray radiation; thus, structures can be described in more detail. Furthermore, these investigations confirm that with the knowledge of the exact composition, obtained from structure analysis, syntheses can be easily optimized, whereas attempts based on the approximate composition determined by EDX often failed. In the case of crystals suitable for laboratory X-ray diffraction, this fact also justifies the single particle diagnosis approach by Xie et al.[40] For smaller (sub)microcrystals, microfocused synchrotron radiation is the method of choice. These approaches may accelerate the development and

optimization of functional materials, as properties of phase-pure samples can be more easily investigated and tuned.

## 4.4.4 Experimental Section

### 4.4.4.1 Synthesis

All synthesis steps were performed under exclusion of oxygen and moisture in either an argon-filled glovebox (Unilab, MBraun, Garching, Germany; $O_2$ < 1 ppm; $H_2O$ < 1 ppm) or in flame-dried glassware using Schlenk techniques. In order to obtain crystals of $La_{11}Si_{13}N_{27.636}O_{1.046}:Ce^{3+}$, La (0.17 mmol, 30.3 mg Smart Elements, 99.9%), $La(NH_2)_3$ (0.22 mmol, 40.5 mg, synthesized according to Jacobs et al.),[25] "$Si(NH)_2$" (0.33 mmol, 19.0 mg, synthesized according to Winter et al.),[26] $BaH_2$ (0.41 mmol, 57.3 mg, Materion, 99.7%), and $CeF_3$ as dopant (0.0086 mmol, 1.7 mg, 2 mol % of Ce, Alfa Aesar, 99.99%) were thoroughly ground and mixed in an agate mortar and filled into a tungsten crucible. The crucible was transferred into a water-cooled silica glass reactor of a radio-frequency furnace (type AXIO 10/450, maximum electrical output 10 kW, Hüttinger Elektronik, Freiburg, Germany)[41] and heated under $N_2$ atmosphere to 900 °C within 5 min, subsequently heated to 1650 °C, maintained at that temperature for 5 h, then cooled to 900 °C within 77 h, and finally quenched to room temperature by switching off the furnace. The reaction yielded a heterogeneous sample with tiny orange crystals of $La_{11}Si_{13}N_{27.636}O_{1.046}:Ce^{3+}$ exhibiting no significant luminescence (measurements at room temperature; luminescence microscope HORIBA Fluoromax4 spectrofluorimeter; Olympus BX51 microscope). The compound is stable to oxygen and moisture. Contact with air and water over several hours did not lead to decomposition.

For the optimized synthesis of $La_{11}Si_{13}N_{27.376}O_{0.936}F$, $LaF_3$ (69.8 mg, 0.36 mmol, Sigma-Aldrich, 99.99%; for sources of other chemicals see above), $La(NH_2)_3$ (50.0 mg, 0.27 mmol), $Si(NH)_2$ (18.9 mg, 0.33 mmol), and $BaH_2$ (63.0 mg, 0.45 mmol) were mixed in an agate mortar and filled into a tungsten crucible. Subsequently, the crucible was heated in a radio-frequency furnace[41] under $N_2$ atmosphere to 1600 °C within 1 h, maintained at that temperature for 10 h, then cooled to 900 °C in 44 h, and finally quenched to room temperature by switching off the furnace. The reaction results in a sample with red crystals next to yellow crystals of $La_{11}Si_{13}N_{27.376}O_{0.936}F$. The latter are inert to oxygen and hydrolysis, whereas the red crystals are sensitive to air and water. Thus, washing the sample with water yielded a single-phase

bulk sample of $La_{11}Si_{13}N_{27.376}O_{0.936}F$. Addition of $CeF_3$ (2.4 mg, 0.012 mmol, 2 mol % Ce) as a doping agent resulted in orange crystals of non-luminescent $La_{11}Si_{13}N_{27.376}O_{0.936}F:Ce^{3+}$ (measurements at room temperature; luminescence microscope HORIBA Fluoromax4 spectrofluorimeter; Olympus BX51 microscope).

Since the nondoped sample consists of light yellow crystals of $La_{11}Si_{13}N_{27.376}O_{0.936}F$, the intense orange color of $La_{11}Si_{13}N_{27.376}O_{0.936}F:Ce^{3+}$/$La_{11}Si_{13}N_{27.636}O_{1.046}:Ce^{3+}$ presumably originates from the $Ce^{3+}$ doping.

#### 4.4.4.2 Elemental Analysis and Spectroscopy

The chemical composition and morphology of the crystals of both compounds were investigated with a JEOL JSM6500F field emission scanning electron microscope (SEM) equipped with a Si/Li EDX detector 7418 (Oxford Instruments). In order to provide electrical conductivity on the sample surfaces, the crystals were prepared on conductive adhesive films and carbon-coated (MED 020, Bal-Tec AG). Infrared (IR) spectra were recorded with a PerkinElmer BXII spectrometer employing ATR (attenuated total reflection) technology.

#### 4.4.4.3 Crystal Structure Analysis

Single crystals of $La_{11}Si_{13}N_{27.636}O_{1.046}:Ce^{3+}$ and $La_{11}Si_{13}N_{27.376}O_{0.936}F$ were mounted on Kapton foil sample holders (micromount, MiTeGen, Ithaca, NY, USA). X-ray diffraction data of $La_{11}Si_{13}N_{27.636}O_{1.046}:Ce^{3+}$ were collected at beamline ID11 of the ESRF in Grenoble, France (Ge(111) double-crystal monochromator, Frelon 2K CCD detector).[42] The beam ($\lambda = 0.3099$ Å) was focused to approximately 10 µm diameter with Be/Al refractive lenses.[43-45] X-ray diffraction data of $La_{11}Si_{13}N_{27.376}O_{0.936}F$ were recorded with a D8 Venture diffractometer (Mo Kα radiation ($\lambda = 0.71073$ Å), rotating anode, and Goebel mirror optics). The reflections of the data set of $La_{11}Si_{13}N_{27.636}O_{1.046}:Ce^{3+}$ were indexed with SMART,[46] integrated with SAINT,[47] and scaled as well as corrected for absorption effects using SADABS.[48] Data handling for $La_{11}Si_{13}N_{27.376}O_{0.936}F$ was performed with the APEX software.[49] The synchrotron data set was further corrected in order to account for the incidence-angle dependence of the beam path through the CCD phosphor.[50] The structures were solved using direct methods and refined by full-matrix least-squares calculations on $F^2$ using SHELX-2014.[51]

Powder X-ray diffraction data were collected on a STOE STADI P diffractometer (Stoe & Cie, Darmstadt, Germany) in modified Debye-Scherrer geometry using Mo $K\alpha_1$ radiation ($\lambda$ = 0.70930 Å) with a Ge(111) monochromator and a MYTHEN 1K detector (Dectris, Baden-Dättwil, Switzerland). Rietveld refinement was performed using the TOPAS-Academic package.[52] Simulated powder diffraction patterns were calculated on the basis of the single-crystal structure data using WinXPOW.[53]

## 4.4.5 References


[1] M. Zeuner, S. Pagano, W. Schnick, *Angew. Chem. Int. Ed.* **2011**, *50*, 7754.

[2] J. Lang, J.-P. Charlot, *Rev. Chim. Miner.* **1970**, *7*, 121.

[3] H. Hillebrecht, J. Churda, L. Schröder, H. G. v. Schnering, *Z. Kristallogr. Suppl.* **1993**, *6*, 80.

[4] D. R. MacFarlane, J. Huang, M. Forsyth, *Nature* **1999**, *402*, 792.

[5] M. S. Bhamra, D. J. Fray, *J. Mater. Sci.* **1995**, *30*, 5381.

[6] S. Lupart, G. Gregori, J. Maier, W. Schnick, *J. Am. Chem. Soc.* **2012**, *134*, 10132.

[7] R. Müller-Mach, G. Müller, M. R. Krames, H. A. Höppe, F. Stadler, W. Schnick, T. Jüstel, P. Schmidt, *Phys. Status Solidi A* **2005**, *202*, 1727.

[8] H. A. Höppe, H. Lutz, P. Morys, W. Schnick, A. Seilmeier, *J. Phys. Chem. Solids* **2000**, *61*, 2001.

[9] W. Schnick, H. Huppertz, *Chem. Eur. J.* **1997**, *3*, 679.

[10] D. Durach, W. Schnick, *Eur. J. Inorg. Chem.* **2015**, 4095.

[11] Z. Inoue, M. Mitomo, N. Li, *J. Mater. Sci.* **1980**, *15*, 2915.

[12] T. Schlieper, W. Milius, W. Schnick, *Z. Anorg. Allg. Chem.* **1995**, *621*, 1380.

[13] H. Huppertz, W. Schnick, *Acta Crystallogr. Sect. C* **1997**, *53*, 1751.

[14] Z. A. Gàl, P. M. Mallinson, H. J. Orchard, S. J. Clarke, *Inorg. Chem.* **2004**, *43*, 3998.

[15] S. Lupart, M. Zeuner, S. Pagano, W. Schnick, *Eur. J. Inorg. Chem.* **2010**, 2636.

[16] M. Zeuner, S. Pagano, P. Matthes, D. Bichler, D. Johrendt, T. Harmening, R. Pöttgen, W. Schnick, *J. Am. Chem. Soc.* **2009**, *131*, 11242.

[17] W. Schnick, *Angew. Chem. Int. Ed. Engl.* **1993**, *32*, 806.

[18] W. H. Baur, *Nature* **1972**, *240*, 461.

[19] A. Bischoff, T. Grund, T. Jording, B. Heying, R.-D. Hoffmann, U. Ch. Rodewald, R. Pöttgen, *Z. Naturforsch. B* **2005**, *60b*, 1231.

[20] W. Schnick, H. Huppertz, R. Lauterbach, *J. Mater. Chem.* **1999**, *9*, 289.

[21] M. Zeuner, F. Hintze, W. Schnick, *Chem. Mater.* **2009**, *21*, 336.

[22] D. Durach, L. Neudert, P. J. Schmidt, O. Oeckler, W. Schnick**,** *Chem. Mater.* **2015**, *27*, 4832.

[23] D. Durach, F. Fahrnbauer, O. Oeckler, W. Schnick, *Inorg. Chem.* **2015**, *54*, 8727.

[24] F. Fahrnbauer, T. Rosenthal, T. Schmutzler, G. Wagner, G. B. M. Vaughan, J. P. Wright, O. Oeckler, *Angew. Chem. Int. Ed.* **2015**, *54*, 10020.

[25] B. Gieger, H. Jacobs, C. Hadenfeldt, *Z. Anorg. Allg. Chem.* **1974**, *410*, 104.

[26] H. Lange, G. Wotting, G. Winter, *Angew. Chem. Int. Ed.* **1991**, *30*, 1579.

[27] P. E. D. Morgan, *J. Mater. Sci.* **1986**, *21*, 4305.

[28] Further details of the crystal structure investigation can be obtained from the Fachinformationszentrum Karlsruhe, 76344 Eggenstein-Leopoldshafen, Germany (fax: (+49)7247-808-666; e-mail: crysdata@fiz-karlsruhe.de) on quoting the depository number CSD-430509.

[29] F. Liebau, *Structural Chemistry of Silicates*, Springer, Berlin, **1985**.

[30] C. Schmolke, O. Oeckler, D. Bichler, D. Johrendt, W. Schnick *Chem. Eur. J.* **2009**, *15*, 9215.

[31] A. E. J. Gobichon, J. P. Auffrédic, D. Louer, *Solid State Chem.* **1999**, *144*, 68.

[32] The term *dreier* (*vierer*, *sechser, siebener*) ring was coined by Liebau and is derived from the German word “drei” (“vier”, ”sechs”, “sieben”). A *dreier* (*vierer, sechser, siebener*) ring comprises three (four, six, seven) tetrahedral centers.

[33] a) V. A. Blatov, M. O’Keeffe, D. M. Proserpio, *CrystEngComm* **2010**, *12*, 44; b) V. A. Blatov, A. P. Shevchenko, D. M. Proserpio, *Cryst. Growth Des.* **2014**, *14*, 3576.

[34] C. Schmolke, S. Lupart, W. Schnick, *Solid State Sci.* **2009**, *11*, 305.

[35] H. Huppertz, W. Schnick, *Chem. Eur. J*. **1997**, *3*, 249.

[36] Y. I. Smolin, Y.F. Shepelev, *Acta Crystallogr. Sect. B* **1970**, *26*, 484.

[37] E. Günther, R. Hagenmayer, M. Jansen, *Z. Anorg. Allg. Chem.* **2000**, *626*, 1519.

[38] R. D. Shannon, *Acta Crystallogr. Sect. A.* **1976**, *32*, 751.

[39] C. Schmolke, D. Bichler, D. Johrendt, W. Schnick, *Solid State Sci.* **2009**, *11*, 389.

[40] X.-J. Wang, L. Wang, T. Takeda, S. Funahashi, T. Suehiro, N. Hirosaki, R. -J. Xie, *Chem. Mater.* **2015**, *27*, 7689.

[41] W. Schnick, H. Huppertz, R. Lauterbach, *J. Mater. Chem.* **1999**, *9*, 289.

[42] J. C. Labiche, O. Mathon, S. Pascarelli, M. A. Newton, G. G. Ferre, C. Curfs, G. Vaughan, A. Homs, D. F. Carreiras, *Rev. Sci. Instrum.* **2007**, *78*, 091301.

[43] G. B. M. Vaughan, J. P. Wright, A. Bytchkov, C. Curfs, C. Grundlach, M. Orlova, L. Erra, H. Gleyzolle, T. Buslaps, A. Götz, G. Suchet, S. Petitdemange, M. Rossat, L. Margulies, W. Ludwig, A. Snigirey, I. Snigireva, H. O. Sorensen, E. M. Lauridsen, U. L. Olsen, J. Oddershede, H. F. Poulsen, *Science* **2010**, 457.

[44] G. B. M. Vaughan, J. P. Wright, A. Bytchkov, M. Rossat, H. Gleyzolle, I. Snigireva, A. Snigirev, *J. Synchrotron Rad.* **2011**, *18*, 125.

[45] B. Lengeler, C. Schroer, J. Tümmler, B. Benner, M. Richwin, A. Snigirev, I. Snigireva, M. Drakopoulos, *J. Synchrotron Rad.* **1999**, *6*, 1153.

[46] J. L. Chambers, K. L. Smith, M. R. Pressprich, Z. Jin, *SMART*, Bruker-AXS, Madison, USA, **1997-1998**, v. 5.059.

[47] *SAINT*, Bruker-AXS, Madison, USA, **1997-2002**, v. 6.36A.

[48] G. M. Sheldrick, *SADABS, Multi-Scan Absorption Correction*, Bruker-AXS: WA, **2012**, v.2.

[49] *APEX*, Bruker AXS, Madison, USA, **2014**, v. 11-0.

[50] G. Wu, B. L. Rodrigues, P. Coppens, *J. Appl. Crystallogr.* **2002**, *35*, 356**.**

[51] G. M. Sheldrick, *Acta Crystallogr. Sect. A* **2008**, *64*, 112.

[52] A. Coelho, *TOPAS Academic* 2007, Coelho Software, Brisbane, Australia, **2007**.

[53] *WINXPOW, Program for powder data handling*, Stoe & Cie GmbH, Darmstadt, Germany, **2007**, v. 2.21.

# 4.5 $Ba_{1.63}La_{7.39}Si_{11}N_{23}Cl_{0.42}:Ce^{3+}$ - A Nitridosilicate Chloride with a Zeolite-like Structure

published in: *Z. Anorg. Allg. Chem.* **2016**, *642*, 603-608.

authors: Peter Schultz, Dajana Durach, Wolfgang Schnick and Oliver Oeckler

DOI: 10.1002/zaac.201600090



http://onlinelibrary.wiley.com/doi/10.1002/zaac.201600090/abstract

**Abatract.** The nitridosilicate chloride $Ba_{1.63}La_{7.39}Si_{11}N_{23}Cl_{0.42}:Ce^{3+}$ was synthesized by metathesis reaction starting from $LaCl_3$, $BaH_2$, $CeF_3$ and the product of the ammonolysis of $Si_2Cl_6$. The title compound is stable towards air and moisture. Diffraction data of a microcrystal were recorded using microfocused synchrotron radiation. X-ray spectroscopy confirms the chemical composition of the crystal; IR spectra corroborate absence of N-H bonds. The compound is homeotypic to $Ba_2Nd_7Si_{11}N_{23}$ and crystallizes in space group *Cmmm* with $a = 11.009(3)$, $b = 23.243(8)$, $c = 9.706(4)$ Å and $Z = 4$; $R1(\text{all}) = 0.0174$. According to bond valence sum calculations, some crystallographic positions show complete occupancy by Ba or La whereas others contain significant amounts of both elements. In contrast to the structure prototype $Ba_2Nd_7Si_{11}N_{23}$, $Ba_{1.63}La_{7.39}Si_{11}N_{23}Cl_{0.42}:Ce^{3+}$ contains chloride ions in channels of the $SiN_4$ tetrahedra network, hinting at various substitution possibilities of the complex zeolite-like structure.

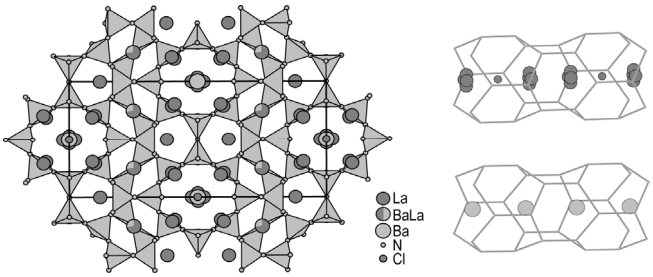

## 4.5.1 Introduction

Due to strong Si-N and Si-O bonds, (oxo-)nitridosilicates combine high thermal and chemical stability. The dimensionality of the respective crystal structures is diverse; there are three-dimensional frameworks, layered or ribbon-like structures as well as such with discrete tetrahedra.[1-6] Possible applications reach from luminescent phosphors doped with $Eu^{2+}$ like $M_2Si_5N_8$ (M = Ca, Sr, Ba) and $MSi_2O_2N_2$ (M = Ca, Sr, Ba)[7-9] to frameworks for ionic conductors ($Li_2SiN_2$, $Li_8SiN_4$, $Li_{14}RE_5[Si_{11}N_{19}O_5]O_2F_2$ with RE = Ce, Nd).[10-14] Compared to oxosilicates, the (partial) exchange of oxygen by nitrogen in $SiO_4$ tetrahedra results in a larger variety of structures, as oxygen usually links only two tetrahedral centers or acts as a terminal atom, whereas in $SiO_{4-x}N_x$ with x = 1-4, N atoms may interconnect up to four tetrahedral centers. (Oxo-)nitridosilicates with zeolite-like structures are very rare. Examples include $Li_2Sr_4Si_4N_8O$[1] in the BCT type framework[15] as well as a few examples of the NPO or NPT type, where chlorine occasionally occupies channels in those structures, e.g. $Ba_6Si_6N_{10}O_2(CN_2)$ and $Ba_3T_3N_5OCl$ (T = Si, Ta).[16-20] The interrupted framework of $M_7Si_6N_{15}$ with M = La, Ce, Pr also resembles zeolite structures.[21]

Problems arising from high reaction temperatures required were tackled using flux methods, as nitrogen exhibits a significant solubility in liquid alkali metals (Na or Li). Additionally, metal amide precursors were used as starting materials, as they are highly reactive and readily decompose at elevated temperatures, which leads to metal nitrides and imides.[1] Silicon diimide "$Si(NH)_2$" is an established precursor, which paved the way to several (oxo-)nitrido-silicates.[5,22] Besides, "$Si_2(NH)_3 \cdot 6\,NH_4Cl$", i. e. the product of the ammonolysis of $Si_2Cl_6$, turned out to be a promising precursor that offers another stoichiometric proportion of Si and N and another oxidation state of Si as in "$Si(NH)_2$", which opens the door to further nitridosilicates.[23]

Still, high-temperature syntheses often result in microcrystalline and inhomogeneous samples. Structure solution and refinement by conventional single crystal or powder methods is hardly possible in such cases. However, the use of microfocused synchrotron radiation has been shown to solve this problem efficiently, enabling high-quality data and structure refinements for very small crystallites.[24] In this article, the crystal structure of $Ba_{1.63}La_{7.39}Si_{11}N_{23}Cl_{0.42}:Ce^{3+}$ represents another successful application of this method.

## 4.5.2 Experimental Section

### 4.5.2.1 Synthesis

In a glove box, 23.2 mg $LaCl_3$, 59.5 mg "$Si_2(NH)_3$ 6 $NH_4Cl$" (obtained by ammonolysis of $Si_2Cl_6$)[25]. 66.7 mg $BaH_2$ and 0.4 mg $CeF_3$ as dopant were filled into a tungsten crucible. The latter was heated from ambient temperature to 900 °C within five minutes in nitrogen atmosphere using a radio-frequency furnace (AXIO 10/450, max. output 10 kW, Hüttinger Elektronik, Freiburg).[26] This step was followed by a slower four-hour temperature ramp to 1400 °C, then the furnace was switched off. The reaction yielded an inhomogeneous sample with colorless, orange and red crystals. The present publication focuses on the red platelet-shaped crystals.

### 4.5.2.2 Scanning electron microscopy and X-ray spectroscopy

Potential crystals for the single crystal structure analysis were mounted on micromounts (Kapton foil sample support, MiTeGen, Ithaca) and selected based on their morphology (Figure S1 in the Supporting Information) using a JEOL JSM-6500F field emission scanning electron microscope (SEM) operated at 12 keV. In order to provide sufficient electrical conductivity of the sample, it was coated with carbon. The chemical composition was determined by energy-dispersive X-ray spectroscopy (EDX) with an Oxford Instruments 7418 Si/Li EDX detector.

### 4.5.2.3 Single-crystal X-ray diffraction

Microfocused synchrotron radiation (beamline ID11, ESRF, Grenoble) was used for data acquisition from a microcrystal of ca. 6 x 6 x 2 µm³. A Ge (111) double crystal monochromator was used for the adjustment of the chosen wavelength (λ = 0.3116 Å) and the beam was focused with a Be/Al lens system to a diameter of approximately 10 µm.[27,28] Diffraction data were recorded with a Frelon4k CCD detector. The software packages SMART[29] and SAINT[30] were used for indexing and data integration. Scaling and semiempirical absorption correction were performed with SADABS.[31] In addition, a correction for incomplete absorption of high-energy radiation in the phosphor of the CCD detector[32] was applied. Graphical Fourier sections were calculated with JANA 2006.[33]

#### 4.5.2.4 Powder X-ray diffraction

Powder X-ray diffraction (PXRD) patterns were measured with a STOE STADI P diffractometer (Mo-$K_{\alpha1}$ radiation, λ = 0.70930 Å**,** Ge(111) monochromator, MYTHEN 1K detector). Simulated powder patterns were calculated on the basis of the single crystal structure data using the WinXPOW program package.[34]

#### 4.5.2.5 FTIR Spectroscopy

A Perkin Elmer BXII spectrometer with an ATR (attenuated total reflection) setup was used for recording the FTIR spectrum.

### 4.5.3 Results and Discussion

#### 4.5.3.1 Synthesis and sample characterization

The driving force behind the reaction is presumably the decomposition of $BaH_2$ (≈ 675 °C)[35] and the formation of $BaCl_2$ with chlorine originating from $LaCl_3$. Among other intermediates, probably La metal is formed, which reacts with the remaining Ba, $LaCl_3$ and the precursor "$Si_2(NH)_3 \cdot 6\ NH_4Cl$" to the observed red crystals of $Ba_{1.63}La_{7.39}Si_{11}N_{23}Cl_{0.42}:Ce^{3+}$. The crystals are stable against air and moisture at ambient temperature. Despite their Ce content, the crystals show no luminescence under UV light. As evident from PXRD data (Figure S2 in the Supporting Information), $Ba_{1.63}La_{7.39}Si_{11}N_{23}Cl_{0.42}:Ce^{3+}$ is only one among several unknown phases in the sample. This confirms that attempts to solve the structure from PXRD data would have been futile.

According to EDX spectra, the ratio of heavy atoms (La, Ba, Ce) : Si = 17(2) : 21(2) = 0.81 which agrees well with the ratio calculated from the single crystal measurement which is 9.02 : 11 = 0.82. Small amounts of Ce were detected. The quantitative EDX results for light elements are unreliable but minor amounts of chlorine were unequivocally detected in agreement with the findings described below (Sections 4.5.3.2 and 4.5.3.4). The FTIR measurement (Figure S3 in the Supporting Information) confirms the absence of N-H bonds and thus the absence of hydrogen.

### 4.5.3.2 Structure solution and refinement

After unsuccessful attempts with laboratory X-ray measurements, the synchrotron data of the microcrystal investigated yielded a straightforward structure solution by direct methods (SHELX program suite).[36] The refinement (full-matrix least-squares algorithm) turned out to be complex. Small amounts of $Ce^{3+}$ were neglected because of the insignificant contribution to the scattering density on the cation positions. As La and Ba are not distinguishable by X-ray scattering, all heavy atoms were initially treated as La. The assignment to Ba/La in the final refinement is described below. Six heavy atom and several possible Si positions resulted from the initial solution. Difference Fourier peaks corresponding to N atoms completed the $SiN_4$-tetrahedra network during the refinement. One additional heavy atom located in the channels of the structure described in Section 4.5.3.4 was found to be disordered into two symmetrically independent split positions (La6A and La6B). Two residual densities not associated with the tetrahedra network were assigned to the positions Ba7 and Cl1; the relevant difference Fourier sections are shown in Figure 1.

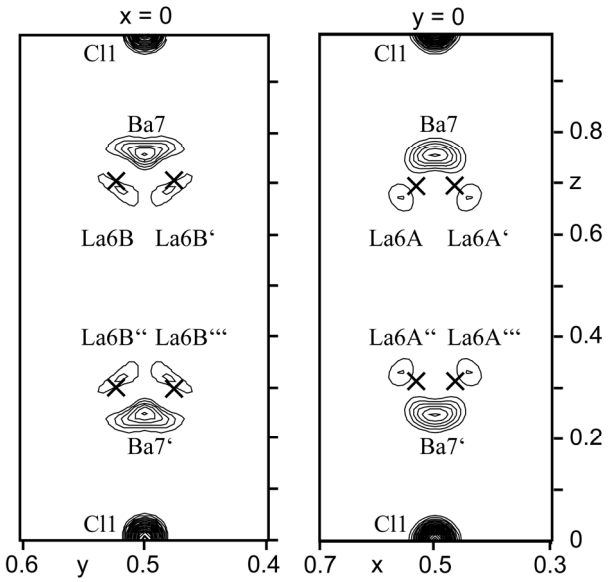


**Figure 1.** Residual electron densities in difference Fourier maps (isoline interval 3 e/Å³) through the “channel” of the structure at x = 0 and y = 0; the occupancy of the Cl1 position is 83.1(4)%, that of Ba7 is 16.9(4)%;. crosses represent La6A/La6B.

Free refinement of the occupancies of La6A and La6B yields a sum of 46.7(8)% + 37.8(8)% = 84.5(8)%, complementary to the occupation of Ba7 which refined to 16.9(5)%. The latter position corresponds to the Ba position reported for the homeotypic compound $Ba_2Nd_7Si_{11}N_{23}$.[37] La6A and LA6B are a fourfold split position around the special position (1/2, 0, *z*), i. e. two closely neighboring more general sites. Cl1 was identified as a Cl atom due to crystal chemical considerations and EDX results. Its occupancy was refined to 83.3(8)%, very similar to the sum of La6A/La6B. This position is too close to the Ba7 positions (distance 2.39 Å) but is in a typical distance relative to the La6A/La6B positions (2.98 Å). Thus, as further discussed in Section 4.5.3.4, it is reasonable to assume a disordered structure where either groups of two Ba occupy the channels or where they are replaced by a combination of La and Cl. The free refinement of the occupancies clearly corroborates this assumption. However, for the sake of numerical consistency, the occupancies of Ba7 and Cl1 were constrained in the final refinement: Ba7 16.9(4)%, Cl1 83.1(4)%. The occupancy of Cl1 corresponds to the overall occupancy of La6A 47.0(4)% + La6B 37.8(4)% = 84.8(4)%, the slightly higher overall occupancy is a typical feature of multiple split positions.[38] One nitrogen atom's position (N11) is also split. All atoms were refined with anisotropic displacement parameters. Coordinates and displacement parameters for atoms on positions with mixed occupation (La4/Ba4 and La5/Ba5) were constrained to be equal, as well as the displacement parameters for the split position La2A/La2B.

Crystallographic data are listed in Table 1, atomic parameters in Table 2. Anisotropic displacement parameters can be found in Table S2 in the Supporting Information. Further details of the crystal structure investigation can be obtained from the Fachinformationszentrum Karlsruhe, 76344 Eggenstein-Leopoldshafen, Germany (fax: (+49)7247-808-666; e-mail: crysdata@fiz-karlsruhe.de) on quoting the depository number CSD-430956.

**Table 1.** Crystallographic data for the single-crystal structure refinement of $Ba_{1.63}La_{7.39}Si_{11}N_{23}Cl_{0.42}:Ce^{3+}$.

| | |
|---|---|
| formula | $La_{7.39}Ba_{1.63}Cl_{0.42}Si_{11}N_{23}:Ce^{3+}$ |
| formula weight in g $mol^{-1}$ | 1895.65 |
| crystal system | orthorhombic |
| space group | *Cmmm* |
| lattice parameters in Å | *a* = 11.009(3) |
| | *b* = 23.243(8) |
| | *c* = 9.706(4) |
| cell volume in $Å^3$ | 2483.6(15) |
| formula units per unit cell (*Z*) | 4 |
| density in g·$cm^{-3}$ | 5.094 |
| μ in $mm^{-1}$ | 8.73 |
| temperature in K | 297(2) |
| radiation | synchrotron (ESRF; ID11, $\lambda$ = 0.3116 Å) |
| F(000) | 3337 |
| θ range in °; resolution in Å | 1.198 – 15.049; 0.6 |
| total no. of reflections | 23828 |
| independent refl. (I/σ > 3; all) | 3147; 3311 |
| $R_\sigma$, $R_{int}$ | 0.0207, 0.0319 |
| refined parameters | 149 |
| goodness of fit | 1.092 |
| *R*1 (I/σ > 3; all) [a] | 0.0160; 0.0174 |
| *wR*2 (I/σ > 3; all) [b] | 0.0398; 0.0413 |
| $\Delta\rho_{max}$ , $\Delta\rho_{min}$ in e $Å^{-3}$ | 2.76, -1.68 |

[a] $R1 = \sum||F_{obs}| - |F_{calc}|| / \sum |F_{obs}|$, [b] $wR2 = \{\sum[w(|F_{obs}|^2 - |F_{calc}|^2)^2] / \sum[w(|F_{obs}|^2)^2]\}^{1/2}$ with $w = 1 / [\sigma^2(|F_{obs}|^2) + (0.0219\,P)^2 + 4.4353\,P]$ where $P = [Max(|F_{obs}|^2,0) + 2\,|F_{calc}|^2)] / 3$

**Table 2.** Atomic coordinates, equivalent isotropic displacement parameters and site occupancies of $Ba_{1.63}La_{7.39}Si_{11}N_{23}Cl_{0.42}:Ce^{3+}$; $U_{eq}$ is defined as one third of the trace of the orthogonalized $U_{ij}$ tensor $\exp[-2\pi^2 (U_{11}h^2a^{*2} + U_{22}k^2b^{*2} + U_{33}l^2c^{*2} + U_{12}hka^*b^* + U_{13}hla^*c^* + U_{23}klb^*c^*)]$.

| Atom | | *x* | *y* | *z* | $U_{eq}$ | *s.o.f.* |
|---|---|---|---|---|---|---|
| La1 | 8*n* | 0 | 0.12028(2) | 0.20611(2) | 0.00657(3) | 1 |
| La2A | 8*p* | 0.29042(9) | 0.10021(5) | 0 | 0.00647(8) | 0.953(9) |
| La2B | 8*p* | 0.3055(12) | 0.0912(7) | 0 | = $U_{eq}$(La2A) | 0.047(9) |
| La3 | 4*j* | 0 | 0.33479(2) | ½ | 0.00769(4) | 1 |
| La4/Ba4 | 4*h* | 0.16485(2) | 0 | ½ | 0.01038(4) | 0.16/0.84[a] |
| La5/Ba5 | 8*m* | ¼ | ¼ | 0.22302(2) | 0.01144(3) | 0.69/0.31[a] |
| La6A | 8*o* | 0.5341(2) | 0 | 0.31009(14) | 0.0348(7) | 0.235(4) |
| La6B | 8*n* | ½ | 0.02321(14) | 0.30245(19) | 0.0273(8) | 0.189(4) |
| Ba7 | 4*l* | ½ | 0 | 0.2478(4) | 0.0703(19) | 0.169(4) |
| Si1 | 8*o* | 0.14905(5) | 0 | 0.17314(6) | 0.00482(8) | 1 |
| Si2 | 8*q* | 0.13422(5) | 0.20109(3) | ½ | 0.00657(9) | 1 |
| Si3 | 16*r* | 0.26860(4) | 0.11467(2) | 0.33890(4) | 0.00535(6) | 1 |
| Si4 | 8*n* | ½ | 0.17341(2) | 0.16126(6) | 0.00495(8) | 1 |
| Si5 | 4*i* | 0 | 0.21556(3) | 0 | 0.00539(12) | 1 |
| N1 | 4*g* | 0.1695(2) | 0 | 0 | 0.0087(4) | 1 |
| N2 | 16*r* | 0.14815(11) | 0.16049(6) | 0.35499(13) | 0.00826(19) | 1 |
| N3 | 16*r* | 0.37549(12) | 0.15217(6) | 0.25130(15) | 0.0118(2) | 1 |
| N4 | 8*n* | ½ | 0.24639(8) | 0.1496(2) | 0.0125(3) | 1 |
| N5 | 4*i* | ½ | 0.14149(11) | 0 | 0.0074(4) | 1 |
| N6 | 8*q* | 0.17558(16) | 0.40963(8) | ½ | 0.0081(3) | 1 |
| N7 | 8*p* | 0.1277(2) | 0.16907(10) | 0 | 0.0154(4) | 1 |
| N8 | 4*k* | 0 | 0. | 0.2338(3) | 0.0098(4) | 1 |
| N9 | 16*r* | 0.22066(13) | 0.05971(6) | 0.23599(14) | 0.0103(2) | 1 |
| N10 | 4*j* | 0 | 0.23619(11) | ½ | 0.0096(4) | 1 |
| N11 | 8*q* | 0.2631(9) | 0.2450(6) | ½ | 0.0119(14) | ½ |
| Cl1 | 2*b* | ½ | 0 | 0 | 0.0161(3) | 0.831(4) |

[a] cation distribution as obtained by BVS analysis,[39] see text.

#### 4.5.3.3 Bond-valence sum calculations

(BVS) calculations [40-42] were performed in order to determine the Ba/La distribution on the cation positions 1-5. The results (Table S1 in the Supporting Information) established a conclusive sum formula that is electroneutral with respect to the standard deviations of site occupancies. BVS for all Si atoms are also in the expected range for $Si^{4+}$. However, BVS for the atoms in the large channels of the structure are below 0.6 and 0.8 for Ba and La, respectively. In such cases, i.e. when the atoms are not part of a rigid framework, the BVS method is not applicable. This is corroborated by BVS calculations for comparable cations in typical zeolites from the literature utilizing published atomic coordinates. For example, the BVS sum of Na atoms in channels of the faujasite structure was determined to values < 0.16 (expected: 1).[43] In a similar case, positions occupied by divalent copper, located in the channels of faujasite yield BVS below 0.3.[44]

#### 4.5.3.4 Structure description

$Ba_{1.63}La_{7.39}Si_{11}N_{23}Cl_{0.42}:Ce^{3+}$ is homeotypic to $Ba_2Nd_7Si_{11}N_{23}$.[37] The three-dimensionally extended nitridosilicate network (Figure 2a, b) is formed exclusively by vertex-sharing $SiN_4$ tetrahedra. The ratio of fourfold ($Q^4$) and twofold ($Q^2$) interconnected ones in the interrupted network is 10:1, with a degree of condensation κ = n(Si) : n(N) = 0.48. The point symbol for the framework as calculated by TOPOS [45] is $\{3.6^2.7^3\}_2\{3.6^3.7^2\}_2\{3.6^4.7\}_4\{3\}\{4.6^5\}_2$. Apart from *dreier*, *vierer, sechser* and *siebener* rings, the characteristic feature of the structure are *achter* rings that form channels along [001].[46,47] Either $[La_2Cl]^{5+}$ units (83.1(4)%) or two $Ba^{2+}$ ions (16.9(4)%; Figure 2c, d) are located in these channels. The assignment of the cations (in spite of lacking scattering contrast and problematic BVS, Section 4.5.3.3) was possible due to a similar situation in $Ba_2Nd_7Si_{11}N_{23}$, crystal chemical considerations and the requirement to achieve charge neutrality. The Ba/La distribution for the heavy atom positions 1-5 obtained from BVS calculations in conjunction with the model of 83% $[La_2Cl]^{5+}$ units and 17% $Ba^{2+}$ cations renders an almost electroneutral sum formula (< 1 charges deviation for more than 270 charges overall).

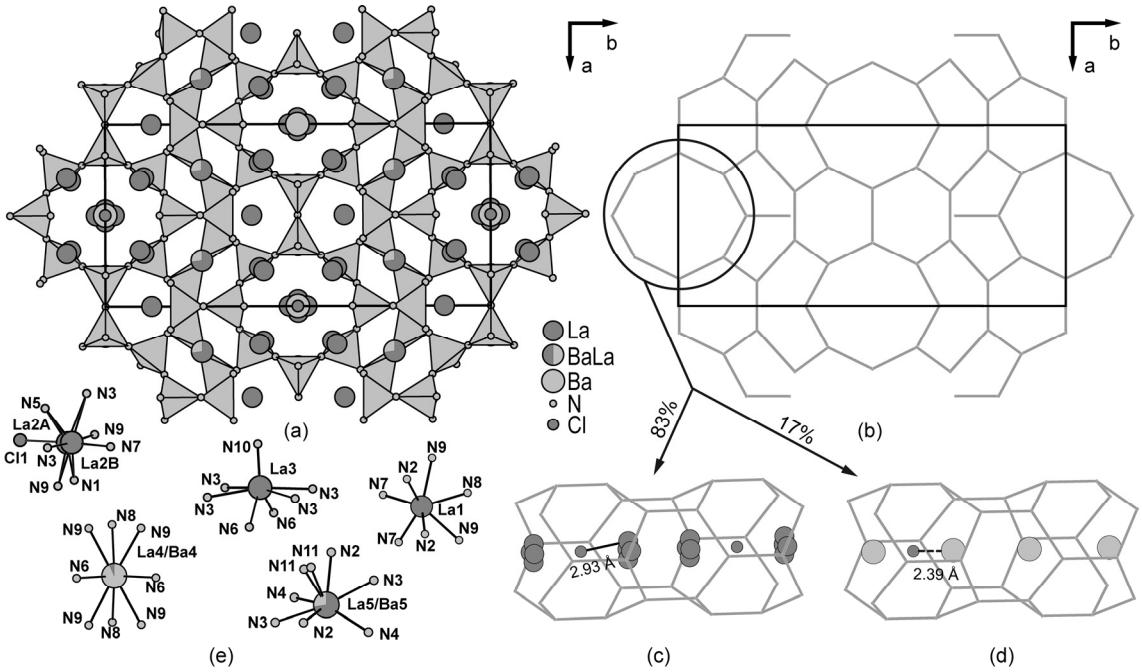


**Figure 2. :** Crystal structure of $Ba_{1.63}La_{7.39}Si_{11}N_{23}Cl_{0.42}:Ce^{3+}$: a) projection of the structure along [001], b) framework skeleton (each line represents a Si-N-Si bond), c and d) the two possible occupancies of the *achter*-ring channel: $[La_2Cl]^{5+}$ units (La on split positions) or $Ba^{2+}$ cations, e) coordination environments of cations not located within the channels.

Similar mixed occupation of channels by Ba and Cl, although not disordered with La, has been reported e.g. for $Ba_3T_3N_5OCl$ (T = Si, Ta). The Si-N distances in $Ba_{1.63}La_{7.39}Si_{11}N_{23}Cl_{0.42}:Ce^{3+}$ range from 1.68 Å to 1.77 Å, well in agreement with those of compounds with similar Si:N ratio and $La^{3+}$ ions like $La_3Si_6N_{11}$ (1.68-1.75 Å).[48.49] Cations located in the *achter* ring channels are coordinated by 16 N (Ba) or 12 N and 1 Cl atom (La). The La-Cl distance (2.98-3.03 Å) lie well between that of pure $LaCl_3$ (2.95 Å)[50] and LaOCl (3.21 Å).[51] In the channels, La-N (3.12-3.79 Å) and Ba-N (3.37-4.36 Å) distances are rather large, owing to the large space present. The weak bonding is in line with high coordination numbers. La-N and Ba-N distances of the remaining 5 (coordination number 7-8) cation positions not located in the channels (Figure 2e) are in the usual rage with 2.29-3.20 Å for the pure La positions (comparable to those in $La_{16}Si_{10}N_{28}O_2$, 2.40-3.19 Å) and 2.67-3.16 Å for the mixed Ba/La positions.[52] (min. Ba-N distance in $BaSiN_2$:[53] 2.89 Å; min. La-N distance in $La_3Si_6N_{11}$:[48] 2.53 Å). The free radius (taking into account van der Waals radii of the networks atoms) for mobile cations in the channels is 2.6 Å, along with a framework density of 17.7 tetrahedra per 1000 Å³. Comparable zeolite-like structures like $Ba_6Si_6N_{10}O_2(CN_2)$,[18] zeolite beta [54] or $[(C_4NH_{12})_4M_4Al_{12}P_{16}O_{64}]$ (M = Co, Zn)[55] have densities of 14.2, 15.1 and 17.9

tetrahedra per 1000 Å³. Continuous channels along [001] along with large cavities suggest possible ion exchange properties.

## 4.5.4 Conclusion

As a variation of the $Ba_2Nd_7Si_{11}N_{23}$ structure type, $Ba_{1.63}La_{7.39}Si_{11}N_{23}Cl_{0.42}:Ce^{3+}$ shows the ability of this nitridic framework to host different atoms or groups in its cavities. The compound is stable against air or moisture at ambient temperature and contains a large channel system, thus substitution and ion exchange experiments seem promising. Along with $La_6Ba_3[Si_{17}N_{29}O_2]Cl$, the title compound is another example that "$Si_2(NH)_3 \cdot 6\ NH_4Cl$" is a valuable precursor for the synthesis of new (oxo)nitridosilicates. The structure determination showed that microfocused synchrotron radiation is a useful way to obtain precise structure analyses of crystals from inhomogeneous and microcrystalline samples. Without such data, it would not have been possible to derive the complex structure model.

## 4.5.5 References

[1] M. Zeuner, S. Pagano, W. Schnick, *Angew. Chem. Int. Ed.* **2011**, *50*, 7754.

[2] D. Durach, W. Schnick, *Eur. J. Inorg. Chem.* **2015**, *24*, 4095.

[3] Z. Inoue, M. Mitomo, N. Li, *J. Mater. Sci.* **1980**, *15*, 2915.

[4] T. Schlieper, W. Milius, W. Schnick, *Z. Anorg. Allg. Chem.* **1995**, *621*, 1380.

[5] M. Zeuner, S. Pagano, P. Matthes, D. Bichler, D. Johrendt, T. Harmening, R. Pöttgen, W. Schnick, *J. Am. Chem. Soc.* **2009**, *131*, 11242.

[6] S. Lupart, M. Zeuner, S. Pagano, W. Schnick, *Eur. J. Inorg. Chem.* **2010**, *18*, 2636.

[7] H. A. Höppe, H. Lutz, P. Morys, W. Schnick, A. Seilmeier, *J. Phys. Chem. Solids* **2000**, *61*, 2001.

[8] R. Müller-Mach, G. Müller, M. R. Krames, H. A. Höppe, F. Stadler, W. Schnick, T. Jüstel, P. Schmidt, *Phys. Status Solidi A* **2005**, *202*, 1727.

[9] M. Seibald, T. Rosenthal, O. Oeckler, W. Schnick, *Crit. Rev. Solid State Mater. Sci.* **2014**, *39*, 215.

[10] J. Lang, J. P. Charlot, *Rev. Chim. Miner.* **1970**, *7*, 121.

[11] H. Hillebrecht, J. Curda, L. Schröder, H. G. v. Schnering, *Z. Kristallogr. Suppl.* **1993**, *6*, 80.

[12] D. R. MacFarlane, J. Huang, M. Forsyth, *Nature* **1999**, *402*, 792.

[13] M. S. Bhamra, D. J. Fray, *Mater. Sci.* **1995**, *30*, 5381.

[14] S. Lupart, G. Gregori, J. Maier, W. Schnick, *J. Am. Chem. Soc.* **2012**, *134*, 10132.

[15] Y. Takeuchi, N. Haga, J. Ito, *Z. Kristallogr.* **1973**, *137*, 380.

[16] S. J. Sedlmaier, M. Döblinger, O. Oeckler, J. Weber, J. Schmedt auf der Günne, W. Schnick, *J. Am. Chem. Soc.* **2011**, *133*, 12069.

[17] S. Correll, O. Oeckler, N. Stock, W. Schnick, Angew. *Chem. Int. Ed.* **2003**, *42*, 3549.

[18] S. Pagano, O. Oeckler, T. Schröder, W. Schnick, *Eur. J. Inorg. Chem.* **2009**, *18*, 2678.

[19] A. J. D. Barnes, T. J. Prior, M. G. Francesconi, *Chem. Commun.* **2007**, *44*, 4638.

[20] A. Marchuk, W. Schnick, *Angew. Chem. Int. Ed.* **2015***, 54*, 2383.

[21] C. Schmolke, O. Oeckler, D. Bichler, D. Johrendt, W. Schnick, *Chem. Eur. J.* **2009**, *15*, 9215.

[22] S. Schmiechen, H. Schneider, P. Wagatha, C. Hecht, P. J. Schmidt, W. Schnick, *Chem. Mater.* **2014**, *26*, 2712.

[23] D. Durach, F. Fahrnbauer, O. Oeckler, W. Schnick, *Inorg. Chem.* **2015**, *54*, 8727.

[24] F. Fahrnbauer, T. Rosenthal, T. Schmutzler, G. Wagner, G. B. M. Vaughan, J. P. Wright, O. Oeckler, *Angew. Chem*. *Int. Ed.* **2015**, *54,* 10020.

[25] J. Besson, *Compt. rend-* **1890**, *110*, 518.

[26] W. Schnick, H. Huppertz, R. Lauterbach, *J. Mater. Chem.* **1999**, *9*, 289.

[27] B. Lengeler, C. Schroer, J. Tümmler, B. Benner, M. Richwin, A. Snigirev, I. Snigireva, M. Drakopoulos, *J. Synchrotron Rad.* **1999**, *6*, 1153.

[28] G. B. M. Vaughan, J. P. Wright, A. Bytchkov, M. Rossat, H. Gleyzolle, I. Snigireva, A. Snigirev, *J. Synchrotron Rad.* **2011**, *18*, 125.

[29] J. L. Chambers, K. L. Smith, M. R. Pressprich, Z. Jin, *SMART*, Bruker-AXS, Madison, USA, **1997-1998**, v. 5.059.

[30] *SAINT*, Bruker-AXS, Madison, USA, **1997-2002**, v. 6.36A.

[31] G. M. Sheldrick, *SADABS, Multi-Scan Absorption Correction*, Bruker-AXS, WA, USA, **2012**, v. 2.

[32] G. Wu, B. L. Rodrigues, P. Coppens, *J. Appl. Crystallogr.* **2002**, *35*, 356.

[33] V. Petricek, M. Dusek, L. Palatinus, *Z. Kristallogr*. **2014**, *229*, 345.

[34] *WINXPOW, Program for powder data handling*, Stoe & Cie GmbH, Darmstadt, Germany, **2007**, v. 2.21.

[35] W. Grochala, P. Edwards, *Chem. Rev.* **2004**, *104*, 1283.

[36] G. M. Sheldrick, *Acta Crystallogr. Sect. C* **2015**, *71*, 3.

[37] H. Huppertz, W. Schnick, *Angew. Chem., Int. Ed. Engl.* **1997**, *36*, 2651.

[38] G. Miehe, T. Vogt, H. Fuess, U. Müller, *Acta Crystallogr. Sect. B* **1993**, *49*, 745.

[39] A. S. Wills, *VaList,* University College London, UK, **2010**, v. 4.0.7.

[40] I. D. Brown, D. Altermatt, *Acta Crystallogr. Sect. B* **1985**, *41*, 244.

[41] N. E. Brese, M. O'Keeffe, *Acta Crystallogr. Sect. B* **1991**, *47*, 192.

[42] A. Trzesowska, R. Kruszynski, T. J. Bartczak, *Acta Crystallogr. Sect. B* **2005**, *61,* 429.

[43] J. Marti, J. Soria, F. H. Cano, *J. Colloid Interface Sci.* **1977**, *60*, 82.

[44] I. E. Maxwell, J. J. de Boer, *J. Phys. Chem.* **1975**, *79*, 1874.

[45] V. A. Blatov, A. P. Shevchenko, D. M. Proserpio, *Cryst. Growth Des.* **2014**, *14*, 3576.

[46] F. Liebau, *Structural Chemistry of Silicates*, Springer: Berlin, **1985**.

[47] The term *dreier* (*vierer*, *sechser*, *siebener*, *achter*) ring was coined by Liebau and is derived from the German word “drei” (“vier, “sechs”, “sieben”, “acht”); a *dreier* (*vierer*, *sechser, siebener*, *achter*) ring comprises three (four, six, seven, eight) tetrahedra centers.

[48] M. Woike, W. Jeitschko, *Inorg. Chem.* **1995**, *34*, 5105.

[49] W. M. Meier, D. H. Olson, *Atlas of Zeolite Structure Types*, Butterworths, London, **1987**.

[50] B. Morosin, *J. Chem. Phys*. **1968**, *49*, 3007.

[51] E. N. Maslen, V. A. Streltsov, N. R. Streltsova, N. Ishizwa, *Acta Crystallogr. Sect. B* **1996**, *52*, 576.

[52] C. Schmolke, S. Lupart, W. Schnick, *Solid State Sci*. **2009**, *11*, 305.

[53] Z. A. Gal, P. M. Mallinson, H. J. Orchard, S. J. Clarke, *Inorg. Chem.* **2004**, *43*, 3998.

[54] J. B. Higgins, R. B. LaPierre, J. L. Schlenker, A. C. Rohrman, J. D. Wood, G. T. Kerr, W. J. Rohrbaugh, *Zeolites* **1988**, *8*, 446.

[55] Z. Liu, X. Song, J. Li, Y. Li, J. Yu, R. Xu, *Inorg. Chem*. **2012**, *51*, 1969.

# 5 Conclusion and Outlook

Lanthanum (oxo)nitridosilicates are intriguing compounds, not only from a structural point of view but also as they are promising candidates for application in efficient neutral to warm-white 1pc-LEDs. Thus, the first focus of this thesis was set on the development of an innovative synthesis route leading to novel lanthanum (oxo)nitridosilicates.

Since precursor approaches, combining crystalline metal amide precursors and "$Si(NH)_2$", already yielded several (oxo)nitridosilicates[1] this route served as starting point. But to avoid thermodynamic sinks and the synthesis of already known compounds, this approach was developed. In order to access novel phases by modified reaction conditions, next to the precursors $La(NH_2)_3$ and "$Si(NH)_2$", lanthanum halides ($LaX_3$, X = F, Cl, Br) and earth alkali hydrides ($EAH_2$, *EA* = Ca, Sr, Ba) were used as starting materials. This seems to be promising as the decomposition of the $EAH_2$ around 600 °C ($CaH_2$: 600 °C, $BaH_2$/$SrH_2$: 675 °C)[2] and its reaction to $EAX_2$ with the halide originating from $LaX_3$ can probably be used as driving force for the reaction. Among other intermediates, presumably finely dispersed and reactive La metal is formed, which reacts with the remaining *EA*, $LaX_3$, the precursors and $La_2O_3$, which was added in some syntheses as oxygen source. $CeF_3$ was added to all reactions as doping agent. With this approach seven so far unknown lanthanum (oxo)nitridosilicates with intriguing structures have been obtained. Whether the *EA* or X ions are incorporated in the lanthanum (oxo)nitridosilicate or not presumably depends on the composition of the starting materials. For example, $La_3[SiN_3O]$ represents a lanthanum oxonitridosilicate consisting only of La, Si, N and O, whereas for the synthesis of $La_{13.68}Sr_{12.32}[Si_{60}N_{96}]F_{6.32}O_{5.68}$ the F ions of $LaF_3$ as well as the Sr ions of $SrH_2$ are necessary. Additionally, syntheses are possible in which either the halide or the earth alkaline ions are incorporated as shown e.g. with the syntheses of $La_3SiN_4F$ and $La_5CaSi_{12}N_{17}O_7\square_2:Ce^{3+}$. Moreover, this route allows for a great structural variety, since it leads to e.g. $La_3BaSi_5N_9O_2:Ce^{3+}$, a yellow phosphor with a fascinating three-dimensional network of $SiN_4$ and $SiN_2O_2$ tetrahedra, as well as to $La_3SiN_4F$, which is the only known non-condensed nitridosilicate next to $Ca_4SiN_4$. Furthermore, "$Si_2(NH)_3{\cdot}6NH_4Cl$" comprises a great potential as a precursor for the synthesis of intriguing lanthanum (oxo)nitridosilicates, since this compound provides another stoichiometric proportion of Si and N and another oxidation state of Si as the common precursors $Si_3N_4$ and "$Si(NH)_2$" (chapter 4.3). Therefore, "$Si_2(NH)_3{\cdot}6NH_4Cl$" was used as starting material for some

syntheses instead of "$Si(NH)_2^{''}$". Its combination with $EAH_2$ (*EA* = Ca, Ba) and $LaCl_3$ yielded $La_{3.7}Ca_{2.3}Si_{12}N_{11.7}O_{14.3}:Ce^{3+}$, a promising phosphor material, and $La_6Ba_3[Si_{17}N_{29}O_2]Cl$, an oxonitridosilicate chloride with a complex three-dimensional network, which is a hierarchical derivative of the simple NiAs structure type. These reactions demonstrate the great capability of this precursor.

Based on the enormous variation possibilities concerning the starting materials, the composition of the starting materials as well as the thermal treatment of the samples, the developed synthesis approach might also enable the synthesis of further new lanthanum (oxo)nitridosilicates in future. Moreover, it will probably be applicable to other (oxo)nitridosilicates and will thus help to expand the compound class of (oxo)nitridosilicates in general. Due to the promising materials properties of some (oxo)nitridosilicates (chapter 1 and 3) this approach might lead to new auspicious functional materials, as proved with the synthesis of the phosphor materials $La_3BaSi_5N_9O_2:Ce^{3+}$, $La_5CaSi_{12}N_{17}O_7\square_2:Ce^{3+}$ and $La_{3.7}Ca_{2.3}Si_{12}N_{11.7}O_{14.3}:Ce^{3+}$. Especially $La_5CaSi_{12}N_{17}O_7\square_2:Ce^{3+}$ and $La_{3.7}Ca_{2.3}Si_{12}N_{11.7}O_{14.3}:Ce^{3+}$ will probably revolutionize the LED market, since these phosphors presumably enable the production of highly efficient neutral to warm-white 1pc-LEDs. $La_3BaSi_5N_9O_2:Ce^{3+}$ served as a powerful example for the demonstration of the capability of the combination of electron microscopy and synchrotron microdiffraction for detailed structure elucidation of microcrystals even in inhomogeneous samples. Electron microscopy helps with the crystal selection and synchrotron microdiffraction yielded high-quality X-ray data. The latter was also confirmed with the investigation of the microcrystals of $La_6Ba_3[Si_{17}N_{29}O_2]Cl$, $Ba_{1.63}La_{7.39}Si_{11}N_{23}Cl_{0.42}:Ce^{3+}$ and $La_{11}Si_{13}N_{27.636}O_{1.046}:Ce^{3+}$. This elaborated approach is a powerful tool, as it enables to draw conclusions about the relation between structures and properties even for inhomogeneous samples with microcrystals. Additionally, the knowledge of the exact composition, obtained from structure analysis, enables synthesis optimization, whereas attempts based on the approximate composition determined by EDX often failed, as proved with the investigation of $La_{11}Si_{13}N_{27.636}O_{1.046}:Ce^{3+}$. Consequently, the combination of electron microscopy and synchrotron microdiffraction may accelerate the development and optimization of functional materials, as properties of phase-pure samples can be more easily investigated and tuned.

## References

[1] M. Zeuner, F. Hintze, W. Schnick, *Chem. Mater.* **2009**, *21*, 336.

[2] W. Grochala, P. Edwards, *Chem. Rev.* **2004**, *104*, 1283.

# 6 Summary

## 6.1 Lanthanum (Oxo)nitridosilicates: From Ordered to Disordered Crystal Structures

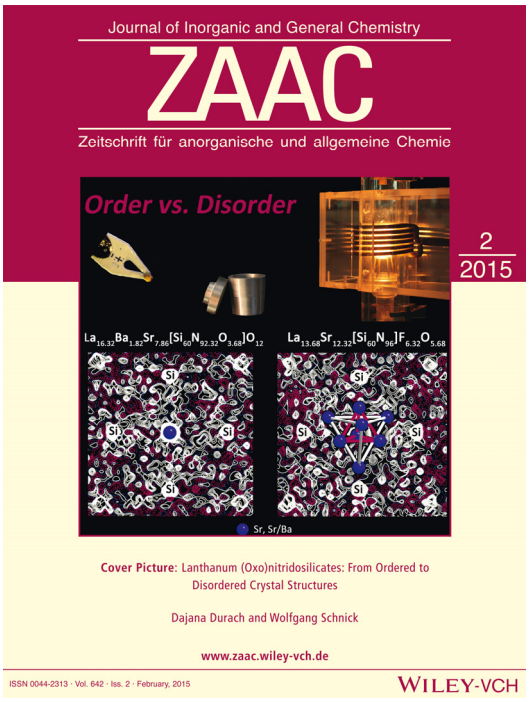


The homeotypic compounds $La_{16.32}Ba_{1.82}Sr_{7.86}[Si_{60}N_{92.32}O_{3.68}]O_{12}$ and $La_{13.68}Sr_{12.32}[Si_{60}N_{96}]F_{6.32}O_{5.68}$ were synthesized in a radio-frequency furnace at high temperatures (1600/1500 °C). The crystal structures [$I\bar{4}3m$ (no. 217), $Z$ = 1, $a$ = 13.3360(10)/13.3258(10) Å and $V$ = 2371.8(5)/2366.4(5) Å$^3$] were elucidated from single-crystal X-ray diffraction data and corroborated by lattice-energy calculations (Madelung part of lattice energy, MAPLE) powder X-ray diffraction data and FTIR spectroscopy. Both compounds are built up by a three-dimensional network of all side corner sharing $SiN_{4-x}O_x$ tetrahedra. The framework is characterized by double *dreier* rings. Besides, the crystal structures contain non-condensed ($O^{[0]}$/O,$F^{[0]}$) anions. $La_{16.32}Ba_{1.82}Sr_{7.86}[Si_{60}N_{92.32}O_{3.68}]O_{12}$ is isotypic to $Sr_3Ln_{10}Si_{18}Al_{12}O_{18}N_{36}$ (*Ln* = Ce, Pr, Nd; $Z$ = 2), whereas $La_{13.68}Sr_{12.32}[Si_{60}N_{96}]F_{6.32}O_{5.68}$ describes a disordered model of the crystal structure, which is homeotypic to the mentioned SiAlONs. It could be shown that syntheses based on $LaF_3$, hydrides and amides permit a promising synthetic approach to new lanthanum (oxo)nitridosilicates.

## 6.2 Non-Condensed (Oxo)nitridosilicates: $La_3[SiN_4]F$ and the Polymorph o-$La_3[SiN_3O]O$

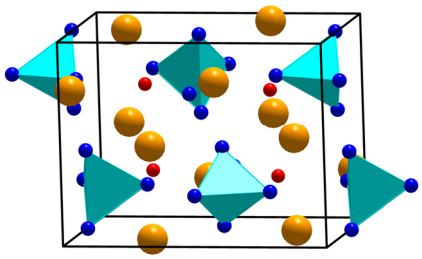

The isotypic compounds $La_3[SiN_4]F$ and $La_3[SiN_3O]O$ were synthesized in a radio-frequency furnace at 1600 °C. The crystal structures [*Pnma* (no. 62), $Z = 4$; $La_3(SiN_4)F$: $a = 9.970(3)$, $b = 7.697(2)$, $c = 6.897(2)$ Å, $V = 529.3(3)$ Å$^3$; $La_3(SiON_3)O$: $a = 9.950(2)$, $b = 7.6160(15)$, $c = 6.9080(14)$ Å, $V = 523.48(18)$ Å$^3$] were solved and refined on the basis of single-crystal X-ray diffraction data. Accuracy of the structure determinations were confirmed by Rietveld refinement, lattice-energy calculations (Madelung part of lattice energy, MAPLE) and Raman/FTIR spectroscopy. Both compounds are homeotypic with $Na_2Pr[GeO_4]OH$ forming a network of vertex-sharing $FLa_6/OLa_6$ octahedra, whose voids are filled with non-condensed $SiN_4/SiN_3O$ tetrahedra. o-$La_3[SiON_3]O$ is the orthorhombic polymorph of this compound, which probably represents the high-temperature modification, whereas the tetragonal polymorph t-$La_3[SiON_3]O$ represents the low-temperature modification. While the space group of the t-polymorph [*I*4/*mcm* (no. 140)] differs from that of the new $La_3[SiN_4]F$ and o-$La_3[SiN_3O]O$, the crystal structure contains the same linking pattern. It has been shown that the synthetic approach based on $LaHal_3$ (Hal = halides), hydrides and amides also allows for the synthesis of new less-condensed lanthanum (oxo)nitridosilicates.

## 6.3 $La_5CaSi_{12}N_{17}O_7\square_2$ and $La_{3.7}Ca_{2.3}Si_{12}N_{11.7}O_{14.3}$: Two Promising Host Lattices for $Eu^{2+}$- and $Ce^{3+}$-doping Towards Phosphor Materials with Highly Tunable Luminescence

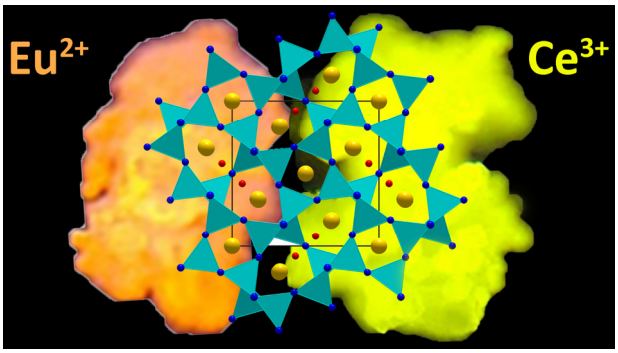


$La_5CaSi_{12}N_{17}O_7\square_2$ and $La_{3.7}Ca_{2.3}Si_{12}N_{11.7}O_{14.3}$ were obtained by high-temperature reactions (1600 / 1400 °C) in a radio-frequency furnace. The crystal structures [*P*4*bm* (no. 100), $Z = 1$, $a = 10.1505(3)$ / 10.0881(4) Å, $c = 4.8806(2)$/ 4.9234(2) Å, $V = 502.86(4)$ / 501.05(4) Å$^3$] were elucidated from single-crystal X-ray diffraction data. Rietveld refinements confirm that the target phases could be obtained as bulk samples. FTIR spectroscopy proves the absence of N-H bonds. $La_5CaSi_{12}N_{17}O_7\square_2$ and $La_{3.7}Ca_{2.3}Si_{12}N_{11.7}O_{14.3}$ are homeotypic to $La_3Si_6N_{11}$ ($Z = 2$) as they are characterized by the same network, consisting of *vierer* and *achter* rings of all side vertex sharing $Si(N,O)_4$, but contain an additional isolated O site. Moreover, both compounds show intriguing luminescence properties upon doping with $Ce^{3+}$ or $Eu^{2+}$ or being codoped with $Ce^{3+}$ and $Eu^{2+}$. Consequently, the luminescence of doped $La_5CaSi_{12}N_{17}O_7\square_2$ and $La_{3.7}Ca_{2.3}Si_{12}N_{11.7}O_{14.3}$ can be easily tuned, thus both are promising candidates for application in neutral to warm-white 1pc-LEDs (LEDs based on a single-phosphor approach).

## 6.4 $La_3BaSi_5N_9O_2:Ce^{3+}$ - A Yellow Phosphor with an Unprecedented Tetrahedra Network Structure Investigated by Combination of Electron Microscopy and Synchrotron X-ray Diffraction

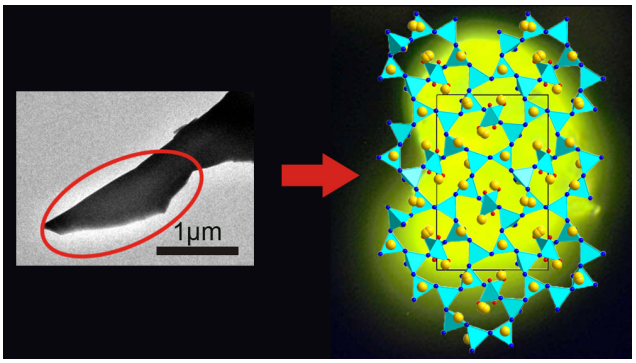


A high-temperature reaction starting from $LaF_3$, $La(NH_2)_3$, $BaH_2$, $Si(NH)_2$, and $CeF_3$ yielded an inhomogeneous sample with small aggregates of the yellow phosphor $La_3BaSi_5N_9O_2:Ce^{3+}$ ($\lambda_{max}$ = 578 nm; fwhm ~4700 $cm^{-1}$). The latter were characterized by a combination of transmission electron microscopy (TEM) and synchrotron microfocus diffraction which allows for the analysis of particles with a volume even smaller than 1 $\mu m^3$ and furthermore provides the possibility of analyzing the same particle by TEM and X-ray diffraction. Consequently, this elaborate characterization approach could help to push forward the research of phosphor materials for LEDs. $La_3BaSi_5N_9O_2:Ce^{3+}$ crystallizes in space group $Pmn2_1$ (no. 31) with $a$ = 9.5505(8), $b$ = 19.0778(16), $c$ = 12.1134(9) Å, and $Z$ = 8. Its interrupted three-dimensional tetrahedra network contains *zehner* and *dreier* rings of vertex-sharing $SiN_4$ and $SiN_2O_2$ tetrahedra. The crystal structure was confirmed by high-resolution TEM and Z-contrast scanning TEM. The element distribution was derived by bond-valence sum calculations. Rietveld refinement proves that the sample contains $La_3BaSi_5N_9O_2:Ce^{3+}$ as main phase. The infrared spectrum confirms the absence of N-H bonds.

## 6.5 $La_6Ba_3[Si_{17}N_{29}O_2]Cl$ – An Oxonitridosilicate Chloride with Exceptional Structural Motifs

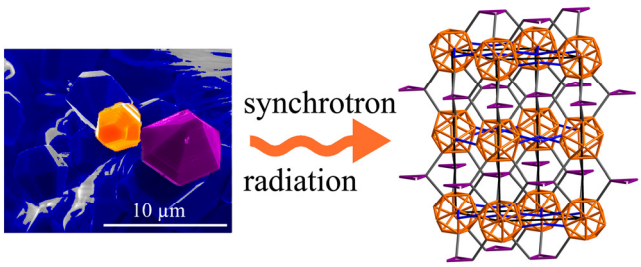


Crystals of the oxonitridosilicate chloride $La_6Ba_3[Si_{17}N_{29}O_2]Cl$ were obtained by high-temperature synthesis starting from $LaCl_3$, $BaH_2$, and the ammonolysis product of $Si_2Cl_6$. As only crystals with a maximum size of a few µm could be obtained, diffraction data were collected using microfocused synchrotron radiation at beamline ID11 at the ESRF. EDX measurements on the same crystal confirm the chemical composition. The crystal structure [space group $P6_3/m$ (no. 176), $a$ = 9.8117(14), $c$ = 19.286(6) Å, $Z$ = 2] is built up by an unprecedented complex three-dimensional network, which is a hierarchical derivative of the simple NiAs structure type. Rietveld refinements confirm that the final product contains only a small amount of impurities. The element distribution was derived by bond-valence sum (BVS) and lattice energy (MAPLE) calculations, which also show that the structure is electrostatically well-balanced. Infrared spectroscopy confirms the absence of N-H bonds. Next to the importance of microfocused synchrotron radiation, which enables the precise determination of the structure of microcrystals, the relevance of the precursor "$Si_2(NH)_3{\cdot}6NH_4Cl$" could be shown, which seems to be a promising starting material for the synthesis of novel (oxo)nitridosilicates.

## 6.6 From Minor Side Phases to Bulk Samples of Lanthanum Oxonitridosilicates – An Investigation with Microfocused Synchrotron Radiation

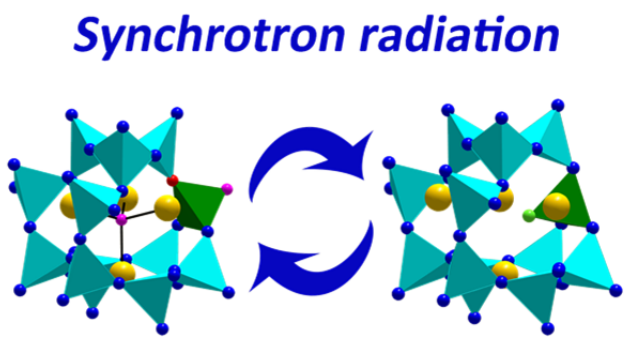


Crystals of $La_{11}Si_{13}N_{27.636}O_{1.046}:Ce^{3+}$ were synthesized in a radio-frequency furnace at high temperatures starting from La, $La(NH_2)_3$, $Si(NH)_2$, $BaH_2$ and $CeF_3$. Diffraction data of a micrometer-sized single crystal were obtained using microfocused synchrotron radiation at beamline ID11 at the ESRF [space group *Cmc*$2_1$ (no. 36), $a = 9.5074(4)$, $b = 32.0626(9)$, $c = 18.5076(8)$ Å, $Z = 8$, $R1(all) = 0.0267$]. The crystal structure contains an unprecedented interrupted three-dimensional network of vertex-sharing $SiN_{4-x}O_x$ tetrahedra that form channels of *siebener* rings along [100], *sechser* rings in boat conformation and *vierer* rings, which are alternatingly stacked with layers of *vierer* and *dreier* rings. Several split positions indicate two different local structure variants. Infrared spectroscopy confirms the absence of N-H bonds. Powder X-ray diffraction data prove that the product contains only a small amount of $La_{11}Si_{13}N_{27.636}O_{1.046}:Ce^{3+}$. With the knowledge of the exact composition, as unambiguously derived by the structure analysis (and supported by matching yet imprecise EDX measurements), it was possible to optimize the synthesis, using fluorides as starting materials. Thereby bulk samples of the homeotypic compound $La_{11}Si_{13}N_{27.376}O_{0.936}F$ were obtained and investigated. Consequently, the described characterization approach may accelerate the development and optimization of functional materials, as properties of phase-pure samples can be more easily investigated and tuned.

## 6.7 $Ba_{1.63}La_{7.39}Si_{11}N_{23}Cl_{0.42}:Ce^{3+}$ - A Nitridosilicate Chloride with a Zeolite-like Structure

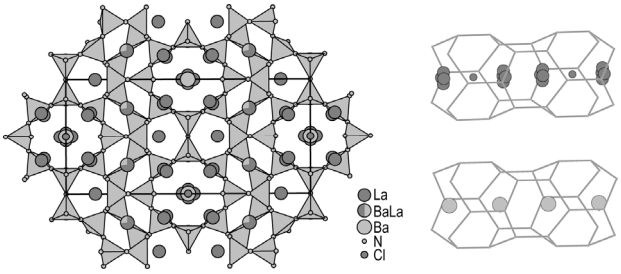


A high-temperature metathesis reaction starting from $LaCl_3$, $BaH_2$, $CeF_3$ and the product of the ammonolysis of $Si_2Cl_6$ yielded an inhomogeneous sample with microcrystals of $Ba_{1.63}La_{7.39}Si_{11}N_{23}Cl_{0.42}:Ce^{3+}$. Due to the small size of the crystals, diffraction data of a microcrystal were collected using microfocused synchrotron radiation at beamline ID11 at the ESRF [space group *Cmmm* (no. 65), with $a$ = 11.009(3), $b$ = 23.243(8), $c$ = 9.706(4) Å, $Z$ = 4; $R1$(all) = 0.0174]. X-ray spectroscopy confirms the chemical composition of the crystal. IR spectra corroborate absence of N-H bonds. The crystal structure of $Ba_{1.63}La_{7.39}Si_{11}N_{23}Cl_{0.42}:Ce^{3+}$ is homeotypic to $Ba_2Nd_7Si_{11}N_{23}$ and is built up by a three-dimensional network of vertex-sharing $SiN_4$ tetrahedra that form channels of *achter* rings along [001]. According to bond valence sum calculations, some crystallographic positions show complete occupancy by Ba or La whereas others contain significant amounts of both elements. In contrast to the structure prototype $Ba_2Nd_7Si_{11}N_{23}$, $Ba_{1.63}La_{7.39}Si_{11}N_{23}Cl_{0.42}:Ce^{3+}$ contains chloride ions in channels of the $SiN_4$ tetrahedra network, hinting at various substitution possibilities of the complex zeolite-like structure. It could be shown that "$Si_2(NH)_3 \cdot 6\ NH_4Cl$" is a valuable precursor for the synthesis of new (oxo)nitridosilicates and that microfocused synchrotron radiation is a useful way to obtain precise structure analyses of crystals, even with complex crystal structures, from inhomogeneous and microcrystalline samples.

# 7 Appendix

## 7.1 Supporting Information for Chapter 2.2

Dajana Durach and Wolfgang Schnick, *Z. Anorg. Allg. Chem.* **2016**, *642*, 101-106.

**Table S1.** Anisotropic displacement parameters ($U_{ij}$ in Å$^2$) of $La_{16.32}Ba_{1.82}Sr_{7.86}[Si_{60}N_{92.32}O_{3.68}]O_{12}$ and $La_{13.68}Sr_{12.32}[Si_{60}N_{96}]F_{6.32}O_{5.68}$ with standard deviations in parentheses.

| atom | $U_{11}$ | $U_{22}$ | $U_{33}$ | $U_{23}$ | $U_{13}$ | $U_{12}$ |
|---|---|---|---|---|---|---|
| $La_{16.32}Ba_{1.82}Sr_{7.86}[Si_{60}N_{92.32}O_{3.68}]O_{12.}$ | | | | | | |
| La/Sr1 | 0.01216(9) | $U_{11}$ | 0.00889(12) | 0.00006(6) | $U_{23}$ | -0.00394(11) |
| Ba/Sr2 | 0.0421(6) | $U_{11}$ | $U_{11}$ | 0 | 0 | 0 |
| Si1 | 0.0073(7) | 0.0067(4) | $U_{22}$ | 0.0009(6) | 0 | *0* |
| Si2 | 0.0070(3) | $U_{11}$ | 0.0070(5) | -0.0002(3) | $U_{23}$ | -0.0001(4) |
| Si3 | 0.0071(3) | $U_{11}$ | 0.0070(5) | 0.0001(3) | $U_{23}$ | -0.0002(4) |
| O1 | 0.019(3) | 0.0148(16) | $U_{22}$ | 0 | 0 | 0 |
| N/O2 | 0.0112(9) | $U_{11}$ | 0.0101(15) | -0.0015(9) | $U_{23}$ | -0.0037(11) |
| N3 | 0.0128(11) | $U_{11}$ | 0.0103(16) | -0.0009(9) | $U_{23}$ | -0.0045(14) |
| N4 | 0.0073(9) | $U_{11}$ | 0.0125(17) | 0.0020(9) | $U_{23}$ | 0.0007(11) |
| N5 | 0.0091(9) | $U_{11}$ | 0.0072(14) | -0.0005(8) | $U_{23}$ | 0.0021(12) |
| | | | | | | |
| $La_{13.68}Sr_{12.32}[Si_{60}N_{96}]F_{6.32}O_{5.68}$ | | | | | | |
| La/Sr1 | 0.01021(7) | $U_{11}$ | 0.00693(9) | -0.00007(6) | $U_{23}$ | -0.00368(10) |
| Si1 | 0.0047(6) | 0.0050(4) | $U_{22}$ | -0.0003(4) | 0 | 0 |
| Si2 | 0.0051(2) | $U_{11}$ | 0.0046(4) | 0.0000(2) | $U_{23}$ | 0.0001(3) |
| Si3 | 0.0052(3) | $U_{11}$ | 0.0051(4) | 0.0000(2) | $U_{23}$ | -0.0001(3) |
| F1/O1 | 0.0118(17) | 0.0125(11) | $U_{22}$ | 0 | 0 | 0 |
| N2 | 0.0084(7) | $U_{11}$ | 0.0056(11) | 0.0001(7) | $U_{23}$ | -0.0028(8) |
| N3 | 0.0111(9) | $U_{11}$ | 0.0090(13) | -0.0017(7) | $U_{23}$ | -0.0040(11) |
| N4 | 0.0054(7) | $U_{11}$ | 0.0108(13) | 0.0016(7) | $U_{23}$ | 0.0000(9) |
| N5 | 0.0065(7) | $U_{11}$ | 0.0060(12) | 0.0002(7) | $U_{23}$ | 0.0016(9) |

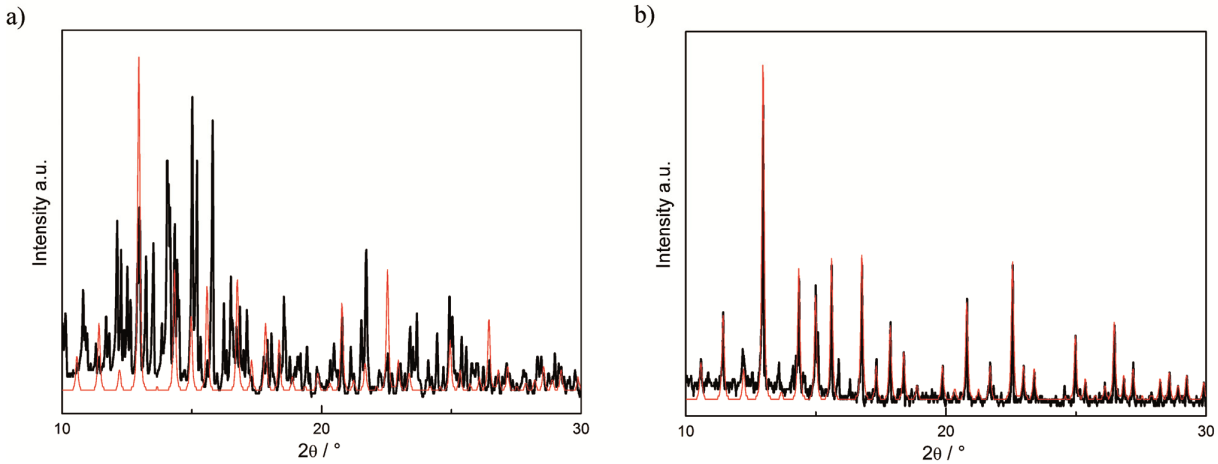


**Figure S1.** Characteristic section of the experimental powder diffraction pattern (black) of the sample containing $La_{16.32}Ba_{1.82}Sr_{7.86}[Si_{60}N_{92.32}O_{3.68}]O_{12}$ (a) and $La_{13.68}Sr_{12.32}[Si_{60}N_{96}]F_{6.32}O_{5.68}$, respectively. (b). Red lines describe the simulation of the structural models obtained from single-crystal structure elucidation of the respective compound.Unassigned reflections belong to common side phases, e.g., $La_3Si_6N_{11}$ (green), or unknown side phases.

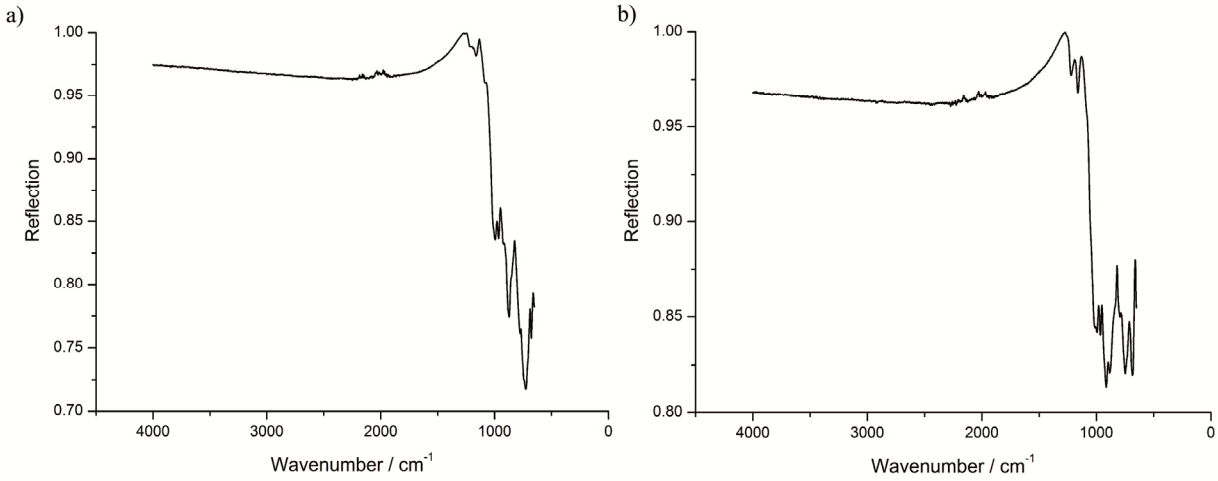


**Figure S2.** IR spectrum of $La_{16.32}Ba_{1.82}Sr_{7.86}[Si_{60}N_{92.32}O_{3.68}]O_{12}$ (a) and $La_{13.68}Sr_{12.32}[Si_{60}N_{96}]F_{6.32}O_{5.68}$ (b).

## 7.2 Supporting Information for Chapter 2.3

Dajana Durach and Wolfgang Schnick, *Eur. J. Inorg. Chem.* **2015**, 4095-4100.

**Table S1.** Anisotropic displacement parameters ($U_{iy}$, in Å$^2$) of $La_3[SiN_4]F$ and o-$La_3[SiN_3O]O$ with standard deviations in parentheses.

| atom | $U_{11}$ | $U_{22}$ | $U_{33}$ | $U_{23}$ | $U_{13}$ | $U_{12}$ |
|---|---|---|---|---|---|---|
| $La_3[SiN_4]F$ | | | | | | |
| La1 | 0.00829(10) | 0.00859(10) | 0.01004(11) | -0.00333(7) | 0.00086(6) | 0.00013(6) |
| La2 | 0.00651(13) | 0.00534(13) | 0.00636(12) | 0 | -0.00102(9) | 0 |
| Si1 | 0.0051(5) | 0.0046(5) | 0.0054(5) | 0 | -0.0001(4) | 0 |
| F1 | 0.0126(14) | 0.0241(16) | 0.0178(15) | 0 | 0.0004(12) | 0 |
| N1 | 0.0090(12) | 0.0056(12) | 0.0121(13) | -0.0015(10) | -0.0011(10) | 0.0006(10) |
| N2 | 0.0048(17) | 0.0117(18) | 0.0078(18) | 0 | 0.0019(14) | 0 |
| N3 | 0.0061(17) | 0.0106(18) | 0.0065(17) | 0 | -0.0008(14) | 0 |
| o-$La_3[SiN_3O]O$ | | | | | | |
| La1 | 0.0087(2) | 0.0105(2) | 0.0107(2) | -0.0030(2) | 0.0003(2) | 0.00038(19) |
| La2 | 0.0075(3) | 0.0079(3) | 0.0084(3) | 0 | -0.0012(3) | 0 |
| Si1 | 0.0071(18) | 0.0066(16) | 0.0066(17) | 0 | -0.0008(13) | 0 |
| O1 | 0.016(5) | 0.024(5) | 0.010(5) | 0 | -0.005(4) | 0 |
| N/O2 | 0.009(3) | 0.009(4) | 0.012(4) | -0.003(3) | -0.006(3) | 0.001(3) |
| N/O3 | 0.009(5) | 0.015(6) | 0.008(5) | 0 | -0.003(4) | 0 |
| N/O4 | 0.009(5) | 0.011(5) | 0.021(7) | 0 | 0.009(4) | 0 |

**Table S2.** Crystallographic data of Rietveld refinement of $La_3[SiN_4]F$ and o-$La_3[SiN_3O]O$.

| Formula | $La_3[SiN_4]F$ | o-$La_3[SiN_3O]O$ |
|---|---|---|
| Crystal system | Orthorhombic | |
| Space group | *Pnma* (no. 62) | |
| *a* [Å] | 9.97076(7) | 9.96745(17) |
| *b* [Å] | 7.69966(5) | 7.6267(12) |
| *c* [Å] | 6.89324(5) | 6.90725(11) |
| Cell volume [$Å^3$] | 529.204(6) | 525.050(14) |
| Formula units per unit cell | 4 | |
| Density [$g \cdot cm^{-3}$] | 6.524 | 6.563 |
| Temperature [K] | 293(2) | |
| Diffractometer | STOE STADI P | |
| Radiation [Å] | Mo-K$\alpha_1$ (λ = 0.70930) | |
| 2θ range [°] | 2-63 | |
| Data points | 4120 | 4087 |
| Total no. of reflections | 970 | 999 |
| Refined parameters | 40 | 143 |
| Background function | Shifted Chebychev | |
| $R_{wp}$ | 0.05537 | 0.04457 |
| $R_{exp}$ | 0.01761 | 0.01859 |
| $R_p$ | 0.03691 | 0.03336 |
| $R_{Bragg}$ | 0.01943 | 0.01580 |
| $\chi^2$ | 3.145 | 2.397 |

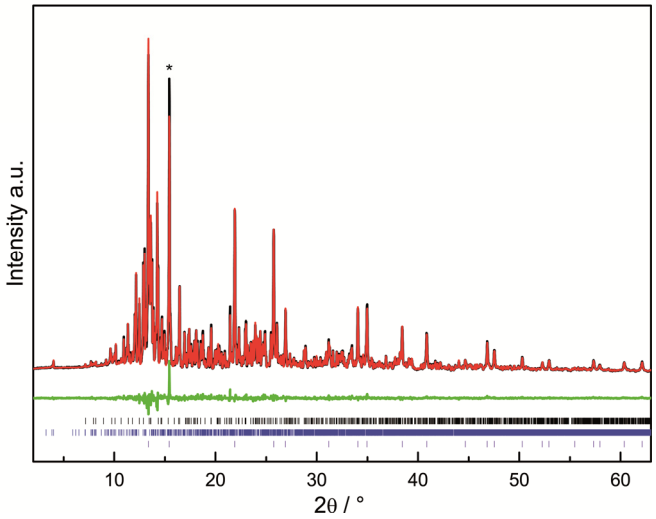


**Figure S1.** Rietveld refinement of the sample containing o-$La_3[SiN_3O]O$. Observed (black line) and calculated (red line) X-ray powder diffraction pattern as well as difference profile (green line). The vertical bars indicate positions of Bragg reflections (black: o-$La_3[SiN_3O]O$ (25%), blue: $La_{16}[Si_8N_{22}][SiON_3]_2$ (54%) purple: LaN (21%). The marked reflection (*) is from LaN.

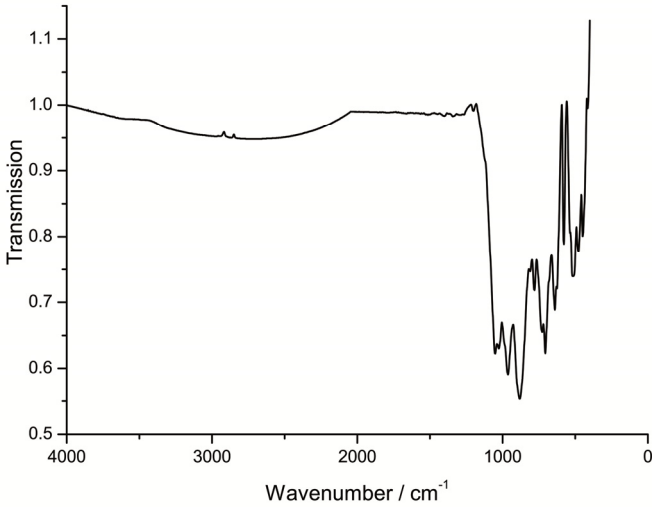


**Figure S2.** IR spectrum of the sample containing $La_3[SiN_4]F$.

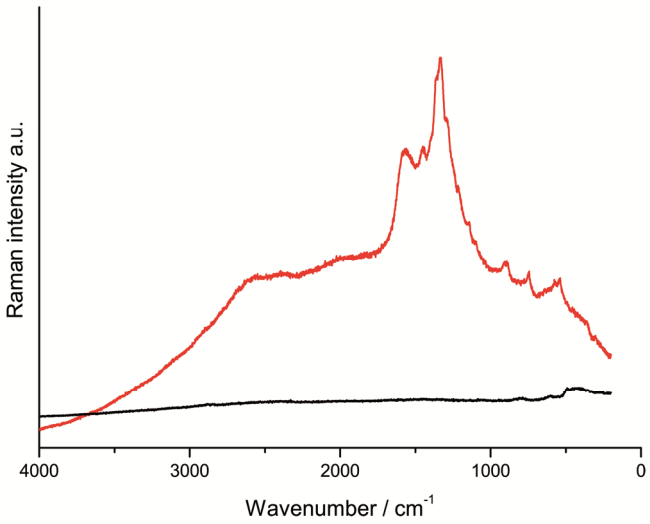


**Figure S3.** Raman spectrum of a crystal of o-$La_3[SiN_3O]O$ (red) and background of the capillary (black).

## 7.3 Supporting Information for Chapter 3.2

Dajana Durach, Peter J. Schmidt and Wolfgang Schnick, *patent in progress.*

**Table S1.** Atomic coordinates, isotropic displacement parameters [Å$^2$] and site occupancies of $La_5CaSi_{12}N_{17}O_7\square_2$ and $La_{3.7}Ca_{2.3}Si_{12}N_{11.7}O_{14.3}$ at room temperature with standard deviations in parentheses.

| atom | | *x* | *y* | *z* | $U_{eq}$ | s.o.f. |
|---|---|---|---|---|---|---|
| $La_5CaSi_{12}N_{17}O_7\square_2$ | | | | | | |
| La1 | 2*a* | 0 | 0 | -0.00003(13) | 0.00525(16) | 1 |
| La,Ca2A | 4*c* | 0.68037(3) | 0.18037(3) | 0.02320(19) | 0.00788(16) | 0.7; 0.25 |
| La2B | 4*c* | 0.6754(7) | 0.1754(7) | 0.198(3) | 0.00788(16) | 0.05 |
| Si1 | 8*d* | 0.20879(13) | 0.07935(13) | 0.5348(5) | 0.0045(3) | 1 |
| Si2 | 4*c* | 0.11796(13) | 0.61796(13) | 0.0449(6) | 0.0037(5) | 1 |
| N1 | 4*c* | 0.1516(5) | 0.6516(5) | 0.6963(14) | 0.0045(14) | 1 |
| N,O2 | 8*d* | 0.2319(5) | 0.0744(5) | 0.1854(10) | 0.0089(10) | 13/18; 5/18 |
| N,O3 | 8*d* | 0.0796(5) | 0.1796(5) | 0.6414(11) | 0.0095(10) | 13/18; 5/18 |
| N,O4 | 2*b* | 0 | ½ | 0.072(2) | 0.014(2) | 13/18; 5/18 |
| O1 | 4*c* | 0.5704(9) | 0.0704(9) | 0.569(3) | 0.021(3) | ½ |
| | | | | | | |
| $La_{3.7}Ca_{2.3}Si_{12}N_{11.7}O_{14.3}$ | | | | | | |
| La,Ca1 | 2*a* | 0 | 0 | 0.00003(18) | 0.00878(17) | 0.95; 0.05 |
| La,Ca2A | 4*c* | 0.67945(6) | 0.17945(6) | 0.0246(3) | 0.0189(3) | 0.4; 0.4 |
| La,Ca2B | 4*c* | 0.6744(4) | 0.1744(4) | 0.1969(18) | 0.0189(3) | 0.05; 0.15 |
| Si1 | 8*d* | 0.20715(14) | 0.08102(13) | 0.5356(4) | 0.0085(3) | 1 |
| Si2 | 4*c* | 0.11985(14) | 0.61985(14) | 0.0449(5) | 0.0070(4) | 1 |
| N1 | 4*c* | 0.1495(5) | 0.6495(5) | 0.6967(13) | 0.0067(13) | 1 |
| N,O2 | 8*d* | 0.2311(5) | 0.0760(5) | 0.1890(10) | 0.0160(10) | 77/180; 103/180 |
| N,O3 | 8*d* | 0.0786(5) | 0.1816(5) | 0.6415(12) | 0.0173(10) | 77/180; 103/180 |
| N,O4 | 2*b* | 0 | ½ | 0.067(2) | 0.028(3) | 77/180; 103/180 |
| O1 | 4*c* | 0.5689(4) | 0.0689(4) | 0.5668(11) | 0.0116(14) | 1 |

**Table S2.** Anisotropic displacement parameters ($U_{iy}$, in Å$^2$) of $La_5CaSi_{12}N_{17}O_7\square_2$ and $La_{3.66}Ca_{2.34}Si_{12}N_{11.66}O_{14.34}$.

| atom | $U_{11}$ | $U_{22}$ | $U_{33}$ | $U_{23}$ | $U_{13}$ | $U_{12}$ |
|---|---|---|---|---|---|---|
| $La_5CaSi_{12}N_{17}O_7\square_2$ | | | | | | |
| La1 | 0.00495(19) | $U_{11}$ | 0.0057(3) | 0 | 0 | 0 |
| La/Ca2A | 0.00364(17) | $U_{11}$ | 0.0176(4) | -0.0002(3) | $U_{23}$ | -0.00055(17) |
| La/Ca2B | 0.00364(17) | $U_{11}$ | 0.0176(4) | -0.0002(3) | $U_{23}$ | -0.00055(17) |
| Si1 | 0.0045(6) | 0.0040(6) | 0.0044(8) | 0.0006(8) | 0.0011(9) | -0.0020(5) |
| Si2 | 0.0033(5) | $U_{11}$ | 0.0046(12) | -0.0003(7) | $U_{23}$ | 0.0001(7) |
| N1 | 0.0047(19) | $U_{11}$ | 0.003(3) | -0.0011(18) | $U_{23}$ | 0.000(3) |
| N/O2 | 0.008(2) | 0.011(2) | 0.007(2) | 0.0001(18) | 0.0001(18) | -0.0013(19) |
| N/O3 | 0.008(2) | 0.010(3) | *0.010(3)* | 0.0008(19) | 0.0003(19) | -0.0011(19) |
| N/O4 | 0.012(3) | $U_{11}$ | 0.019(6) | 0 | 0 | -0.006(3) |
| O1 | 0.021(4) | $U_{11}$ | 0.023(9) | -0.003(4) | $U_{23}$ | 0.002(5) |
| | | | | | | |
| $La_{3.66}Ca_{2.34}Si_{12}N_{11.66}O_{14.34}$ | | | | | | |
| La/Ca1 | 0.0088(2) | $U_{11}$ | 0.0091(3) | 0 | 0 | 0 |
| La/Ca2A | 0.0097(3) | $U_{11}$ | 0.0377(7) | -0.0027(5) | $U_{23}$ | -0.0007(3) |
| La/Ca2B | 0.0097(3) | $U_{11}$ | 0.0377(7) | -0.0027(5) | $U_{23}$ | -0.0007(3) |
| Si1 | 0.0094(6) | 0.0098(6) | 0.0064(7) | 0.0000(7) | 0.0002(7) | -0.0034(5) |
| Si2 | 0.0076(5) | $U_{11}$ | 0.0066(10) | -0.0006(6) | $U_{23}$ | 0.0004(7) |
| N1 | 0.0074(18) | $U_{11}$ | 0.006(3) | 0.0002(16) | $U_{23}$ | 0.001(2) |
| N/O2 | 0.016(2) | 0.020(3) | 0.013(2) | -0.0017(18) | -0.0001(18) | -0.0042(18) |
| N/O3 | 0.017(2) | 0.018(3) | 0.017(3) | -0.001(2) | 0.002(2) | -0.0002(19) |
| N/O4 | 0.022(3) | $U_{11}$ | 0.039(9) | 0 | 0 | -0.004(4) |
| O1 | 0.0105(15) | $U_{11}$ | 0.014(4) | 0.0004(15) | $U_{23}$ | 0.0033(19) |

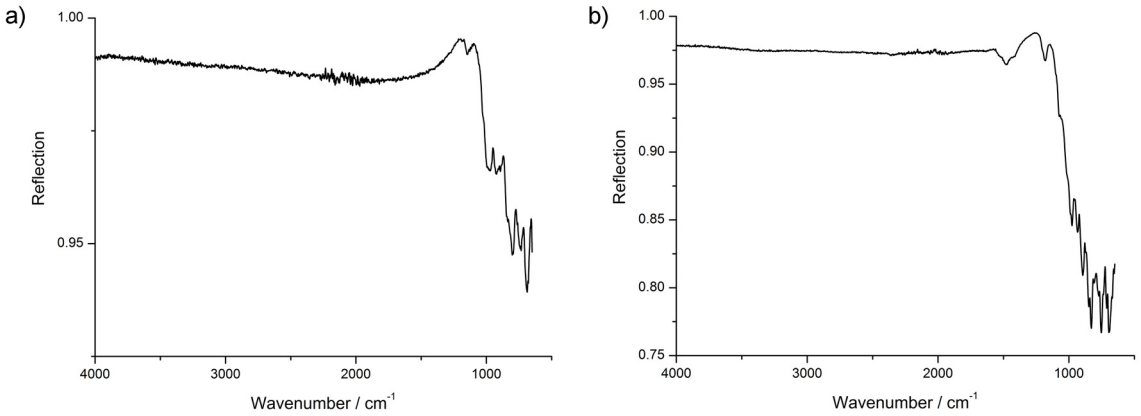


**Figure S1.** IR spectrum of (a) $La_5CaSi_{12}N_{17}O_7\square_2$ and (b) a washed sample containing $La_{3.7}Ca_{2.3}Si_{12}N_{11.7}O_{14.3}$.

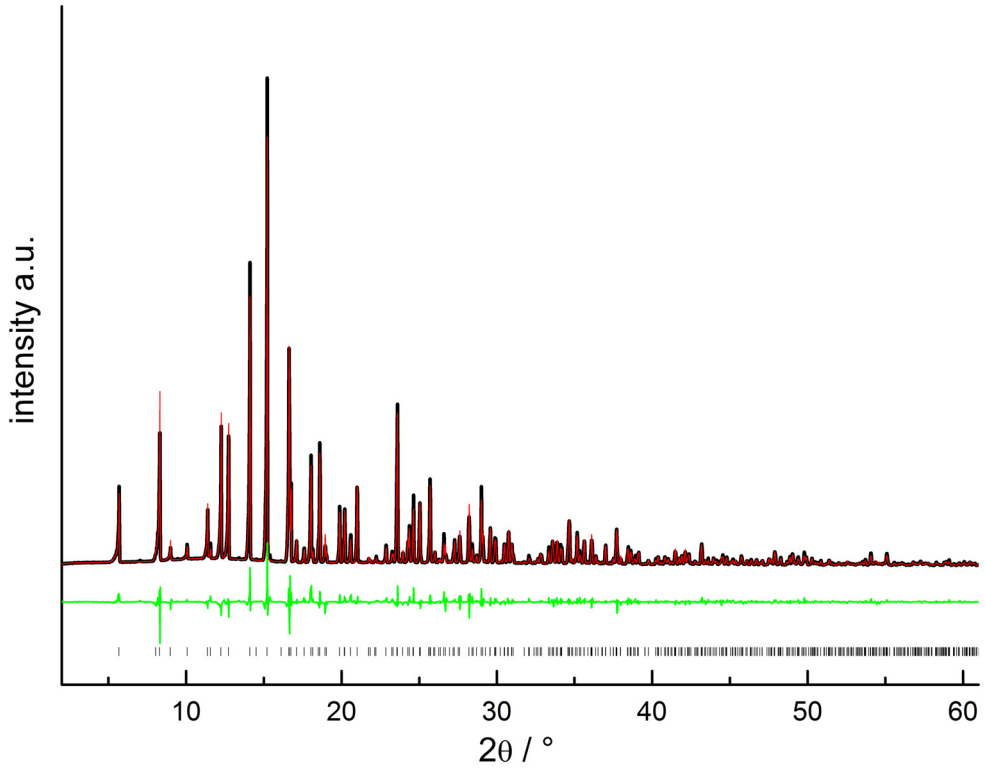


**Figure S2.** Observed (black line) and calculated (red line) powder diffraction pattern, positions of Bragg reflections (vertical bars) and difference profile (green line) for the Rietveld refinement of a sample of $La_5CaSi_{12}N_{17}O_7\square_2$.

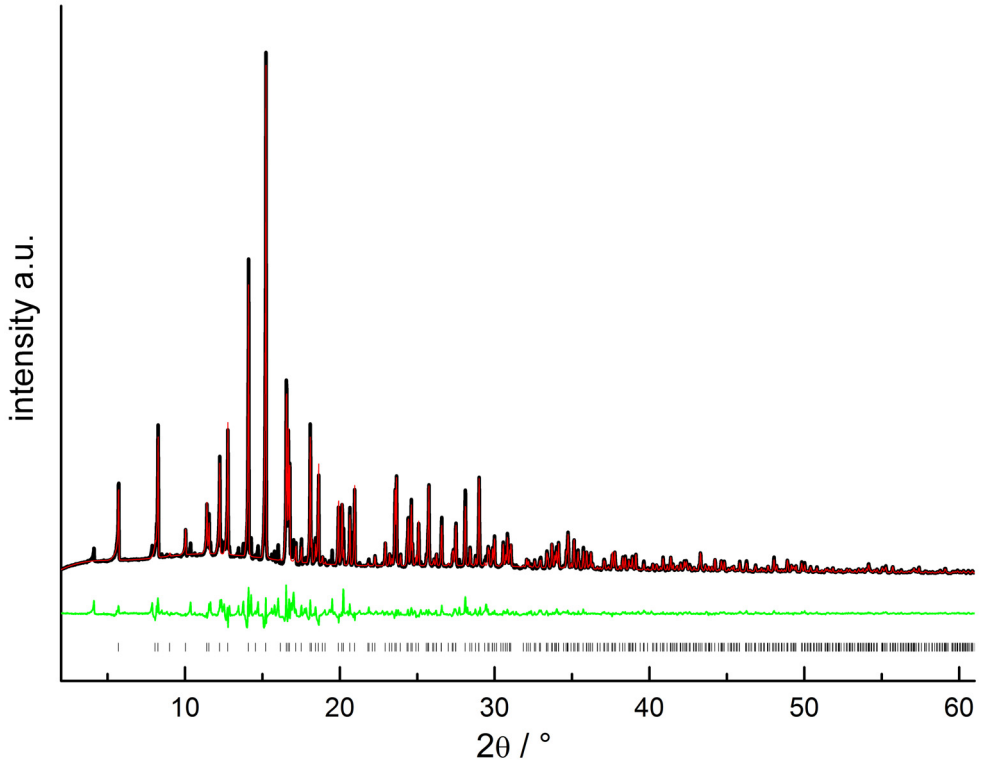


**Figure S3.** Observed (black line) and calculated (red line) powder diffraction pattern, positions of Bragg reflections (vertical bars) and difference profile (green line) for the Rietveld refinement of a washed sample containing $La_{3.66}Ca_{2.34}Si_{12}N_{11.66}O_{14.34}$.

**Table S3.** Crystallographic data of Rietveld refinement of $La_5CaSi_{12}N_{17}O_7\square_2$ and $La_{3.66}Ca_{2.34}Si_{12}N_{11.66}O_{14.3}$.

| | | |
|---|---|---|
| Formula | $La_5CaSi_{12}N_{17}O_7\square_2$ | $La_{3.66}Ca_{2.34}Si_{12}N_{11.66}O_{14.3}$ |
| Crystal system | Tetragonal | |
| Space group | *P*4*bm* (no. 100) | |
| *a* [Å] | 10.12634(10) | 10.09483(14) |
| *c* [Å] | 4.90341(7) | 4.93130(9) |
| Cell volume [Å$^3$] | 502.819(12) | 502.52(16) |
| Formula units per unit cell | 1 | |
| Density [g·cm$^{-3}$] | 4.69534(11) | 4.41406(15) |
| Diffractometer | STOE STADI P | |
| Radiation [Å] | Mo-K$\alpha_1$ (λ = 0.70930) | |
| 2θ range [°] | 2.0-63.785 | 2.0-63.485 |
| Data points | 4120 | 4100 |
| Total no. of reflections | 525 | 520 |
| Refined parameters | 47 | 48 |
| Background function | Shifted Chebychev | |
| $R_{wp}$ | 9.946 | 9.813 |
| $R_{exp}$ | 1.722 | 1.899 |
| $R_p$ | 7.058 | 6.771 |
| $R_{Bragg}$ | 4.68728082 | 4.01751294 |

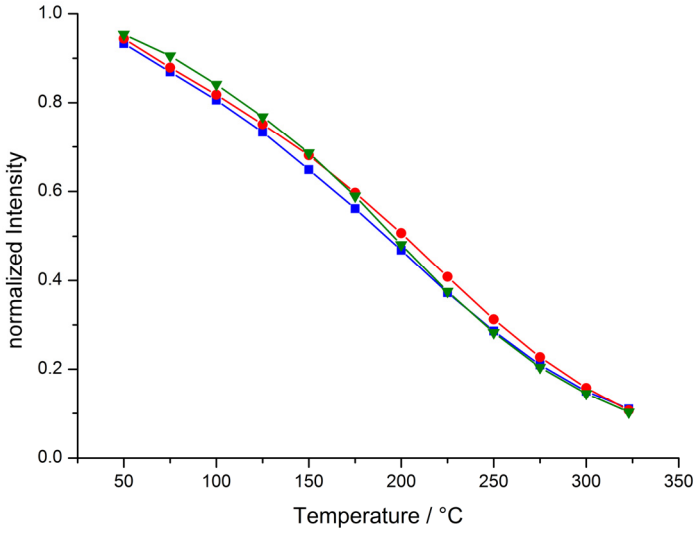


**Figure S4.** Temperature dependence of the emission intensity of $La_5CaSi_{12}N_{17}O_7\square_2:Ce^{3+}$ (1.2 mol% Ce) (red), $La_{3.7}Ca_{2.3}Si_{12}N_{11.7}O_{14.3}:Ce^{3+}$ (2.1 mol% Ce) (blue) and $La_5CaSi_{12}N_{17}O_7\square_2:Ce^{3+},Eu^{2+}$ (1.9 mol% Ce and 0.1 mol% Eu) (green).

## 7.4 Supporting Information for Chapter 4.2

Dajana Durach, Lukas Neudert, Peter J. Schmidt, Oliver Oeckler and Wolfgang Schnick, *Chem. Mater.* **2015**, *27*, 4832-4838.

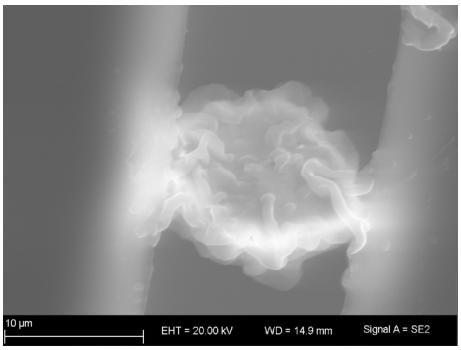


**Figure S1.** SEM image of an aggregate of $La_3BaSi_5N_9O_2:Ce^{3+}$ mounted on a Kapton foil sample holder.

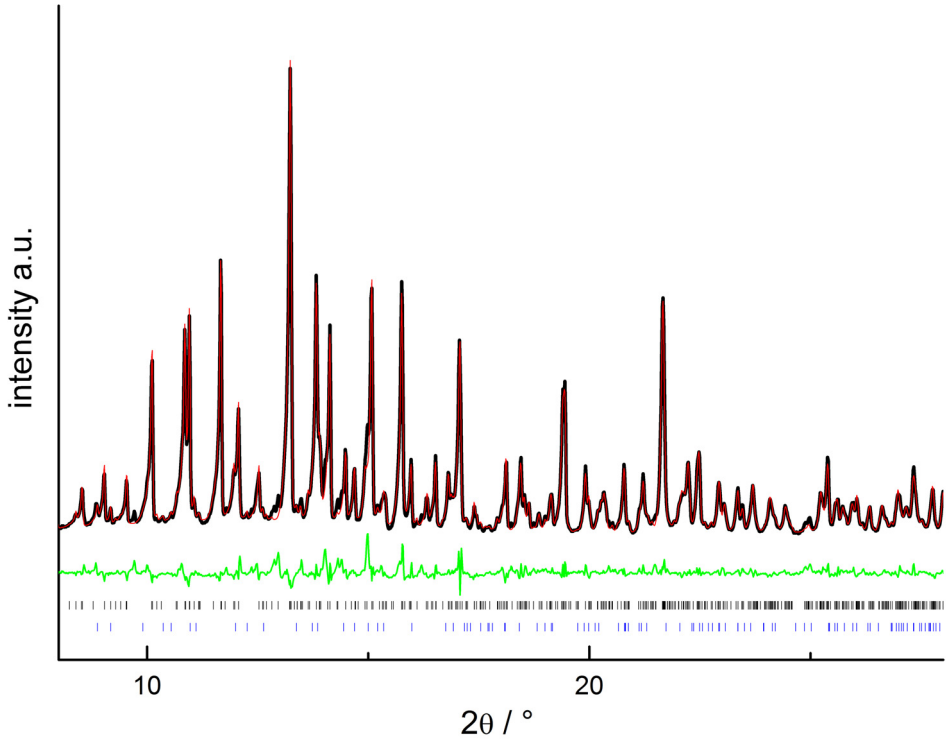


**Figure S2.** Characteristic section of the Rietveld profile fit for a sample of $La_3BaSi_5N_9O_2$: observed (black line) and calculated (red line) powder diffraction pattern as well as position of Bragg reflections (black: $La_3BaSi_5N_9O_2$ (93%), blue: $LaSi_3N_5$(7%)) and difference profile (green line).

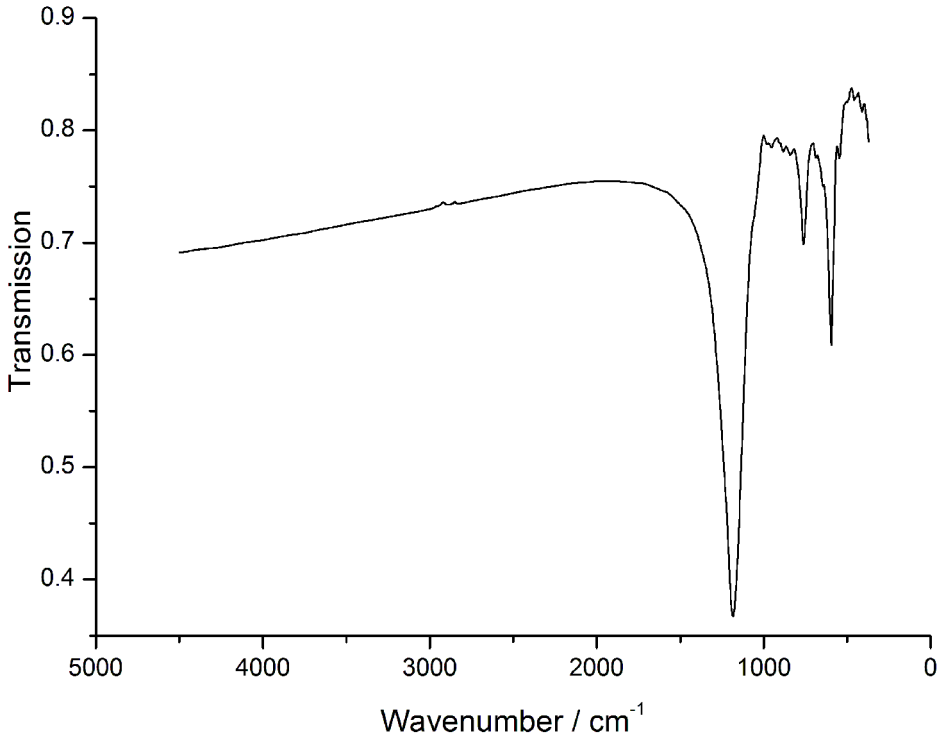


**Figure S3.** IR spectrum of the sample whose powder pattern is shown in Figure S1.

**Table S1.** Atomic coordinates, site occupancies and isotropic (for O/N) or equivalent isotropic atomic displacement parameters (for Si/La/Ba) of $La_3BaSi_5N_9O_2$ (in $Å^2$) with standard deviations in parentheses.

| atom | | *x* | *y* | *z* | $U_{iso}/U_{eq}$ | s.o.f. |
|---|---|---|---|---|---|---|
| La1 | 4b | 0.22420(8) | 0.03047(4) | 0.92256(6) | 0.00950(16) | 0.9144 |
| Ba1 | 4b | 0.22420(8) | 0.03047(4) | 0.92256(6) | 0.00950(16) | 0.0856 |
| La2 | 4b | 0.22608(7) | 0.28788(3) | 0.59655(6) | 0.00728(15) | 0.9544 |
| Ba2 | 4b | 0.22608(7) | 0.28788(3) | 0.59655(6) | 0.00728(15) | 0.0456 |
| La3A | 4b | 0.2717(2) | 0.21079(9) | 0.09552(13) | 0.0113(3) | 0.5433 |
| Ba3A | 4b | 0.2717(2) | 0.21079(9) | 0.09552(13) | 0.0113(3) | 0.2067 |
| La3B | 4b | 0.2725(8) | 0.2223(4) | 0.0692(5) | 0.0113(3) | 0.1936 |
| Ba3B | 4b | 0.2725(8) | 0.2223(4) | 0.0692(5) | 0.0113(3) | 0.0564 |
| La4 | 4b | 0.27890(8) | 0.48297(4) | 0.48236(6) | 0.00865(16) | 0.9044 |
| Ba4 | 4b | 0.27890(8) | 0.48297(4) | 0.48236(6) | 0.00865(16) | 0.0956 |
| La5A | 2a | 0 | 0.0542(6) | 0.2231(14) | 0.0071(10) | 0.3459 |
| Ba5A | 2a | 0 | 0.0542(6) | 0.2231(14) | 0.0071(10) | 0.0841 |
| La5B | 2a | 0 | 0.0402(4) | 0.2316(10) | 0.0071(10) | 0.4585 |
| Ba5B | 2a | 0 | 0.0402(4) | 0.2316(10) | 0.0071(10) | 0.1115 |
| La6 | 2a | 0 | 0.09669(6) | 0.63200(9) | 0.0115(2) | 0.2344 |

| | | | | | | |
|---|---|---|---|---|---|---|
| Ba6 | 2a | 0 | 0.09669(6) | 0.63200(9) | 0.0115(2) | 0.7656 |
| La7 | 2a | 0 | 0.27154(5) | 0.30800(8) | 0.0092(2) | 0.8344 |
| Ba7 | 2a | 0 | 0.27154(5) | 0.30800(8) | 0.0092(2) | 0.1656 |
| La8 | 2a | 0 | 0.34883(5) | 0.88810(12) | 0.0175(3) | 0.4544 |
| Ba8 | 2a | 0 | 0.34883(5) | 0.88810(12) | 0.0175(3) | 0.5456 |
| La9A | 2a | 0 | 0.6070(7) | 0.7095(16) | 0.0141(3) | 0.0403 |
| Ba9A | 2a | 0 | 0.6070(7) | 0.7095(16) | 0.0141(3) | 0.0396 |
| La9B | 2a | 0 | 0.61423(6) | 0.65333(12) | 0.0141(3) | 0.1788 |
| Ba9B | 2a | 0 | 0.61423(6) | 0.65333(12) | 0.0141(3) | 0.7412 |
| La10 | 2a | 0 | 0.77904(5) | 0.28360(8) | 0.0097(2) | 0.8244 |
| Ba10 | 2a | 0 | 0.77904(5) | 0.28360(8) | 0.0097(2) | 0.1756 |
| La11 | 2a | 0 | 0.51509(5) | 0.26193(8) | 0.00816(19) | 0.9344 |
| Ba11 | 2a | 0 | 0.51509(5) | 0.26193(8) | 0.00816(19) | 0.0656 |
| La12 | 2a | 0 | 0.85597(5) | 0.91257(8) | 0.00748(19) | 0.6744 |
| Ba12 | 2a | 0 | 0.85597(5) | 0.91257(8) | 0.00748(19) | 0.3256 |
| Si1 | 4b | 0.1636(3) | 0.20837(14) | 0.8093(2) | 0.0050(5) | 1 |
| Si2 | 4b | 0.1757(3) | 0.38100(15) | 0.1514(2) | 0.0051(5) | 1 |
| Si3 | 4b | 0.1769(3) | 0.64476(14) | 0.3985(3) | 0.0053(5) | 1 |
| Si4 | 4b | 0.1808(3) | 0.14229(14) | 0.4051(3) | 0.0053(5) | 1 |
| Si5 | 4b | 0.3227(3) | 0.09717(15) | 0.6405(3) | 0.0050(5) | 1 |
| Si6 | 4b | 0.3359(3) | 0.29008(15) | 0.3446(3) | 0.0058(5) | 1 |
| Si7 | 4b | 0.3368(3) | 0.53404(14) | 0.2322(3) | 0.0047(5) | 1 |
| Si8 | 4b | 0.3377(3) | 0.05057(15) | 0.2084(2) | 0.0054(5) | 1 |
| Si9 | 2a | 0 | 0.1457(2) | 0.0003(4) | 0.0073(8) | 1 |
| Si10 | 2a | 0 | 0.4030(2) | 0.5446(3) | 0.0049(8) | 1 |
| Si11 | 2a | 0 | 0.6385(2) | 0.0144(3) | 0.0056(8) | 1 |
| Si12 | 2a | 0 | 0.8995(2) | 0.5091(4) | 0.0088(8) | 1 |
| N1 | 4b | 0.1479(11) | 0.1594(5) | 0.9263(8) | 0.0099(18) | 1 |
| N2 | 4b | 0.2275(10) | 0.5678(5) | 0.3317(8) | 0.0080(17) | 1 |
| N3 | 4b | 0.2315(14) | 0.3581(7) | 0.0208(12) | 0.025(3) | 1 |
| N4 | 4b | 0.2360(10) | 0.3120(5) | 0.2323(9) | 0.0092(18) | 1 |
| N5 | 4b | 0.2401(12) | 0.7167(5) | 0.3283(10) | 0.013(2) | 1 |
| N6 | 4b | 0.2425(14) | 0.1089(7) | 0.2843(11) | 0.023(2) | 1 |
| N7 | 4b | 0.2472(11) | 0.2257(5) | 0.4161(9) | 0.0106(18) | 1 |
| N8 | 4b | 0.2491(11) | 0.4614(5) | 0.1836(9) | 0.012(2) | 1 |

| | | | | | | |
|---|---|---|---|---|---|---|
| N9 | 4b | 0.2552(11) | 0.0912(5) | 0.5071(8) | 0.0093(18) | 1 |
| N10 | 4b | 0.2583(11) | 0.1707(5) | 0.7051(9) | 0.0098(18) | 1 |
| N11 | 4b | 0.2646(11) | 0.0242(5) | 0.7107(9) | 0.0110(19) | 1 |
| N12 | 4b | 0.3496(11) | 0.3583(5) | 0.4388(8) | 0.0094(18) | 1 |
| N13 | 4b | 0.3520(10) | 0.0843(5) | 0.0779(8) | 0.0100(18) | 1 |
| N14 | 4b | 0.3537(10) | 0.5900(5) | 0.1222(8) | 0.0088(17) | 1 |
| N15 | 2a | 0 | 0.1423(7) | 0.4073(13) | 0.013(3) | 1 |
| N16 | 2a | 0 | 0.2321(7) | 0.7564(12) | 0.013(3) | 1 |
| N17 | 2a | 0 | 0.3861(7) | 0.1695(13) | 0.014(3) | 1 |
| N18 | 2a | 0 | 0.4830(6) | 0.7935(11) | 0.007(2) | 1 |
| N19 | 2a | 0 | 0.6470(8) | 0.4111(15) | 0.020(3) | 1 |
| N20 | 2a | 0 | 0.7388(6) | 0.7994(11) | 0.006(2) | 1 |
| N21 | 2a | 0 | 0.8956(7) | 0.1313(13) | 0.014(3) | 1 |
| N22 | 2a | 0 | 0.9648(7) | 0.7753(13) | 0.013(3) | 1 |
| O1 | 2a | 0 | 0.0582(6) | 0.0247(10) | 0.012(2) | 1 |
| O2 | 2a | 0 | 0.1899(7) | 0.1230(11) | 0.021(3) | 1 |
| O3 | 2a | 0 | 0.3211(6) | 0.4971(10) | 0.011(2) | 1 |
| O4 | 2a | 0 | 0.4607(7) | 0.4436(12) | 0.019(3) | 1 |
| O5 | 2a | 0 | 0.5571(6) | 0.0686(10) | 0.011(2) | 1 |
| O6 | 2a | 0 | 0.6995(6) | 0.1159(10) | 0.015(2) | 1 |
| O7 | 2a | 0 | 0.8132(7) | 0.4828(12) | 0.019(3) | 1 |
| O8 | 2a | 0 | 0.9477(8) | 0.3948(13) | 0.027(3) | 1 |

**Table S2.** Anisotropic displacement parameters ($U_{iy}$, in Å$^2$) (for Si/La/Ba) of $La_3BaSi_5N_9O_2$.

| atom | $U_{11}$ | $U_{22}$ | $U_{33}$ | $U_{23}$ | $U_{13}$ | $U_{12}$ |
|---|---|---|---|---|---|---|
| La1 | 0.0085(4) | 0.0110(3) | 0.0089(3) | -0.0012(3) | -0.0003(3) | 0.0007(2) |
| Ba1 | 0.0085(4) | 0.0110(3) | 0.0089(3) | -0.0012(3) | -0.0003(3) | 0.0007(2) |
| La2 | 0.0081(3) | 0.0089(3) | 0.0049(3) | 0.0015(2) | 0.0010(3) | 0.0014(2) |
| Ba2 | 0.0081(3) | 0.0089(3) | 0.0049(3) | 0.0015(2) | 0.0010(3) | 0.0014(2) |
| La3A | 0.0110(4) | 0.0119(8) | 0.0110(9) | -0.0043(5) | -0.0013(7) | 0.0023(5) |
| Ba3A | 0.0110(4) | 0.0119(8) | 0.0110(9) | -0.0043(5) | -0.0013(7) | 0.0023(5) |
| La3B | 0.0110(4) | 0.0119(8) | 0.0110(9) | -0.0043(5) | -0.0013(7) | 0.0023(5) |
| Ba3B | 0.0110(4) | 0.0119(8) | 0.0110(9) | -0.0043(5) | -0.0013(7) | 0.0023(5) |
| La4 | 0.0089(3) | 0.0099(3) | 0.0072(3) | 0.0033(2) | 0.0002(3) | 0.0005(2) |
| Ba4 | 0.0089(3) | 0.0099(3) | 0.0072(3) | 0.0033(2) | 0.0002(3) | 0.0005(2) |

| | | | | | | |
|---|---|---|---|---|---|---|
| La5A | 0.0041(5) | 0.011(3) 0 | 0.0068(18) | -0.001(2) | 0 | 0 |
| Ba5A | 0.0041(5) | 0.011(3) 0 | 0.0068(18) | -0.001(2) | 0 | 0 |
| La5B | 0.0041(5) | 0.011(3) 0 | 0.0068(18) | -0.001(2) | 0 | 0 |
| Ba5B | 0.0041(5) | 0.011(3) 0 | 0.0068(18) | -0.001(2) | 0 | 0 |
| La6 | 0.0071(5) | 0.0163(5) | 0.0110(4) | 0.0022(4) | 0 | 0 |
| Ba6 | 0.0071(5) | 0.0163(5) | 0.0110(4) | 0.0022(4) | 0 | 0 |
| La7 | 0.0047(5) | 0.0133(4) | 0.0095(4) | 0.0048(4) | 0 | 0 |
| Ba7 | 0.0047(5) | 0.0133(4) | 0.0095(4) | 0.0048(4) | 0 | 0 |
| La8 | 0.0064(5) | 0.0105(4) | 0.0356(7) | -0.0039(4) | 0 | 0 |
| Ba8 | 0.0064(5) | 0.0105(4) | 0.0356(7) | -0.0039(4) | 0 | 0 |
| La9A | 0.0066(6) | 0.0130(5) | 0.0226(7) | -0.0018(5) | 0 | 0 |
| Ba9A | 0.0066(6) | 0.0130(5) | 0.0226(7) | -0.0018(5) | 0 | 0 |
| La9B | 0.0066(6) | 0.0130(5) | 0.0226(7) | -0.0018(5) | 0 | 0 |
| Ba9B | 0.0066(6) | 0.0130(5) | 0.0226(7) | -0.0018(5) | 0 | 0 |
| La10 | 0.0039(5) | 0.0160(4) | 0.0091(4) | 0.0001(3) | 0 | 0 |
| Ba10 | 0.0039(5) | 0.0160(4) | 0.0091(4) | 0.0001(3) | 0 | 0 |
| La11 | 0.0049(4) | 0.0131(4) | 0.0065(4) | 0.0024(3) | 0 | 0 |
| Ba11 | 0.0049(4) | 0.0131(4) | 0.0065(4) | 0.0024(3) | 0 | 0 |
| La12 | 0.0050(5) | 0.0098(4) | 0.0076(4) | -0.0018(3) | 0 | 0 |
| Ba12 | 0.0050(5) | 0.0098(4) | 0.0076(4) | -0.0018(3) | 0 | 0 |
| Si1 | 0.0037(14) | 0.0070(12) | 0.0043(12) | 0.0000(10) | -0.0004(11) | -0.0009(9) |
| Si2 | 0.0028(14) | 0.0088(12) | 0.0038(13) | 0.0007(9) | -0.0004(10) | -0.0001(10) |
| Si3 | 0.0043(14) | 0.0073(12) | 0.0042(13) | -0.0004(9) | -0.0007(11) | 0.0009(10) |
| Si4 | 0.0039(14) | 0.0065(11) | 0.0056(13) | -0.0003(9) | -0.0001(11) | 0.0004(10) |
| Si5 | 0.0033(13) | 0.0073(11) | 0.0042(12) | 0.0009(10) | 0.0011(11) | -0.0006(9) |
| Si6 | 0.0047(14) | 0.0080(12) | 0.0046(12) | 0.0008(9) | -0.0007(11) | -0.0010(10) |
| Si7 | 0.0045(14) | 0.0049(11) | 0.0048(12) | 0.0014(9) | 0.0006(11) | -0.0001(9) |
| Si8 | 0.0056(15) | 0.0069(12) | 0.0037(12) | -0.0003(9) | 0.0002(10) | -0.0001(10) |
| Si9 | 0.006(2) | 0.0115(18) | 0.0047(18) | 0.0014(14) | 0 | 0 |
| Si10 | 0.002(2) | 0.0092(18) | 0.0033(17) | -0.0009(14) | 0 | 0. |
| Si11 | 0.005(2) | 0.0068(17) | 0.0048(18) | -0.0010(14) | 0 | 0 |
| Si12 | 0.005(2) | 0.017(2) | 0.0044(18) | -0.0017(15) | 0 | 0 |

**Table S3.** Bond-valence sums for the anions and Si in $La_3BaSi_5N_9O_2$.

| atom | BVS | oxidation state | atom | BVS | oxidation state | atom | BVS | oxidation state |
|---|---|---|---|---|---|---|---|---|
| Si1 | 4.05 | 4 | N3 | 2.79 | 3 | N17 | 2.85 | 3 |
| Si2 | 4.02 | 4 | N4 | 2.99 | 3 | N18 | 2.52 | 3 |
| Si3 | 4.03 | 4 | N5 | 2.96 | 3 | N19 | 2.62 | 3 |
| Si4 | 4.07 | 4 | N6 | 2.68 | 3 | N20 | 2.62 | 3 |
| Si5 | 4.02 | 4 | N7 | 3.05 | 3 | N21 | 2.72 | 3 |
| Si6 | 3.93 | 4 | N8 | 2.94 | 3 | N22 | 2.56 | 3 |
| Si7 | 3.95 | 4 | N9 | 3.05 | 3 | O1 | 1.87 | 2 |
| Si8 | 3.95 | 4 | N10 | 3.05 | 3 | O2 | 1.46 | 2 |
| Si9 | 3.80 | 4 | N11 | 2.86 | 3 | O3 | 2.10 | 2 |
| Si10 | 4.03 | 4 | N12 | 2.98 | 3 | O4 | 1.94 | 2 |
| Si11 | 3.78 | 4 | N13 | 3.19 | 3 | O5 | 2.24 | 2 |
| Si12 | 4.08 | 4 | N14 | 3.27 | 3 | O6 | 1.84 | 2 |
| N1 | 3.00 | 3 | N15 | 2.72 | 3 | O7 | 1.75 | 2 |
| N2 | 3.18 | 3 | N16 | 2.71 | 3 | O8 | 1.57 | 2 |

**Table S4.** Bond-valence sums for the heavy atom sites in $La_3BaSi_5N_9O_2$.

| atom | BVS | oxidation state | s.o.f. | weighted average BVS | weighted average oxidation state |
|---|---|---|---|---|---|
| La1 | 2.76 | 3 | 0.91 | 2.92 | 2.91 |
| Ba1 | 4.60 | 2 | 0.09 | | |
| La2 | 2.86 | 3 | 0.95 | 2.96 | 2.95 |
| Ba2 | 4.77 | 2 | 0.05 | | |
| La3A | 2.30 | 3 | 0.54 | 2.04 | 2.16 |
| Ba3A | 3.81 | 2 | 0.21 | | |
| La3B | 2.40 | 3 | 0.19 | 0.69 | 0.69 |
| Ba3B | 3.97 | 2 | 0.06 | | |
| La4 | 2.72 | 3 | 0.90 | 2.90 | 2.90 |
| Ba4 | 4.52 | 2 | 0.10 | | |
| La5A | 2.48 | 3 | 0.35 | 1.20 | 1.21 |
| Ba5A | 4.04 | 2 | 0.08 | | |
| La5B | 2.47 | 3 | 0.46 | 1.59 | 1.60 |
| Ba5B | 4.06 | 2 | 0.11 | | |
| La6 | 1.41 | 3 | 0.23 | 2.23 | 2.23 |
| Ba6 | 2.48 | 2 | 0.77 | | |
| La7 | 2.56 | 3 | 0.83 | 2.84 | 2.83 |
| Ba7 | 4.23 | 2 | 0.17 | | |
| La8 | 1.73 | 3 | 0.45 | 2.46 | 2.45 |
| Ba8 | 3.05 | 2 | 0.55 | | |
| La9A | 1.79 | 3 | 0.04 | 0.21 | 0.20 |
| Ba9A | 3.16 | 2 | 0.04 | | |
| La9B | 1.36 | 3 | 0.18 | 2.02 | 2.02 |
| Ba9B | 2.39 | 2 | 0.74 | | |
| La10 | 2.54 | 3 | 0.82 | 2.83 | 2.82 |
| Ba10 | 4.15 | 2 | 0.18 | | |
| La11 | 2.82 | 3 | 0.93 | 2.94 | 2.93 |
| Ba11 | 4.57 | 2 | 0.07 | | |
| La12 | 2.13 | 3 | 0.67 | 2.66 | 2.67 |
| Ba12 | 3.75 | 2 | 0.33 | | |

## 7.5 Supporting Information for Chapter 4.3

Dajana Durach, Felix Fahrnbauer, Oliver Oeckler and Wolfgang Schnick, *Inorg. Chem.* **2015**, *54*, 8727-8732.

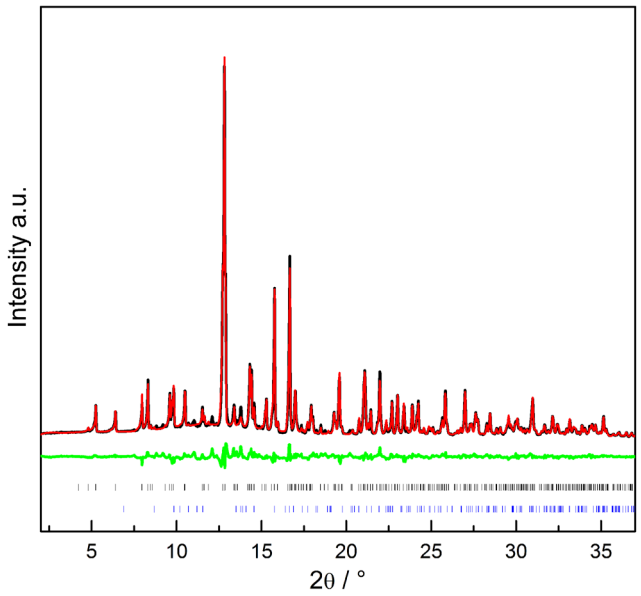


**Figure S1.** Characteristic section of the Rietveld profile fit for a sample of $La_6Ba_3Si_{17}N_{29}O_2Cl$: observed (black line) and calculated (red line) powder diffraction patterns of the sample as well as position of Bragg reflections (black: $La_6Ba_3[Si_{17}N_{29}O_2]Cl$ (95.1%), blue: $BaCl_2$ (4.9%)) and difference profile (green line).

**Table S1.** Crystallographic data of Rietveld refinement of $La_6Ba_3[Si_{17}N_{29}O_2]Cl$ at room temperature.

| | |
|---|---|
| formula | $La_6Ba_3[Si_{17}N_{29}O_2]Cl$ |
| crystal system | hexagonal |
| space group | $P6_3/m$ (no. 176) |
| $a$ (in Å) | 9.7974(5)[i] |
| $c$ (in Å) | 19.2415(10)[i] |
| cell volume (in Å$^3$) | 1599.53(17) |
| Z | 2 |
| density (in g·cm$^{-3}$) | 4.5606(5) |
| Diffractometer | STOE STADI P |
| Radiation | Mo-K$\alpha_1$ (λ = 0.70930 Å) |
| $2\theta$ range (°) | 2.0 - 60.3 |
| data points | 3886 |
| total no. of reflections | 1662 |
| refined parameters | 94 |
| background function | shifted Chebychev |
| $R_{wp}$ | 0.0690 |
| $R_{exp}$ | 0.0168 |
| $R_p$ | 0.0500 |
| $R_{Bragg}$ | 0.0321 |

[i]for crystal structure refinement, single crystal data were used

**Table S2.** Anisotropic displacement parameters ($U_{iy}$, in Å$^2$) of $La_6Ba_3[Si_{17}N_{29}O_2]Cl$.

| atom | $U_{11}$ | $U_{22}$ | $U_{33}$ | $U_{23}$ | $U_{13}$ | $U_{12}$ |
|---|---|---|---|---|---|---|
| La1 | 0.00638(6) | 0.00758(7) | 0.00935(7) | -0.00011(4) | 0.00072(4) | 0.00313(5) |
| Ba2 | 0.01125(9) | 0.01768(10) | 0.00826(9) | 0 | 0 | 0.00861(8) |
| Si1 | 0.0051(3) | 0.0041(3) | $U_{11}$ | 0 | 0 | 0.0020(3) |
| Si2 | 0.0041(2) | $U_{11}$ | 0.0076(4) | 0 | 0 | 0.00207(11) |
| Si3 | 0.0044(2) | 0.0048(2) | 0.0049(2) | 0.00014(17) | 0.00018(17) | 0.00224(18) |
| Si4 | 0.0045(2) | $U_{11}$ | 0.0058(2) | 0.00018(17) | 0.00038(17) | 0.00227(18) |
| N1 | 0.0045(7) | $U_{11}$ | 0.0084(12) | 0 | 0 | 0.0023(3) |
| N2 | 0.0070(7) | 0.0084(7) | 0.0052(7) | 0.0009(5) | 0.0010(5) | 0.0053(6) |
| N3 | 0.0069(7) | 0.0055(7) | 0.0076(7) | -0.0003(5) | 0.0009(5) | 0.0030(6) |
| N4 | 0.0045(6) | 0.0058(7) | 0.0133(8) | -0.0001(6) | 0.0008(6) | 0.0022(6) |
| N5 | 0.0090(7) | 0.0082(7) | 0.0076(7) | -0.0026(6) | -0.0016(6) | 0.0034(6) |
| N6 | 0.0055(10) | 0.0049(9) | 0.0123(11) | 0 | 0 | 0.0017(8) |
| O7 | 0.0088(6) | $U_{11}$ | 0.0082(11) | 0 | 0 | 0.0044(3) |
| Cl1 | 0.0257(7) | $U_{11}$ | 0.111(5) | 0 | 0 | 0.0129(4) |

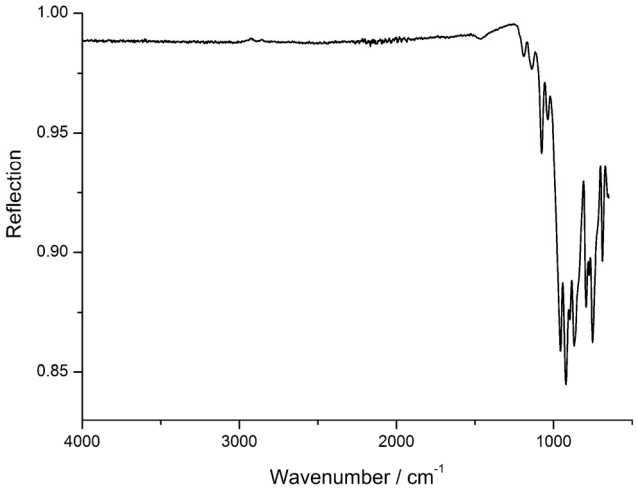


**Figure S2.** IR spectrum of $La_6Ba_3[Si_{17}N_{29}O_2]Cl$.

## 7.6 Supporting Information for Chapter 4.4

Dajana Durach, Peter Schultz, Oliver Oeckler and Wolfgang Schnick, *Inorg. Chem.* **2016**, *55*, 3624-3629.

**Table S1.** Atomic coordinates, site occupancies and isotropic ($U_{iso}$, for Si15A/Si15B, Si16A/Si16B and all O and N atoms) or equivalent isotropic atomic displacement parameters ($U_{eq}$, in Å$^2$) of $La_{11}Si_{13}N_{27.636}O_{1.046}$ with estimated standard deviations in parentheses. $U_{eq}$ is defined as one third of the trace of the orthogonalized $U_{ij}$ tensor exp[-2π$^2$ ($U_{11}h^2a^{*2} + U_{22}k^2b^{*2} + U_{33}l^2c^{*2} + U_{12}hka^*b^* + U_{13}hla^*c^* + U_{23}klb^*c^*$)].

| atom | | *x* | *y* | *z* | $U_{iso}/U_{eq}$ | s.o.f. |
|---|---|---|---|---|---|---|
| La1 | 4*a* | 0 | 0.58418(2) | 0.06079(3) | 0.00620(7) | 1 |
| La2 | 8*b* | 0.28940(3) | 0.08916(2) | 0.41059(2) | 0.00762(5) | 1 |
| La3 | 4*a* | 0 | 0.17562(2) | 0.35004(3) | 0.01097(8) | 1 |
| La4 | 4*a* | 0 | 0.48543(2) | 0.35207(3) | 0.00824(7) | 1 |
| La5 | 8*b* | 0.27814(4) | 0.26268(2) | 0.40011(2) | 0.00965(6) | 1 |
| La6 | 4*a* | 0 | 0.16838(2) | 0.03201(3) | 0.00705(7) | 1 |
| La7 | 4*a* | 0 | 0.05619(2) | 0.71944(3) | 0.00917(8) | 1 |
| La8C | 4*a* | 0 | 0.25015(12) | 0.5569(3) | 0.0126(3) | 0.79(4) |
| La8D | 4*a* | 0 | 0.2428(8) | 0.5711(13) | 0.012(2) | 0.21(4) |
| La9 | 8*b* | 0.29129(4) | 0.16447(2) | 0.17756(2) | 0.01069(6) | 1 |
| La10 | 8*b* | 0.30195(3) | 0.38924(2) | 0.37888(2) | 0.00762(5) | 1 |
| La11 | 4*a* | 0 | 0.43409(2) | 0.08172(3) | 0.00833(7) | 1 |
| La12 | 4*a* | 0 | 0.24850(2) | 0.22376(3) | 0.00896(8) | 1 |
| La13 | 4*a* | 0 | 0.32814(2) | 0.01726(3) | 0.00934(8) | 1 |
| La14A | 4*a* | 0 | 0.00336(2) | -0.00005(7) | 0.00782(19) | 0.636(3) |
| La14B | 4*a* | 0 | 0.00315(4) | 0.03582(15) | 0.0123(4) | 0.364(3) |
| La15 | 8*b* | 0.26314(4) | 0.34391(2) | 0.17511(2) | 0.01255(6) | |
| La16A | 8*b* | 0.27108(14) | 0.04158(2) | 0.21484(4) | 0.01183(16) | 0.636(3) |
| La16B | 8*b* | 0.2129(2) | 0.04436(3) | 0.21221(6) | 0.0109(3) | 0.364(3) |
| Si1 | 8*b* | 0.17795(15) | 0.25015(4) | 0.07923(8) | 0.0047(2) | 1 |
| Si2 | 8*b* | 0.17028(15) | 0.16820(4) | 0.49788(8) | 0.0053(2) | 1 |
| Si3 | 8*b* | 0.33842(15) | 0.48558(4) | 0.35643(8) | 0.0053(2) | 1 |

| | | | | | | |
|---|---|---|---|---|---|---|
| Si4 | 8*b* | 0.16292(15) | 0.43555(4) | 0.23036(8) | 0.0055(2) | 1 |
| Si5 | 4*a* | 0 | 0.60279(6) | 0.27303(12) | 0.0057(3) | 1 |
| Si6 | 8*b* | 0.16194(16) | 0.08563(5) | 0.06580(10) | 0.0102(3) | 1 |
| Si7 | 8*b* | 0.31997(15) | 0.00871(4) | 0.00628(8) | 0.0049(2) | 1 |
| Si8 | 8*b* | 0.34679(15) | 0.17653(4) | 0.34348(8) | 0.0055(2) | 1 |
| Si9 | 4*a* | 0 | 0.30769(6) | 0.37442(13) | 0.0082(3) | 1 |
| Si10 | 8*b* | 0.34132(15) | 0.16622(4) | 0.00373(8) | 0.0054(2) | 1 |
| Si11 | 8*b* | 0.34697(16) | 0.24950(4) | 0.23520(8) | 0.0053(2) | 1 |
| Si12 | 4*a* | 0 | 0.17810(6) | 0.80725(12) | 0.0060(3) | 1 |
| Si13 | 4*a* | 0 | 0.36202(7) | 0.24973(13) | 0.0093(4) | 1 |
| Si14 | 8*b* | 0.32815(15) | 0.42400(4) | 0.07203(8) | 0.0060(2) | 1 |
| Si15A | 4*a* | 0 | 0.11873(13) | 0.2018(2) | 0.0061(5) | 0.636(3) |
| Si15B | 4*a* | 0 | 0.1205(2) | 0.1889(4) | 0.0061(5) | 0.364(3) |
| Si16A | 4*a* | 0 | 0.05318(10) | 0.30694(19) | 0.0070(5) | 0.636(3) |
| Si16B | 4*a* | 0 | 0.06573(17) | 0.3383(3) | 0.0070(5) | 0.364(3) |
| N1 | 4*a* | 0 | 0.50721(19) | 0.0088(4) | 0.0093(10) | 1 |
| N2 | 8*b* | 0.2833(5) | 0.37566(15) | 0.0412(3) | 0.0114(8) | 1 |
| N3A | 4*a* | 0 | 0.1048(3) | 0.2925(6) | 0.0138(19) | 0.636(3) |
| O3B | 4*a* | 0 | 0.0864(6) | 0.2554(12) | 0.021(4) | 0.364(3) |
| N4 | 8*b* | 0.3539(5) | 0.13147(14) | 0.2944(3) | 0.0084(7) | 1 |
| N5 | 4*a* | 0 | 0.0627(2) | 0.5810(5) | 0.0185(14) | 1 |
| N6 | 4*a* | 0 | 0.0816(2) | 0.0253(4) | 0.0123(11) | 1 |
| N7 | 4*a* | 0 | 0.2698(2) | 0.6986(4) | 0.0115(11) | 1 |
| N8 | 8*b* | 0.2304(5) | 0.16569(14) | 0.4113(3) | 0.0109(8) | 1 |
| N9 | 4*a* | 0 | 0.03826(19) | 0.8634(4) | 0.0086(10) | 1 |
| N10 | 8*b* | 0.1488(5) | 0.03773(14) | 0.3494(3) | 0.0097(7) | 1 |
| N11 | 8*b* | 0.2632(5) | 0.21329(14) | 0.2899(3) | 0.0080(7) | 1 |
| N12 | 8*b* | 0.2329(6) | 0.25423(15) | 0.1648(3) | 0.0121(8) | 1 |
| N13 | 8*b* | 0.3540(5) | 0.29495(12) | 0.2805(2) | 0.0070(7) | 1 |
| N14 | 4*a* | 0 | 0.1808(2) | 0.4988(4) | 0.0143(12) | 1 |
| N15 | 8*b* | 0.1482(5) | 0.32878(13) | 0.4131(3) | 0.0080(7) | 1 |
| N16 | 8*b* | 0.2560(5) | 0.42535(14) | 0.1553(3) | 0.0095(7) | 1 |
| N17 | 8*b* | 0.2570(5) | 0.04055(13) | 0.0740(2) | 0.0072(7) | 1 |
| N18 | 4*a* | 0 | 0.24789(18) | 0.0745(4) | 0.0071(10) | 1 |
| N19 | 4*a* | 0 | 0.3141(2) | 0.2841(4) | 0.0135(12) | 1 |

| | | | | | | |
|---|---|---|---|---|---|---|
| N20 | 8*b* | 0.2478(5) | 0.45977(13) | 0.0169(3) | 0.0083(7) | 1 |
| N21 | 8*b* | 0.1482(5) | 0.38903(14) | 0.2751(3) | 0.0091(7) | 1 |
| N22 | 8*b* | 0.2580(6) | 0.12068(16) | 0.0161(3) | 0.0156(9) | 1 |
| N23 | 8*b* | 0.2419(5) | 0.20576(14) | 0.0399(3) | 0.0097(7) | 1 |
| N24 | 4*a* | 0 | 0.69561(18) | 0.3809(4) | 0.0078(10) | 1 |
| N25 | 4*a* | 0 | 0.45762(18) | 0.2148(4) | 0.0078(10) | 1 |
| N26 | 8*b* | 0.2571(5) | 0.46951(14) | 0.2801(3) | 0.0107(8) | 1 |
| N27 | 4*a* | 0 | 0.33341(19) | 0.5487(4) | 0.0087(10) | 1 |
| N28 | 8*b* | 0.2283(5) | 0.47046(14) | 0.4246(3) | 0.0101(8) | 1 |
| N29 | 8*b* | 0.2388(6) | 0.29131(18) | 0.0342(3) | 0.0179(10) | 1 |
| N30 | 8*b* | 0.1473(7) | 0.1047(2) | 0.1514(4) | 0.0244(12) | 1 |
| N31 | 4*a* | 0 | 0.3539(2) | 0.1547(4) | 0.0163(13) | 1 |
| N32 | 4*a* | 0 | 0.5556(2) | 0.3177(4) | 0.0126(12) | 1 |
| N33 | 4*a* | 0 | 0.8255(2) | 0.4022(4) | 0.0120(11) | 1 |
| N34 | 4*a* | 0 | 0.5961(3) | 0.1808(5) | 0.0207(15) | 1 |
| N35 | 4*a* | 0 | 0.1281(2) | 0.7721(4) | 0.0139(12) | 1 |
| N36 | 4*a* | 0 | 0.2544(2) | 0.3884(5) | 0.0202(15) | 1 |
| O37B | 4*a* | 0 | 0.1037(5) | 0.3969(9) | 0.011(3) | 0.364(3) |
| N38 | 4*a* | 0 | 0.1718(2) | 0.2044(5) | 0.0184(14) | 1 |
| N39A | 4*a* | 0 | 0.0259(3) | 0.2287(6) | 0.0091(16) | 0.636(3) |
| O40 | 4*a* | 0 | 0.60356(16) | 0.4733(3) | 0.0080(9) | 1 |
| O41B | 4*a* | 0 | 0.0108(5) | 0.1673(10) | 0.013(3) | 0.364(3) |

**Table S2.** Anisotropic displacement parameters (in Å$^2$) (for La and Si except Si15A/Si15B, Si16A/Si16B) of $La_{11}Si_{13}N_{27.636}O_{1.046}$.

| atom | $U_{11}$ | $U_{22}$ | $U_{33}$ | $U_{23}$ | $U_{13}$ | $U_{12}$ |
|---|---|---|---|---|---|---|
| La1 | 0.00485(17) | 0.00642(14) | 0.00734(18) | -0.00064(13) | 0 | 0 |
| La2 | 0.00731(12) | 0.00708(11) | 0.00847(13) | 0.00121(9) | -0.00218(11) | -0.00181(9) |
| La3 | 0.00627(19) | 0.01481(19) | 0.0118(2) | 0.00224(16) | 0 | 0 |
| La4 | 0.00541(17) | 0.00902(16) | 0.01029(19) | -0.00203(14) | 0 | 0 |
| La5 | 0.01049(14) | 0.01047(12) | 0.00798(13) | -0.00186(10) | 0.00037(11) | 0.00290(10) |
| La6 | 0.00406(17) | 0.00702(15) | 0.01006(19) | 0.00009(13) | 0 | 0 |
| La7 | 0.00418(17) | 0.01617(19) | 0.00715(19) | -0.00013(15) | 0 | 0 |
| La8C | 0.0064(3) | 0.0052(5) | 0.0262(8) | 0.0037(7) | 0 | 0 |
| La8D | 0.0064(12) | 0.008(4) | 0.020(4) | -0.006(3) | 0 | 0 |

| | | | | | | |
|---|---|---|---|---|---|---|
| La9 | 0.01492(15) | 0.00935(12) | 0.00780(13) | 0.00097(10) | -0.00200(12) | -0.00153(10) |
| La10 | 0.00578(12) | 0.00851(11) | 0.00859(13) | 0.00070(9) | 0.00037(10) | 0.00000(9) |
| La11 | 0.00584(18) | 0.01215(17) | 0.00701(18) | -0.00086(14) | 0 | 0 |
| La12 | 0.00692(18) | 0.00856(16) | 0.0114(2) | -0.00153(14) | 0 | 0 |
| La13 | 0.00682(19) | 0.00725(16) | 0.0140(2) | 0.00245(14) | 0 | 0 |
| La14A | 0.0057(6) | 0.0068(5) | 0.0244(13) | 0.0008(5) | 0 | 0 |
| La14B | 0.0060(3) | 0.0106(3) | 0.0069(5) | 0.0030(2) | 0 | 0 |
| La15 | 0.01575(16) | 0.00879(12) | 0.01311(15) | 0.00035(10) | 0.00065(13) | 0.00012(10) |
| La16A | 0.0126(8) | 0.0117(4) | 0.0084(4) | 0.0028(3) | 0.0023(4) | 0.0027(4) |
| La16B | 0.0095(4) | 0.0180(2) | 0.0080(2) | 0.00447(18) | -0.0001(2) | -0.0035(2) |
| Si1 | 0.0025(6) | 0.0049(5) | 0.0066(6) | -0.0002(4) | -0.0003(4) | 0.0003(4) |
| Si2 | 0.0032(6) | 0.0059(5) | 0.0067(6) | 0.0004(4) | -0.0004(5) | -0.0001(4) |
| Si3 | 0.0036(6) | 0.0065(5) | 0.0058(6) | -0.0010(4) | 0.0004(5) | 0.0001(4) |
| Si4 | 0.0036(6) | 0.0077(5) | 0.0052(6) | -0.0008(4) | -0.0004(4) | -0.0002(4) |
| Si5 | 0.0049(8) | 0.0063(7) | 0.0059(8) | -0.0001(6) | 0 | 0 |
| Si6 | 0.0030(6) | 0.0068(5) | 0.0208(8) | -0.0048(5) | -0.0008(5) | 0.0003(4) |
| Si7 | 0.0034(6) | 0.0051(5) | 0.0063(6) | 0.0002(4) | 0.0001(4) | 0.0002(4) |
| Si8 | 0.0040(6) | 0.0065(5) | 0.0061(6) | 0.0005(4) | 0.0007(5) | 0.0005(4) |
| Si9 | 0.0040(8) | 0.0071(7) | 0.0135(9) | -0.0006(7) | 0 | 0 |
| Si10 | 0.0037(6) | 0.0054(5) | 0.0070(6) | 0.0001(4) | 0.0001(5) | 0.0003(4) |
| Si11 | 0.0034(6) | 0.0065(5) | 0.0060(6) | -0.0005(4) | -0.0004(4) | -0.0006(4) |
| Si12 | 0.0042(8) | 0.0057(7) | 0.0081(9) | 0.0020(6) | 0 | 0 |
| Si13 | 0.0056(9) | 0.0123(8) | 0.0100(9) | -0.0001(7) | 0 | 0 |
| Si14 | 0.0033(6) | 0.0098(5) | 0.0049(6) | 0.0002(4) | -0.0001(4) | 0.0016(4) |

**Table S3.** Crystallographic data and details of the structure refinement of $La_{11}Si_{13}N_{27.376}O_{0.936}F$.[i]

| | |
|---|---|
| formula | $La_{11}Si_{13}N_{27.376}O_{0.936}F$ |
| crystal system | orthorhombic |
| space group | $Cmc2_1$ (no. 36) |
| *a* (in Å) | 9.5602(3) |
| *b* (in Å) | 32.3092(14) |
| *c* (in Å) | 18.7599(8) |
| cell volume (in Å$^3$) | 5794.6(4) |
| Z | 8 |
| density (in g·cm$^{-3}$) | 5.297 |
| μ (in mm$^{-1}$) | 16.436 |
| Temperature (in K) | 293(2) |
| radiation | Bruker D8 Venture (Mo-*Kα*; *λ* = 0.71073 Å) |
| F(000) | 8137 |
| θ range (in °) | 2.171 ≤ θ ≤ 27.483 |
| total no. of rflns | 27388 |
| independent rflns | 6968 [R(int) = 0.0543] |
| refined params | 389 |
| twin ratio | 0.37(3) / 0.63 |
| GOF | 1.392 |
| *R*1 (all data / for $F^2 > 2\sigma(F^2)$) | 0.0575 / 0.0405 |
| *wR*2 (all data / for $F^2 > 2\sigma(F^2)$) | 0.0598 / 0.0577 |
| $\Delta\rho_{max}$ , $\Delta\rho_{min}$ (in e/Å$^3$) | 5.312; -1.730 |

i: compared to $La_{11}Si_{13}N_{27.636}O_{1.046}$ the crystal structure of $La_{11}Si_{13}N_{27.376}O_{0.936}F$ contains an additional isolated anion position occupied with F

**Table S4.** Atomic coordinates, site occupancies and isotropic ($U_{iso}$, for Si15A/Si15B, Si16A/Si16B and all O and N atoms) or equivalent isotropic atomic displacement parameters ($U_{eq}$, in Å$^2$) of $La_{11}Si_{13}N_{27.376}O_{0.936}F$ with estimated standard deviations in parentheses. $U_{eq}$ is defined as one third of the trace of the orthogonalized $U_{ij}$ tensor $\exp[-2\pi^2 (U_{11}h^2a^{*2} + U_{22}k^2b^{*2} + U_{33}l^2c^{*2} + U_{12}hka^*b^* + U_{13}hla^*c^* + U_{23}klb^*c^*)]$.

| atom | | *x* | *y* | *z* | $U_{iso}/U_{eq}$ | s.o.f. |
|---|---|---|---|---|---|---|
| La1 | 4*a* | 0 | 0.58379(5) | 0.05638(9) | 0.0094(4) | 1 |
| La2 | 8*b* | 0.28503(11) | 0.08801(4) | 0.41019(6) | 0.0126(3) | 1 |
| La3 | 4*a* | 0 | 0.17441(6) | 0.35177(9) | 0.0172(4) | 1 |
| La4 | 4*a* | 0 | 0.48278(5) | 0.35645(9) | 0.0117(4) | 1 |
| La5 | 8*b* | 0.27805(11) | 0.26185(4) | 0.40193(6) | 0.0118(2) | 1 |
| La6 | 4*a* | 0 | 0.16843(5) | 0.03338(9) | 0.0085(4) | 1 |
| La7 | 4*a* | 0 | 0.05860(5) | 0.72122(9) | 0.0102(4) | 1 |
| La8D | 4*a* | 0 | 0.24690(6) | 0.56663(10) | 0.0157(4) | 1 |
| La9 | 8*b* | 0.29191(11) | 0.16301(4) | 0.17683(6) | 0.0140(3) | 1 |
| La10 | 8*b* | 0.29470(12) | 0.38970(4) | 0.38099(6) | 0.0159(3) | 1 |
| La11 | 4*a* | 0 | 0.43262(6) | 0.08382(9) | 0.0127(4) | 1 |
| La12 | 4*a* | 0 | 0.24730(6) | 0.22460(9) | 0.0129(4) | 1 |
| La13 | 4*a* | 0 | 0.32679(5) | 0.01776(9) | 0.0149(4) | 1 |
| L14B | 4*a* | 0 | 0.0020(6) | 0.0007(4) | 0.0091(14) | 0.624(10) |
| L14A | 4*a* | 0 | 0.0022(10) | 0.0184(8) | 0.0091(14) | 0.376(10) |
| La15 | 8*b* | 0.26882(10) | 0.34195(4) | 0.17727(6) | 0.0126(3) | 1 |
| L16B | 8*b* | 0.2804(6) | 0.03826(17) | 0.2122(3) | 0.0190(9) | 0.624(10) |
| L16A | 8*b* | 0.2388(8) | 0.0479(3) | 0.2170(5) | 0.0190(9) | 0.376(10) |
| Si1 | 8*b* | 0.1782(5) | 0.25034(17) | 0.0803(3) | 0.0065(12) | 1 |
| Si2 | 8*b* | 0.1689(5) | 0.16837(17) | 0.4971(3) | 0.0080(11) | 1 |
| Si3 | 8*b* | 0.3396(5) | 0.48765(16) | 0.3541(3) | 0.0081(11) | 1 |
| Si4 | 8*b* | 0.1626(5) | 0.43387(16) | 0.2315(3) | 0.0088(11) | 1 |
| Si5 | 4*a* | 0 | 0.6018(3) | 0.2729(4) | 0.0100(17) | 1 |
| Si6 | 8*b* | 0.1616(5) | 0.08439(18) | 0.0685(3) | 0.0138(14) | 1 |
| Si7 | 8*b* | 0.3197(5) | 0.00667(16) | 0.0071(3) | 0.0057(11) | 1 |
| Si8 | 8*b* | 0.3460(5) | 0.17559(17) | 0.3426(3) | 0.0073(11) | 1 |
| Si9 | 4*a* | 0 | 0.3083(3) | 0.3741(4) | 0.0146(18) | 1 |
| Si10 | 8*b* | 0.3407(5) | 0.16679(17) | 0.0061(3) | 0.0074(12) | 1 |
| Si11 | 8*b* | 0.3472(5) | 0.24843(16) | 0.2370(3) | 0.0066(11) | 1 |

| | | | | | | |
|---|---|---|---|---|---|---|
| Si12 | 4*a* | 0 | 0.1792(2) | 0.8109(4) | 0.0081(16) | 1 |
| Si13 | 4*a* | 0 | 0.3609(3) | 0.2509(5) | 0.025(2) | 1 |
| Si14 | 8*b* | 0.3297(5) | 0.42234(16) | 0.0735(3) | 0.0061(11) | 1 |
| S15B | 4*a* | 0 | 0.1184(2) | 0.1968(4) | 0.0113(16) | 1 |
| S16B | 4*a* | 0 | 0.0684(5) | 0.3404(8) | 0.012(2) | 0.624(10) |
| S16A | 4*a* | 0 | 0.0594(8) | 0.3212(13) | 0.012(2) | 0.376(10) |
| N1 | 4*a* | 0 | 0.5059(7) | 0.0094(11) | 0.008(5) | 1 |
| N2 | 8*b* | 0.2838(13) | 0.3741(5) | 0.0422(8) | 0.009(3) | 1 |
| O3B | 4*a* | 0 | 0.0975(12) | 0.2649(19) | 0.038(9) | 0.624(10) |
| N3A | 4*a* | 0 | 0.165(3) | 0.487(5) | 0.038(9) | 0.376(10) |
| N4 | 8*b* | 0.3548(14) | 0.1301(5) | 0.2955(8) | 0.011(3) | 1 |
| N5 | 4*a* | 0 | 0.0628(8) | 0.5809(13) | 0.017(6) | 1 |
| N6 | 4*a* | 0 | 0.0793(7) | 0.0278(12) | 0.008(5) | 1 |
| N7 | 4*a* | 0 | 0.2715(7) | 0.7015(11) | 0.007(5) | 1 |
| N8 | 8*b* | 0.2340(14) | 0.1650(4) | 0.4116(8) | 0.008(3) | 1 |
| N9 | 4*a* | 0 | 0.0361(7) | 0.8650(11) | 0.007(5) | 1 |
| N10 | 8*b* | 0.1505(16) | 0.0394(5) | 0.3395(9) | 0.025(4) | 1 |
| N11 | 8*b* | 0.2574(12) | 0.2113(5) | 0.2903(8) | 0.008(3) | 1 |
| N12 | 8*b* | 0.2348(15) | 0.2543(5) | 0.1640(8) | 0.014(4) | 1 |
| N13 | 8*b* | 0.3541(12) | 0.2932(5) | 0.2843(8) | 0.006(3) | 1 |
| N14 | 4*a* | 0 | 0.1836(8) | 0.4900(15) | 0.020(7) | 1 |
| N15 | 8*b* | 0.1505(14) | 0.3280(4) | 0.4157(8) | 0.010(3) | 1 |
| N16 | 8*b* | 0.2575(13) | 0.4247(4) | 0.1556(7) | 0.005(3) | 1 |
| N17 | 8*b* | 0.2567(14) | 0.0392(5) | 0.0742(8) | 0.013(4) | 1 |
| N18 | 4*a* | 0 | 0.2506(6) | 0.0762(11) | 0.004(4) | 1 |
| N19 | 4*a* | 0 | 0.3126(7) | 0.2874(11) | 0.010(5) | 1 |
| N20 | 8*b* | 0.2428(13) | 0.4580(4) | 0.0187(7) | 0.008(3) | 1 |
| N21 | 8*b* | 0.1505(13) | 0.3872(4) | 0.2747(7) | 0.008(3) | 1 |
| N22 | 8*b* | 0.2558(13) | 0.1208(5) | 0.0203(8) | 0.011(3) | 1 |
| N23 | 8*b* | 0.2408(15) | 0.2062(5) | 0.0417(8) | 0.010(3) | 1 |
| N24 | 4*a* | 0 | 0.6959(7) | 0.3794(11) | 0.011(5) | 1 |
| N25 | 4*a* | 0 | 0.4542(7) | 0.2148(12) | 0.007(4) | 1 |
| N26 | 8*b* | 0.2530(16) | 0.4678(5) | 0.2826(8) | 0.016(4) | 1 |
| N27 | 4*a* | 0 | 0.3319(6) | 0.5508(10) | 0.004(4) | 1 |
| N28 | 8*b* | 0.2345(16) | 0.4751(5) | 0.4266(9) | 0.018(4) | 1 |

| | | | | | | |
|---|---|---|---|---|---|---|
| N29 | 8*b* | 0.2419(15) | 0.2911(5) | 0.0312(8) | 0.012(3) | 1 |
| N30 | 8*b* | 0.1495(15) | 0.1018(5) | 0.1539(8) | 0.020(4) | 1 |
| N31 | 4*a* | 0 | 0.3519(8) | 0.1517(13) | 0.026(6) | 1 |
| N32 | 4*a* | 0 | 0.5516(7) | 0.3162(11) | 0.009(5) | 1 |
| N33 | 4*a* | 0 | 0.8230(7) | 0.4055(12) | 0.013(5) | 1 |
| N34 | 4*a* | 0 | 0.5933(7) | 0.1795(13) | 0.022(6) | 1 |
| N35 | 4*a* | 0 | 0.1287(8) | 0.7788(11) | 0.015(5) | 1 |
| N36 | 4*a* | 0 | 0.2531(8) | 0.3798(13) | 0.028(7) | 1 |
| O37B | 4*a* | 0 | 0.0961(11) | 0.408(2) | 0.035(9) | 0.624(10) |
| N38 | 4*a* | 0 | 0.1709(6) | 0.1851(11) | 0.010(5) | 1 |
| N39A | 4*a* | 0 | 0.0174(18) | 0.200(3) | 0.004(5) | 0.376(10) |
| F1 | 4*a* | 0 | 0.6040(5) | 0.4728(8) | 0.025(4) | 1 |
| O41B | 4*a* | 0 | 0.0118(9) | 0.1711(14) | 0.004(5) | 0.624(10) |
| F2 | 4*a* | ½ | 0.3169(5) | 0.1392(9) | 0.026(4) | 1 |

**Table S5.** Crystallographic data of Rietveld refinement for $La_{11}Si_{13}N_{27.376}O_{0.936}F$; the refinement was based on the results of the single-crystal investigation of $La_{11}Si_{13}N_{27.376}O_{0.936}F$, only lattice parameters were refined.

| | |
|---|---|
| formula | $La_{11}Si_{13}N_{27.376}O_{0.936}F$ |
| crystal system | orthorhombic |
| space group | $Cmc2_1$ (no. 36) |
| *a* (in Å) | 9.56301(8) |
| *b* (in Å) | 32.2977(4) |
| *c* (in Å) | 18.75796(19) |
| cell volume (in Å$^3$) | 5793.64(10) |
| Z | 8 |
| density (in g·cm$^{-3}$) | 5.297 |
| temperature (in K) | 293(2) |
| diffractometer | STOE STADI P |
| radiation | Mo-K$\alpha_1$ (λ = 0.70930 Å) |
| 2θ range (°) | 2.0 - 62.6 |
| data points | 4042 |
| total no. of rflns | 5265 |
| refined params | 28 |
| background function | shifted Chebychev |
| $R_{wp}$ | 0.0490 |
| $R_{exp}$ | 0.0192 |
| $R_p$ | 0.0344 |
| $R_{Bragg}$ | 0.0253 |

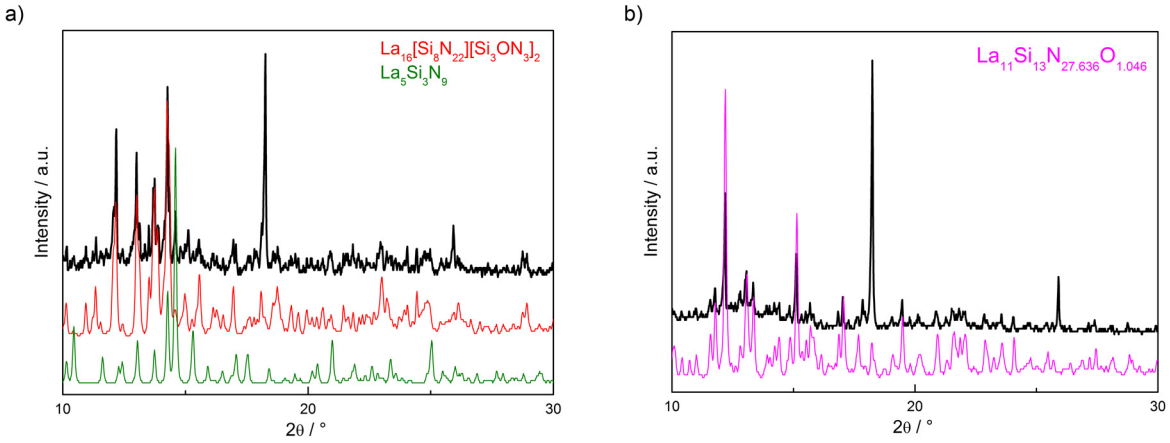


**Figure S1.** a) Characteristic section of the experimental powder diffraction pattern (black) of the sample containing $La_{11}Si_{13}N_{27.636}O_{1.046}:Ce^{3+}$: red peaks belong to the calculated pattern of $La_{16}[Si_8N_{22}][Si_3ON_3]_2$ and green ones to that of $La_5Si_3N_9$; b) characteristic section of the experimental powder diffraction pattern (black) of the same sample washed with $H_2O$, pink peaks correspond to a diagram calculated according to the structure model of $La_{11}Si_{13}N_{27.636}O_{1.046}$ obtained from single-crystal data of the respective compound; unassigned reflections belong to unknown side phases.

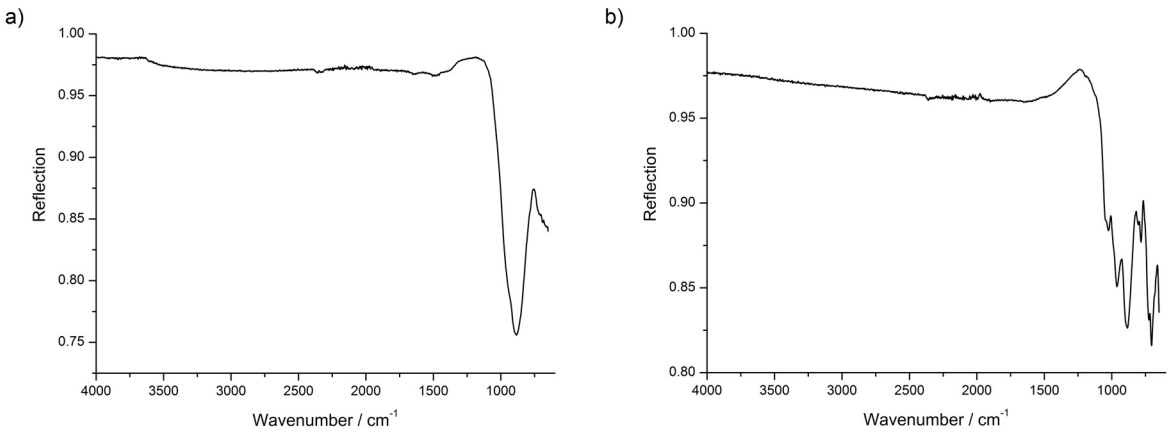


**Figure S2.** FTIR spectra of washed samples: a) containing $La_{11}Si_{13}N_{27.636}O_{1.046}:Ce^{3+}$; b) of single-phase $La_{11}Si_{13}N_{27.376}O_{0.936}F$.

## 7.7 Supporting Information for Chapter 4.5

Peter Schultz, Dajana Durach, Wolfgang Schnick and Oliver Oeckler, *Z. Anorg. Allg. Chem.* **2016**, *642*, 603-608.

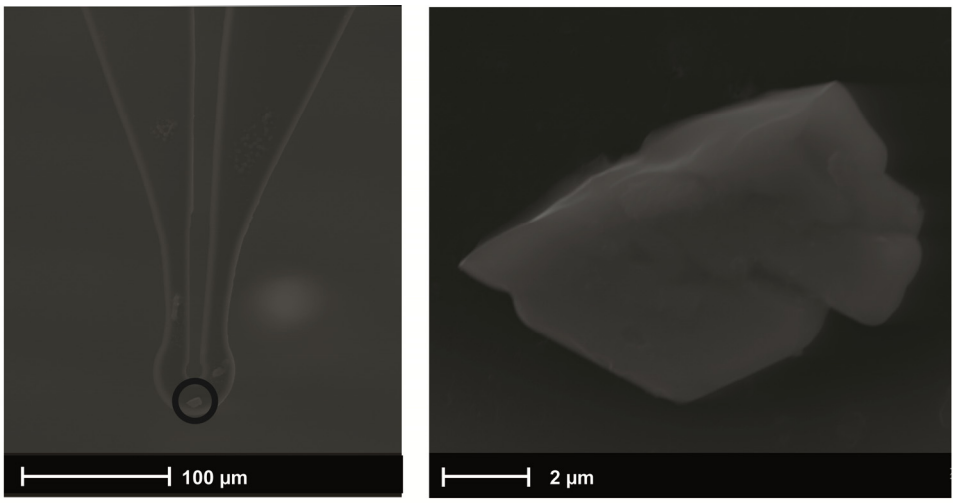


**Figure S1.** SEM images of the crystal used for data collection: a) position on the micromount (encircled), b) enlarged view.

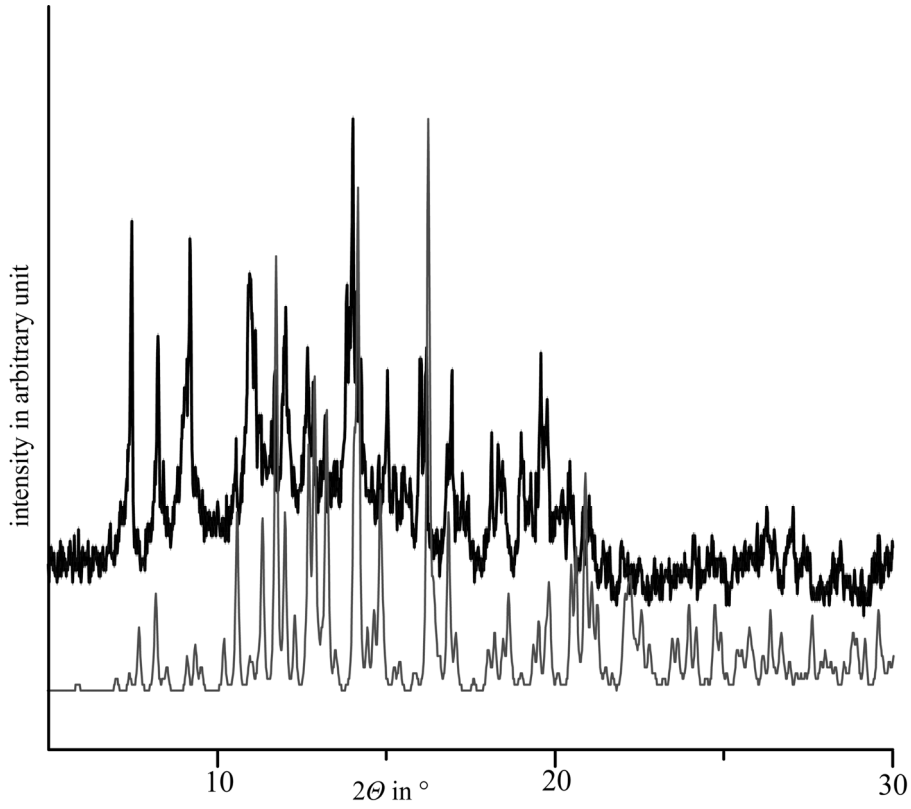


**Figure S2.** Characteristic section of the experimental powder diffraction pattern (black) of the sample (washed in $H_2O$) containing $Ba_{1.63}La_{7.39}Si_{11}N_{23}Cl_{0.42}:Ce^{3+}$ as a minority phase; the gray histogram depicts the simulation according to the structure model obtained from single-crystal structure elucidation; unassigned additional reflections belong to unknown side phases.

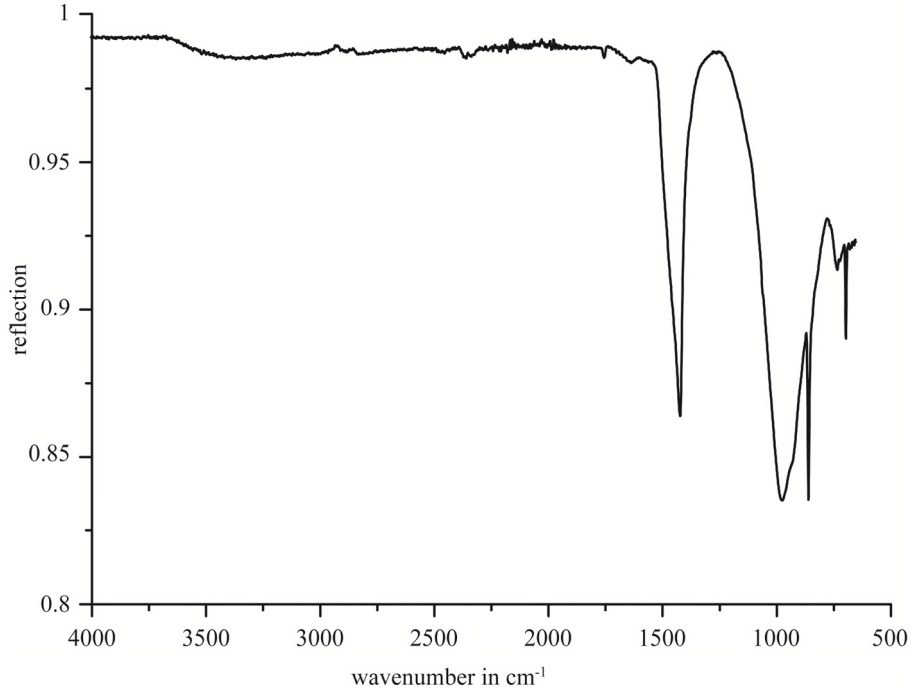


**Figure S3.** FTIR spectrum of the sample (washed in $H_2O$) containing $Ba_{1.63}La_{7.39}Si_{11}N_{23}Cl_{0.42}:Ce^{3+}$; no bands are visible at typical N-H or O-H wavenumbers.

**Table S1.** Bond valence sums for some cations in $Ba_{1.63}La_{7.39}Si_{11}N_{23}Cl_{0.42}:Ce^{3+}$.

| | BVS | oxidation state | occupancy |
|---|---|---|---|
| La1 | 2.89 | 3 | 1 |
| La2A | 2.89 | 3 | 1 |
| La2B | 2.85 | 3 | 1 |
| La3 | 2.86 | 3 | 1 |
| La4 | 1.32 | 3 | 0.16 |
| Ba4 | 2.324 | 2 | 0.84 |
| La5 | 2.20 | 3 | 0.70 |
| Ba5 | 3.88 | 2 | 0.30 |
| Si1 | 4.14 | 4 | 1 |
| Si2 | 4.39 | 4 | 1 |
| Si3 | 4.09 | 4 | 1 |
| Si4 | 4.22 | 4 | 1 |
| Si5 | 3.91 | 4 | 1 |

**Table S2.** Anisotropic displacement parameters of all atomic positions in $Ba_{1.63}La_{7.39}Si_{11}N_{23}Cl_{0.42}:Ce^{3+}$ in the form $\exp[-2\pi^2 (U_{11}h^2a^{*2} + U_{22}k^2b^{*2} + U_{33}l^2c^{*2} + U_{12}hka^*b^* + U_{13}hla^*c^* + U_{23}klb^*c^*)]$

| atom | $U_{11}$ | $U_{22}$ | $U_{33}$ | $U_{23}$ | $U_{13}$ | $U_{12}$ |
|---|---|---|---|---|---|---|
| La1 | 0.00657(5) | 0.00696(5) | 0.00618(5) | -0.00016(3) | 0 | 0 |
| La2A | 0.00695(12) | 0.00552(17) | 0.00694(5) | 0 | 0 | -0.00061(13) |
| La2B | 0.00695(12) | 0.00552(17) | 0.00694(5) | 0 | 0 | -0.00061(13) |
| La3 | 0.00798(7) | 0.00660(7) | 0.00850(7) | 0 | 0 | 0 |
| La4 | 0.01583(8) | 0.00785(7) | 0.00746(7) | 0 | 0 | 0 |
| Ba4 | 0.01583(8) | 0.00785(7) | 0.00746(7) | 0 | 0 | 0 |
| La5 | 0.01653(6) | 0.00762(6) | 0.01018(6) | 0 | 0 | 0.00226(4) |
| Ba5 | 0.01653(6) | 0.00762(6) | 0.01018(6) | 0 | 0 | 0.00226(4) |
| La6A | 0.0309(6) | 0.0529(17) | 0.0205(6) | 0 | -0.0054(4) | 0 |
| La6B | 0.0312(11) | 0.0342(13) | 0.0166(7) | -0.0077(5) | 0 | 0 |
| Ba7 | 0.056(2) | 0.139(5) | 0.0161(16) | 0 | 0 | 0 |
| Si1 | 0.00659(19) | 0.0035(2) | 0.0044(2) | 0 | -0.00009(16) | 0 |
| Si2 | 0.0096(2) | 0.0050(2) | 0.0051(2) | 0 | 0 | -0.00223(17) |
| Si3 | 0.00644(14) | 0.00526(15) | 0.00433(14) | -0.00033(11) | 0.00018(11) | -0.00114(11) |
| Si4 | 0.00555(19) | 0.0051(2) | 0.0042(2) | 0.00065(16) | 0 | 0 |
| Si5 | 0.0081(3) | 0.0034(3) | 0.0047(3) | 0 | 0 | 0 |
| N1 | 0.0130(10) | 0.0078(9) | 0.0052(8) | 0 | 0 | 0 |
| N2 | 0.0086(4) | 0.0098(5) | 0.0064(4) | -0.0019(4) | -0.0009(3) | 0.0013(4) |
| N3 | 0.0108(5) | 0.0149(6) | 0.0096(5) | -0.0002(4) | 0.0032(4) | -0.0043(4) |
| N4 | 0.0247(9) | 0.0055(7) | 0.0074(7) | 0.0007(5) | 0 | 0 |
| N5 | 0.0096(9) | 0.0074(9) | 0.0051(8) | 0 | 0 | 0 |
| N6 | 0.0098(6) | 0.0089(7) | 0.0055(6) | 0 | 0 | -0.0001(5)a |
| N7 | 0.0172(8) | 0.0165(9) | 0.0124(8) | 0 | 0 | 0.0105(7) |
| N8 | 0.0080(9) | 0.0116(10) | 0.0098(9) | 0 | 0 | 0 |
| N9 | 0.0160(5) | 0.0075(5) | 0.0075(5) | -0.0015(4) | -0.0004(4) | -0.0049(4) |
| N10 | 0.0120(10) | 0.0078(9) | 0.0089(9) | 0 | 0 | 0 |
| N11 | 0.011(4) | 0.013(4) | 0.0114(12) | 0 | 0 | -0.007(3) |
| Cl1 | 0.0198(6) | 0.0113(5) | 0.0171(6) | 0 | 0 | 0 |

# 8 Publications

## 8.1 List of Publications Included in this Thesis

**1** **Lanthanum (Oxo)nitridosilicates: From Ordered to Disordered Crystal Structures**
Dajana Durach and Wolfgang Schnick
*Z. Anorg. Allg. Chem.* **2016**, *642*, 101-106.

*For this article, writing the manuscript, synthesis of the samples, single-crystal refinements, evaluation of spectroscopic data, analysis of the electron density as well as topological analyses and MAPLE calculations were performed by D. Durach. W. Schnick supervised the work and revised the manuscript.*

**2** **Non-Condensed (Oxo)nitridosilicates: $La_3[SiN_4]F$ and the Polymorph o-$La_3[SiN_3O]O$**
Dajana Durach and Wolfgang Schnick
*Eur. J. Inorg. Chem.* **2015**, 4095-4100.

*For this publication, writing the manuscript, synthesis of the samples, single-crystal and Rietveld refinements, evaluation of spectroscopic data, topological analyses and MAPLE calculations were done by D. Durach. W. Schnick supervised the work and revised the manuscript.*

**3** **$La_5CaSi_{12}N_{17}O_7\square_2$ and $La_{3.7}Ca_{2.3}Si_{12}N_{11.7}O_{14.3}$: Two Promising Host Lattices for $Eu^{2+}$- and $Ce^{3+}$-doping Towards Phosphor Materials with Highly Tunable Luminescence**
patent in progress: Dajana Durach, Peter J. Schmidt and Wolfgang Schnick

*In this contribution, writing the manuscript, synthese of the samples, and structure determination based on single-crystal and powder XRD data were done by D. Durach. Luminescence investigations and interpretation of measured values were done in the LDC Aachen by P. J. Schmidt. Supervision of the research project was carried out by W. Schnick.*

**4 $La_3BaSi_5N_9O_2:Ce^{3+}$ - A Yellow Phosphor with an Unprecedented Tetrahedra Network Structure Investigated by Combination of Electron Microscopy and Synchrotron X-ray Diffraction**

Dajana Durach, Lukas Neudert, Peter J. Schmidt, Oliver Oeckler and Wolfgang Schnick
*Chem. Mater.* **2015**, *27*, 4832-4838.

*D. Durach did the synthesis, PXRD analyses, topological analysis, bond valence calculations and prepared the main part of the manuscript. It was revised by all co-authors. O. Oeckler did the synchrotron measurements and structure refinement, the latter supported by D. Durach. TEM investigations and the interpretation of obtained results were done by L. Neudert and O. Oeckler. Luminescence investigations and interpretation of measured values were done in the LDC Aachen by P. J. Schmidt. W. Schnick and O. Oeckler supervised the work. Help of F. Heinke, P. Urban, P. Schultz, F. Fahrnbauer, L. Erra, G. Vaughan and J. Wright during synchrotron measurements is acknowledged.*

**5 $La_6Ba_3[Si_{17}N_{29}O_2]Cl$ - An Oxonitridosilicate Chloride with Exceptional Structural Motifs**

Dajana Durach, Felix Fahrnbauer, Oliver Oeckler and Wolfgang Schnick
*Inorg. Chem.* **2015**, *54*, 8727-8732.

*W. Schnick supervised the work. D. Durach did the synthesis, crystal selection and preparation, PXRD analyses, evaluation of spectroscopic data, the MAPLE calculations, bond valence calculations and prepared the manuscript. It was revised by all co-authors. O. Oeckler and F. Fahrnbauer did the synchrotron measurements and structure refinement, the latter supported by D. Durach. Help of F. Heinke, P. Urban, P. Schultz, L. Erra, G. Vaughan and J. Wright during synchrotron measurements is acknowledged. N. Auner, University of Frankfurt provided $Si_2Cl_6$ as a starting material.*

**6 From Minor Side Phases to Bulk Samples of Lanthanum Oxonitridosilicates – An Investigation with Microfocused Synchrotron Radiation**

Dajana Durach, Peter Schultz, Oliver Oeckler and Wolfgang Schnick

*Inorg. Chem.* **2016**, *55*, 3624-3629.

*W. Schnick supervised the work. D. Durach did the synthesis, crystal selection and preparation, PXRD analyses, evaluation of spectroscopic data and prepared the manuscript. It was revised by all co-authors. O. Oeckler and P. Schultz did the synchrotron measurements and in close collaboration with D. Durach the structure refinement. Help of F. Heinke, P. Urban, F. Fahrnbauer, L. Erra, G. Vaughan and J. Wright during synchrotron measurements is acknowledged.*

**7 $Ba_{1.63}La_{7.39}Si_{11}N_{23}Cl_{0.42}:Ce^{3+}$ - A Nitridosilicate Chloride with a Zeolite-like Structure**

Peter Schultz, Dajana Durach, Wolfgang Schnick and Oliver Oeckler

*Z. Anorg. Allg. Chem.* **2016**, *642*, 603-608.

*In this contribution, synthesis of the sample, crystal selection and preparation, PXRD analyses and the evaluation of spectroscopic data were done by D. Durach. P. Schultz did the bond valence calculations, the structure refinement and prepared the manuscript. All co-authors revised the manuscript. Synchrotron measurements were done by O. Oeckler and P. Schultz. Help of F. Heinke, P. Urban, F. Fahrnbauer, L. Erra, G. Vaughan and J. Wright during synchrotron measurements is acknowledged.*

## 8.2 Other Publications

**1** **Increasing crystallinity for improved electrical conductivity of TiO2 blocking layers**

A. S. Wochnik, M. Handloser, D. Durach, A. Hartschuh, and C. Scheu

*ACS Appl. Mater. Interfaces* **2013**, *5*, 5696.

**2** **$Li_{35}Ln_9Si_{30}N_{59}O_2F$ with *Ln* = Ce, Pr - Highly Condensed Nitridosilicates**

S. Lupart, D. Durach, W. Schnick

*Z. Anorg. Allg. Chem.* **2011**, *637*, 1841

## 8.3 Conference Contributions

**1** **Structure determination of microcrystalline oxonitridosilicates and oxonitridoimidophosphates by combination of TEM and synchrotron methods (poster)**

L. Neudert, F. Pucher, D. Durach, O. Oeckler, W. Schnick

Microscopy Conference, Göttingen, 2015.

**2** **Microfocused Synchrotron Radiation as a Powerful Tool for Structure Elucidation of Lanthanum Barium Oxonitridosilicates (poster)**

D. Durach, F. Fahrnbauer, L. Neudert, O. Oeckler, W. Schnick

15th European Conference on Solid State Chemistry, Wien, 2015.

**3** **Neue Lanthannitridosilicate und ihre strukturelle Vielfalt (talk)**

D. Durach, F. Fahrnbauer, O. Oeckler, W. Schnick,

Seminar für Festkörperchemie, Hirschegg, 2015.

**4** **Neue zeolithartige Silicatstrukturen aus Einkristallmessungen mit mikrofokussierter Synchrotronstrahlung (talk)**

P. Schultz, D. Durach, W. Schnick, O. Oeckler

Seminar für Festkörperchemie, Hirschegg, 2015.

**5 Structure determination of luminescent oxonitridosilicates by a combination of electron microspcopy and microfocus synchrotron diffraction (poster)**

L. Neudert, D. Durach, O. Oeckler, W. Schnick

23th Annual Meeting of the German Crystallographic Society (DGK), Göttingen, 2015.

**6 Structure determination of luminescent oxonitridosilicates by a combination of electron microspcopy and microfocus synchrotron diffraction (poster)**

L. Neudert, D. Durach, O. Oeckler, W. Schnick

Wöhler-Tagung, Saarbrücken, 2014.

**7 TEM und Synchrotron-Mikrodiffraktion zur Strukturaufklärung neuer Oxonitridophosphate und -silicate (talk)**

P. Schultz, D. Durach, L. Neudert, A. Marchuk, T. Rosenthal, W. Schnick, O. Oeckler

Mitteldeutsches Anorganiker Nachwuchs Symphosium (MANS), 2014, Freiberg.

**8 Neue Lanthannitridosilicate und ihr Potential als Leuchtstoff (talk)**

D. Durach, P. Suchultz, L. Neudert, O. Oeckler, W. Schnick,

Obergurgl-Seminar Festkörperchemie, Obergurgl, 2014.

**9 Synthetic Approach to Promising Nitride Host Lattices (poster)**

D. Durach, F. Hintze, C. Pösl, W. Schnick,

11th International Krutyn Summer School, Krutyn, 2012.

## 8.4 CSD Numbers

Crystallographic data (cif files) for the compounds synthesized as part of this work were deposited at the Fachinformationszentrum Karlsruhe, 76344 Eggenstein-Leopoldshafen, Germany (fax: +49-7247-808-666; e-mail: crysdata@fiz-karlsruhe.de) and are available on quoting the following depository numbers.

| | |
|---|---|
| $La_{16.32}Ba_{1.82}Sr_{7.86}[Si_{60}N_{92.32}O_{3.68}]O_{12}$ | CSD-429945 |
| $La_{13.68}Sr_{12.32}[Si_{60}N_{96}]F_{6.32}O_{5.68}$ | CSD-429946 |
| o-$La_3[SiON_3]O$ | CSD-429559 |
| $La_3[SiN_4]F$ | CSD-429558 |
| $La_3BaSi_5N_9O_2$ | CSD-429510 |
| $La_6Ba_3[Si_{17}N_{29}O_2]Cl$ | CSD-429711 |
| $La_{11}Si_{13}N_{27.636}O_{1.046}$ | CSD-430509 |
| $Ba_{1.63}La_{7.39}Si_{11}N_{23}Cl_{0.42}$ | CSD-430956 |

# 9 Curriculum Vitae

| | |
|---|---|
| **Personal Details** | |
| Name | Dajana Durach |
| Date of Birth | 29.09.1987 |
| Place of Birth | Bonn, Germany |
| Nationality | German |
| **Professional experience** | |
| Since 02/2016 | **Phosphors Development Engineer**<br>*Osram Opto Semiconductors, Regensburg, Germany* |
| **Education** | |
| 06/2012-01/2016 | **Research assistant** in the group of Prof. Dr. W. Schnick (Department of Chemistry, *Ludwig-Maximilians-Universität München, Germany* )<br>**Doctoral thesis**<br>*Ludwig-Maximilians-Universität München, Germany*<br>(supervisor: Prof. Dr. W. Schnick)<br>Title*: "Lanthanum (Oxo)nitridosilicates: Syntheses, Properties and the Use of Synchrotron Radiation for Structure Elucidation"* |
| 11/2011 - 05/2012 | **Master thesis** (Inorganic Chemistry)<br>*Ludwig-Maximilians-Universität München, Germany*<br>(supervisor: Prof. Dr. W. Schnick)<br>Title: "*Characterization of $Li_5Nd_5Si_4N_{12}$ and $La_4Si_5N_{10}0$ as well as synthetic approaches to reduced nitridosilicates by employment of $Si_2(NH)_3$"* |
| 03/2010 - 05/2010 | **Master of Science** (Chemistry) |

| | |
|---|---|
| | *Ludwig-Maximilians-Universität München, Germany* |
| 08/2009 - 12/2009 | **Bachelor thesis** (Inorganic Chemistry)<br>*Ludwig-Maximilians-Universität München, Germany*<br>(supervisor: Prof. Dr. W. Schnick)<br>Title: "*Charakterisierung von $Li_{35}Pr_9Si_{30}N_{59}O_2F$ sowie Syntheseuntersuchungen an quaternären Cäsiumnitridosilicaten*" |
| 10/2006 - 03/2010 | **Bachelor of Science** (Chemistry and Biochemistry)<br>*Ludwig-Maximilians-Universität München, Germany* |
| 06/2006 | **Allgemeine Hochschulreife** |
| 09/1994 - 06/2006 | **Secondary School**<br>*Leonhard-Wagner-Gymnasium Schwabmünchen, Germany* |